This is to certify that the
dissertation entitled

ALLANITE WEATHERING AND RARE EARTH ELEMENTS IN MASS BALANCE CALCULATIONS OF CLAY GENESIS RATES AT THE COWEETA HYDROLOGIC LABORATORY, WESTERN NORTH CAROLINA, USA: THE RESPONSE TIMES OF CHANGES IN CLAY MINERAL ASSEMBLAGES TO FLUCTUATIONS IN CLIMATE

presented by

Jason R. Price

has been accepted towards fulfillment
of the requirements for the

Ph.D. degree in Geological Sciences

Michael Anthony Velbel
Major Professor's Signature

MAY 16, 2003
Date

ALLANITE WEATHERING AND RARE EARTH ELEMENTS IN MASS BALANCE CALCULATIONS OF CLAY GENESIS RATES AT THE COWEETA HYDROLOGIC LABORATORY, WESTERN NORTH CAROLINA, USA: THE RESPONSE TIMES OF CHANGES IN CLAY MINERAL ASSEMBLAGES TO FLUCTUATIONS IN CLIMATE

By

Jason R. Price

A DISSERTATION

Submitted to
Michigan State University
in partial fulfillment of the requirements
for the degree of

DOCTOR OF PHILOSOPHY

Department of Geological Sciences

2003

ABSTRACT

ALLANITE WEATHERING AND RARE EARTH ELEMENTS IN MASS BALANCE CALCULATIONS OF CLAY GENESIS RATES AT THE COWEETA HYDROLOGIC LABORATORY, WESTERN NORTH CAROLINA, USA: THE RESPONSE TIMES OF CHANGES IN CLAY MINERAL ASSEMBLAGES TO FLUCTUATIONS IN CLIMATE

By

Jason R. Price

Flux-based mass balance methods have been used to calculate rates of clay formation/dissolution in three watersheds located at the Coweeta Hydrologic Laboratory, western North Carolina. The mass balance calculations of this study include rare earth elements (REE), which is fundamentally different from any study performed at Coweeta or elsewhere. The primary advantage of using additional elements such as the rare earths is that a larger number of equations can be constructed, allowing determination of a larger number of unknowns. This situation does not always exist in mass balance calculations.

The REE in Coweeta stream waters are strongly influenced by the weathering of previously unrecognized allanite which is a very important source of Ca in stream waters. Due to the inclusion of allanite that also contains and releases Na during weathering, the primary mineral weathering rates calculated as part of this study differ from those of previous studies (i.e., Taylor and Velbel 1991). All new plagioclase dissolution rates are lower but still within 20% of those reported by Taylor and Velbel (1991). Similarly, the biotite weathering rates reported herein are within 40% of those reported by Taylor and Velbel (1991). The garnet weathering rates of this study are up to approximately 75%

slower than those calculated by Taylor and Velbel (1991). Without allanite, large weathering rates were needed to balance the Ca in stream waters.

The results of this study demonstrate that kaolin precipitation/formation is favored in warmer and/or drier climates, and gibbsite is favored in cooler and/or wetter climates. Vermiculite appears to be influenced by lithology and climate.

The clay genesis/dissolution rates determined by mass balance methods have been used to calculate the time needed for a 5% (50 g kg^{-1}) change in relative clay abundance in the saprolite at Coweeta; i.e., the "response time" of the clay mineral to a change in climate. Response times occur on time scales of tens of thousand to hundreds of thousands of years. The results of this study concur with the arguments of Thiry (2000) that the best resolution of the paleoclimatic record in clay-rich sediments and mudrocks is 1 or 2 Ma.

To Sumi, who has been my girlfriend, fiancée, and wife during my tenure as a Ph.D. student. Your understanding and support have been extraordinary, and I cannot thank you enough for all that you have done. You are awesome!

For the late Dick Noreen, whose caring, compassion, and humanitarianism should be a model for all.

For the late Dr. James L. Massey, who knew what education should be, and indomitably strove to make it that way.

ACKNOWLEDGEMENTS

The individual who requires the greatest acknowledgement is my wife, Sumi. Her copy editing, support, patience, understanding, and love have been amazing. She has done more than she will ever know. Thank you Sumi.

I owe many thanks to my dissertation advisor Dr. Michael Velbel who has assisted me in so many ways, for so many years, in spite of all his collateral demands. In addition to his scarce time he has also very generously provided me financial support for multiple semesters. All of his help has been very much appreciated.

One of the most patient and selfless individuals I have ever met has been Dr. Lina Patiño. This project has only come to fruition with her technical and analytical assistance, not to mention all of the research and career advice she has given me. Dr. Patiño is what every faculty member should strive to be, and I am delighted and privileged to have been able to work with her.

Dr. Brian Teppen is another individual whom I feel very fortunate to have met. He is truly one of the clearest thinkers I know, and I have enjoyed every interaction that I have had with him. Clay Mineralogy (CSS 825) has been the best class I have ever taken, graduate or undergraduate. Dr. Teppen deserves a great deal of thanks for all of the help he has provided me as I pursued my Ph.D.

Dr. Randy Schaetzl, too, has been a genuine benefit to my guidance committee. I'm very pleased that the Department of Geological Sciences relaxed its faculty affiliation requirements for guidance committee members, otherwise I probably never would have gotten to interact with Dr. Schaetzl. Thanks for all of your assistance, despite joining my committee a bit later on.

Dr. Robert D. Hatcher, Jr. of the University of Tennessee, Knoxville has been more helpful than he humbly admits. His knowledge of the petrology and structure of the bedrock at Coweeta is amazing and has been invaluable. His willingness to answer my numerous questions is very much appreciated, and I've thoroughly enjoyed our interactions.

Although there are many people worthy of mention, I certainly cannot go any further without acknowledging Diane Baclawski, Librarian of the Geology Library. I do not think the Department of Geological Sciences has a greater asset than her. She assists students and faculty in so many ways, and with such sincerity, humor, and humility. She is, unfortunately, under-recognized for all that she does. I will not, however, forget all that she has done for me during my time as a graduate student at MSU. Many many thanks Diane. You're one of a kind and MSU should feel fortunate to have you.

I am also extremely grateful to Dr. Jennifer Knoepp, Research Soil Scientist at Coweeta, for her assistance, cooperation, and suggestions during field activities, and for providing splits of lysimeter cores from Watershed 27. She is another individual whom I am pleased to have met and interacted.

The entire staff at the Center for Advanced Microscopy are also deserving of a great deal of thanks for all of their help and terrific classes. These individuals include (in no specific order) Dr. Stanley Flegler, Dr. Karen Klomparens, Dr. Xudong Fan, Dr. Alicia Pastor, Dr. Shirley Owens, Ewa Danielewicz, and Carol Flegler. After visiting the University of Michigan's electron microscopy center I realized what an outstanding facility CAM is.

Fellow graduate students David Szymanski and Meredith Lindeman also deserve thanks for their help with stream water sampling and analyses.

Funding for this project was partially provided by a Grant-in-Aid of Research, from Sigma Xi, The Scientific Research Society. Additional funding has also been provided by a Michigan Space Grant Consortium Graduate Fellowship, Clay Minerals Society Student Grant, and a Lucile Drake Pringle Fellowship.

TABLE OF CONTENTS

LIST OF TABLES

LIST OF FIGURES

INTRODUCTION

Continental weathering processes generate unconsolidated material available for erosion, which ultimately contribute clastic materials to sedimentary basins. Thus, the physical record of erosion and [chemical] weathering is found in clastic sedimentary deposits (Derry and France-Lanord 1997). As the weathering of silicate rocks is typically incongruent, clays are formed, which may then accumulate in sedimentary basins and serve as direct evidence of continental silicate weathering (Derry and France-Lanord 1997). Secondary minerals, or their associations, may be diagnostic for certain types of climatic environments (Migoń and Lidmar-Bergström 2002, John et al. 2003). Nonetheless, disparity exists between researchers who find detrital clays to be an accurate proxy for continental source area paleoclimate interpretations (e.g., Menking 1997, Chamley 1997, Yuretich et al. 1999, Price et al. 2000, Tabor et al. 2002, John et al. 2003), and those who express caution with respect to the use of clay mineralogy in retrospective analysis of source area climate (e.g., Gibbs 1977, Singer 1980, 1984, Gerrard 1994, Power and Smith, 1994, Curtis 1990, Thiry 2000, Migoń and Lidmar-Bergström 2002). These latter researchers recognize that terrigenous clay sediment may undergo significant modifications not only during transport to, and diagenesis within, the depositional basin, but also in the source area prior to erosion. Parent rock composition, local geomorphology and hydrology, stage of weathering, and/or duration of weathering may influence clay genesis rates in a continental source area (Migoń and Lidmar-Bergström 2002). Therefore, any investigation of terrigenous clay mineral modification within the sedimentary cycle should begin by addressing those factors capable of influencing clay mineral assemblages and formation rates in the continental source area.

Knowing the rates of clay genesis in a regolith permits calculation of response times of a weathering profile to changes in climate. This knowledge will permit constraints to be placed on the resolution of the paleoclimatic record in clay-rich sediments and mudrocks; Thiry (2000) suggests that the best resolution is 1 or 2 Ma. Thiry (2000) states that terrigenous material in sedimentary deposits reflects only climate if the source area landscape is covered with a substantial blanket of mature soils in equilibrium with the environment. Based on geochemical calculations and the geomorphic occurrences of soils and paleosols, Thiry (2000) argues that a time span of at least 1 Ma is necessary to form a landscape blanketed with a thick kaolinitic regolith.

Rates of clay formation in source areas are influenced not only by climate, but also by the chemical reactivity of the bedrock (Potter et al. 1975, Velbel 1984a, Righi and Meunier 1995, Migoń and Lidmar-Bergström 2002). However, John et al. (2003) have found clay minerals in sediments to be a climate proxy even when the type of source area bedrock is unknown. The chemical reactivity of the bedrock controls the solutes present in regolith solutions, subsequently controlling the clays which are able to form and their respective genesis rates (Potter et al. 1975, Lowe 1986). Constraining bedrock lithologic influences on weathering and clay genesis in heterogeneous metamorphic orogenic belts is extremely difficult, if not impossible.

One facet of the complex process of landscape evolution and denudation that has been difficult to measure is the timescale over which secondary minerals form (Weaver 1989, Schroeder et al. 2001). The purpose of this study is to calculate the rates of clay (hydrous aluminosilicates and hydroxides) formation in a modern weathering profile, in a setting where the effects of climate and bedrock composition can be constrained. These

clay genesis rates are then used to calculate the response times of clay minerals to changes in climate; that is, to test Thiry's (2000) 1 to 2 Ma hypothesis

CHAPTER 1

BACKGROUND

Study Area

The study areas are three watersheds (Table 1) of the U.S. Forest Service Coweeta Hydrologic Laboratory located in the southeastern Blue Ridge Province of western North Carolina (Figures 1 and 2). Coweeta is located approximately 15 km southwest of Franklin, North Carolina, and about 3 km north of the Georgia state line. This research facility was established in 1934 (Douglass and Hoover 1988), and in 1968 collection of nutrient cycling data in Coweeta watersheds was initiated with joint USDA Forest Service and National Science Foundation funding (Swank and Crossley 1988). Relief at Coweeta is quite rugged (average slope of approximately 45%/23°); Albert Mountain (elevation 1,592 m) the western boundary forms the highest point within Coweeta, with the lowest point being 670 m in the valley of Coweeta Creek on the east side of the facility (Figure 2). The highest and lowest points in Coweeta are approximately 4.5 km apart (Figure 2).

Bedrock Geology

The southern Blue Ridge Province includes low to high grade metamorphic rocks that have been thrust northwestward over the unmetamorphosed sedimentary rocks of the Valley and Ridge Province (O'Hara et al. 1995, Mossa 1998, Miller et al. 2000; Figure 1). The eastern Blue Ridge is generally similar lithologically to the adjacent Inner Piedmont, and together these two belts comprise the Piedmont Terrane (Williams and Hatcher 1982, 1983, Miller et al. 2000; Figure 1). The Brevard Fault Zone separates the eastern Blue Ridge from the Inner Piedmont, but it is equivocal whether or not it is a

Table 1. Watershed data for use in this study (data from Swank and Crossley 1988, Swift et al. 1988, and Swank and Waide 1988).

Water-shed	Bedrock	Area (ha)	Elevation at weir (m)	Maximum elevation (m)	Midslope elevation (m)	Land slope (%)	Mean annual precipitation (cm)	Mean annual runoff (cm)	Mean annual temperature (°C)	Aspect
2	Otto Formation	12.26	709	1004	857	60	177.17	85.39	11.7	South-southeast
34	Otto Formation	32.70	866	1184	1025	52	200.94	117.47	10.6	South-southeast
27	Coweeta Group (Persimmon Creek Gneiss, Coleman River Formation, Ridgepole Mountain Formation)	39.05	1061	1454	1257	55	245.08	173.74	9.1	North-northeast

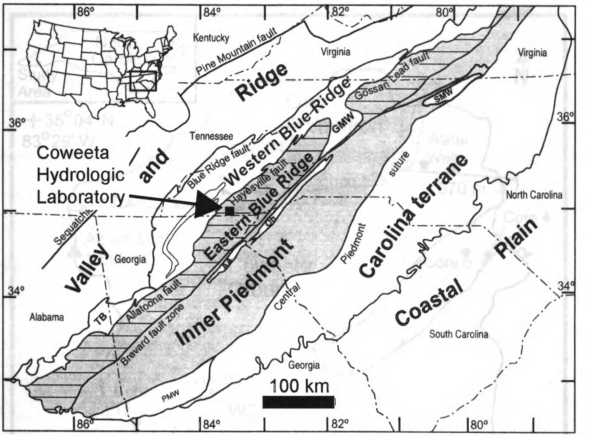

Figure 1. Generalized geologic map of the southern Appalachian orogen showing the Valley and Ridge Province, eastern Blue Ridge, Brevard Fault Zone, Inner Piedmont, and Coweeta Hydrologic Laboratory. The eastern Blue Ridge and Inner Piedmont together form the Piedmont Terrane (shaded) (Williams and Hatcher 1982, 1983, Miller et al. 2000). Modified from Mershat and Kalbas (2002), their Figure 1(a).

fundamental terrane boundary (Williams and Hatcher 1983, Dennis and Wright 1997, Miller et al. 2000).

The Coweeta Basin is underlain by complexly folded, thrust faulted, and amphibolite facies (staurolite-kyanite subfacies) metamorphosed sediments of the Coweeta Group (mid-Ordovician; Miller et al. 2000) and the Otto Formation (Upper Pre-Cambrian; Hatcher 1980, 1988). The Otto Formation at Coweeta was previously mapped as the Tallulah Falls Formation, but has since been revised (Hatcher 1980, 1988, personal communication 2001). The Coweeta Group may be subdivided into three

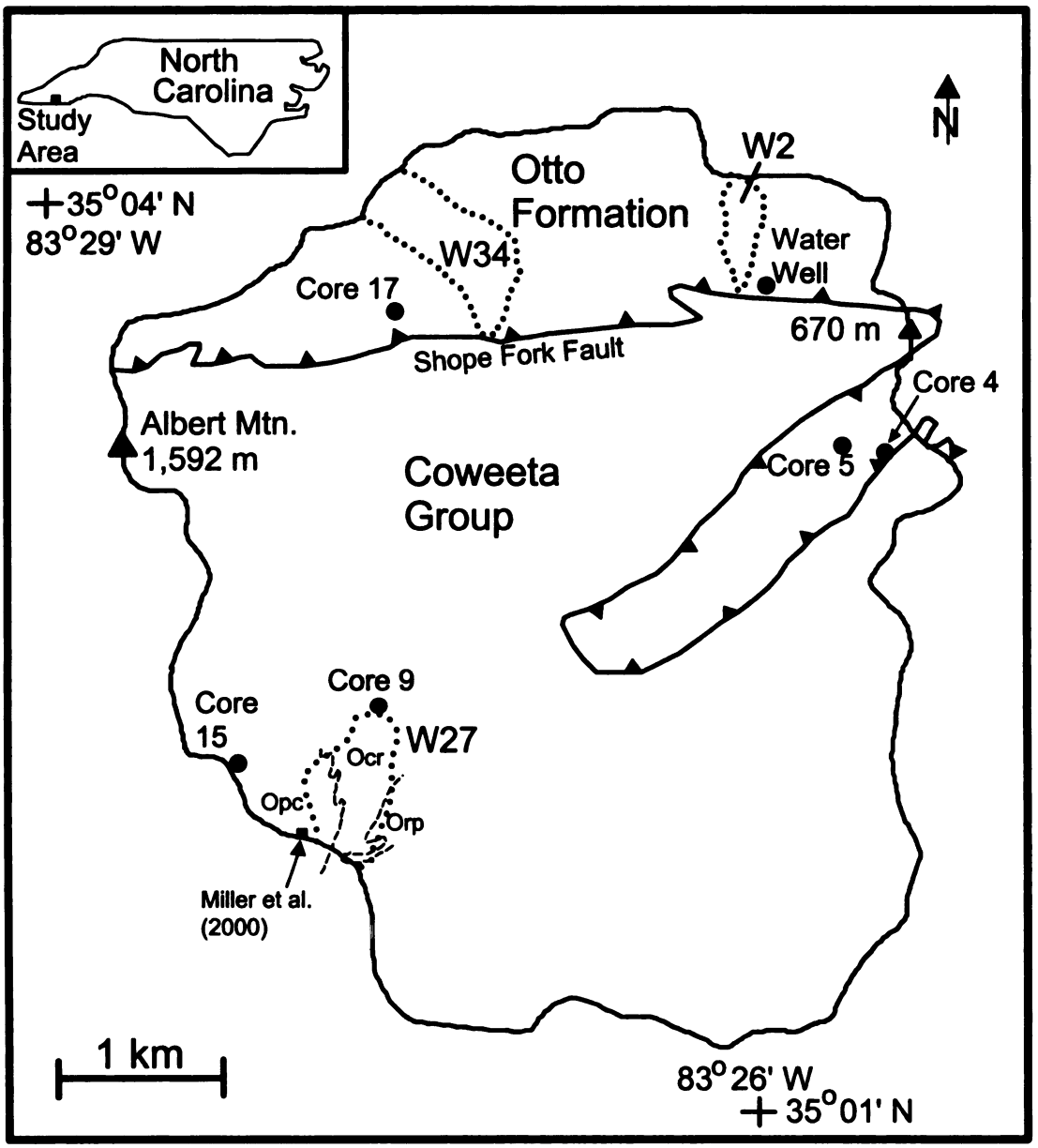

Figure 2. Map of Coweeta Hydrologic Laboratory showing watershed locations, bedrock geology, and core and water well locations. Bedrock units for W27 are: Opc=Persimmon Creek Gneiss, Ocr=Coleman River Formation, and Orp=Ridgepole Mountain Formation.

lithostratigraphic units. The basal Persimmon Creek Gneiss is dominantly a massive quartz diorite orthogneiss with interlayers of metasandstone, quartz-feldspar gneiss, and pelitic schist (Hatcher 1980). The overlying Coleman River Formation is characterized

by metasandstone and quartz-feldspar gneiss with lesser pelitic schist and calc-silicate quartzite. The Coleman River Formation is overlain by the Ridgepole Mountain Formation; a cleaner coarse biotite-garnet schist, pelitic schist, metaorthoquartzite, garnetiferous metasandstone, and muscovite-chlorite quartzite (Hatcher 1980). In contrast to the maturity of the Coweeta Group protolith sediments (e.g., arkoses and quartz arenites), the Otto Formation is derived from sedimentary protoliths of low compositional maturity (e.g., graywackes) and comprises a sequence of metasandstones which are feldspar- and biotite-rich, and are interlayered with mafic volcanics and aluminous schists (Hatcher 1988). The Otto Formation is predominantly biotite paragneiss and biotite schist (Hatcher 1980). The amphibolite facies regional metamorphism is associated with the Ordovician Taconic Orogeny when the Piedmont Terrane was probably accreted (or reattached) to Laurentia (Hatcher 1988, Miller et al. 2000). Coweeta Group and Otto Formation rocks are juxtaposed as a result of thrusting of the premetamorphic Shope Fork Fault (Hatcher 1988; Figure 2). The eastern Blue Ridge Province has, however, been affected by all the major tectonic events that shaped the southern Appalachian orogen (Miller et al. 2000). There is evidence of Early Cretaceous through Holocene compressive intraplate tectonism in the southern Appalachians with greatest uplifts in the Blue Ridge Mountains (Prowell and Owens 1987, Prowell 1989, Prowell and Obermeier 1991, Prowell and Christopher 1993, 2000).

Surficial Geology

Saprolite mantles the landscape at Coweeta, although bedrock occasionally may crop out, especially near ridge crests. The term saprolite was first used by Becker (1895), who referred to it as "a general name for thoroughly decomposed, earthy, but

untransported rock." Saprolite is an isovolumetric residuum of chemical weathering, in which the altered mineralogy, petrography, and structural fabric of the saprolite reflects the original crystalline rock types (Mills et al. 1987, Velbel 1990b). The average weathering profile (saprolite and soil) at Coweeta is approximately 6 m thick (Berry 1976, Yeakley et al. 1998). The saprolite at Coweeta is not an ancient, relict, deep weathering profile, as evidenced by their great thickness (up to 18 m; Ciampone 1995) despite residing on very steep slopes (average slope of approximately 45%/23°; Velbel 1984a, 1985a). The soil, mostly Ultisols and Inceptisols (Velbel 1988), comprises the uppermost 30 cm of the profile and is the friable material in which parent rock structure and fabric have been destroyed by mass-wasting, root throw, soil infauna, etc. (Velbel 1984a, 1985a). Ultisols reflect soil development on untransported, and therefore geomorphically older, residual parent material. In contrast, Inceptisols have developed on transported substrate (i.e., mass wasting materials or fluvially transported sediments), and subsequently reflect younger soils.

The weathering profile at Coweeta is developed on a heterogeneous metamorphic parent rock, and consequently is also heterogeneous (Figure 3). This heterogeneity greatly complicates the interpretation of weathering profile depth trends in mineralogy and major element bulk chemistry (Price and Velbel in review). Under such circumstances, differences in the regolith chemistry and mineralogy between samples may simply reflect variation in parent rock bulk chemistry and mineralogy, rather than the degree or extent to which the sample has been geochemically weathered.

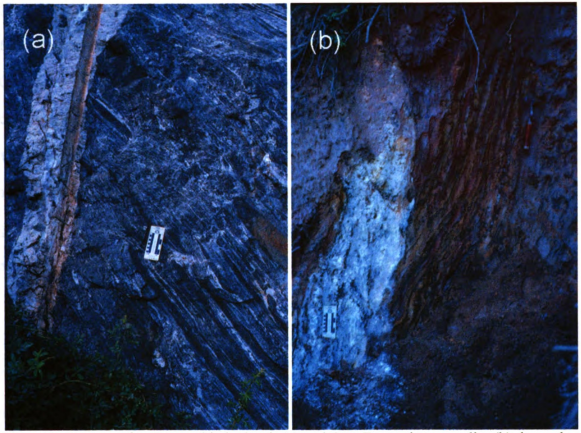

Figure 3. Images of metamorphic bedrock (a) and Otto Formation saprolite (b), in, and near Coweeta, showing the heterogeneity of both. Scale on cards is 10 cm. Bedrock image (a) was taken approximately 10 km northeast of Coweeta, and the saprolite image (b) was taken in a soil pit in W7; W7 is the next watershed to the west of W2. Note presence of quartz veins and alternating layers of felsic and mafic minerals in both images.

Climate and Hydrology

Coweeta Basin is a small topographic basin with appreciable climate variability along its length. Mean annual precipitation varies from 250 cm on the upper slopes to 170 cm at the lower elevations (Swank and Douglass 1977). Stream discharge from the areas of high precipitation is more than double that from areas of low precipitation (Grantham and Velbel 1988). Precipitation is distributed fairly evenly throughout the year with only a minor amount falling as snow (Swank and Douglass 1977, Swift et al. 1988). Overland flow on a well-forested watershed at Coweeta is essentially nonexistent

(Swank and Douglass 1977), as rain almost always soaks into the forest floor as fast as it falls (Helvey and Patric 1988). Velbel (1984a, 1985b) demonstrated that the streams at Coweeta are merely samples of subsurface water which have undergone no significant change after leaving the saprolite to enter the streams, except re-equilibration with atmospheric gases which would affect pH. Coweeta has a temperate climate with a mean annual temperature of 12.6°C (Swift et al. 1988). There is no evidence for alpine glaciation during the Pleistocene in or near Coweeta (Michalek 1969, Velbel 1984a, Mills et al. 1987).

An extensive ground water aquifer has not been shown to exist at Coweeta (Hewlett 1961). Instead, earlier studies of water in wells at Coweeta suggest variations in "cistern" storage. That is, nearly all stream water at Coweeta has passed through the soil mantle, with continuous base flow to perennial streams resulting from water draining from pore space in the unsaturated zone (Hewlett 1961, Hewlett and Hibbert 1963). Velbel (1984a, 1985a, and references therein) concisely summarizes these findings by stating that both base flow and storm flow in streams draining deeply-weathered, saprolite landscapes are sustained by water from depth in the saprolite.

Geomorphic History of the Southern Blue Ridge

Early interest in the geomorphology of the Appalachian Mountains and Plateaus was facilitated by William Morris Davis, who introduced the idea of the peneplain in the late nineteenth century (Mossa 1998). Until recently, however, Appalachian geomorphology has received little attention (Mills et al 1987, Gardner and Sevon 1989, Liebens and Schaetzl 1997). Even with a renewed interest in Appalachian

geomorphology, much of the recent research has focused on the northern and central Appalachians (e.g., Gardner and Sevon 1989).

Appalachian slopes and elevations are typically highest in the Blue Ridge (Mossa 1998), and are likely the result of the prevalence of debris slides and flows (Mills et al. 1987). Debris slides constitute the most common form of mass wasting in the Blue Ridge Province, with the absolute number of debris slides being greater in this province than in other parts of the Appalachians (Scott 1972, Mills et al. 1987). Hack (1980) determined denudation rates by debris slides to be 0.04 mm yr^{-1} for the southern Appalachians. However, a large percentage (50-95%) of the erosion of the upland slopes of the Blue Ridge occurs during high-magnitude, low-frequency events (Velbel 1985a, Mills et al. 1987, Eaton and McGeehin 1997, Daniels and Kochel 1998). That is, rare events of large magnitude are more important for long-term denudation in the Blue Ridge than in the Appalachian Plateau (Mills et al. 1987). Mass wasting processes in which slope failure occurs at the saprolite-bedrock interface (Grant 1988) result in eroded debris that contains all of the clay minerals that may exist in the Coweeta weathering profile. Any or all of these clay minerals may be transported to the depositional basin.

Periods of landscape instability in the Southern Blue Ridge have been have been assessed using the relative ages of debris flow deposits (Mills 1982, Liebens and Schaetzl 1997). Liebens and Schaetzl (1997) used four different relative-age indicators of soil developed on the debris flows, and demonstrated that the topographically highest debris flows are slightly older than those at lower elevations. Furthermore, the similarity of ages between three different localities suggests that an external factor, likely extreme precipitation, accounts for the formation of the debris flows at approximately the same

time in the geologic past (Liebens and Schaetzl 1997). However, the general difference in age of sites within relative proximity of each other shows that intrinsic factors affect the formation of debris flows locally (Liebens and Schaetzl 1997).

It has been suggested that formation of debris flows in the Southern Blue Ridge is associated with periods of post-glacial climate change (Mills 1981, 1982, 1983, Kochel and Johnson 1984). Michalek (1969) argued that glacial climates provided optimum conditions for growth of foot-slope fans. However, such a conclusion cannot be accepted with certainty (Mills et al 1987). Mills et al. (1987) states that the building of most foot-slope fans probably spans at least several Pleistocene stadials and interstadials, if not glaciations and interglaciations. Therefore, although Michalek (1969) suggested that fan sediment is derived by solifluction, his suggestion that fans were related to former periglacial climates may be at least partly correct (Mills et al. 1987).

Recurrence intervals for debris slides of the Blue Ridge have been proposed by several authors. Neary and Swift (1984) suggest intervals of between 50 and 200 years for smaller events, while other researchers propose intervals of 1,000 to 6,000 years for the largest slides (Thompson 1969, Kochel and Johnson 1984, Swift et al. 1988).

Although no evidence for permafrost or alpine glaciation has been found south of the glacial border, there is evidence of periglacial activity in the Appalachian and Interior Highlands (Michalek 1969, Mills 1981, Velbel 1984a, Clark and Ciolkosz 1988). Velbel (1984a) analyzed valley form at Coweeta, and found that the valleys are distinctly V-shaped at higher elevations, with lower elevation valleys exhibiting abrupt transitions from valley walls to flat bottoms. These observations indicate colluvial channel material rather than a U-shape valley (Velbel 1984a). In summary, there is no evidence for alpine

glaciation at Coweeta, and colluvial material is the product of mass wasting events. However, the influence(s) and timing of mass wasting events in the southeastern Blue Ridge are still enigmatic.

Background

Geomorphic Considerations

Source areas for terrigenous clay sediment may be classified along a continuum between two end-members (Stallard and Edmond 1983, Johnsson 1992): "Weathering-limited" source areas are characterized by steep slopes where transport processes are more rapid than the weathering processes generating the clay, while "transport-limited" landscapes have gentle slopes where the maximum weathering rate exceeds the ability of transport processes to remove sediment. Both end-members pose concerns for paleoclimatologists trying to use clay mineral assemblages from mudrocks and sediments to interpret source area climate changes through geologic time. These concerns arise because clay detritus eroded from a transport-limited landscape may originate from paleosols, and not reflect the climatic conditions during erosion and transport of the clay to the depositional basin (Thiry 2000, Migoń and Lidmar-Bergström 2002). A transport-limited environment may require several million years to develop a deep mature profile, and under such circumstances only long-term (1 or 2 Ma) paleoclimatic changes may be recorded in the clay mineral assemblages of the sedimentary deposits (Thiry 2000). Weathering-limited landscapes also present problems for paleoclimatic interpretations, because the regolith present may not be retained for adequate duration to permit equilibrium of clay mineral assemblages with climate. The Coweeta landscape may be interpreted to be intermediate between weathering- and transport-limited landscapes. The

presence of a modern (100 Ky mean age; Velbel 1985a) saprolite on such steep slopes at Coweeta favors this interpretation. Furthermore, the consistency between the saprolitization rate (38 m Ma^{-1}; Velbel 1984a, 1985a) and the landscape reduction rate (40 m Ma^{-1}; Hack 1980) supports the interpretation that the regolith at Coweeta is in approximately steady-state (constant thickness; Velbel 1984a, 1985a).

Coweeta Hydrologic Laboratory provides a unique opportunity to evaluate the temporal resolution of clay mineral assemblages in paleoclimatic reconstructions, as Coweeta is characterized by relatively high rainfall (~200 cm $year^{-1}$), substantial erosion rates (0.038 mm yr^{-1}), a thick (6 m) modern regolith, and extensive hydrochemical data for use in mass balance determinations of clay genesis rates (Berry 1976, Velbel 1985a, Yeakley et al. 1998). The long-term average solute-flux data for Coweeta watersheds are based on weekly measurements and constitute one of the longest running catchment flux records in North America (the published period of record is 20 years; Swank and Waide 1988, Velbel 1993a). The weathering profiles (saprolite and soil) at Coweeta are modern, as evidenced by their great thickness (up to 18 m; Ciampone 1995) despite residing on very steep slopes (average slope of approximately 45%/23°; Velbel 1984a, 1985a).

Epidote Group Mineral Weathering

The weathering of epidote is controversial. Epidote is a common constituent of the heavy mineral fraction of clastic sediments (e.g., Frye et al. 1960, Willman et al. 1963, Carver 1986, Friis 1974, Poppe et al. 1995, Dill 1995, Logan and Dyer 1996, Uddin and Lundberg 1998, Khan and Kim 1998, Cocker 1998) and the residual mineral fraction of soils (e.g., Suwa et al., 1958, Gupta and Talwar 1997, Ezzaïm et al. 1999). Epidote has been reported to have a comparable field weatherability to that of quartz

(Allen and Hajek 1995, their Table 4-1) and zircon (Lång 2000). In contrast, epidote has been reported to dissolve relatively fast (Sverdrup 1990), and included with plagioclase, K-feldspar, hornblende, and apatite, as being the major mineralogic controls for calculation of field weathering rates using the PROFILE model (Warfvinge and Sverdrup 1992, Sverdrup and Warfvinge 1993, 1995, and references contained therein). These authors routinely, perhaps injudiciously, include epidote in field weathering rate calculations, but do so without any mineralogic observations to support its occurrence in the parent material or its extent of weathering. Sverdrup and Warfvinge (1995) state that it is their experience that epidote is present in very many locations, but almost always in small amounts. It is noteworthy that Warfvinge and Sverdrup (1992) and Sverdrup and Warfvinge (1993, 1995) do not find biotite to be of importance when calculating field weathering rates, despite the ubiquity of literature outlining the significance and importance of biotite weathering (e.g., Gilkes and Suddhiprakarn 1979a, 1979b, Rebertus et al. 1986, Ahn and Peacor 1987, Banfield and Eggleton 1988, Dong et al. 1998, Murphy et al. 1998, Jolicoeur et al. 2000, Jacobson et al. 2003). However, evidence favoring the incorporation of epidote weathering into models of weathering has been reported from selected localities. Schroeder et al. (2000) reports epidote to be completely dissolved in the A horizon of a Georgia Piedmont soil, and Braun and Pagel (1994) find epidote to be destroyed within the first stages of syenite weathering in southwest Cameroon.

Allanite has been found to be highly weatherable in Coweeta. Epidote is relatively unweatherable, and persists into the solum with only minor evidence of weathering. However, as will be demonstrated, for the lithostratigraphic units at Coweeta

epidote and allanite are typically identical petrographically, and are only distinguished by trace element analytical analyses.

Watershed Mass Balance

Geochemical mass balance (input-output budgeting) is commonly used to calculate weathering rates, and is a subject with a long history in the geochemical literature (e.g., Garrels 1967, Garrels and Mackenzie 1967, Cleaves et al. 1970, 1974, Clayton 1979, 1986, Bricker et al. 1983, Pačes 1983, 1986, Katz et al. 1985, Katz 1989, Velbel 1985a, 1986a, 1992, 1995, Drever and Hurcomb 1986, Taylor and Velbel 1991, Finley and Drever 1997, Furman et al. 1998, Bowser and Jones 2002 and references therein). These authors employ the "balance sheet" approach, which is a system of simultaneous linear equations with constant coefficients that represent the steady-state input-output behavior of the modeled systems. The mathematical treatment of geochemical mass balances in small watersheds is conceptually identical to the mathematics of single reservoirs in global geochemical cycles (Velbel 1986a, Taylor and Velbel 1991), and is considered the most reliable means for making quantitative determinations of elemental transfers in the Earth's surface environment (Clayton 1979).

To date, all of the studies that have employed mass balance calculations in watersheds underlain by silicate bedrock address consumption of atmospheric inputs (CO_2 and acid rain) (e.g., Katz et al. 1985, Bricker 1986, White and Blum 1995b, Likens and Bormann 1995, Drever 1997b, Taylor et al. 2000), dissolution of primary rock-forming minerals (e.g., Cleaves et al. 1970, 1974, Clayton 1979, Afifi and Bricker 1983, Velbel 1984a, 1985a, 1993a, 1995, Furman et al. 1998, Bowser and Jones 2002), or generation of stream solutes (e.g., Berner and Berner 1987, Velbel 1993a, O'Brien et al.

1997). Numerous watershed studies using mass balance methods provide preliminary and often speculative discussions on clay mineral genesis (e.g., Cleaves et al. 1970, 1974, Velbel 1985a, Finley and Drever 1997), but none provide detailed and rigorous evaluations of the solid weathering products. Watersheds represent an important resource in discerning the interconnection between climate and chemical weathering, and can provide important information on chemical weathering under different climatic conditions existing today (White and Blum 1995b).

The Calcium Problem

Bowser and Jones (1993) introduced the term "calcium problem" to refer to the observation that solute analyses of many streams draining small watersheds underlain by crystalline silicate bedrock often contain Ca/Na ratios higher than can be predicted by congruent dissolution of plagioclase feldspar. In silicate-dominated natural hydrologic systems, plagioclase dissolution is the most important weathering reaction (Bowser and Jones 1993, 2002; Drever 1997b, Jacobson et al. 2003), and the calcium problem has become an essential part of watershed mass balance studies (Drever 1997b).

The calcium problem was recognized as part of the pioneering mass balance work of Garrels and Mackenzie (1967) in their study of perennial springs in the Sierra Nevada Mountains. They attributed the excess Ca to the dissolution of calcite, but did not have mineralogic observations to support such a conclusion. Furthermore, the calcium problem has been noted in watersheds worldwide (e.g., Pačes 1986, Stauffer 1990, Turk and Spahr 1991, Drever 1997b), where calcite is demonstrably absent, such as Trout Lake, Wisconsin (Kenoyer and Bowser 1992, Bowser and Jones 2002), and appears in

the mass balance modeling of all the watersheds developed on plutonic rocks studied by Bowser and Jones (2002).

Clayton et al. (1979) and Clayton (1986, 1988) explained the calcium problem they encountered in the Silver Creek watershed of Idaho by preferential weathering of calcic cores in zoned plagioclase grains. However, they were unable to explain the non-stoichiometric Ca/Na ratio in stream water by other mechanisms, such as cation exchange or preferential uptake of Na by biomass.

Drever and Hurcomb (1986) reported plagioclase stoichiometric Ca/Na ratios between 0.39 (An_{28}) and 1.22 (An_{55}) for the South Cascade Glacier area of Washington State. However, the Ca/Na ratios in Cascade Lake of their study area are much higher, so much so that the stoichiometric weathering of plagioclase could not be the exclusive source of Ca in the water. Drever and Hurcomb (1986) found calcite in the catchment as veins deposits, occasional marble bands, and as a superficial subglacial deposit associated with regelation processes under glacial ice.

In a more controversial study, Mast et al. (1990) and Mast (1992) invoked calcite weathering as a source of the excess Ca at Loch Vale, Colorado, despite an absence of microscopically visible calcite. However, cathodoluminescence microscopy did reveal very fine-grained calcite in the bedrock in hydrothermally altered zones and along grain boundaries. Mast et al. (1990) argued that deglaciation had occurred relatively recently, with sufficiently high rates of physical erosion to permit fresh rock surfaces to remain in contact with meteoric water. Otherwise, accessible calcite would become depleted over time and would no longer serve as a significant source of Ca. However, Romero (1989) explained the excess Ca in the stream water at Loch Vale by the weathering of mafic

inclusions in the bedrock. Based on what is currently known, either explanation is equally feasible (Drever 1997b).

Several explanations are commonly offered to explain the calcium problem (Drever 1997b, Bowser and Jones 2002). These are: (1) there is an additional, unrecognized, source of Ca; (2) there is an unidentified Na sink; (3) plagioclase dissolution is incongruent with respect to Ca and Na; or (4) Ca is released from cation exchange sites.

Additional sources of Ca may be Ca-rich silicate minerals that typically occur in minor to trace abundances (e.g., epidote group minerals), minerals that occur in relatively large abundances but contain lesser Ca (e.g., amphiboles or pyroxenes), or, as previously discussed, calcite. Biomass, too, may be a source of Ca, however such sources are usually limited to surficial recharge (Bowser and Jones 2002). Furthermore, Ca could be derived from a net decrease in biomass, but watersheds showing a net decrease in biomass are relatively rare. Epidote weathering is difficult to support, as epidote is typically reported as being relatively unweatherable (e.g., Allen and Hajek 1995) and a common constituent of heavy mineral assemblages in sediments (e.g., Uddin and Lundberg 1998, Khan and Kim 1998, Cocker 1998). However, Warfvinge and Sverdrup (1992) and Sverdrup and Warfvinge (1993, 1995) routinely invoked epidote weathering when applying PROFILE to watershed stream solutes. The weathering of Ca-bearing primary rock forming minerals such as pyroxenes and amphiboles is a possibility in watershed studies, but should be assessed for each watershed individually (Drever 1997b). Drever (1997b) also points out that the weathering reactions associated with Ca-

bearing mafic phases are difficult to constrain by mass balance equations because the secondary products are often smectites, whose compositions are poorly known.

Viers et al. (2000) found that the Ca/Na ratios for rivers of the Nyong basin in Cameroon plotted between the silicate and carbonate bedrock end-members, where the bedrock of the area is silicate. However, they would not invoke disseminated calcite weathering because the weathering surface is old and should be depleted in calcite (White et al. 1999b). Instead, weathering of minerals containing abundant Ca, Sr, and Mg was invoked, with the relatively low pH of the river waters (4.5-6.5) creating favorable conditions for preferential weathering of such minerals (Viers et al. 2000).

The possibility of calcite weathering to explain the calcium problem is worth special discussion. Drever (1997b) argues that, on the scale of a watershed, calcite will always be present initially in granitic rocks. However, even if present initially in the rock, calcite will be rapidly depleted as the rock is exposed to meteoric water (Bowser and Jones 2002). The sustainability of weatherable calcite will vary from watershed to watershed, and will be a function of the rate of physical erosion (Drever 1997b).

The presence of a Na sink (Na-bearing weathering product and Na conservation) during weathering is very difficult to support, although some researchers have invoked a Na-montmorillonite weathering product (e.g., Furman et al. 1998), but do so without analytical data to support its presence. With respect to cation exchange, in natural dilute water systems alkaline earth elements and K will be favored over Na (Appelo and Postma 1996, Drever 1997b). However, cation exchange is only a concern for mass balance studies if there is mixing of waters of different chemistries, or if water chemistry changes

with time (Drever 1997b, Bowser and Jones 2002). At the present time there is no support in the literature for proposing conservation of Na in the weathering profile.

Plagioclase dissolution has been suggested to be incongruent with respect to Ca and Na. The more anorthitic the plagioclase, the greater the weathering rate, whether at the landscape scale or at the scale of a zoned grain (e.g., Clayton et al. 1979, Clayton 1986, Clayton 1988, Blum 1994, White et al. 2001). Clayton et al. (1979) and Clayton (1986, 1988) explained the calcium problem they encountered in the Silver Creek watershed of Idaho by preferential weathering of a calcic core in a zoned plagioclase grain. However, it must be noted that the selective stoichiometric weathering of calcic portions of zoned plagioclase grains cannot yield waters with Ca/Na ratios higher than that of the most calcic portion of the grain (Clayton 1986, 1988, Drever 1997b, Bowser and Jones 2002). Bowser and Jones (2002) also pointed out that the Ca/Na ratios can be reduced or reversed by solute cation build-up and the formation of a more relatively aluminum-rich weathering product such as kaolinite.

Calcium may be released from cation exchange sites. Clayton (1986) found that Ca is preferentially adsorbed in Silver Creek soils by between one and two orders of magnitude over Na. Furthermore, and as stated previously, cation exchange is only a concern for mass balance studies if there is mixing of waters of different chemistries or a change in water chemistry over time (Drever 1997b, Bowser and Jones 2002). Drever (1997b) does acknowledge that Ca may be preferentially released from cation exchange sites if there are anthropogenic inputs of acidity. However, the calcium problem has been reported in regions of the world where acid precipitation is minor or nonexistent.

Previous Work

Allanite Weathering

Perhaps the earliest formal description of the weathering of allanite is that of Watson (1917). He examined an extensive collection of fresh and weathered allanite samples collected from pegmatites in the Atlantic States. All of Watson's (1917) weathered allanite samples contained a "...usual reddish brown alteration product from weathering." Watson (1917) was able to conclude that the reddish brown weathered product of allanite was composed of varying abundances of Si, Al, Fe^{3+}, Ce, and H_2O. Furthermore, it was noted that in several cases, all of the rare earth elements (except Ce) present in the fresh mineral were completely lost from the weathering crust (Watson 1917). Hata (1939) made identical conclusions when studying allanite from the granite region of the Abukama Range, Japan, and also determined that allanite weathering started with the dissolution of rare earth elements. Variations in the REE concentration in the allanite did not seem to have any influence on the weatherability of allanite (Hata 1939).

In his classic work on chemical weathering, Goldich (1938) reported that the allanite found in the Morton Gneiss of Minnesota was one of the least stable minerals during weathering, and categorized it with the other relatively weatherable minerals plagioclase, epidote, hornblende, titanite, and apatite. Similarly, Ramspott (1965) reports that accessory allanite weathers very rapidly in the Elberton Granite of Georgia, although epidote rims on allanite are not discernibly weathered at the thin section scale. In the Elberton Granite allanite is present as both unaltered single grains, as well as colorless, nearly isotropic, metamict grains (Ramspott 1965).

Delvigne (1998; his Plates 231 and 232, p. 185) provides a thin section photomicrograph of a metamict allanite that has been completely weathered and pseudomorphically replaced by poorly crystalline saponite. The pseudomorph is irregularly surrounded by an incomplete rim of skeletal primary epidote. Delvigne (1998) also notes that the only other mineral observed weathering in same thin section as the allanite is biotite, which is only partially weathered to saponite.

The release of REE during rapid weathering of allanite is also reported in more recent literature (e.g., Meintzer 1981, Banfield and Eggleton 1989, Braun et al. 1993, Braun and Pagel 1994, Harlavan and Erel 2002). At least 70% of the light REE in a rock may be contained in the accessory minerals allanite, apatite, titanite, and epidote (Gromet and Silver 1983, Braun et al. 1993, Braun and Pagel 1994); Hermann (2002) found that over 90% of bulk rock light REE may be incorporated into accessory allanite.

Weathering Studies at the Coweeta Hydrologic Laboratory

The pioneering efforts in characterizing the weathering profiles at Coweeta were those of Berry (1976, 1977). He is responsible for acquiring the cores (Figure 2) that have been collected, generating bulk chemistry data for the bedrock and saprolite, and providing initial weathering reactions from petrographic observations. Berry's core cuttings and data have been extensively used in studies of the saprolite at Coweeta (e.g., Velbel 1984a, 1985a, Ciampone 1995, Price and Velbel in review). Major element oxide analyses of saprolite and bedrock aggregate cuttings sampled during installation of the potable water well at Coweeta (Figure 2) have also been completed by Ciampone (1995). The bulk chemical data generated by Berry (1976) and Ciampone (1995) are utilized in this study.

After Berry's (1976, 1977) pioneering work, most research on weathering at Coweeta is that of Velbel (e.g., 1983, 1984a,b, 1985a,b, 1986a,b, 1987, 1988, 1989a,b, 1990a,b 1992, 1993a,b,c,d, 1995) and his students (e.g., Grantham and Velbel 1988, Taylor 1988, Taylor and Velbel 1991, Bryan 1994, Velbel et al. 1996, Price and Velbel in review). Velbel's primary research at Coweeta addressed the weathering of primary minerals, specifically garnet (Velbel 1984b, 1993b) and plagioclase (Velbel 1983, 1986b, 1990a). The weathering rates of these minerals (and also biotite) at Coweeta have been calculated using watershed mass balance methods (e.g., Velbel 1984a, 1985a,b, 1986a,b, 1988, 1989, 1990a, 1992, 1993a,c, Taylor 1988, Taylor and Velbel 1991). Such kinetic calculations have permitted estimation of the mean age of the saprolite (approximately 100 Ky) and the rate of saprolitization (0.038 mm yr^{-1}) (Velbel 1984a, 1985a, 1988). In addition, mass balance calculations using watersheds at Coweeta have also been used by Velbel (1993a) to determine the Arrhenius activation energy of natural feldspar weathering. Additional contributions made by Velbel to the understanding of Coweeta weathering have been with regards to the role of biomass in mass balance calculations (Taylor 1988, Taylor and Velbel 1991, Velbel 1995), and constraining factors that control the composition of sand-sized detrital sediment in streams draining Coweeta watersheds (Grantham and Velbel 1988).

The only works to date which studied the Coweeta clay mineralogy are by Velbel (1984a, 1985b), Taylor (1988), Bryan (1994), and Ciampone (1995). Velbel (1984a, 1985b) has found hydroxy-interlayered vermiculite (HIV), expandable (smectitic) material, hydrobiotite, kaolinite, and gibbsite at Coweeta, and has addressed the hydrologic and lithologic controls on kaolinite-gibbsite clay mineralogy of the

weathering profiles. The kaolinite/gibbsite ratio is higher in saprolite developed on the more chemically reactive Otto Formation, indicating a lithologic influence on clay mineralogy. Climate also influences clay mineralogy, as the watersheds in the wetter western part of the basin have a lower kaolinite/gibbsite ratio than do drier watersheds further east on similar rock types (Velbel 1984a). The clay minerals specific to W2 have been identified as kaolinite, gibbsite, hydrobiotite, HIV, and expandable material. Bryan (1994) focused only on the iron oxides and iron oxyhydroxides in the weathering profile, and found that factors such as soil maturity, precipitation, lithologic variations, and temperature control hematite and goethite proportions in soils. Garnet and magnetite appear to be the only primary minerals weathering to hematite, with garnet more commonly altering to goethite (Bryan 1994). Saprolite cuttings collected from the water well (Figure 2) do not display a classic clay mineral weathering profile (Ciampone et al. 1992); that is, the expected mature gibbsitic soil at the surface, underlain by an intermediate layer composed of kaolinite and hydrobiotite, and immature basal saprolite at greater depth characterized by ubiquitous plagioclase and biotite are not observed. Ciampone (1995) suggests that this non-systematic profile may reflect variations in bulk composition of the parent rock and/or variations in the composition of ground water.

Clay Mineralogy of the Southern Blue Ridge Province

The clay mineralogy of southern Blue Ridge weathering profiles outside of Coweeta are generally similar to those of Coweeta, with a few exceptions. In western North Carolina, Loferski (1981) found that rock type did not appear to influence the clay mineralogy of the overlying saprolite, and that kaolin abundance is independent of depth within the weathering profile. Norfleet and Smith (1989) and Norfleet et al. (1989, 1993)

found that gibbsite abundance increased with a decrease in kaolinite, with increasing slope, elevation, and rainfall. These same authors also determined that vertical profiles often have gibbsite initially increasing with depth to a maximum abundance in argillic horizons, and then starting to decrease. Gibbsite was also found in the nonclay fraction of each pedon, suggesting that it may have formed alteromorphically (terminology of Delvigne 1998) after feldspars at the weathering front. Blue Ridge kaolinite is often found to be a product of biotite weathering (Norfleet and Smith 1989, Graham et al. 1989a,b), and HIV may dominate the soil horizons and decrease with depth (Norfleet and Smith 1989). Graham et al. (1989a,b) studied the weathering of iron-bearing minerals in soil and saprolite developed on mica gneiss and schist of the North Carolina Blue Ridge Mountains and found ubiquitous gibbsite in both the saprolite and soil. However, in colluvial soil horizons the abundance of gibbsite was greatly reduced relative to the underlying saprolite (Graham et al. 1989b, Graham and Buol 1990) where kaolinite dominates (Graham and Buol 1990). Graham and Buol (1990) suggest that Al is leached from the acidic surface horizons and then precipitates as gibbsite in the higher-pH environments of the saprolite. Most Blue Ridge clay researchers agree that gibbsite is a weathering product of plagioclase (e.g., Norfleet and Smith 1989, Stolt et al. 1991, Norfleet et al. (1993), although traces of gibbsite were identified in weathered biotite (Graham et al. 1989a). More recently, Jolicoeur et al. (2000) described the pseudomorphic replacement of mica by kaolinite, halloysite, and gibbsite, with or without a vermiculite intermediary. Jolicoeur et al. (2000) suggested that these multimineralic assemblages reflect the control of microenvironments on secondary clays, rather than the anti-gibbsite effect (Jackson 1963, Losche et al. 1970). The anti-gibbsite effect was

initially described by Jackson (1963), who found that the intercalation of expanded 2:1 layer silicates with aluminum hydroxide interlayers in soils tends to inhibit the formation of free gibbsite.

Clay Mineralogy of the Southern Piedmont Province

Similar clay mineral assemblages are also reported for regolith of the southern Piedmont. In a buried weathering profile in the South Carolina Piedmont, Gardner et al. (1978, 1981) identified only kaolinite in a granite saprolite, and smectite and kaolinite in a diabase saprolite. The latter authors concluded that the oxidizing conditions in the upper portion of the weathering profile favored the formation of Fe-rich smectite over kaolinite, while deeper in the profile reducing conditions favored the formation of kaolinite over Al-rich smectite. Calvert et al. (1980a,b) reported muscovite altering at the surface to a randomly mixed-layer mica-vermiculite and kaolinite in a rock-saprolite-soil sequence developed on a granitic gneiss from the North Carolina Piedmont. These authors believed gibbsite to have initially formed near the weathering front, followed by resilication to a kaolin mineral. The increase of gibbsite near the surface of the profile is reported to be the result of a decrease in weatherable Si-rich minerals, and probable biocycling of Al. Calvert et al. (1980b) further reported that amorphous aluminosilicates produced by the rapid weathering of feldspar resilicate to tubular halloysite, and the gibbsite resilicates (often pseudomorphously) to tabular halloysite. The halloysite of either form then recrystallizes to kaolinite via a randomly interstratified transition phase (Calvert et al. 1980b).

Pavich (1989) determined that HIV is the dominant clay phase in the soil of the Piedmont regolith. HIV results from the weathering of muscovite, and is absent in the

saprolite (Pavich 1989). This same author states that kaolinite is the dominant clay phase in the saprolite, and is the product of plagioclase weathering. In a study of weathering mantles developed on quartzofeldspathic bedrock of the Virginia Piedmont, Pavich et al. (1989) found vermiculite, kaolinite, and halloysite to be ubiquitous, while gibbsite was only present in profiles developed on metapelites. Vermiculite was typically dioctahedral, suggesting parent muscovite, and smectite was only identified in saprolite developed on granite (Pavich et al. 1989). Pedogenic kaolinite found in saprolite of the Virginia Piedmont Province was analyzed for oxygen isotope ratios in order to estimate the ambient climatic conditions during formation of the saprolite (Elliott et al. 1995, 1997). These authors determined that the kaolinite formed under a cooler climatic regime, possibly during or shortly after Pleistocene glaciation. Such an interpretation is consistent with the age of the saprolite (<1 Ma) determined using ^{10}Be dating methods. For a weathering profile developed on meta-gabbro in the Georgia Piedmont, Schroeder et al. (2000) found that HIV and gibbsite formed as tertiary phases in the soil A horizon.

Schroeder et al. (2001) performed ^{14}C dating of carbon bound in gibbsite from a weathering profile developed on granite in the Georgia Piedmont. These authors found that ^{14}C-gibbsite model ages of gibbsite in the saprolite average approximately 8,000 years, while soil horizon gibbsite yields ages which range from 2,100 to 4,200 years. These data suggest that gibbsite undergoes significant recrystallization as the weathering front propagates into the landscape (Schroeder et al. 2001).

Clay Genesis Rates

Barshad (1955, 1957) is likely the earliest researcher to provide an estimate of total clay formation rates in soils. Based on bulk chemical analyses of the whole soil and

the amount of clay in the soil, Barshad (1957) found that total clay formation in soils was enhanced by poor drainage (influenced by topography), grass-type vegetation (as opposed to tree-type), and finer grained and more basic bedrock. Total clay formation rates are reported as ranging from 0.01 to 0.02 g kg^{-1} yr^{-1} (Barshad 1957). For the Maryland Piedmont, Cleaves et al. (1970) used mass balance methods to calculate the amount of clay minerals (vermiculite, kaolinite, and gibbsite) formed in soil and saprolite (in kilomoles). Based on their data the following clay mineral formation rates may be calculated: gibbsite is forming at a rate of 60 moles ha^{-1} $year^{-1}$, kaolinite at a rate of 77 moles ha^{-1} yr^{-1}, and vermiculite at 8 mol ha^{-1} yr^{-1}.

Using soil sequences ranging in age from less than 100 years to about 5,500 years in the Hudson Bay area, Canada, Protz et al. (1984, 1988; data summarized by Righi and Meunier 1995) combined quantitative XRD analyses with soil age, permitting determination of a rate of clay mineral formation. They found that the clay mineralogy of C horizons in all soils was practically the same, but changed with time in the A horizons. X-ray diffraction analysis indicated a decrease in chlorite and mica contents with increasing age, and an increase in vermiculite content which, after 4,500 years, becomes the only clay mineral present with the exception of a small amount of smectite (Protz et al. 1984). Their XRD data for the Hudson Bay coastal area suggest a formation rate of vermiculite in the clay size fraction of soil of approximately 0.06 g kg^{-1} yr^{-1}. In a similar study of a soil chronosequence (developed on nearly identical parent material as the Hudson Bay study) from the southern James Bay area, Canada, Protz et al. (1988) found that vermiculite formed at a rate twice as fast as that of the cooler/drier Hudson Bay area.

They also found that both chlorite and mica weathered rapidly to vermiculite and ultimately to smectite.

Lowe (1986) provides an excellent literature review, results of his research on weathered New Zealand tephras, and summary on the factors that control rates of clay genesis during weathering of airfall tephras. Based on his work, he found that temperature and duration of weathering were subordinate factors to mineralogical and chemical composition of the parent rock, and macro- and microenvironmental factors in governing clay genesis and weathering rates. Environmental factors that are most important are those that affect the concentration of SiO_2 in solution, and the movement and availability of Al; specifically, pH and drainage (a function of precipitation/climate). Total clay formation rates for the tephras of New Zealand when calculated using percent clay and age of weathering profile range from approximately 0.001 to 0.1 g kg^{-1} yr^{-1}.

Clay Mineral Assemblages and Climate

Interest in relating climate to clays in mudrocks and sediments was primarily pioneered by the French (e.g., Millot 1964, Pédro 1968, Tardy et al. 1973, Righi and Meunier 1995), and furthered by researchers who found a correlation between clay minerals in ocean sediments and contemporary climates on the continents (i.e., latitude) (e.g., Biscaye 1965, Griffin et al. 1968, Rateev et al. 1969, Windom 1976, Gibbs 1977). These authors were also able to distinguish authigenic from terrigenous clay minerals, further strengthening the link between climate and clay mineral assemblages. More recent studies have supported the relationship between clay minerals and continental climate in both terrestrial and marine basins, using complimentary data such as isotopes, detrital sand and silt mineralogy, and biostratigraphic changes to support the clay mineral

data (e.g., Robert and Kennett 1992, Gibson et al. 1993, Menking 1997, Finkelstein et al. 1998, Yuretich et al. 1999, Price et al. 2000, Tabor et al. 2002; see also Table 2).

Table 2. Summary of studies which relate clay minerals in sediments and mudrocks to source area climate.

	Temperature		Moisture		
Clay Mineral	**Warm**	**Cool**	**Humid**	**Arid**	**Alternating wet and dry seasons**
Gibbsite	Q, V	U	Q, U, V		
Kaolinite	A, F, G, I, L, M, N, Q, R, W, X, Y, Z, AB, AD, AE, AF, AH		B, C, F, G, I, J, M, N, P, Q, R, W, X, Y, Z, AA, AB, AD, AE, AF, AH		
Chlorite	E	A, D, G, H, L, Q	E	G	
Vermiculite	AG	N, W		C	
Illite	AC, AH	A, D, G, H, L, O, T, W, Y, AB, AH	AC	C, G, O, Y, AH	
Smectite	E, G, H, I, K, O, S, W, Z, AA, AB, AE, AF, AH	R	C, E, H, S, Z, AB	D, J, N, P, R, X, Y, AD	G, I, K, O, W, AA, AE, AF, AH
Illite-smectite	A	F, W	G	B, F	
Chlorite-Smectite		G	G		
Palygorskite	I, W			C, I, J, W, AA, AH	
Sepiolite				C, I, AH	

A=Yuretich et al. (1999)
B=Finkelstein et al. (1998)
C=El-Younsy et al. (1998)
D=Menking (1997)
E=Wagner et al. (1997)
F=Gibson et al. (1993)
G=Robert and Kennett (1992)
H=Ehrmann et al. (1992)
I=Robert and Chamley (1991)
J=Hallam et al. (1991)
K=DeConinck and Bernoulli (1991)
L=Chamley (1989)
M=Kronberg et al. (1986)
N=Pe-Piper and Piper (1985)
O=Chamley & Debrabant (1984)
P=Stoffers and Hecky (1978)
Q=Biscaye (1965)
R=Price et al. (2000)
S=Ehrmann (1998)
T=Hartmann et al. (1999)
U=Norfleet (1993)
V=Hill et al. (2000)
W=Righi and Meunier (1995)
X=Kalindekafe et al. (1996)
Y=Net et al. (2002)
Z=Hiscott (1984)
AA=Chamley and Müller (1991)
AB=Debrabant et al. (1993)
AC=Clayton et al. (1999)
AD=Griffin (1962)
AE=Robert and Kennett (1994)
AF=Tabor et al. (2002)
AG=Protz et al. (1988)
AH=John et al. (2003)

Despite the strong link between continental [paleo]climate and clay mineralogy in the literature, several authors warn that such a link should be made only with caution (e.g., Gibbs 1977, Singer 1980, 1984, Gerrard 1994, Power and Smith, 1994, Curtis 1990, Thiry 2000, Migoń and Lidmar-Bergström 2002). Gibbs (1977) determined that differential settling processes of clay minerals leads to deposition of illite, chlorite, and kaolinite in proximal areas of the basin and transport of smectite to more distal areas. Curtis (1990) found that the sediments delivered to major basins today do not reflect global soil distribution patterns, but rather local topography which strongly influences both the rate and products of chemical weathering and erosion. Potter et al. (1975) studied the alluvial muds of the Mississippi River basin and found that their clay mineralogy reflected source rocks rather than either climate or relief. These findings are in contrast with Barshad (1966), who found that frequency distribution patterns of source area clay minerals is a function of precipitation and not the nature of the parent material, with the exception of illite. Additional concerns include the likely requirement of a tropical climate to produce deep weathering profiles (Thiry 2000) and the several million years it may take to develop a deep mature profile (Weaver 1989, Thiry 2000). In a study of the clay mineralogy of suspended river sediments of Puerto Rico, Ehlmann (1968) found an absence of gibbsite, despite ubiquitous gibbsite in the weathering profiles of the watershed. The loss of gibbsite in the river sediments is attributed to gibbsite converting in the stream waters to allophane or poorly crystalline kaolinite (Ehlmann 1968). The loss of gibbsite in streams is interesting considering that Biscaye (1965) found gibbsite in low to mid-latitudes of recent Atlantic Ocean sediments. Also during transport, clay mineral assemblages may become modified due to mixing of sediment from different

source areas (Thiry 2000), physical sorting by size (Gibbs 1977), and/or post-depositional (burial) alteration (Curtis 1990).

Table 2 provides a summary of previous studies that were able to correlate sedimentary clay minerals assemblages with [paleo]climate. The studies included in Table 2 reflect a combination of both ancient and modern sediments, and terrestrial and marine basins. From Table 2, several observations are noteworthy. First, the only mineral consistently associated with specific climate is kaolinite, in warm and humid climates. Smectite is generally agreed to occur in warm climates, but may appear in humid or arid environments, or in a climate with seasonal variability. There is basic agreement that illite reflects cool and arid climates. Gibbsite appears to form in humid conditions, but there is no consensus on temperature regime. Macías Vazquez (1981) states that there is no evidence that gibbsite is a feature of hot and humid climates, but rather reflects open, well-drained systems in the initial stages of weathering of various aluminosilicates, especially plagioclase. There is a general agreement that chlorite occurs in cool climates, and that palygorskite and sepiolite occur in arid climates. For the mixed-layer expandable phases in Table 2, there are either insufficient data to determine a relationship, or the information reflects a lack of agreement by researchers. In general, Table 2 suggests that if clay mineral assemblages can be correlated with climate, confident delineation of [paleo]climate can be accomplished using only certain clay minerals.

Power and Smith (1994) present a similar table to Table 2 (their Table 2.1), but with much older data. They concluded that, in general, smectite and chlorite dominate arid landscapes, illite is dominant in dry-temperate regions, vermiculite is dominant in

humid-temperate areas (montmorillonite if poorly drained), and very wet-temperate areas are dominated by kaolinite, which in turn is the most commonly reported product of tropical weathering. In addition, kaolinite and montmorillonite can occur in less humid tropical regions, while gibbsite is present in the wettest (Power and Smith 1994).

Significance of this Study

Mass balance methods have been criticized for the following reasons:

(1) They may use poorly quantified mineral stoichiometries (e.g., Finley and Drever 1997, Bowser and Jones 2002).

(2) Weathering products that are determined using thermodynamic arguments from activity-activity diagrams rather than being determined using microscopic observations and x-ray diffraction data (Finley and Drever 1997). Drever and Zobrist (1992) demonstrated that the interpretation of mineral-water interactions based solely on phase diagrams may lead to spurious results.

(3) Biomass stoichiometry is not included in the mass balance calculations. Excluding a biomass term is only valid if the biomass is in steady state during the period of sampling. However, in forested watersheds the biomass is rarely in a steady state (Velbel 1995, Drever 1997b). Taylor and Velbel (1991) demonstrated that exclusion of a biological term from Coweeta watershed mass balance calculations can result in underestimation of mineral weathering rates by up to a factor of four.

(4) Mass balance calculations may involve more unknowns than equations, yielding a system of linear equations that cannot be solved mathematically (Finley and Drever 1997, Bowser and Jones 2002).

(5) A minimum seven-year record of data is needed in order to average out the effects of biomass, seasonal variations in climate, and water storage in the watershed (Likens and Bormann 1995).

This mass balance study has attempted to overcome these criticisms. Mineral stoichiometries have been determined by performing extensive electron microprobe phase analyses (EMPA) and laser ablation inductively coupled plasma mass spectrometry (LA-ICP-MS) on all minerals involved in weathering. The only exceptions are kaolinite and gibbsite; however, these phases do not host REE (Burt 1989) and have little compositional variability (Nesbitt 1979, Duddy 1980, Braun et al. 1993, Finley and Drever 1997). The weathering products used in the mass balance calculations have been determined using microscopic observations and x-ray diffraction data, rather than activity-activity diagrams. Biomass stoichiometry is included in the mass balance calculations of this study. The Coweeta biomass stoichiometry is taken from Day and Monk (1977) and Boring et al. (1981). In order to make the number of unknowns equal the number of equations, REE have been included in the mass balance calculations of this study. With the exception of the REE analyses, the stream water solute data used in this study exceeds the seven-year record of data that is needed in order to average out the effects of seasonal climatic and hydrologic variations in the watersheds. The one-time REE sample episode has been adjusted to an approximate long-term average.

This study differs from not only from previous watershed solute-based mass balance studies performed at Coweeta (e.g., Velbel 1984a, 1985a, 1992, 1993a, 1993c, 1993d, 1995, Taylor and Velbel 1991), but also from other mass balance studies performed elsewhere, in the following ways:

(1) In all watersheds investigated allanite is included in the mass balance calculations;

(2) In Watershed 27, previously unrecognized hornblende weathering is included in the mass balance calculations;

(3) Clay genesis rates are included in the mass balance solution; and

(4) Rare earth elements (REE) are included in the both the mineral chemistries and the stream flux data used in the mass balance calculations.

Hypotheses

The following three hypotheses are proposed for this study:

(1) Detectable (by x-ray diffraction [XRD]) changes in the relative abundances of clay minerals in a weathering profile to changes in climate will occur at time scales that are less than 1 to 2 Ma, as proposed by Thiry (2000). Thiry (2000) has suggested that sedimentary clay mineral records of short-term (<1 Ma) changes in paleoclimates are unrealistic. By calculating rates of clay genesis (abundance of a given clay produced per unit area of saprolitic landscape per time; i.e., moles hectare^{-1} year^{-1}, or mol ha^{-1} yr^{-1} hereafter) in watersheds where the climate is constrained, the 1 to 2 Ma response time of clay mineral assemblages to changes in climate may be determined. A 5% change in relative clay abundance is equivalent to a relative increase or decrease of 50 g kg^{-1}, and is the minimum change in clay abundance that is detectable by XRD (Brown and Brindley 1984, Moore and Reynolds 1997).

(2) The hydrous aluminosilicate clay genesis rates will be more rapid under warmer climatic conditions following Arrhenius Law. Furthermore, the more rapid consumption of Si by the formation of aluminosilicate clays will reduce the rate of gibbsite formation;

rates of kaolinite and gibbsite formation are antithetic (e.g., Medeira and Sanches Furtado 1987). White and Blum (1995a,b) determined that the weathering fluxes of SiO_2 for worldwide distributions of 68 watersheds underlain by granitoid rock types exhibit systematic increases with both precipitation (or "effective precipitation" whereby evapotranspiration is substracted from precipitation) and temperature. Furthermore, these same authors suggested that for watersheds in the 0-16°C temperature range, precipitation is a much stronger influence on weathering rates than is temperature. Previous research has shown that the weathering rates of plagioclase and biotite are higher in W2 than in W34 (Velbel 1984a, 1985a,b, 1993a, Taylor and Velbel 1991), suggesting an Arrhenius relationship (Velbel 1993a) despite the higher precipitation and runoff conditions of W34. Stream solute fluxes (minus precipitation inputs) for SiO_2 are published in Swank and Waide (1988; Their Table 4.11). Watershed 34 (higher precipitation/runoff) has higher SiO_2 flux values than does W2 (lower precipitation/runoff), consistent with the findings of White and Blum (1995a,b) for their global watershed database. With a lower rate of solutes released into the pore waters of W34, and greater loss of SiO_2 from the watershed, it follows that W34 should have lower rates of aluminosilicate clay genesis relative to W2. With the higher loss of SiO_2 from W34, however, gibbsite formation rates will likely be greater than W2. Despite the influence of precipitation/runoff on weathering rates, White et al. (1999a) provide strong support for significant temperature effects on rates of chemical weathering of granitoid rocks both under experimental and natural conditions.

The climate hypothesis should hold for both neoformed clays (i.e., precipitated from solution such as kaolinite and gibbsite) and transformed clays (i.e., remodeling of an

existing structure in which parts of the parent mineral are retained such as vermiculite which has parent biotite) (Moore and Reynolds 1997).

(3) Genesis rates will be lowest for a watershed (W27; Figure 2) underlain by the least chemically reactive bedrock (although all three lithostratigraphic units occur in W27, any combination of Coweeta Group lithologies is less reactive than the Otto Formation; e.g., Velbel 1985b; please see Study Area section for a description of lithostratigraphic units). Velbel (1984a) found that due to the high flushing, and low reactivity of the bedrock, SiO_2 could not reach adequate concentrations (>~20 $\mu g\ ml^{-1}$; Parfitt et al. 1983) for kaolinite to precipitate in the soil and upper saprolite. Therefore, under intense flushing conditions in a watershed developed on low chemical reactivity bedrock, gibbsite will form at the expense of kaolinite, antithetically reducing the rate of kaolinite formation.

In addition, field observations of profiles developed on the Persimmon Creek Gneiss (one lithostratigraphic unit of the Coweeta Group and present in W27) suggest that they are of a grussic nature (in contrast to kaolinite-rich saprolites). The presence of grussic, sandy saprolites has been suggested to reflect a less aggressive weathering environment (Migoń and Lidmar-Bergström 2002), however other researchers find such weathering mantles a contentious issue (Gerrard 1994, Migoń and Thomas 2002).

CHAPTER 2

METHODS

Field Sampling

Watersheds sampled at Coweeta for this study were W2, W34, and W27 (Figure 2, Table 1). Only the control (undisturbed since 1927) watersheds were sampled in order to minimize the influence of biomass state on the stream mineral nutrient budgets, although the biomass component of the mass balance has been included in calculations. All watersheds used in this study are covered with mixed mature hardwoods characterized in greater detail by Swank and Douglass (1977) and Swank and Crossley (1988).

Watersheds 2 and 34 represent the warmer/drier and cooler/wetter climate watersheds, respectively, used in order to assess the effect of climate on clay genesis rates. Within each of these two watersheds samples were collected vertically through the profile in order to constrain up-profile changes in the regolith. In addition, cuttings of saprolite and bedrock were generated during drilling of the on-site potable water well (e.g., Ciampone 1995; Figure 2), and splits of samples were readily available. To date, no clay mineral analysis has been performed on weathering materials from W34.

Watershed 27 has been extensively studied by Coweeta researchers, and, thus, yields an extensive data set. Berry (1976) cored very near W27 (Cores 9 and 15; Figure 2), cuttings have also been obtained from lysimeters installed within W27.

Outcrop samples were collected using 3 cm-diameter chrome tubes. These tubes were hammered into the saprolite in order to collect samples that preserved petrographic/micromorphologic features. This method has been successfully used by

Gardner et al. (1978) for sampling an ancient saprolite exposed in the South Carolina Piedmont.

Stream waters were sampled at the weir and filtered in the field using 0.45 μm pore-size Millipore™ filters. The filtered stream water was collected in acid-cleaned polypropylene (Nalgene) bottles. The approximately 60 ml of filtered stream water was acidified with 200 μl of HNO_3. The field sampling kits were provided by the aqueous geochemistry research group at Michigan State University. The ultra clean sampling protocols used to sample the Coweeta streams were established by this same group and follow methods outlined by Nriagu et al. (1993, 1996), Benoit et al. (1994, 1997), Horowitz et al. (1994, 1996), and Hurley et al. (1996).

Petrography

As a first attempt to delineate weathering reactions, petrography was employed. Thin sections of bedrock, soil, and saprolite were prepared by standard methods for determination of parent mineralogy and weathering product identification. All samples collected as part of this study were prepared commercially by Petrographic International located in Choiceland, Saskatchewan Canada. Due to the friable nature of the saprolite and soil, clear epoxy was used to vacuum impregnate the samples in chrome tubes. The epoxy consisted of a standard two-part epoxy resin and hardener kit. Numerous small holes had to be drilled into the chrome tubes in order to facilitate epoxy impregnation, and vacuum impregnation had to be repeated multiple times in order to achieve complete impregnation. Images in this dissertation are presented in color.

Point count data from other studies (Velbel 1984a, 1985a, Ciampone 1995) have been augmented by additional point counts completed for this study. Point counting as

part of this study utilized standard methods, and was completed using bedrock samples of Berry (1976). A minimum of 500 points per thin section were counted.

X-ray Diffraction (XRD)

Separation into the clay size fraction was performed by gravity settling, with the clay-size fraction being separated with a pipette, and the aliquots being filtered onto a 0.45 μm Millipore™ filter following rapid-suction mounting techniques (production of oriented mounts; also termed the Millipore™ Filter Transfer Method of Drever (1973); this method is well described by Moore and Reynolds 1997). In order to ensure homogeneity of the clay cakes on the filter, the clay solution was stirred during suction. The filter cake was transferred to standard petrographic slides following the methods for quantitative analysis as outlined by Moore and Reynolds (1997). That is, the filter was not rolled after inverting onto the glass slide as outlined in the original method by Drever (1973). Rolling the filter may cause segregations of clay minerals in the cake, disrupting the homogeneity (Moore and Reynolds 1997).

The most effective method of identifying and characterizing the minerals of weathering profiles is x-ray diffraction (Hughes et al. 1994). The XRD used belongs to the Department of Geological Sciences at Michigan State University, and is a Rigaku Geigerflex XRD that has been recently equipped with a new goniometer and software. The XRD uses CuKα radiation and is equipped with a nickel foil filter to ensure monochromatic radiation and low background count. XRD analyses have been conducted on samples collected at all levels in the weathering profile (including bedrock), using divergence, receiving, and anti-scatters slits of 1/2°, 0.3 mm, and 2°, respectively, a step size of 0.02° 2θ, and count times of 20 seconds.

Quantitative representation (QR) is used to characterize the clay mineral content of the samples. QR implies that a set of numbers have been generated that represent the mineral content of a sample, but does not necessarily reflect an accurate measure of the absolute amounts of minerals present (Hughes et al. 1994). For a given clay mineral in an x-ray diffractogram, QR values were generated by multiplying the peak height by its breadth at half maximum height, often referred to as full width at half maximum (FWHM; Brindley 1984, Moore and Reynolds 1997). Moore and Reynolds (1997) term this method as the "height-width" method. The height-width method was applied to the 001 peaks for vermiculite, mica (10 Å), kaolinite, and gibbsite, to the 002 peaks for hydrobiotite, and to the nonbasal 02/11 peak for halloysite. All QR values of interest in a given diffractogram were then normalized to 100% in order account for fluctuations in beam intensity between individual sample scans. Calculation of peak areas using the height-width method are typically superior to simply integrating the area under the peak, as the "tails" of the diffraction peaks often cannot be measured due to overlap with adjacent peaks, and a large portion of the peak area lies in its "tails" (for a detailed comparison between height-width and integration methods the reader is referred to Moore and Reynolds 1997). The diffraction pattern background was carefully accommodated using a low-order polynomial (Howard and Preston 1989), as the choice of background in quantitative methods is crucial (Bish 1994). The detailed XRD scans performed as part of this investigation (20 second count times and 0.02° step sizes) are conducive to yielding relatively precise, albeit not necessarily accurate, QR values. As QR was employed in this study, diffractogram clay mineral peak areas were not corrected using mineral intensity factors (MIF; Kahle et al. 2002). The weighing of peak intensities

and hence areas is unnecessary for most practical purposes (Whitton and Churchman 1987). Whitton and Churchman (1987) argue that the relatively large breadth of low 2θ angle clay peaks may actually require an increase, rather than decrease, in intensity, which in turn approximately offsets the need to make any adjustments to peak intensities for low angle phases. In addition, there is substantial variability in MIF values reported in the literature (e.g., Table 2 of Kahle et al. 2002).

Identification of diffractogram peaks followed Brown and Brindley (1984), Wilson (1987), Eslinger and Pevear (1988), and Moore and Reynolds (1997). The 10 Å peaks on XRD patterns are herein referred to as "mica", because biotite weathering dominates the regolith relative to muscovite. Mixed-layer materials were modeled using NEWMOD-For-Windows™ (Reynolds and Reynolds 1996). No baseline correction was applied to diffractograms.

Bulk Major Element Oxide Analyses

This study utilizes bulk major element oxide analyses reported by Berry (1976) and Ciampone (1995). Ciampone (1995) performed major element oxide analyses on saprolite and bedrock aggregate cuttings sampled during installation of the potable water well at Coweeta (Figure 2). The composite water well samples were collected over 3 m intervals. Whole-rock geochemical analyses were performed by x-ray fluorescence (XRF) using a Rigaku 3070 x-ray spectrometer at the University of Cincinnati (Ciampone, 1995). Because composite cuttings from 3 m intervals were collected (rather than intact samples), bulk density could not be measured on the well samples. Berry (1976) provides bulk major element oxide chemical data of samples collected during a regolith coring investigation (see Figure 2 for core locations). All cores sampled

complete regolith profiles (bedrock parent material and saprolite developed from that bedrock). Cores 4, 5, and 17 reached Otto Formation bedrock and penetrated saprolite developed by weathering of the Otto Formation. Core 9 sampled a regolith profile on the Coleman River Formation of the Coweeta Group; Core 15 sampled regolith developed on the Persimmon Creek Gneiss of the Coweeta Group. Berry (1976) sampled the weathering profile by driving a standard engineering split spoon into the regolith and by diamond-drilling into the unweathered rock. Major element oxide analyses were performed by atomic adsorption methods at the University of Georgia. Bulk density was measured with a Jolly Balance. Samples were weighed in air, and then weighed in water after being coated with aerosol acrylic lacquer (Berry, 1976).

As Berry's (1976) study included bulk density measurements of saprolite, his data are used to generate reaction progress diagrams. One way to interpret the bulk chemistry of heterogeneous weathering profiles is by using isovolumetric techniques. Millot and Bonifas (1955; summarized in English by Millot 1970) were the first to apply the isovolumetric method to the geochemical study of weathering profiles. This technique is based on the assumption that, during subaerial weathering, elements are removed from or added to the weathering profile without dilation or compaction. Therefore, a unit volume of weathered rock is presumed to have evolved from an equivalent volume of fresh rock (Gardner et al. 1978). Saprolite forms by isovolumetric weathering (Schoeller 1942, Millot and Bonifas 1955, Gardner et al. 1978, Velbel 1990b, Gardner 1980, 1992). An empirical reaction progress diagram is created by plotting the oxide volumetric concentration (in g cm^{-3}) against bulk density (e.g., Millot 1970, Gardner et al. 1978, 1981, Gardner 1980, 1992). The bulk density--not depth--of the sample serves as a

measure of the extent of weathering (e.g., Grant 1963, 1964). Sample depth may be inferior to bulk density as a measure of the extent of weathering even in lithologically homogeneous materials, because deeper samples may be highly weathered adjacent to joints or other parent-rock discontinuities not directly related to distance from the land surface.

Gardner et al. (1978, 1981) successfully applied the isovolumetric approach to understanding saprolite formation on homogeneous granite and diabase. This study differs from that of Gardner et al. (1978) in that it applies isovolumetric bulk chemical methods to a weathering profile developed on heterogeneous bedrock. This pre-weathering heterogeneity is exacerbated during chemical weathering, making interpretation of bulk chemistry very difficult. Trend lines for the reaction progress diagrams have been fit using low order polynomials. The trend lines used reflect the overall major element oxide behavior with decreasing sample bulk density without displaying excessive and geochemically unreasonable curvature. Due to the heterogeneity of the system, correlation coefficient (R^2) values for the reaction progress diagrams may be as low as 0.2 (i.e., K_2O, MgO, and Al_2O_3), but as high as 0.77 for SiO_2. Price and Velbel (in review) argue that poor correlation coefficients (as low as 0.2) for bulk chemical data collected from heterogeneous systems can still be significant and meaningful.

Scanning Electron Microscopy Secondary (SEM) and Backscattered Electron Imaging (BSE)

Polished and carbon or gold-coated thin sections, and SEM stubs of Coweeta bedrock and regolith were prepared for examination by SEM and analyzed by energy

dispersive x-ray spectroscopy (EDS) for element composition. Imaging and analyses were performed at Michigan State University's Center for Advanced Microscopy (CAM) using a JEOL JSM-35CF SEM with EDS and BSE capabilities.

Transmission Electron Microscopy (TEM)

A JEOL 100CX II TEM at Michigan State University's CAM has provided high phase-contrast images (lattice images) of weathered Coweeta biotite. The samples imaged were prepared by ion milling at Australia National University, and provided by Dr. Michael Velbel.

Electron Microprobe Phase Analyses (EMPA)

Electron microprobe analyses of Coweeta bedrock and regolith in thin section were completed at the University of Michigan's Electron Microbeam Analysis Laboratory (EMAL), using a wavelength dispersive Cameca SX 100 electron microprobe analyzer. Accelerating voltage and beam current were 15 keV and 10 nA, respectively, and a 2 μm beam diameter. Calculation of the structural formula for primary minerals from the EMPA data followed conventional methods. The structural formula of vermiculite was calculated using a method that assumes that the aluminosilicate layers have not been altered during the transformation of biotite to vermiculite (Newman, 1987; Velbel, 1984a, 1985a).

Rare Earth Element Analyses by Inductively Coupled Plasma Mass Spectrometry (ICP-MS)

Rare earth element analyses of both stream water and mineral phases was performed on a Micromass Platform Inductively Coupled Plasma Mass Spectrometer

(ICP-MS) at Michigan State University. This ICP-MS has a hexapole collision cell interface that minimizes the interferences caused by argon molecules. The REE included in this study are lanthanum (La), cerium (Ce), neodymium (Nd), gadolinium (Gd), dysprosium (Dy), and ytterbium (Yb). All six of these have been included in the mineral structural formulae; however, only stream flux data for La, Nd, Gd, and Dy have been utilized in the mass balance calculations. These six REE were selected based on their relatively high abundance (above background) in a preliminary scan of Coweeta stream waters. Stream solutions were analyzed by the ICP-MS using a concentric nebulizer and indium (In) was used as an internal standard. The concentrations (in $\mu g\ ml^{-1}$) were calculated using regression lines with standard solutions.

Laser ablation ICP-MS (LA-ICP-MS) analyses were performed using a Cetac LSX 200^{+} laser ablation system on sample thin sections. LA-ICP-MS provides high resolution sampling capabilities and multi-element high sensitivity (Fryer et al 1995, Neal et al. 1995). For all minerals analyzed (biotite, vermiculite, plagioclase, garnet, epidote, allanite, and hornblende), the beam size was 25 μm (using a UV, 266 nm beam), and the pulse rate was 20 Hz, with the exception of the phyllosilicates for which a pulse rate of 10 Hz was used. A reduced pulse rate for the phyllosilicates was necessary as the perfect basal cleavage resulted in a mineral that was susceptible to extensive damage at higher pulse rates. LA-ICP-MS and EMPA analyses spots were adjacent to one another, and Ca was used as the internal standard for all laser ablation analyses (Fryer et al. 1995, Longerich et al. 1996). NIST 612 glass was used as a calibration standard and results were obtained in $\mu g\ g^{-1}$. LA-ICP-MS detection limits are influenced by instrument operating conditions, scanning parameters, mass of material ablated, and the

homogeneity of the mineral at the sample scale (Jackson et al. 1992, Perkins et al. 1993, Jenner et al. 1994, Jeffries et al. 1995). Therefore, detection limits have been calculated following methods presented by Norman et al. (1996) (Table 3).

Table 3. Detection limits for REE analyzed by LA-ICP-MS.

	La (ppb)	Ce (ppb)	Nd (ppb)	Gd (ppb)	Dy (ppb)	Yb (ppb)
Detection Limit	5.20	28.83	10.73	4.70	8.14	10.68

Watershed Mass Balance Methods and Clay Genesis Rates

All methods for calculating rates of mineral weathering from the results of mass balance calculations are ultimately based on the method first presented by Garrels and Mackenzie (1967) and Garrels (1967). Mass balance methods follow those of Plummer and Back (1980), Velbel (e.g., 1985a, 1986a), and Drever (1997a), with rates of clay mineral genesis determined following methods outlined by Cleaves et al. (1970), Finley and Drever (1997), and recently by Bowser and Jones (2002 and references therein). For mass balance modeling of watersheds, input fluxes include precipitation, atmospheric dust, biomass decomposition (for degrading biomass), and mineral weathering reactions, while output fluxes include evapotranspiration, botanical uptakes (for aggrading biomass), clay genesis, and stream discharge. Analytical techniques outlined above have permitted determination of clay composition and provide the stoichiometries of clay genesis. These data have been combined with published hydrological and hydrogeochemical data (i.e., Swift et al. 1988, Swank and Waide 1988).

Weathering rates have been calculated by solving a system of linear equations that represent the steady-state input-output behavior of the watershed (Plummer and Back 1980). Velbel (1986a) modifies the method of Plummer and Back (1980) by defining the

change in mass of a given element as temporal fluxes across the boundary of the system, rather than concentration differences between output and input waters in ground water systems. In this study the forest biomass has been included in the mass balance calculations, as omitting this compartment from studies of even small catchments has been demonstrated to result in errors in silicate weathering rates; the assumption that biomass is at "steady state" is generally incorrect (e.g., Taylor and Velbel 1991, Velbel 1995, Drever 1997b). Nutrient data for Coweeta biomass is from Day and Monk (1977) and Boring et al. (1981). Chloride is approximately in balance in all watersheds, and, hence, ground water storage, depletion, or leakage is not of concern (Swank and Douglass 1977). The mass balance systems of linear equations have been solved using the software MATLAB® Release 12.

Following matrix algebraic methods, to perform solute-based mass balance calculations the number of unknowns (i.e., the rate of weathering of a primary mineral and/or the rate of formation of a secondary mineral) must equal the number of equations (i.e., the number of elements for which stream solute fluxes are available). For any element included in the solute flux, every phase involved in weathering which contains that element must be included in the mass balance matrix. In order to obtain equal numbers of unknowns and equations, REE have been included in the calculations of this study (specifically, La, Nd, Gd, and Dy). This investigation is the first time that trace elements have been included in mass balance methods. The REE are an ideal choice to include in the mass balance model, as allanite is an important weathering phase at Coweeta and is also a substantial REE host (Meintzer 1981, Braun and Pagel 1994, Braun et al. 1993, 1998, Harlavan and Erel 2002, Ercit 2002).

CHAPTER 3

RESULTS

Field Sampling, Petrography, and X-ray Diffraction

A map showing the localities sampled as part of this study is contained in Appendix A. The modal mineralogies for Otto Formation and Coweeta Group bedrock at Coweeta are presented in Table 4, and includes point count data from Velbel (1984a, 1985a), Ciampone (1995), and this study. Quantitative representation of XRD analyses for W2 and W34 are provided in Tables 5 and 6, respectively. Representative diffractograms may be found in Appendix B. In addition to the clay minerals quantified in Tables 5 and 6, smectitic material and variscite ($AlPO_4 \cdot 2H_2O$) have also been identified at Coweeta (Appendix B). Because the water well is located near W2, the data from W2 field-collected samples have been combined with the data from the well cuttings. Similarly, sample data from Core 17 have been combined with data from samples collected in and near W34. The XRD analyses for samples collected from Cores 9 and 15, as well as field-collected samples from in and near W27, have been subdivided by lithostratigraphic unit; QR measurements for the Coleman River Formation, Persimmon Creek Gneiss, and Ridgepole Mountain Formation are provided in Tables 7, 8, and 9, respectively.

Bulk Major Element Oxide Analyses

The bulk major element oxide analyses of rock, saprolite, and soil completed by Berry (1976) and Ciampone (1995) are provided in Tables 10, 11, and 12. Berry's (1976) data also include bulk density measurement for bedrock and saprolite (Table 10 and 11).

Table 4. Modal mineralogies for Otto Formation and Coweeta Group bedrock at the Coweeta Hydrologic Laboratory.

Study	Sample	Bedrock[1]	Depth (m)	Quartz (%)	Plagioclase (%)	Biotite (%)	Muscovite (%)	Garnet (%)	Epidote Group Minerals[2] (%)	Other (%)	Total (%)
Velbel (1984a, 1985a)		CG (n=18)		61.6	8.3	11.6	12.9	1.9	0.1	3.6	100.0
Ciampone (1995)	COWW 60-70	OF	21.34	47.0	14.0	20.0	11.5	0.0		7.5	100.0
	COWW 70-80	OF	24.38	46.5	20.5	14.0	12.5	2.0		4.5	100.0
	COWW 80-90	OF	27.43	29.5	26.5	13.0	20.5	0.5		10.0	100.0
	COWW 90-100	OF	30.48	40.0	15.0	12.5	26.0	0.5		6.0	100.0
	COWW 100-110	OF	33.53	13.0	31.5	14.5	23.0	8.0		10.0	100.0
	COWW 110-120	OF, F	36.58	12.5	35.5	15.0	20.5	3.5		13.0	100.0
	COWW 120-130	CG	39.62	42.5	19.5	12.0	15.0	1.5		9.5	100.0
	COWW 130-140	CG	42.67	64.5	15.0	9.0	6.5	0.5		4.5	100.0
	COWW 140-150	CG	45.72	42.0	12.5	13.0	21.0	2.0		9.5	100.0
	COWW 150-160	CG	48.77	44.0	12.0	13.5	21.0	0.0		9.5	100.0
	COWW 160-170	CG	51.82	33.0	15.0	12.5	23.0	0.5		16.0	100.0
	COWW 170-180	CG	54.86	49.0	21.5	14.5	8.0	1.0		6.0	100.0
	COWW 180-190	CG	57.91	50.5	19.5	8.5	11.5	2.5		7.5	100.0
	COWW 190-200	CG	60.96	56.0	9.0	13.5	14.0	0.5		7.0	100.0
This Study (Ca-bearing phases only)	C17-3	OF	1.3		16.2			0.7	1.4	81.7	100.0
	C9-5	CG	6.3		9.9			2.0	0.8	87.3	100.0
	C9-7	CG	11.3		16.1			2.2	0.5	81.2	100.0
	C15-9	CG	11.6		17.1			0.0	0.7	82.2	100.0
Mean[3]				52.5	13.2	12.3	14.6	1.7	0.9		
Minimum				12.5	8.3	8.5	6.5	0.0	0.5		
Maximum				64.5	35.5	20	26	8.0	1.4		

[1]CG = Coweeta Group rocks, OF = Otto Formation, F=Shope Fork Fault

[2]Velbel (1984a, 1985a) uses the term "epidote". However, based on analytical methods (e.g., EDS, ICP-MS) the epidote group mineral point counted as part of this study is recognized to be allanite.

[3]The mean modal abundance for the epidote group minerals is calculated from the allanite point count data from this study.

Table 5. XRD data for samples collected from W2 (including water wells samples). Clay mineral abundances are relative, and all samples are Mg-saturated.

Sample	Depth (m)	Horizon	Hydrobiotite d-spacing (Å)	Vermiculite (%)	Hydrobiotite (%)	Mica (10 Å) (%)	Kaolinite (%)	Halloysite (%)	Gibbsite (%)
W2-6	0.03	A	12.20	20	4	8	53	9	6
W2-7	0.03	A	12.45	28	9	13	39	5	7
W2-11	0.06	A	12.34	32	11	10	27	11	10
W2-14	0.06	A	12.20	23	26	12	28	3	8
W2-16	0.06	A	12.30	22	17	6	30	8	16
W2-5	0.12	B	12.37	7	6	5	71	3	7
W2-9	0.15	A	12.27	47	4	4	41	1	3
W2-12	0.21	B	12.30	26	9	10	28	8	19
W2-13	0.27	B	12.10	8	15	16	21	7	32
W2-8	0.30	B	12.27	27	4	7	51	2	9
W2-15	0.30	B	12.27	16	27	6	23	11	17
W2-17	0.30	B	12.27	15	20	5	30	9	21
W2-10	0.52	B	12.23	14	10	5	59	5	7
W2-1	0.90	C	12.00	7	15	1	43	10	24
W2-2	1.90	C	12.00	2	12	2	74	7	4
W2-3	2.40	C	12.03	0	10	3	80	6	0
W2-4	3.50	C	11.94	4	24	1	26	16	29
COWW 10-20	4.60	C	12.10	9	19	2	38	12	20
COWW 20-30	7.60	C	11.84	1	9	18	48	11	13
COWW 30-40	10.70	C	12.13	9	16	18	35	10	12
COWW 40-50	13.70	C	12.10	3	12	3	47	17	18
COWW 50-60	16.80	C	12.10	5	7	33	33	12	11
COWW 60-70	19.80	R	12.13	3	4	86	7	0	1

Table 6. XRD data for samples collected from W34 (including Core 17). Clay mineral abundances are relative. All samples are Mg-saturated with the exception of sample C17-7 (K) which is K-saturated.

Sample	Depth (m)	Horizon	Hydrobiotite d-spacing (Å)	Vermiculite (%)	Hydrobiotite (%)	Mica (10 Å) (%)	Kaolinite (%)	Halloysite (%)	Gibbsite (%)
W34-12	0.06	A	12.13	17	12	4	53	7	8
C17-1	0.20	A/B	12.44	8	9	1	27	11	43
W34-13	0.27	B	11.84	4	8	5	53	13	16
W34-1	0.50	C	11.94	1	0	5	82	5	6
W34-2	1.00	C	11.97	3	7	1	43	15	31
W34-4	0.60	C	11.81	1	1	2	18	14	64
W34-5	1.10	C	11.94	14	7	1	60	6	12
W34-6	1.80	C	12.00	7	3	4	72	5	10
W34-7	2.30	C	12.10	4	0	0	58	20	17
C17-3	1.30	C		0	0	0	67	9	24
C17-4	2.10	C	12.00	2	15	6	71	5	2
C17-5	2.80	C	11.97	1	10	1	69	6	13
C17-6	4.30	C	11.97	4	2	0	20	22	51
C17-7	7.90	R	12.10	34	1	21	17	14	13
C17-7 (K)	7.90	R		2	1	57	15	13	12

Table 7. XRD data for Coleman River Formation samples collected in and near W27. Clay mineral abundances are relative. All samples are Mg-saturated with the exception of samples C9-5 (K), C9-7 (K), and C9-7J (K) which are K-saturated.

Sample	Depth (m)	Horizon	Hydrobiotite d-spacing (Å)	Vermiculite (%)	Hydrobiotite (%)	Mica (10 Å) (%)	Kaolinite (%)	Halloysite (%)	Gibbsite (%)
LMS27-1	0.09	A	12.10	38	3	7	11	15	26
LRS27-1	0.05	A	12.69	23	9	11	24	14	19
LSS27-1	0.10	A	12.27	55	9	6	9	10	10
LMS27-2	0.37	B	12.34	38	13	4	9	18	18
LRS27-3	0.28	B	12.62	19	12	6	17	17	28
LSS27-3	0.45	B	12.13	44	6	6	10	14	19
C9-1J	0.53	C	11.94	36	9	7	18	8	21
C9-2	1.40	C	12.00	1	7	1	17	14	59
C9-3	0.61	C	11.94	5	44	5	10	10	27
C9-3B	2.10	C	11.78	7	69	12	12	0	0
C9-4	4.30	C	11.94	8	41	12	16	9	14
C9-4A	5.80	C	11.97	1	19	11	33	21	15
C9-4J	2.80	C	11.84	4	67	16	13	0	0
C9-5	6.30	C		44	0	48	7	1	0
C9-5J	4.50	C	11.84	5	51	16	19	5	4
C9-7	11.30	C		53	0	36	8	0	3
C9-7J	10.40	C	12.03	8	8	5	66	13	0

Table 7 (cont'd).

Sample	Depth (m)	Horizon	Hydrobiotite d-spacing (Å)	Vermiculite (%)	Hydrobiotite (%)	Mica (10 Å) (%)	Kaolinite (%)	Halloysite (%)	Gibbsite (%)
W27-10	0.67	C	11.81	5	15	4	24	14	38
W27-11	1.00	C	11.81	6	17	5	26	12	34
W27-12	1.30	C	11.84	3	19	2	17	14	45
W27-13	1.80	C	11.87	4	42	9	15	7	23
W27-3	0.70	C	11.97	1	9	2	12	12	64
W27-4	1.00	C	12.10	2	8	2	7	20	61
W27-5	1.30	C	12.03	2	8	4	9	24	53
W27-6	1.60	C	11.90	0	4	2	10	19	65
W27-7	2.00	C	11.84	1	7	0	5	20	66
W27-9	0.43	C	11.81	13	10	3	21	12	40
W27-8	2.20	R	11.84	2	6	1	9	26	57
C9-5 (K)	6.30	C		4	4	82	8	1	1
C9-7 (K)	11.30	C		8	2	74	12	0	4
C9-7J (K)	10.40	C		2	5	20	60	11	0

Table 8. XRD data for Persimmon Creek Gneiss samples collected in and near W27. Clay mineral abundances are relative. All samples are Mg-saturated with the exception of samples C15-7 (K) and C15-9 (K) which are K-saturated.

Sample	Depth (m)	Horizon	Hydrobiotite d-spacing (Å)	Vermiculite (%)	Hydrobiotite (%)	Mica (10 Å) (%)	Kaolinite (%)	Halloysite (%)	Gibbsite (%)
C15-1	0.15	A	12.37	35	10	7	17	15	16
W27-1	1.40	C	12.51	19	5	0	6	12	58
W27-14	0.46	C	12.00	6	10	0	9	9	66
W27-15	0.94	C	11.90	8	14	0	13	20	44
W27-16	1.60	C	12.00	7	11	0	7	13	62
W27-17	2.40	C	11.97	9	12	1	8	14	56
W27-18	2.70	C	11.94	8	38	1	1	19	33
W27-19	3.40	C	11.97	7	52	2	2	5	32
W27-2	1.60	C	11.81	5	7	0	3	18	67
W27-21	5.00	C	12.00	1	35	3	1	17	43
C15-7	6.10	R		63	0	27	8	0	2
C15-9	11.60	R		55	0	30	13	0	3
W27-20	4.10	R	11.94	10	7	8	18	20	37
C15-7 (K)	6.10	R		4	0	81	13	0	2
C15-9 (K)	11.60	R		3	0	77	17	0	3

Table 9. XRD data for Ridgepole Mountain Formation samples collected in and near W27. Clay mineral abundances are relative. All samples are Mg-saturated with the exception of samples W27-22 (K), W27-25 (K), and W27-26 (K) which are K-saturated.

Sample	Depth (m)	Horizon	Hydrobiotite d-spacing (Å)	Vermiculite (%)	Hydrobiotite (%)	Mica (10 Å) (%)	Kaolinite (%)	Halloysite (%)	Gibbsite (%)
W27-23	0.46	C	12.07	0	4	0	35	14	46
W27-24	1.20	C	12.00	0	4	28	31	20	17
W27-27	0.52	C	11.97	8	30	11	7	12	31
W27-28	1.10	C	12.00	1	20	5	6	16	52
W27-29	1.60	C	11.90	1	7	3	8	20	62
W27-22	1.70	R		49	3	23	7	0	18
W27-25	1.90	R	12.13	10	12	13	4	17	44
W27-26	2.40	R	12.23	15	9	7	22	26	22
W27-22 (K)	1.70	R		5	3	69	7	0	17
W27-25 (K)	1.90	R		1	13	16	4	18	48
W27-26 (K)	2.40	R		8	8	7	24	29	24

Table 10. Chemical analyses of Otto Formation bedrock and saprolite from cores located at Coweeta Hydrologic Laboratory (data from Berry 1976).

Core Sample	Depth (m)	Soil Horizon or Saprolite/ Bedrock Bulk Density ($g\ cm^{-3}$)	Weight Percent Oxide											
			SiO_2	Al_2O_3	Fe_2O_3	MgO	CaO	Na_2O	K_2O	TiO_2	P_2O_5	MnO	LOI	Total
C17-1	0.12	B	49.11	19.46	12.53	1.81	0.23	0.17	1.70	1.99	0.26	0.08	12.64	100.00
C17-2	0.46	1.72	38.77	27.14	10.50	3.08	2.90	0.15	1.32	1.00	0.27	0.06	14.80	100.00
C17-3	8.69	2.6	71.13	12.66	4.92	1.96	3.17	2.47	1.43	0.88	0.17	0.04	1.17	100.00
C17-4	1.37	2.21	63.44	15.15	7.27	1.90	0.10	0.12	1.14	1.88	0.25	0.40	8.36	100.00
C4-1	0.12	A	56.77	19.17	8.38	0.84	0.40	0.28	1.06	1.35	0.22	0.17	11.36	100.00
C4-4	0.85	2.25	51.79	24.21	9.99	1.32	0.03	0.37	3.17	1.24	0.25	0.40	7.23	100.00
C4-6	11.58	2.5	41.88	24.16	16.68	3.14	0.31	0.54	3.11	2.42	0.21	0.22	7.33	100.00
C5-1	0.06	A	61.52	18.10	7.95	0.46	0.01	0.35	0.79	1.41	0.13	0.06	9.22	100.00
C5-2	0.43	B	40.74	30.36	12.08	1.17	0.01	0.20	0.92	1.96	0.22	0.10	12.24	100.00
C5-4	0.67	B	48.46	24.76	14.50	0.75	0.01	0.16	0.98	2.33	0.13	0.09	7.83	100.00
C5-5	19.64	1.61	66.32	15.76	6.61	1.86	1.40	1.36	1.61	1.35	0.06	0.11	3.56	100.00
C5-6	23.18	2.92	47.62	25.00	11.05	3.64	2.27	2.54	3.77	1.82	0.17	0.31	1.81	100.00
C5-7	4.82	1.64	67.31	17.48	5.90	0.99	0.01	0.09	1.04	1.10	0.06	0.09	5.93	100.00

Table 11. Chemical analyses of Coweeta Group bedrock and saprolite from cores located at Coweeta Hydrologic Laboratory (data from Berry 1976).

Core Sample	Depth (m)	Soil Horizon or Saprolite/ Bedrock Bulk Density ($g\ cm^{-3}$)	Weight Percent Oxide											
			SiO_2	Al_2O_3	Fe_2O_3	MgO	CaO	Na_2O	K_2O	TiO_2	P_2O_5	MnO	LOI	Total
C15-1	0.12	A	57.04	17.36	7.73	0.86	0.20	0.24	0.87	1.42	0.15	0.06	14.07	100.00
C15-2	0.34	B	56.69	20.41	9.69	1.22	0.33	0.41	1.94	1.09	0.12	0.21	7.89	100.00
C15-4	0.67	1.3	41.67	24.97	10.01	4.04	1.13	1.14	3.11	2.01	0.09	0.10	11.73	100.00
C15-7	5.73	1.81	50.37	21.52	10.18	3.17	0.35	0.40	5.02	1.43	0.08	0.18	7.30	100.00
C15-9	12.8	2.76	64.88	16.10	6.65	1.58	2.00	2.04	3.59	1.11	0.13	0.04	1.88	100.00
C9-1	0.09	A	41.67	22.56	14.80	2.05	0.01	0.46	1.70	1.70	0.12	0.06	14.87	100.00
C9-3	0.37	1.7	48.34	23.05	13.12	2.51	0.02	0.41	2.69	1.85	0.11	0.04	7.86	100.00
C9-4	4.33	2.29	46.96	24.01	13.86	3.17	0.02	0.47	3.64	1.84	0.11	0.04	5.88	100.00
C9-5	6.31	2.83	73.85	12.27	4.89	1.97	1.11	0.74	1.61	1.95	0.24	0.03	1.34	100.00
C9-7	11.29	2.8	72.04	12.18	5.34	1.73	2.83	2.19	1.28	1.22	0.10	0.02	1.07	100.00

Table 12. Chemical analyses of cuttings sampled from the Coweeta Hydrologic Laboratory potable water well (data from Ciampone 1995).

Well Sample	Bed-rock[1]	Depth (m)	Weight Percent Oxide													
			SiO_2	Al_2O_3	Fe_2O_3	FeO	Total Fe	MgO	CaO	Na_2O	K_2O	TiO_2	P_2O_5	MnO	LOI	Total
COWW 0-10	OF	3.05	60.05	17.67	8.49	0.80	9.38	1.15	0.21	0.18	1.42	0.92	0.14	0.18	8.50	99.80
COWW 10-20	OF	6.10	65.52	14.68			8.83	1.79	0.87	0.76	1.18	1.39	0.18	0.15	5.09	100.44
COWW 20-30	OF	9.14	58.09	19.78			7.86	2.39	0.60	0.80	3.61	1.14	0.11	0.23	5.08	99.69
COWW 30-40	OF	12.19	69.67	13.99			6.21	1.53	0.64	0.74	1.85	1.24	0.10	0.14	3.67	99.78
COWW 40-50	OF	15.24	63.28	14.90	6.26	2.20	8.70	3.05	2.74	0.88	1.29	0.89	0.13	0.19	3.82	99.87
COWW 50-60	OF	18.29	71.02	13.28			4.95	1.54	1.86	1.88	2.09	1.14	0.12	0.08	2.31	100.27
COWW 60-70	OF	21.34	66.47	15.24	2.02	3.80	6.24	2.00	1.69	2.24	3.25	0.92	0.15	0.10	1.44	99.74
COWW 70-80	OF	24.38	69.54	13.46			6.28	1.81	1.91	1.95	2.37	1.27	0.17	0.11	1.54	100.41
COWW 80-90	OF	27.43	64.91	15.97			8.39	2.36	1.60	2.59	2.59	1.27	0.16	0.16	1.32	101.32
COWW 90-100	OF	30.48	61.76	17.14			9.77	2.62	1.54	2.39	2.92	1.28	0.18	0.17	1.55	101.32
COWW 100-110	OF	33.53	55.24	19.41			13.71	3.51	1.39	2.19	3.13	1.44	0.18	0.31	1.52	102.03
COWW 110-120	OF, F	36.58	58.04	18.59			11.95	3.27	1.68	2.65	2.53	1.75	0.16	0.37	1.19	102.18
COWW 120-130	CG	39.62	65.53	16.23	2.60	3.20	6.15	2.04	2.23	3.69	1.53	1.56	0.18	0.12	1.04	100.30
COWW 130-140	CG	42.67	66.97	15.53			7.16	2.25	2.21	3.40	1.37	1.36	0.18	0.16	1.07	101.66
COWW 140-150	CG	45.72	62.17	16.85			10.01	2.57	1.76	2.50	2.01	1.50	0.20	0.22	1.28	101.07
COWW 150-160	CG	48.77	65.30	15.92			8.34	2.33	2.02	2.98	1.53	1.88	0.17	0.18	1.17	101.82
COWW 160-170	CG	51.82	64.46	16.05			9.07	2.43	1.37	2.07	2.32	1.69	0.14	0.17	1.54	101.31
COWW 170-180	CG	54.86	64.59	16.31			8.51	2.46	1.85	2.77	2.00	1.35	0.16	0.22	1.15	101.37
COWW 180-190	CG	57.91	64.35	15.87			8.78	2.56	1.82	2.57	2.00	1.33	0.20	0.30	0.92	100.70
COWW 190-200	CG	60.96	67.13	14.87	2.93	3.70	7.04	2.45	2.03	2.47	2.10	1.45	0.22	0.14	1.31	101.21

[1]CG = Coweeta Group rocks, OF = Otto Formation, F=Shope Fork Fault.

Electron Microprobe Phase Analyses and Inductively Coupled Plasma Mass Spectrometry

Major and rare earth element analyses for all minerals used in both the solid-phase and solute-based mass balance calculations of this study are provided in Tables 13, 14, 15, and 16. Each table contains the data for a different lithostratigraphic unit. Table 17 contains the major and rare element analyses of stream waters from W2, W34, and W27.

The combined EMPA and LA-ICP-MS analyses for allanite yield relatively low totals (Tables 13 and 14). Deer et al. (1986) report allanite analyses which sum to near 100%, but include analyses for structural and non-structural water, uranium, thorium, and additional REE not included in the analyses of this study. If uranium, thorium, and water are subtracted from the allanite totals reported by Deer et al. (1986), then totals may be as low as 90%. However, the allanite totals reported in Tables 13 and 14 are still typically below 90%, and as low as 65% (sample C9-7 E4C, Table 14). Such low totals likely reflect the metamict nature of the allanite grains, but do not prevent calculation of a structural formula. The CaO concentrations in allanite (Tables 13 and 14) are well within the range reported by Deer et al. (1986), despite the low totals. Crystal-chemically Ca is located in interchain tunnels in epidote group minerals and would be most readily lost during alteration and metamictization (e.g., Peng and Ruan 1986, Barman et al. 1992, Varadachari et al. 1992, Kalinowski et al. 1998).

Hornblende Weathering

An interesting result of this study is the discovery of hornblende in the Persimmon Creek Gneiss and the Ridgepole Mountain Formation (Table 1, Figure 4),

Table 13. Combined EMPA and LA-ICP-MS data for Otto Formation minerals used in the mass balance calculations.

	Weight Percent Oxide									
	Allanite					Plagioclase				
Oxide	C17-3 E1C	C17-3 E1R	C17-3 E1C3	C17-3 E1R4	Mean[1]	C17-3 P6	C17-3 P7	C17-3 P8	C17-3 P9	Mean[1]
SiO_2	31.63	34.17	31.80	34.54	33.04	60.21	61.67	60.59	58.50	60.24
TiO_2	0.03	0.05	0.05	0.05	0.04	0.01	BDL	0.01	0.02	0.01
Al_2O_3	17.34	21.64	17.86	21.99	19.71	24.74	23.86	22.82	24.83	24.06
FeO*	4.35	6.26	5.25	7.34	5.80	0.01	0.02	0.03	0.39	0.11
MgO	0.83	0.28	0.44	0.22	0.44	BDL	0.23	BDL	0.36	0.15
MnO	0.13	0.19	0.20	0.23	0.19	0.02	0.01	BDL	0.01	0.01
CaO	12.83	17.72	12.95	18.18	15.42	6.37	5.03	5.07	6.93	5.85
Na_2O	1.28	0.77	0.99	0.31	0.84	7.80	8.44	9.61	7.15	8.25
K_2O	0.01	0.06	0.03	0.04	0.03	0.04	0.04	0.05	0.04	0.04
La_2O_3	0.143	0.157	0.144	0.161	0.151	BDL	BDL	BDL	BDL	BDL
Ce_2O_3	0.275	0.303	0.278	0.310	0.292	BDL	BDL	BDL	BDL	BDL
Nd_2O_3	0.181	0.201	0.182	0.206	0.192	BDL	BDL	BDL	BDL	BDL
Gd_2O_3	0.033	0.038	0.034	0.039	0.036	BDL	BDL	BDL	BDL	BDL
Dy_2O_3	0.018	0.029	0.018	0.030	0.024	BDL	BDL	BDL	BDL	BDL
Yb_2O_3	0.014	0.020	0.014	0.021	0.017	BDL	BDL	BDL	BDL	BDL
Total	69.09	81.89	70.24	83.65	76.22	99.19	99.31	98.19	98.23	98.73

Table 13 (cont'd).

	Weight Percent Oxide									
	Garnet							Biotite		
Oxide	**C17-3 G1C**	**C17-3 G1R**	**C17-3 G2C**	**C17-3 G2R**	**C17-3 G3C**	**C17-3 G3R**	**Mean[1]**	**C17-3 B3[1]**	**C17-3 B6**	**C17-3 B7**
SiO_2	36.61	37.27	38.16	37.42	37.57	37.41	37.41	36.58	34.30	35.95
TiO_2	0.01	BDL	0.01	0.01	0.03	BDL	0.01	1.71	1.43	1.66
Al_2O_3	20.29	20.79	21.03	21.32	20.93	21.21	20.93	17.74	15.90	17.16
FeO*	24.97	26.28	26.28	26.39	26.47	26.59	26.16	16.76	15.59	16.89
MgO	2.63	3.21	2.94	2.31	3.30	3.60	3.00	12.65	11.73	12.80
MnO	7.91	6.98	7.24	7.34	7.30	7.31	7.35	0.09	0.12	0.11
CaO	4.90	4.63	5.10	4.71	4.87	4.63	4.81	0.02	0.02	0.03
Na_2O	0.02	0.02	0.01	0.03	0.01	0.01	0.02	0.28	0.27	0.25
K_2O	BDL	0.03	BDL	0.01	0.01	0.01	0.01	9.16	8.68	9.21
La_2O_3	BDL	BDL	BDL	BDL	BDL	BDL	BDL	BDL	BDL	BDL
Ce_2O_3	BDL	BDL	BDL	BDL	BDL	BDL	BDL	0.035	0.04	BDL
Nd_2O_3	BDL	BDL	BDL	BDL	BDL	BDL	BDL	BDL	BDL	BDL
Gd_2O_3	BDL	BDL	BDL	BDL	BDL	BDL	BDL	BDL	BDL	BDL
Dy_2O_3	0.003	0.002	0.002	0.004	BDL	0.002	0.002	BDL	BDL	BDL
Yb_2O_3	0.014	0.023	0.010	0.027	BDL	0.023	0.016	BDL	BDL	BDL
Total	97.36	99.22	100.78	99.58	100.48	100.80	99.70	95.02	88.07	94.06

Table 13 (cont'd).

Oxide	Weight Percent Oxide			
	Vermiculite			
	W2-9 V1	W2-9 V2	W2-9 V3	W2-9 V4[1]
SiO_2	38.33	38.78	37.42	37.67
TiO_2	1.84	0.79	1.22	1.26
Al_2O_3	19.12	28.10	19.64	20.98
FeO*	15.08	7.99	15.82	14.98
MgO	13.94	6.52	13.80	14.16
MnO	0.11	0.04	0.09	0.08
CaO	0.14	0.19	0.16	0.34
Na_2O	0.17	0.08	0.26	0.23
K_2O	8.90	2.88	7.34	5.14
La_2O_3	0.001	0.008	BDL	0.038
Ce_2O_3	0.001	0.001	BDL	0.017
Nd_2O_3	BDL	0.007	BDL	0.046
Gd_2O_3	BDL	0.001	BDL	0.009
Dy_2O_3	BDL	0.001	BDL	0.006
Yb_2O_3	BDL	BDL	BDL	0.003
Total	97.64	85.40	95.74	94.94

[1]Indicates composition used in the mass balance calculations.
BDL = Below detection limit.

Table 14. Combined EMPA and LA-ICP-MS data for Coleman River Formation minerals used in the mass balance calculations.

	Weight Percent Oxide									
	Allanite									
Oxide	**C9-7 E1C**	**C9-7 E2C**	**C9-7 E2R**	**C9-7 E3C**	**C9-7 E3R**	**C9-7 E4C**	**C9-7 E4R**	**C9-7 E5C**	**C9-7 E5R**	**Mean[1]**
SiO_2	36.78	35.54	35.87	32.34	36.94	29.87	34.65	29.97	29.14	33.46
TiO_2	0.06	0.09	0.09	0.05	0.06	0.05	0.06	0.07	0.06	0.07
Al_2O_3	22.99	22.91	22.93	20.97	23.65	16.71	20.99	19.11	16.98	20.80
FeO*	8.77	8.16	9.02	5.90	9.17	5.22	8.24	5.38	4.27	7.13
MgO	0.16	BDL	BDL	0.06	0.33	0.13	2.72	0.32	0.80	0.50
MnO	0.17	0.26	0.30	0.14	0.22	0.06	0.07	0.24	0.10	0.17
CaO	18.83	19.58	19.49	15.80	21.12	8.60	12.76	12.97	12.90	15.78
Na_2O	0.50	0.01	0.01	BDL	0.03	0.59	0.48	1.62	0.20	0.38
K_2O	0.09	BDL	BDL	BDL	0.02	0.26	0.17	0.07	BDL	0.07
La_2O_3	0.547	0.303	0.166	0.081	0.212	0.898	0.613	0.061	0.066	0.422
Ce_2O_3	0.680	0.517	0.272	0.142	0.388	1.377	0.955	0.098	0.086	0.650
Nd_2O_3	0.567	0.270	0.139	0.087	0.242	0.886	0.571	0.062	0.073	0.412
Gd_2O_3	0.158	0.046	0.028	0.028	0.072	0.220	0.117	0.024	0.022	0.100
Dy_2O_3	0.175	0.028	0.020	0.050	0.101	0.163	0.084	0.048	0.032	0.090
Yb_2O_3	0.037	0.016	0.011	0.028	0.036	0.034	0.025	0.031	0.016	0.028
Total	90.52	87.73	88.35	75.67	92.61	65.07	82.50	70.06	64.74	80.06

Table 14 (cont'd).

	Weight Percent Oxide								
	Plagioclase				Garnet				
Oxide	**C9-7 P3**	**C9-7 P4**	**C9-7 P5**	**Mean[1]**	**C9-7 G1C**	**C9-7 G1R**	**C9-7 G2C**	**C9-7 G3C**	**Mean[1]**
SiO_2	60.30	59.08	60.24	59.87	35.34	36.79	36.82	36.86	36.45
TiO_2	BDL	BDL	BDL	BDL	BDL	0.04	0.01	BDL	0.01
Al_2O_3	24.72	24.30	24.68	24.57	20.52	20.17	21.54	21.26	20.87
FeO*	0.04	0.03	0.03	0.03	31.29	31.25	31.08	32.14	31.44
MgO	0.15	0.12	0.31	0.19	3.38	3.73	3.68	3.71	3.62
MnO	0.01	BDL	0.01	0.01	4.52	2.63	2.69	2.69	3.13
CaO	6.18	5.87	6.29	6.11	2.47	3.74	4.30	3.46	3.49
Na_2O	7.95	7.99	7.81	7.91	0.02	0.04	0.01	0.01	0.02
K_2O	0.08	0.08	0.07	0.08	BDL	0.01	BDL	BDL	BDL
La_2O_3	BDL	BDL	BDL	BDL	BDL	BDL	BDL	BDL	BDL
Ce_2O_3	BDL	0.025	0.021	0.015	BDL	BDL	BDL	BDL	BDL
Nd_2O_3	BDL	BDL	BDL	BDL	BDL	BDL	BDL	BDL	BDL
Gd_2O_3	BDL	BDL	BDL	BDL	BDL	BDL	BDL	BDL	BDL
Dy_2O_3	BDL	BDL	BDL	BDL	0.011	0.009	0.013	0.0022	0.008
Yb_2O_3	BDL	BDL	BDL	BDL	0.021	0.011	0.019	0.0035	0.013
Total	99.42	97.49	99.46	98.79	97.57	98.42	100.17	100.14	99.07

Table 14 (cont'd).

	Weight Percent Oxide										
	Biotite						Vermiculite				
Oxide	C9-7 B1	C9-7 B2	C9-7 B3	C9-7 B4	C9-7 B5	Mean[1]	LMS27-1 V4	LMS27-1 V5	LMS27-1 V1	LMS27-1 V2	Mean[1]
SiO_2	35.42	36.63	35.60	35.92	36.65	36.04	31.60	34.66	32.91	33.53	33.17
TiO_2	1.44	1.91	1.50	1.54	1.67	1.61	1.86	1.94	2.17	2.02	2.00
Al_2O_3	17.25	17.50	17.41	17.22	18.08	17.49	20.65	18.74	18.01	19.67	19.27
FeO*	18.06	18.48	18.14	18.19	17.97	18.17	20.13	19.41	24.16	21.87	21.39
MgO	11.08	12.04	11.51	11.51	11.52	11.53	8.45	8.00	7.92	6.99	7.84
MnO	0.05	0.02	0.06	BDL	0.05	0.04	0.10	0.06	0.08	0.11	0.09
CaO	BDL	0.01	BDL	0.01	BDL	0.003	0.44	0.11	0.13	0.09	0.19
Na_2O	0.22	0.23	0.18	0.16	0.16	0.19	0.07	0.25	0.19	0.24	0.19
K_2O	9.38	9.57	9.18	9.33	9.45	9.38	0.37	2.20	1.67	0.65	1.22
La_2O_3	BDL	BDL	BDL	BDL	BDL	BDL	0.0058	0.0418	0.0580	0.0064	0.0187
Ce_2O_3	BDL	0.054	BDL	0.011	BDL	0.013	0.0057	0.0016	0.0086	0.0010	0.0032
Nd_2O_3	BDL	BDL	BDL	BDL	BDL	BDL	0.0067	0.0442	0.0898	0.0074	0.0243
Gd_2O_3	BDL	BDL	BDL	BDL	BDL	BDL	0.0011	0.0068	0.0145	0.0013	0.0040
Dy_2O_3	BDL	BDL	BDL	BDL	BDL	BDL	0.0009	0.0047	0.0090	0.0009	0.0026
Yb_2O_3	BDL	BDL	BDL	BDL	BDL	BDL	BDL	0.0020	0.0041	0.0005	0.0011
Total	92.91	96.44	93.57	93.89	95.55	94.47	83.67	85.47	87.43	85.18	85.41

[1]Indicates composition used in the mass balance calculations.

BDL = Below detection limit.

Table 15. Combined EMPA and LA-ICP-MS data for plagioclase and hornblende of the Ridgepole Mountain Formation.

	Weight Percent Oxide								
	Plagioclase				Hornblende				
Oxide	W27-25 P1	W27-25 P2	W27-25 P3	Mean	W27-26 H1	W27-26 H2	W27-26 H3	W27-26 H4	Mean[1]
SiO_2	60.03	58.16	58.46	58.88	41.96	41.98	41.04	43.36	42.08
TiO_2	BDL	BDL	0.01	BDL	0.47	0.47	0.47	0.46	0.47
Al_2O_3	25.13	25.36	26.22	25.57	15.22	15.01	14.13	14.65	14.75
FeO*	BDL	0.06	0.02	0.03	15.52	13.83	12.33	13.20	13.72
MgO	BDL	0.36	0.57	0.31	9.51	10.95	9.87	11.57	10.48
MnO	0.01	BDL	0.06	0.02	0.40	0.48	0.50	0.58	0.49
CaO	6.66	7.89	7.87	7.47	11.20	11.26	10.68	11.50	11.16
Na_2O	7.69	6.93	7.06	7.23	1.48	1.42	1.42	1.46	1.45
K_2O	0.07	0.08	0.07	0.07	0.60	0.60	0.52	0.52	0.56
La_2O_3	BDL	BDL	BDL	BDL	BDL	BDL	BDL	BDL	BDL
Ce_2O_3	0.0340	0.0164	BDL	0.0168	0.00031	BDL	BDL	BDL	0.00008
Nd_2O_3	BDL	BDL	BDL	BDL	BDL	BDL	BDL	BDL	BDL
Gd_2O_3	BDL	BDL	BDL	BDL	0.00196	BDL	BDL	BDL	0.00050
Dy_2O_3	BDL	BDL	BDL	BDL	0.00219	BDL	BDL	BDL	0.00056
Yb_2O_3	BDL	BDL	BDL	BDL	BDL	BDL	BDL	BDL	BDL
Total	99.64	98.86	100.32	99.61	96.38	95.99	90.96	97.31	95.16

[1]Indicates composition used in the mass balance calculations.

BDL = Below detection limit.

Table 16. Combined EMPA and LA-ICP-MS data for plagioclase and hornblende of the Persimmon Creek Gneiss.

	Weight Percent Oxide								
	Plagioclase				Hornblende				
Oxide	**C15-7 P1**	**C15-7 P3**	**C15-7 P5**	**Mean**	**W27-20 H1**	**W27-20 H2**	**W27-20 H3**	**W27-20 H4**	**Mean[1]**
SiO_2	61.05	61.67	60.85	61.19	44.12	43.51	44.61	43.72	43.99
TiO_2	0.03	BDL	0.02	0.02	1.00	0.72	0.97	1.09	0.94
Al_2O_3	24.44	24.99	25.16	24.86	12.40	13.61	11.95	11.86	12.46
FeO*	0.05	0.03	0.04	0.04	14.62	14.31	14.04	14.31	14.32
MgO	0.19	BDL	BDL	0.06	11.27	11.94	11.92	12.00	11.78
MnO	BDL	BDL	BDL	BDL	0.31	0.32	0.33	0.32	0.32
CaO	5.76	5.65	6.26	5.89	11.54	11.70	11.62	11.67	11.63
Na_2O	8.15	8.27	7.86	8.09	1.26	1.42	1.21	1.18	1.27
K_2O	0.13	0.07	0.18	0.13	1.12	0.72	1.15	1.29	1.07
La_2O_3	BDL	0.0011	BDL	0.0004	0.0019	0.0017	0.0018	0.0015	0.0017
Ce_2O_3	0.0011	0.0018	BDL	0.0010	0.0062	0.0064	0.0075	0.0056	0.0064
Nd_2O_3	BDL	BDL	BDL	BDL	0.0062	0.0075	0.0087	0.0068	0.0073
Gd_2O_3	BDL	BDL	BDL	BDL	0.0022	0.0020	0.0028	0.0021	0.0023
Dy_2O_3	BDL	BDL	BDL	BDL	0.0025	0.0026	0.0027	0.0018	0.0024
Yb_2O_3	BDL	BDL	BDL	BDL	BDL	BDL	BDL	BDL	BDL
Total	99.78	100.69	100.38	100.28	97.66	98.28	97.83	97.45	97.80

[1]Indicates composition used in the mass balance calculations.

BDL = Below detection limit.

Table 17. Major and rare earth element concentrations in Coweeta stream waters sampled on May 22, 2002.

Element	ppb		
	Watershed 2	**Watershed 34**	**Watershed 27**
SiO_2	4,085	2,643	1,206
Mg	321	364	186
Ca	646	709	273
K	477	355	162
Na	NR	NR	NR
Al	BDL	BDL	34
La	0.08	0.04	0.1
Nd	0.08	0.04	0.09
Gd	0.02	0.01	0.02
Dy	0.02	0.01	0.01

NR = Not reported.

BDL = Below detection limit.

both which underlie W27 (Figure 2). The presence of hornblende in the lithostratigraphic units of W27 has not been previously reported (e.g., Berry 1976, Hatcher 1980, Velbel 1984a, 1985a). The hornblende is weathering in both lithostratigraphic units, although the hornblende of the Ridgepole Mountain Formation is completely weathered to kaolin, goethite, and possibly gibbsite and within a few millimeters of the weathering front (Figure 5).

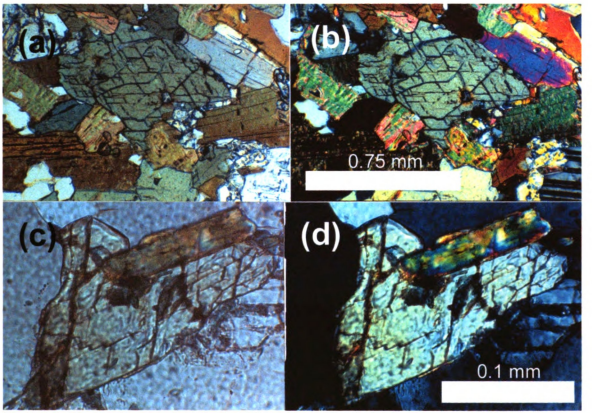

Figure 4. Photomicrographs of unweathered hornblende in the Persimmon Creek Gneiss (a-b) and Ridgepole Mountain Formation (c-d). Left images are plane-polarized light and right images are crossed-polarized light. Persimmon Creek Gneiss sample W27-20 (a-b) and Ridgepole Mountain Formation sample W27-26 (c-d).

The hornblende weathering in W27 is nearly identical to mechanisms described in detail by Velbel (1987, 1989b) for hornblende of the Carroll Knob Mafic Complex, also located in Coweeta. He found hornblende weathering to be a dissolution-reprecipitation

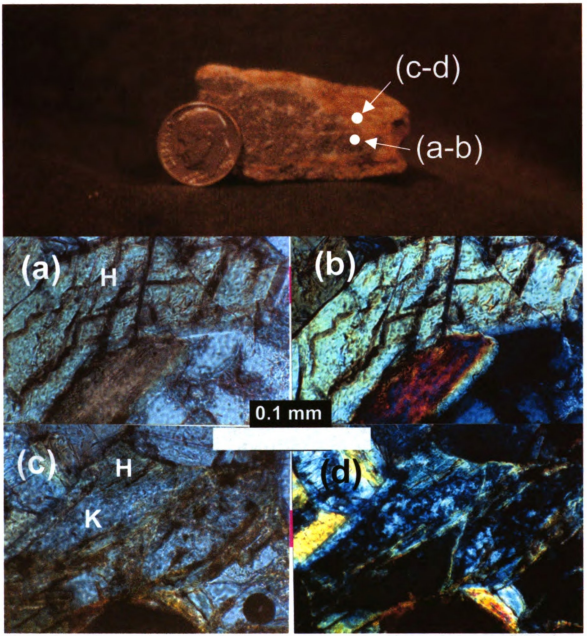

Figure 5. An image of a Ridgepole Mountain Formation rock sample (upper photo) that contains a core and weathering rind (dime for scale), with accompanying micrographs of hornblende (H) weathering at locations indicated on the sample. Note that hornblende weathering is very rapid in the Ridgepole Mountain Formation, with complete replacement of hornblende (a-b) by kaolin (K) (c-d) within a few millimeters of the weathering front. The micrographs on the left are plane-polarized light, and those on the right are crossed-polarized light. Sample W27-26.

reaction, whereby hornblende dissolves stoichiometrically, and the neoformed clay boxworks (kaolinite, gibbsite, and goethite) then precipitate from solution. The

boxworks form as fracture and cleavage linings, and also on crystal surfaces. The presence of void space between the hornblende remnants and boxworks supports the interpretation of a dissolution-reprecipitation mechanism (Velbel 1987, 1989b; Figure 6). Similar to the work of Velbel (1987, 1989b), lenticular etch pits form during an early stage of Coweeta Group hornblende weathering, and clay (kaolin, goethite, and possibly gibbsite) boxworks are composed of paired layers separated by a central parting (Figure 6).

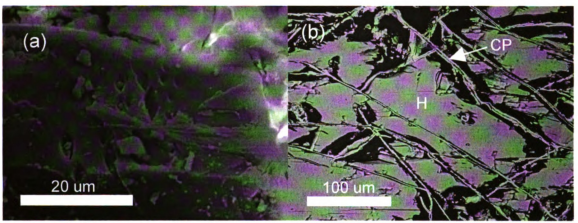

Figure 6. Evidence of hornblende weathering in W27. Image (a) shows lenticular etch pits during an early stage of weathering in the Ridgepole Mountain Formation (sample W27-26). Image (b) is a BSE image of clay (kaolinite, possibly also gibbsite, and goethite) boxwork composed of paired layers separated by a central parting (CP) in the Persimmon Creek Gneiss (sample W27-24).

Hornblende of the Ridgepole Mountain Formation displays alteromorphic replacement (terminology of Delvigne 1998) of hornblende by kaolin, and possibly gibbsite, during the initial stages of rock weathering (Figure 5). This replacement texture was not observed for hornblende weathering in the Persimmon Creek Gneiss. Microscopic observations reveal that hornblende weathering in the Persimmon Creek Gneiss is so rapid that it occurs before the development of substantial permeability within the rock. The relatively low permeability of the incipiently weathered rock permits

retention of solutes, favoring precipitation of neoformed clays within void spaces. This alteromorphic kaolin is removed as weathering progresses and the permeability of the weathered rock increases. Despite the generally low permeability present during the kaolinitization of hornblende, no smectite has been found using XRD or SEM. It has not been determined why the hornblende of the Ridgepole Mountain Formations weathers so rapidly. Distinct compositional differences between the hornblendes of the Persimmon Creek Gneiss and Ridgepole Mountain Formation do exist (Tables 15 and 16).

CHAPTER 4

BIOTITE WEATHERING

The purpose of the chapter is not to present the results of a rigorous investigation into biotite weathering, but rather to present some additional data and conclusions with regard to the nature of biotite weathering at Coweeta. Many of the conclusions presented here are important when interpreting the results of mass balance calculations of mineral weathering rates, which are to follow.

The empirical reaction progress diagrams for K_2O and MgO provide an initial evaluation of Coweeta biotite weathering (Figure 7). Magnesium and K are both lost

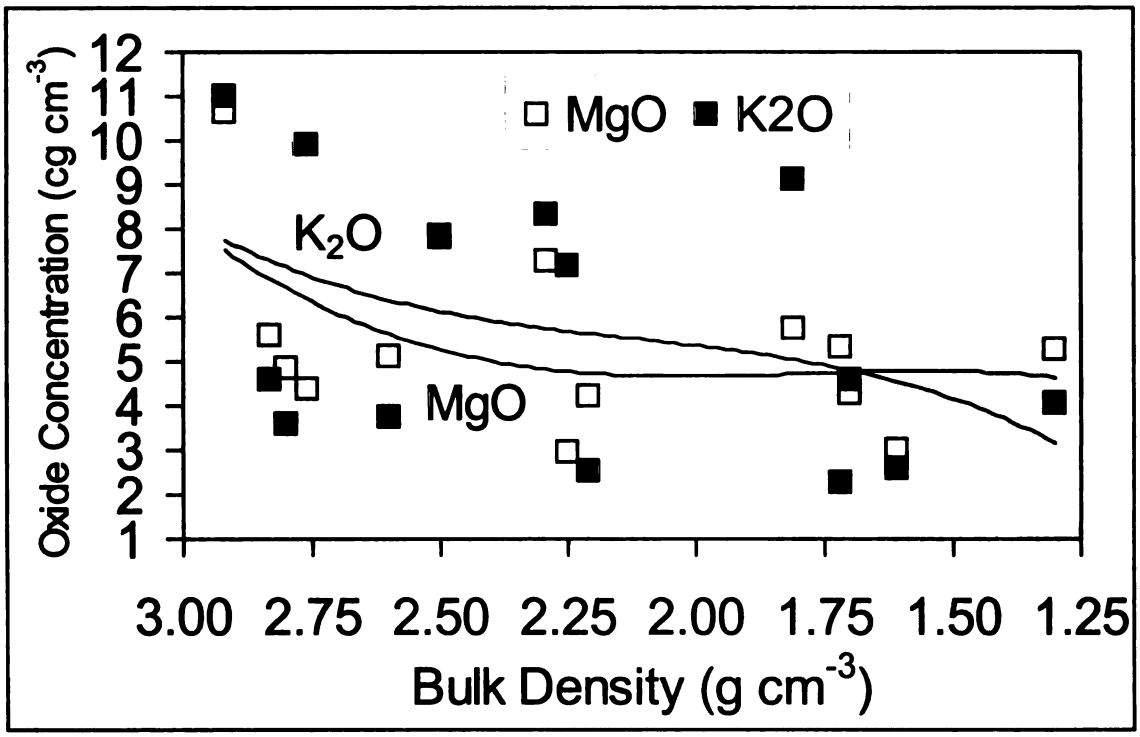

Figure 7. Reaction progress diagrams for K_2O and MgO reflecting biotite weathering at Coweeta.

during the early to middle stages of weathering (bulk densities 2.92 to 2.25 g cm^{-3}; Figure 7).

The loss of both Mg and K at bulk densities greater than 2.25 g cm^{-3} likely reflects some destruction of the biotite silicate structure during the initial stages of weathering. Core 17 (Berry 1976) provides a well constrained weathering sequence that is rarely obtained in the heterogeneous weathering profile at Coweeta. Figure 8 shows XRD patterns for the <2 μm size fraction of bedrock. The three diffractograms shown in Figure 8 display a progression of biotite weathering at and below the weathering front. The earliest stage of biotite weathering is characterized by unexpanded (10Å) vermiculite that contains K in the interlayer (Figure 8(a), Table 6, Appendix B). Upon intercalation with Mg, the 10Å K interlayered vermiculite expands to 14Å (Figure 8(a)). With progressive bedrock weathering the vermiculite is weathered to a hydroxy-interlayered mixed-layer vermiculitic or smectitic material (Figure 8(b)). With the current data set it is not possible to determine if the hydroxy-interlayered phase is vermiculite or smectite, as both clay minerals will have an approximately 14 Å d-spacing. Herein, the hydroxy-interlayered clay mineral will be referred to as "hydroxy-interlayered material" (HIM). Modeling the XRD pattern using NEWMOD-For-Windows™ (Figure 8(b); Reynolds and Reynolds 1996) reveals that the mixed-layer HIM it is an interlayered kaolinite/HIM (K/H) phase. This interlayered clay mineral contains 66% HIM layers, 34% kaolinitic layers, with a Reichweite of 1.5 and the HIM has a nearly complete hydroxide interlayer. The Reichweite value indicates that for the proportions of the HIM and kaolinitic layers, there is only partial ordering of the interlayering. Formation of K/H is accompanied by a nearly complete loss of the early formed vermiculite (Figure 8(a)) and a substantial

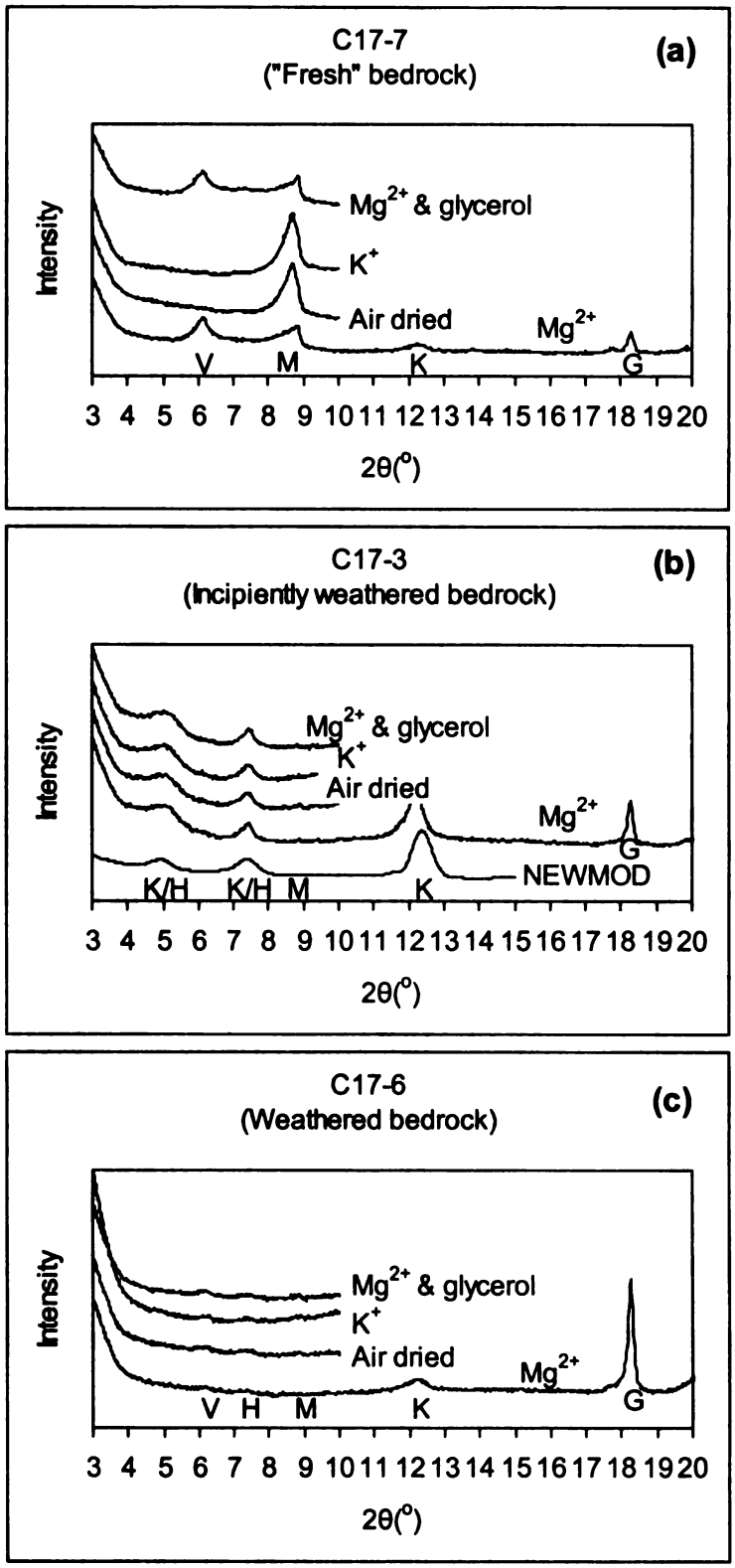

Figure 8. Observed and modeled (b) XRD patterns of the <2 μm size fraction of bedrock from Core 17. V=vermiculite, H=hydrobiotite, M=mica, K=kaolinite, G=gibbsite, and K/H=kaolinite/HIM. The same diffractograms with detailed labeling are contained in Appendix B.

reduction of the intensity of the 10Å mica peak (Figure 8(a,b)). These observations support the conclusion that the K/H is the transformational product of biotite weathering. With further weathering the K/H is destroyed, and relatively small abundances of vermiculite, hydrobiotite, and mica are present in the weathered bedrock (Figure 8(c)). From Figure 8, the progression of weathering is also evident by the steady increase of gibbsite in each diffraction pattern.

In Figure 8(b) the modeled kaolinite peak has a slightly lower d-spacing (7.14Å) than that of the measured Coweeta kaolinite (7.23Å). The slightly higher measured value reflects a substantial halloysite component to the kaolin at Coweeta (Brown and Brindley 1984, Eslinger and Pevear 1988). The modeled K/H pattern in Figure 8(b) also contains a peak near 12Å. This peak could easily be misidentified as a hydrobiotite peak (also common at Coweeta; Figure 8(c)), when in actuality it is simply a higher order K/H peak.

The mixed-layer hydroxy-interlayered material recognized at Coweeta has been termed kaolinite/HIM (K/H) herein, rather than kaolinite/expandables (K/E) as suggested by Hughes et al. (1993). The decision to use K/H is based on the observation that the HIM does not expand or collapse with changes in cation intercalation or relative humidity (Figure 8(b)), and that it cannot unequivocally be determined to be smectitic. All hydroxy-interlayered clay minerals (i.e., vermiculite, smectite, and chlorite) have similar d-spacings of approximately 14Å, and, as stated above, will not expand or collapse with changes in interlayer cation or relative humidity. In fact, when modeling the diffractogram using NEWMOD-For-Windows™, a di-trichlorite was used for the dominant clay mineral. However, the HIM is not believed to be chlorite because there is no evidence of chlorite being present in the sample. Heating the sample to 575° C did

not yield a chlorite (001) peak. Following heating to 575° C, several samples from Core 17 were found to contain chlorite in trace abundances, which were so low that it is unlikely they could produce the abundance of mixed-layer clay material observable in Figure 8(b). Moreover, the largest abundance of chlorite was identified in a sample collected near the top of the saprolite (C17-2), demonstrating the resistance of chlorite to weathering at Coweeta. In general, the scarce chlorite found at Coweeta weathers very slowly, if at all.

There is some evidence that may suggest that the HIM is hydroxy-interlayered smectite (HIS) rather than hydroxy-interlayered vermiculite (HIV). Velbel (1984a) found fracture-filling clays exhibiting a fragile "cornflake" habit in SEM which is often characteristic of authigenic smectite in sedimentary rocks. He found these observations to be consistent with smectite in XRD. Furthermore, Velbel (1984a) only found smectitic material in incipiently weathered materials, where low permeability conditions were conducive to smectite formation. Vermiculite at Coweeta increases with increasing weathering, with there being a dramatic increase in HIV proportions in the solum (Figure 9). Therefore, in the incipiently weathered rock smectite would be more likely than vermiculite. Kaolinite/smectite also has a widespread occurrence in soils and paleosols ranging in age from Pennsylvanian to Holocene (Hughes et al. 1993, Moore and Reynolds 1997), some with Reichweite of 1.5 (Hughes et al. 1993). No other K/14Å phase has been reported as commonly as K/S, especially in a low temperature weathering environment (Moore and Reynolds 1997). The weathering of biotite to vermiculite to smectite to solutes reflects a natural weathering sequence, with a progressive decrease in layer charge of the 2:1 phyllosilicates, followed by solubilization. The presence of

kaolinite and 14Å HIM layers in biotite from incipiently weathered bedrock have been identified in TEM images (Figure 10).

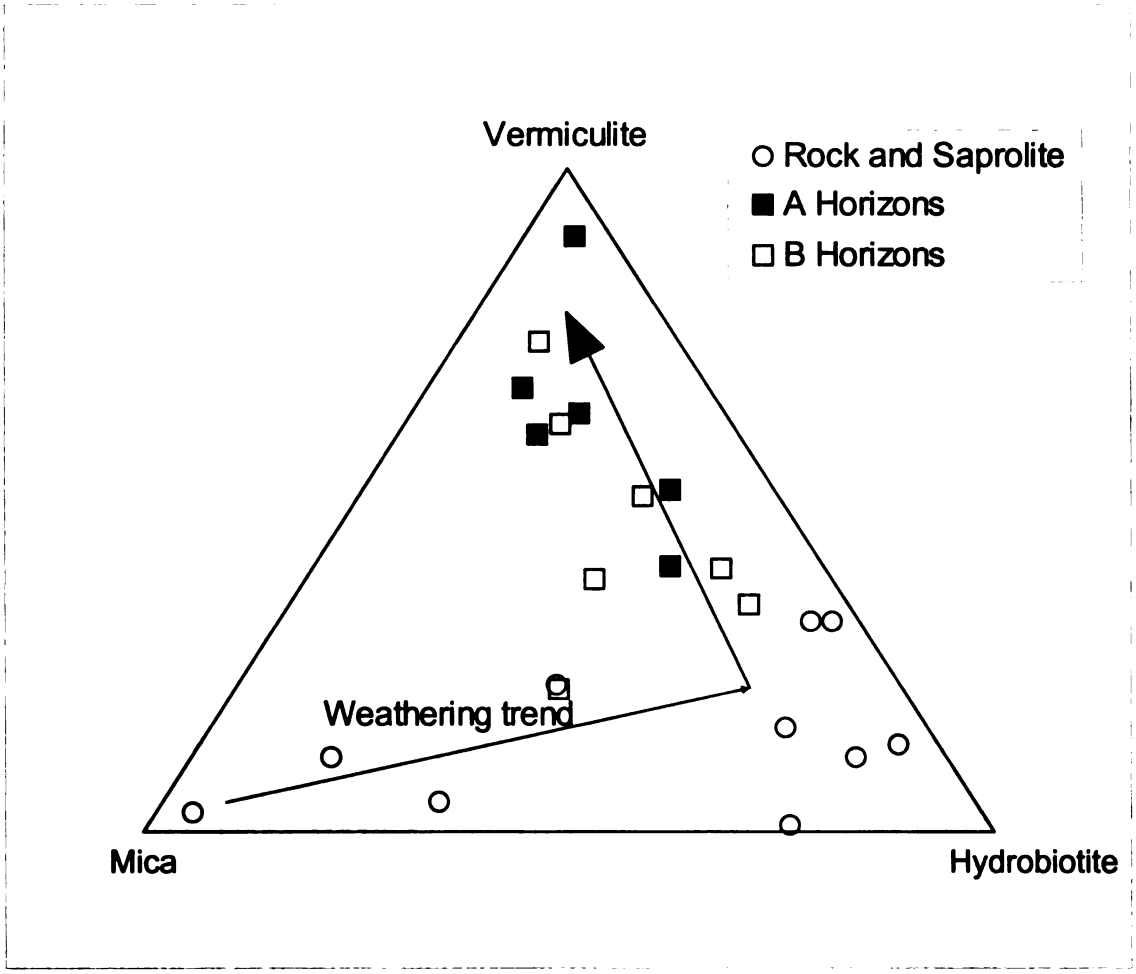

Figure 9. Relative changes in 2:1 clay mineral abundances in Watershed 2. Note pronounced increase in vermiculite (HIV) in the solum. Identical trends are found in weathering profiles throughout Coweeta.

Figure 10 shows biotite altering to HIM, and interstratification of two kaolinite layers. Rebertus et al. (1986) describe a biotite to kaolinite weathering mechanism for North Carolina Blue Ridge weathering profiles. The same mechanism has also been reported for weathered igneous biotite collected from weathering profiles in Puerto Rico

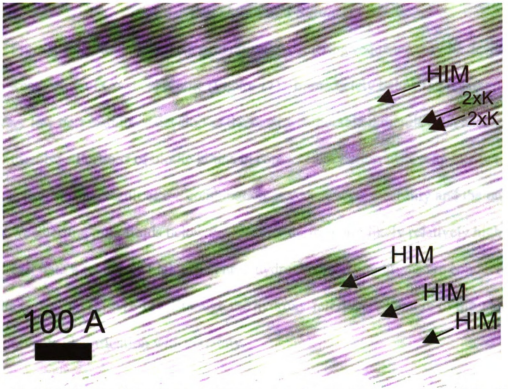

Figure 10. TEM lattice fringe image of biotite showing double layers of kaolinite (2xK) and 14Å HIM layers. Bedrock sample W27-4a.

(Dong et al. 1998, Murphy et al. 1998) and Australia (Gilkes and Suddhiprakarn 1979a,b, Banfield and Eggleton 1988). For metamorphic biotite in New Zealand, Ahn and Peacor (1987) report kaolinite occurring in biotite as either thick packets of layers interstratified within biotite, or as two-layer units irregularly interlayered within biotite. Although similarities exist between the biotite weathering studies of the Blue Ridge and those elsewhere, a substantial difference is that the Blue Ridge biotite weathers to hydrobiotite early in the weathering sequence, with the hydrobiotite persisting up-profile to the solum where hydrobiotite weathers to discrete vermiculite. In contrast, Gilkes and Suddhiprakarn (1979a,b) found that hydrobiotite did not appear in x-ray diffraction patterns until the later stages of weathering and then also remained stable.

Discussion and Summary

From the discussion above a generalized weathering sequence may be developed for the weathering of Coweeta biotite (Figure 11). Immediately below the weathering front very low permeabilities develop as the most weatherable minerals such as allanite start to dissolve. Portions of biotite grains in contact with pore spaces may interact with meteoric fluids. As a result of the combination of very low permeability and the onset of silicate weathering, pore fluids below the weathering front are likely relatively high in solutes and with a relatively high pH. These hydrochemical conditions are conducive to smectite formation (Figure 11), although the hydroxy-interlayered nature of the 14Å phase prevents identification with certainty.

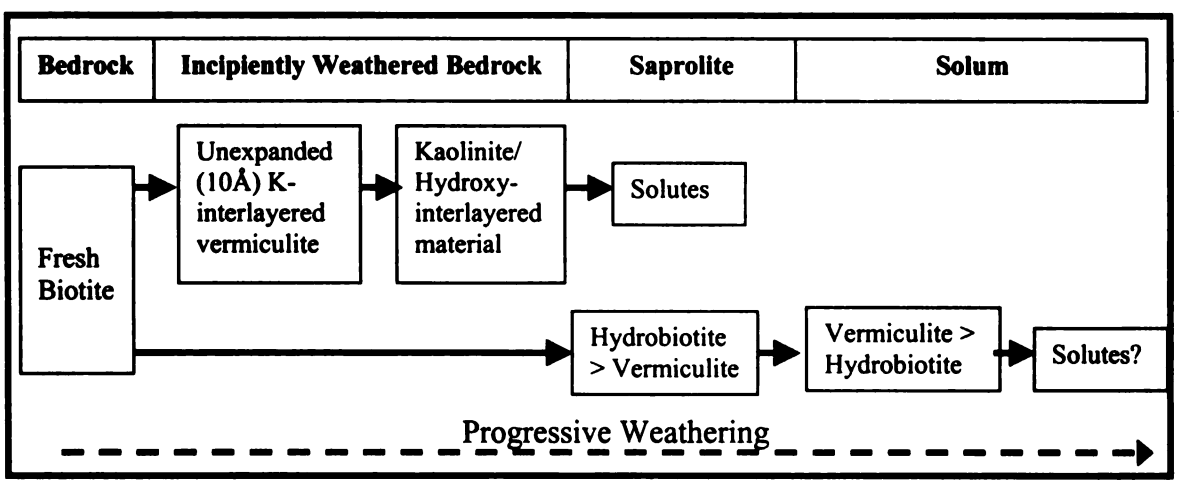

Figure 11. Schematic representation of biotite weathering at Coweeta Hydrologic Laboratory.

Above the weathering front the regolith consists of saprolite and permeability increases dramatically. The increased permeability results in the leaching of solutes from the weathering profile with an accompanied decrease in pH. Under such conditions the HIM is destroyed to solutes (Figure 11). At this stage the remaining biotite weathers to predominantly hydrobiotite and lesser vermiculite. As biotite weathering continues in the

saprolite, the abundances of both hydrobiotite and vermiculite increase (Figures 9 and 11).

The saprolite-solum interface is a distinct geochemical and mineralogical boundary where the hydrobiotite formed in the saprolite weathers to vermiculite (Figures 9 and 11). In the solum, vermiculite dominates over hydrobiotite. With increased weathering in the solum vermiculite may ultimately be destroyed and yield solutes.

CHAPTER 5

EPIDOTE GROUP MINERAL WEATHERING

Crystal-Chemistry of Epidote Group Minerals

Prior to evaluating the secondary minerals in a regolith, the weathering of the primary minerals must be characterized. At Coweeta, the weathering of plagioclase feldspar (Velbel 1983, 1986b, 1989a), almandine garnet (Velbel 1984b, 1993b), biotite (Velbel 1984a, 1985a), hornblende (Velbel 1987, 1989b), and staurolite (Velbel et al. 1996) have already been characterized. However, the weathering of epidote group minerals at Coweeta has only been recognized during the research of this study.

The crystal structure of epidote group minerals is shown in Figure 12. The ideal formula is $A_2M_3Si_3O_{12}OH$, where the A sites contain large, high-coordination number cations such as Ca, Sr, lanthanides, etc., and the M sites are occupied by octahedrally coordinated, trivalent and occasionally divalent cations such as Al, Fe^{3+}, Mn^{3+}, Fe^{2+}, Mg, etc. (Dollase 1971). Both epidote and allanite are monoclinic with $P2_1/m$ symmetry (Mitchell 1966, Dollase 1971, Deer et al. 1986). The structure (Figure 12) contains chains of edge-sharing octahedra of two types; (1) a single chain of M2 octahedra, and (2) a multiple or zig-zag chain composed of a chain of M1 octahedra with peripheral M3 octahedra attached on alternate sides along its length (Dollase 1971, Deer et al. 1986). The chains of octahedra are parallel to b, and are cross-linked in the c-axis direction by groups of single SiO_4 tetrahedra and Si_2O_7 dimers. The large cavities that remain between the chains and cross-links host the A1 and A2 cations in nine- and ten-fold coordination, respectively (Dollase 1971, Deer et al. 1986).

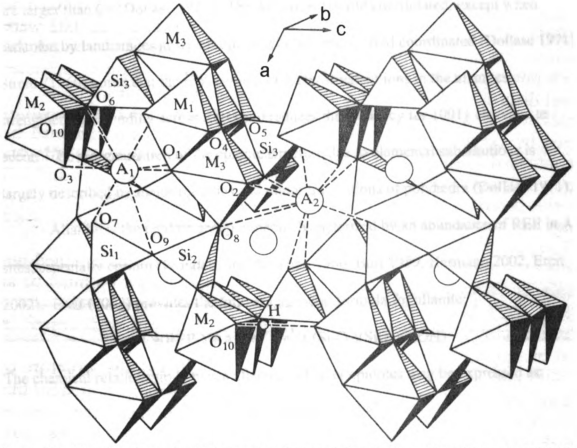

Figure 12. The structure of epidote group minerals (after Dollase 1971, Deer et al. 1986).

Among epidote group minerals the only variations in elemental occupancy involve the A2, M1, and M3 sites. The M2 octahedra contain only Al, with the M3 site containing a larger fraction of the non-aluminum atoms (Dollase 1971). The non-random distribution of the cations in the three octahedral sites likely reflects the preference of Al to coordinate with hydroxyls in M2, and the preference of the transition metals for the larger and more distorted M3 site (Dollase 1971). In epidote the A sites are entirely occupied by Ca, whereas in allanite Ca is partially replaced by other divalent atoms, such as Sr and Pb, or by REE (Dollase 1971). Substitution is non-uniform between the A sites, such that all of the atoms replacing Ca are found only in the A2 site (Dollase 1971). This phenomenon is explained by the larger A2 site hosting atoms that

are larger than Ca (Dollase 1971). The A2 site is 10-fold coordinated, except when occupied by lanthanides at which time it will become 11-fold coordinated (Dollase 1971). Strens (1966) noted that the replacement of Ca by trivalent ions in the allanites strengthens the bonding across (001) and reduces the tendency for {001} cleavage to occur. The reorganization of the epidote structure due to elemental substitutions is largely described by major rotations and minor translations of polyhedra (Dollase 1971).

Allanite is the epidote group mineral characterized by an abundance of REE in A2 sites, especially cerium (Frondel 1964, Mitchell 1966, Burt 1989, Hermann 2002, Ercit 2002). Ercit (2002) provides the following general formula for allanite:

$$Ca(REE,Y)(Al,Fe^{2+},Fe^{3+})_3(Si_2O_7)(SiO_4)O(OH)$$

The chemical relationship between allanite and other epidotes may be expressed as:

$$Ca + Fe^{3+} \Leftrightarrow REE^{3+} + Fe^{2+}$$

Allanite is the only epidote group mineral in which ferrous iron is an essential constituent (Deer et al. 1986).

Allanite often occurs in the metamict state due to the destruction of the crystal structure by α-particle bombardment emitted by uranium and/or thorium contained in the A2 sites (Wilson 1966, Bromley 1964, Mitchell 1966, Ewing 1976, Ewing and Haaker 1981, Deer et al. 1986, Peng and Ruan 1986, Palmquist 1990, Janeczek and Eby 1993, Ercit 2002). The degree of metamictization is influenced by the age of the allanite and the amount of U and Th present, not with any variation of the REE (Frondel 1964). The presence of radioactive elements also makes allanite useful for geochronology (e.g., Wilson 1966, Poitrasson et al. 1998). Metamictization lowers the stability of allanite, making it more susceptible to alteration, including weathering (Deer et al. 1986, Ercit

2002). Metamictization of allanite has been reported to be capable of causing the release of REE from the lattice (Peng and Ruan 1986).

Heating to 650° C in a nitrogen atmosphere for as little as 2 hours is capable of restoring a metamict allanite (Frondel 1964); however Janeczek and Eby (1993) found that in an argon atmosphere annealing may begin at temperatures as low as 400° C and continue up to approximately 800° C. Typically, annealing in argon is a two-stage process with the first stage peaking at 600° C and the second peaking between 700° and 800° C (Janeczek and Eby 1993). When heated in air, other phases begin to develop after allanite above approximately 700° C (Mitchell 1966, Vance and Routcliffe 1976), and the Fe^{3+}/Fe^{2+} ratio increases (Dollase 1971, Vance and Routcliffe 1976).

Metamict minerals usually do not display cleavage, but, rather, conchoidal fracture (Klein and Hurlbut 1999). Many metamict minerals are bounded by crystal faces and are thus amorphous pseudomorphs after an earlier crystalline mineral (Klein and Hurlbut 1999). In thin section, non-metamict allanites are distinguished by their brownish color, whereas metamict grains will behave isotropically and contain anastomosing fractures (Bromley 1964, Deer et al. 1986). Metamict minerals also may not conform to an ideal structural formula (Deer et al. 1986, Ercit 2002).

Epidote Group Mineral Weathering at the Coweeta Hydrologic Laboratory

Chemically, the distinction between isostructural allanite and epidote is in the substitution of Ce for Ca in A2 sites of the former (e.g., Frondel 1964, Dollase 1971, Deer et al. 1986, Janeczek and Eby 1993, Klein and Hurlbut 1999, Ercit 2002). However, appreciable Ce values for epidote are reported (e.g., Grauch 1989), thereby obscuring the distinction between epidote and allanite (Ercit 2002). A complete series

may exist between epidote and allanite (Frondel 1964). In a review of REE abundances in epidote group minerals, Grauch (1989) reports La content ratios for epidote/chondrite as being less than approximately 1,000, whereas the same ratios for allanite are approximately 100,000 or greater (Figure 13). However, many of the epidote group

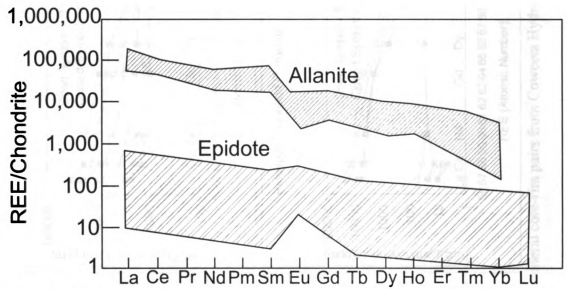

Figure 13. Summary of data for REE contents of metamorphic minerals. Modified from Grauch (1989), his Figures 2 and 16.

minerals at Coweeta fall in between these two values (Figure 14), and may be termed either high-REE epidote or low-REE allanite. Any epidote group mineral at Coweeta that yields a La content ratio of the mineral/chondrite greater than 1,000 will be referred to herein as an allanite (e.g., Deer et al. 1986). It should be recognized, however, that the Coweeta allanite is relatively low in REE (Figure 14) when compared with published data (Figure 13; Deer et al. 1986; Grauch 1989). In thin section, the unweathered allanite grains typically have optical properties that resemble epidote more so than allanite (e.g., optically anisotropic in thin section; Figure 15). Making this distinction is critical, because at Coweeta the bedrock contains both allanite and epidote that are

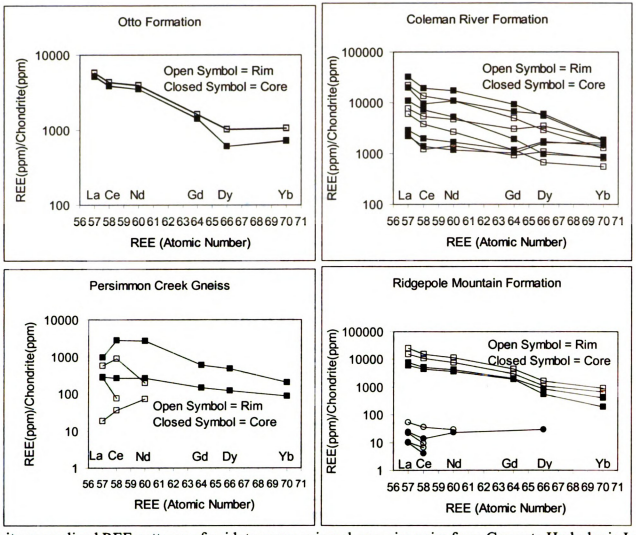

Figure 14. Chondrite normalized REE patterns of epidote group mineral core-rim pairs from Coweeta Hydrologic Laboratory. Chondrite REE abundances from Sun and McDonough (1989).

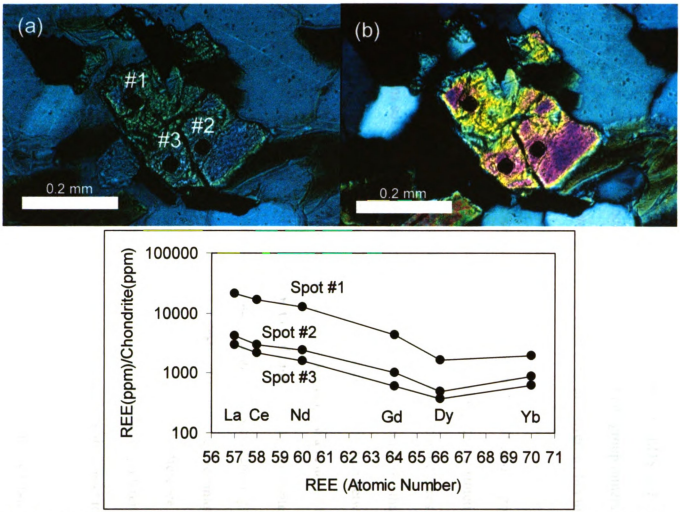

Figure 15. Photomicrographs and REE patterns of an epidote group mineral at Coweeta. This grain has the optical properties of an epidote, but the REE content of an allanite (plot). The three dark circles on grain are laser ablations points and correspond to the REE plot. Images in plane-polarized light (a) and crossed-polarized light (b). Sample C17-3 from the Otto Formation.

indistinguishable in thin section when unweathered (Figure 15). However, the allanite is far more abundant and dissolves rapidly below the weathering front. In contrast, epidote is less abundant and persists into the solum with only minimal evidence of weathering. These observations underscore the importance of analytical (e.g., EDS, ICP-MS) data when conducting studies that include the weathering of epidote group minerals, and may be offered to explain why epidote has been reported to be destroyed within the first stages of weathering (Braun and Pagel 1994).

Figure 14 provides REE contents of both cores and rims of epidote group minerals. Only in the Persimmon Creek Gneiss is there a significant distinction between the REE content of cores and rims. However, Figure 16 shows that the cores of the allanite grains sometimes have higher REE abundances than the rims, and that allanite grains are not always homogeneous (Figure 16). The lack of distinction between the REE content of allanite cores and rims using LA-ICP-MS may be a result of the diameter of the beam being comparable in size with the thin allanite rims (approximately 25 μm), compounded by noting that the core-rim boundary is not always evident (Figure 15), if a rim is present at all. Because laser ablation is a destructive analytical technique, ablating too near grain edges was avoided. In general, the most significant difference between the cores and rims of allanite grains at Coweeta is that the cores weather preferentially to the rims. However, both rims and cores weather relatively rapidly with respect to all other minerals present in the rock.

Although allanite grains, either cores or rims, at Coweeta are generally not sufficiently metamict to be optically isotropic, allanite grains are commonly associated with pleochroic haloes in juxtaposed biotite when observed petrographically (Figure 17).

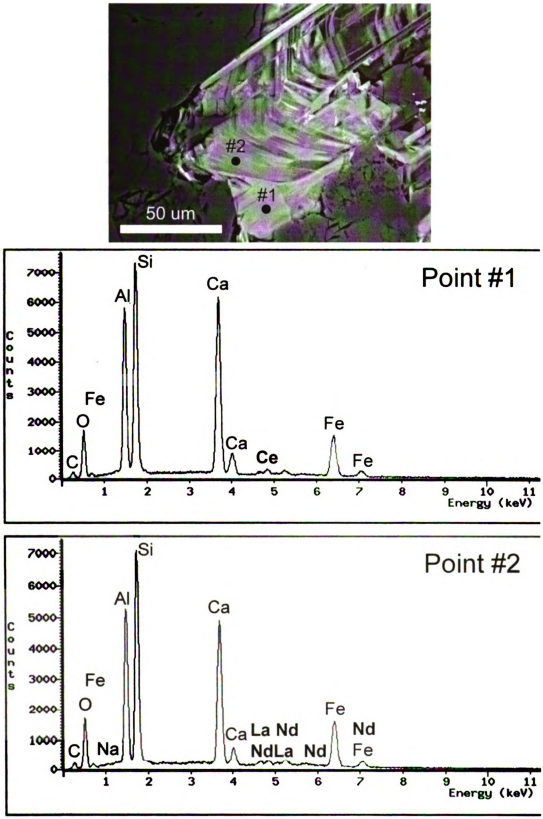

Figure 16. Backscatter image and EDS spectra showing an example of the REE content of a core and rim of an allanite grain at Coweeta; Coleman River Formation sample C9-7.

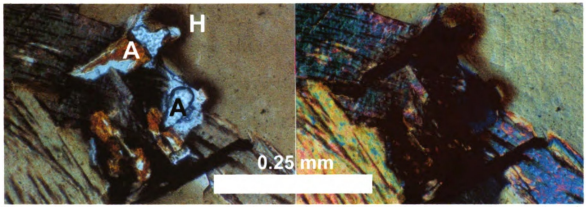

Figure 17. Photomicrographs of pleochroic haloes (H) in biotite juxtaposed to weathered allanite (A). Note ferruginous weathering products (goethite) of allanite (left). Left image is plane-polarized light and right image is crossed-polarized light. Sample C15-9 from the Persimmon Creek Gneiss.

In fact, neither uranium nor thorium has been detected using EDS, even in grains that are petrographically isotropic (Figure 18(a)). Only in the Persimmon Creek Gneiss are some allanite grain cores isotropic and containing fractures that suggest extensive metamictization, but such grains are uncommon (Figure 18(a)). These same grains yield microprobe analyses with very low totals (<65 weight percent) that, like many metamict

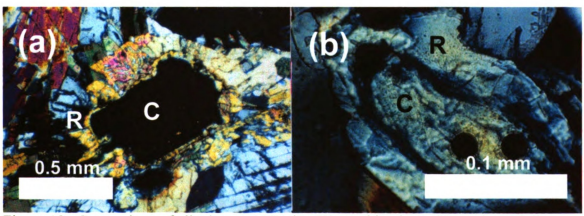

Figure 18. Comparison of allanite core (C)-rim (R) combinations; (a) a substantially metamict core that behaves isotropically, and (b) a minimally metamict core. Photomicrograph (a) is thin section W27-20 from the Persimmon Creek Gneiss in crossed-polarized light, and (b) is thin section C17-3 from the Otto Formation in crossed-polarized light.

minerals, do not permit recalculation of a reasonable structural formula (Deer et al. 1986, Ercit 2002). Since the allanite cores in the metasedimentary rocks at Coweeta are of detrital origin, they have already survived one pass through the sedimentary cycle. The rims on the cores likely formed during the most recent episode of metamorphism (Taconic Orogeny), and thus are younger than the cores. The allanite cores may weather preferentially to the rims because they are older, and likely more metamict, than the rims (Frondel 1964), rather than containing more REE (Hata 1939, Frondel 1964). If so, then the temperature of the amphibolite facies metamorphism in the study area during the Taconian Orogeny was not sufficiently high (<600° C; e.g., Frondel 1964, Janeczek and Eby 1993) to anneal the detrital allanite. This is consistent with the bedrock of Coweeta being in lower to middle amphibolite facies metamorphic conditions (Hatcher 1988). Nonetheless, with the exception of uncommon allanite grains in the Persimmon Creek Gneiss, allanite cores and rims are usually anisotropic in thin section.

Both the Otto Formation and Coweeta Group rocks contain epidote grains that are relatively stable in the regolith (Figure 19). For example, based on REE contents, the Ridgepole Mountain Formation contains both epidote and allanite (Figure 14). Microscopically, the epidote typically does not contain an allanite core (with the exception of the Persimmon Creek Gneiss; Figure 14), although an epidote grain with a thin (approximately 3 μm) rim that is also epidote has been noted (Figure 20). Epidote at Coweeta is characterized as being relatively unweatherable, and persists into the solum (Figures 19 and 20). These observations support the relative stability of epidote in a weathering environment (e.g., Allen and Hajek 1995, Lång 2000), and demonstrate the danger of invoking epidote weathering without mineralogic observations (e.g., Warfvinge

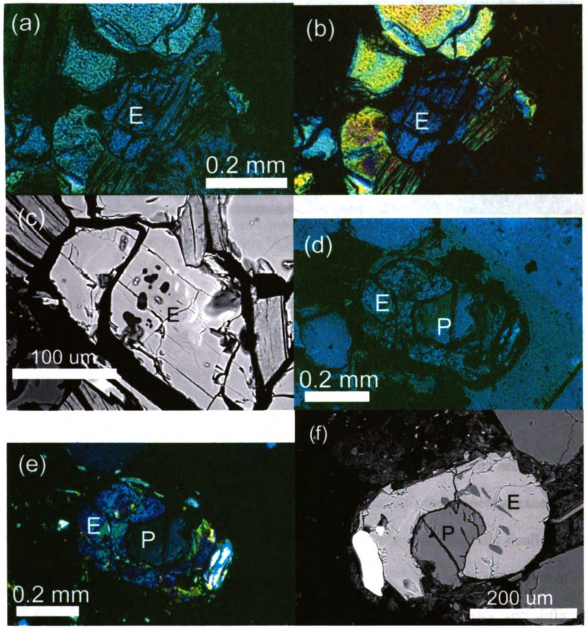

Figure 19. Examples of epidote (E) grains found in the solum at Coweeta. Note absence of allanite core. Small dark inclusions in BSE images are quartz. Otto Formation B horizon sample W2-12 in plane-polarized light (a), crossed-polarized light (b), and BSE (c). Coleman River Formation A horizon sample LSS27-1 with epidote surrounding a plagioclase (P) grain in plane-polarized light (d), crossed-polarized light (e), and BSE (f).

and Sverdrup 1992, Sverdrup and Warfvinge 1993, 1995). However, solum epidote grains at Coweeta often have etch pits. The etch pits are not widespread but do provide information on the crystal-chemistry of epidote group minerals during weathering. For

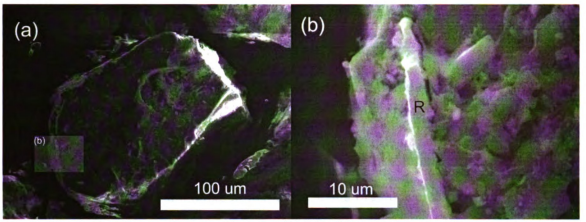

Figure 20. An epidote grain (a) with a rim (R) of epidote (b). Inset of image (a) is image (b). Otto Formation B horizon sample W2-12.

this reason, observations of epidote weathering are included in the investigation of allanite weathering. Because allanite and epidote are isostructural, they provide complementary data on the nature of weathering of epidote group minerals at Coweeta.

The Crystal-Chemistry of Epidote Group Mineral Weathering at the Coweeta Hydrologic Laboratory

Allanite weathering at Coweeta is rapid, with complete dissolution occurring below the weathering front and prior to the weathering of any other minerals, except perhaps biotite. Furthermore, both allanite and epidote grains are generally small (<200 μm), anhedral, and present in very low abundances. These factors make separation of epidote group mineral grains, as well as interpretation of crystal-chemistry, very difficult.

Although obtaining relatively large subhedral to euhedral epidote and allanite grains that may be oriented crystallographically is not possible for Coweeta, evaluating the crystal-chemistry of epidote-group minerals may provide insight into this process. The epidote structure contains continuous chains of AlO_6 and $AlO_4(OH)_2$ octahedra oriented parallel to the b-axis, and cross-linked by SiO_4^{4-} groups and $Si_2O_7^{6-}$ dimers (Figure 12). This cross-linking produces large aligned interchain cavities (the A sites that

contain Ca and REE) that form channels parallel to the octahedral chains (Dollase 1971, Deer et al. 1986, Kalinowski et al. 1998; Figure 12).

Crystallographic information may be combined with the results of low-temperature laboratory epidote dissolution experiments (Barman et al. 1992, Varadachari et al. 1992, Kalinowski et al. 1998). Laboratory epidote dissolution experiments have recently been conducted at a range of pH levels, using organic acids (Barman et al. 1992, Varadachari et al. 1992), inorganic acids (Kalinowski et al. 1998), and deionized water (Kalinowski et al. 1998). Despite the variability of experimental methods of these studies, they all agree that the solubilization of cations during epidote dissolution is crystallographically controlled and follows the order Ca > Si > Fe > Al, with the exception of studies that used oxalic, salicylic, or glycine acids (Schalscha et al. 1967, Barman et al. 1992), during which the relative solubilities of Fe and Al were reversed. As stated previously, Hata (1939) determined that allanite weathering started with dissolution of the rare earth elements, consistent with the work of Meintzer (1981) on allanite from the Virginia Blue Ridge. The rapid release of Ca from the epidote and the REE from allanite is attributed to its being located in the interchain tunnels, outside the octahedral chain (Barman et al. 1992, Kalinowski et al. 1998). The interchain tunnels provide uninhibited access by solvents (Barman et al. 1992), as well as an easy path for hydrated Ca and REE out of the crystal structure (Kalinowski et al. 1998). Kalinowski et al. (1998) also suggest that protonation of the Si-O-Al oxygens in the Si-dimers causes oxygens in the dimers to become less negative, reducing the attraction to the Ca, and facilitating release of the Ca. The Si-tetrahedra are only present as links between adjacent Al chains and are more readily removed from the structure than the Al located in

polymeric chains (Barman et al. 1992). In the experiment of Kalinowski et al. (1998) where deionized water of pH 5.6 was used as the solvent, which is most similar to natural weathering conditions, the reactor output solutions were saturated with respect to gibbsite, and as a result no residual surface layer could be calculated for the epidote surface. Based on molar-volume relationship calculations, Velbel (1993b) reports that epidote is not likely to form any type of clay protective surface coating.

Knowing that Ca, REE, and Si are the most easily solubilized cations in the epidote group mineral structure, and that the polymeric octahedral chains containing the Al and $Fe^{2+/3+}$ are very resistant to dissolution, the nature of etch pit formation on allanite and epidote grains during weathering should reflect these principles. It may be hypothesized that etch pits on epidote group mineral grains should be of two types: (1) large etch pits on (010) surfaces that deepen parallel to the octahedral chains (b-axis), and, hence, parallel to the perfect (001) cleavage, potentially with elongation parallel to the cleavage; and (2) small, shallow etch pits on all surfaces other than (010), which will be elongated parallel to the octahedral chains (b-axis) and also possibly cleavage, but deepening will be impeded by the presence of the polymeric chains.

Images of unweathered allanite are displayed in Figure 21, and, despite evidence of metamictization noted in thin section (i.e., pleochroic haloes in juxtaposed biotite, Figure 17), the basal cleavage is well developed (Figure 21(a)). Examples of the hypothesized two types of etch pits found on epidote group mineral grains from Coweeta are presented in Figures 22 and 23. The outline of six-sided "negative crystals" supports the larger pits forming on the more easily etched (010) surfaces (Figure 22). Etch pits with similar morphology to those pictured in Figure 22(b-c) have been illustrated and

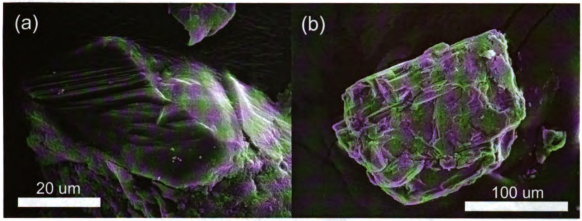

Figure 21. SEM images of unweathered allanite grains. Note perfect basal cleavage on grain in image (a). Both grains hand picked from Coleman River Formation sample C9-7.

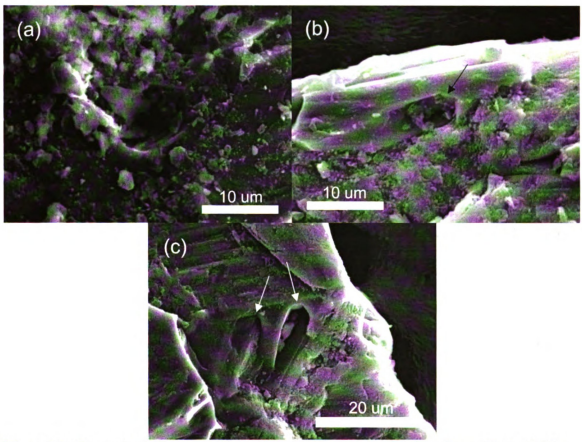

Figure 22. Examples of large etch pits on epidote group mineral surfaces, likely (010). The outline of the "negative crystals" supports the pits being on (010) surfaces, and elongate pits may be parallel to cleavage. Grains are epidote from Otto Formation sample W2-12 (a), and allanite from Coleman River Formation sample C9-7 (b and c).

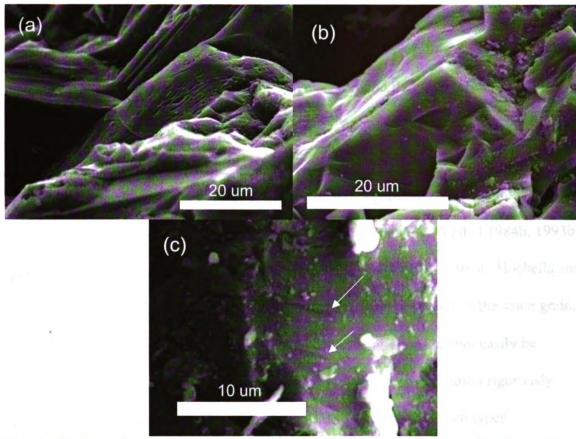

Figure 23. Examples of small, shallow etch pits on epidote group mineral surfaces other than (010). Note elongation of pits. Grains are allanite from the Coleman River Formation sample C9-7 (a) and (b), and epidote from Otto Formation sample W2-12 (c).

described for feldspars and termed "prismatic" etch pits (e.g., Wilson 1975, Keller 1976, 1978, Berner and Holdren 1977, 1979, Velbel 1986b). However, the prismatic etch pits on feldspars noted by these researchers formed by extensive deepening of an etch pit with a relatively small surface expression. That is not believed to be the case for the epidote group minerals of this study, because no etch pits were found which displayed a small surface opening, but with great visible depth.

The hypothesized two types of etch pits pictured in Figures 22 and 23 could be interpreted to simply reflect two different degrees of weathering, with the smaller etch

pits reflecting a lesser degree of weathering relative to the larger, negative-crystal etch pits that would form after more advanced weathering. However, this not believed to be the case for three reasons: (1) no etch pits have been found that may reflect an intermediate stage of weathering between the two types of etch pits pictured; (2) etch pits similar to the smaller etch pits of this study have been noted on minerals very resistant to weathering such as staurolite (Velbel et al. 1996), and negative-crystal etch pits have been noted on relatively weatherable minerals such as garnet (e.g., Velbel 1984b, 1993b) and plagioclase (e.g., Berner and Holdren 1977, 1979, Velbel 1983, 1986b, Hochella and Banfield 1995); and (3) both types have etch pits have been observed on the same grain, but on different surfaces. Although epidote group mineral grains cannot easily be oriented permitting the crystal-chemistry hypothesis of etch pit formation rigorously tested, etch pits on epidote group mineral grains do appear to be of two types.

Epidote Group Mineral Weathering at Coweeta Hydrologic Laboratory: Weathering Products

Although the allanite grains at Coweeta are very small and difficult to liberate and isolate from the incipiently weathered rock, several remarks about the weathering products of allanite dissolution may be made. Perhaps one of the important aspects of allanite weathering at Coweeta is the absence of weathering products. This differs from the weathering of primary REE-bearing accessory phosphate minerals such as apatite and monazite, which are associated with any of several secondary phosphates such as florencite and rhabdophane (e.g., Banfield and Eggleton 1989, Braun et al. 1998, Aubert et al. 2001). Figures 24 and 25 display a single allanite grain from the Persimmon Creek Gneiss in which several stages of weathering have been preserved, and which are summarized in Table 18.

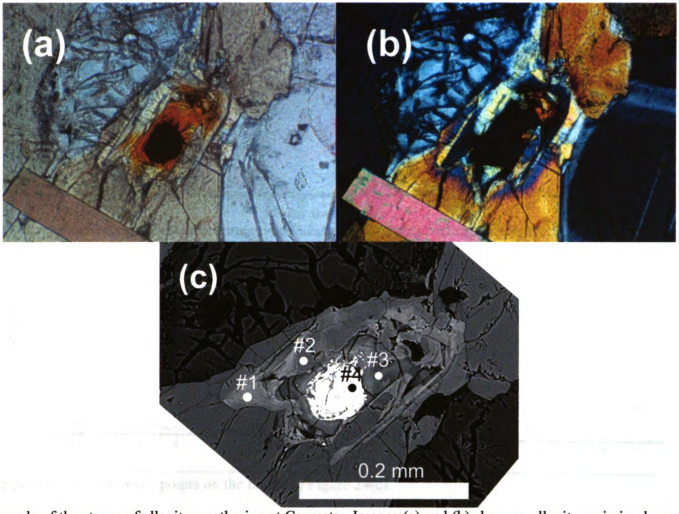

Figure 24. Example of the stages of allanite weathering at Coweeta. Images (a) and (b) show an allanite grain in plane-polarized light and cross polarized light, respectively, and (c) is a BSE image. Numbered points on the BSE image (c) correspond with the numbered EDS patterns in Figure 25. Sample W27-2 from the Persimmon Creek Gneiss.

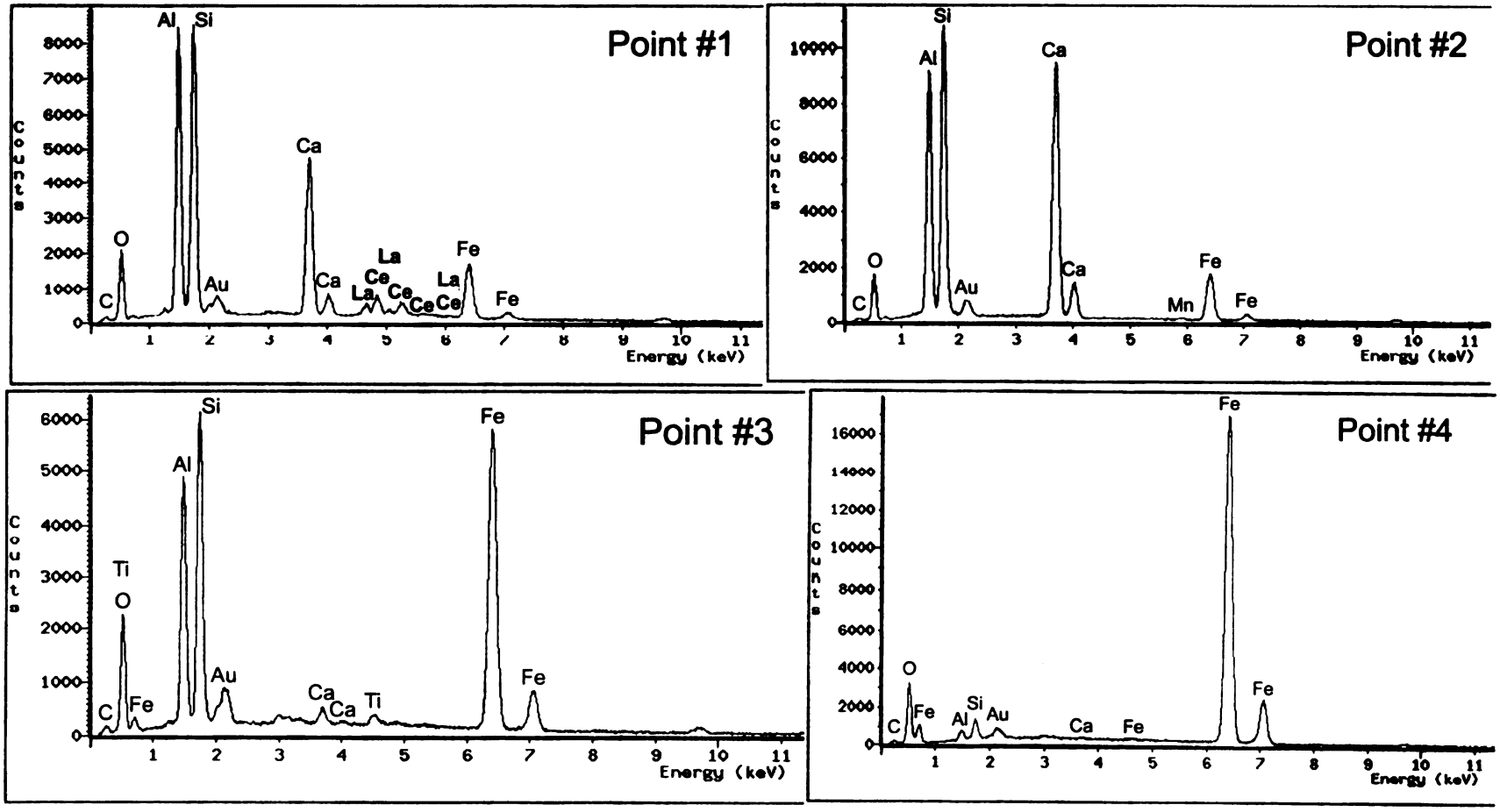

Figure 25. EDS patterns for numbered points on the image in Figure 24(c).

Table 18. Summary of epidote group mineral weathering as depicted in Figures 24 and 25.

Point #1	Point #2	Point #3	Point #4
Relatively unweathered high-REE allanite.	Relatively unweathered low-REE allanite.	Weathered allanite in which Ca is depleted and Fe enriched.	Nearly complete dissolution of allanite with retention of Fe (goethite).

There is preliminary evidence that carbonate may precipitate during allanite dissolution (Figures 26 and 27). As stated previously, with the exception of biotite, allanite is the first phase to weather at Coweeta, and it completely dissolves below the weathering front. Similar observations at other localities have been made by Goldich (1938) and Delvigne (1998). This incipient stage of weathering is certainly characterized by very low permeabilities, and likely a relatively high pH as allanite hydrolysis is a hydrogen consuming reaction. Relatively high pH conditions during allanite weathering are supported by the combined observations that Al is mobile during that time (e.g., Nagy 1995, Drever 1997a, Taylor and Eggleton 2001) and iron is precipitating (Figures 24 and 25; e.g., Schwertmann and Taylor 1995). That is, no gibbsite or kaolinite has been found associated with weathered allanite grains. Carbonate should be readily leached once continued mineral dissolution creates adequate porosity to remove the conditions conducive to carbonate precipitation (i.e., relatively high pH and low leaching). In laboratory experiments of epidote dissolution at pH 10.6, Nickel (1973) found that Ca was not readily released to solution. He invoked carbonate precipitation to explain his observations. SEM images of the suspect carbonate show a spar-like texture, and EDS spectra indicate the presence of Ca, Fe, and anomalously high C counts (Figures 26 and 27).

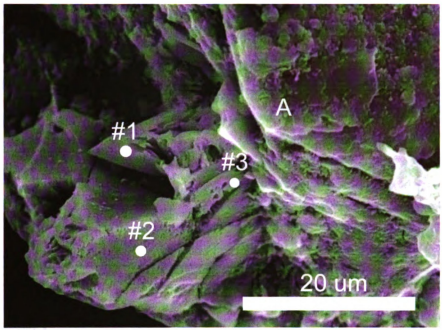

Figure 26. Suspect carbonate on the surface of a nearly fresh allanite (A) and undergoing dissolution. Note sparry nature of the portion of grain on which point #1 is located. Numbered points correspond to the numbered EDS patterns in Figure 27. Grain from the Coleman River Formation sample C9-7.

Discussion of Epidote Group Mineral Weathering at Coweeta Hydrologic Laboratory

The rate-determining step of the hydrolysis of silicate minerals during chemical weathering occurs by one of three mechanisms: (1) transport control in which either transport of solvents to, or products from, the dissolving mineral is rate-limiting; (2) interface control whereby the detachment of ions or molecules from the mineral surface is rate-limiting; or (3) a combination of transport and interface control (Berner 1978, 1981, Blum and Lasaga 1987, Schott and Petit 1987, Velbel et al. 1996). In pure transport-controlled dissolution ions are detached so rapidly from the surface of a crystal that they become concentrated in the solution adjacent to the mineral surface (Berner 1978, 1981). As a result, dissolution is regulated by transport of these ions via advection

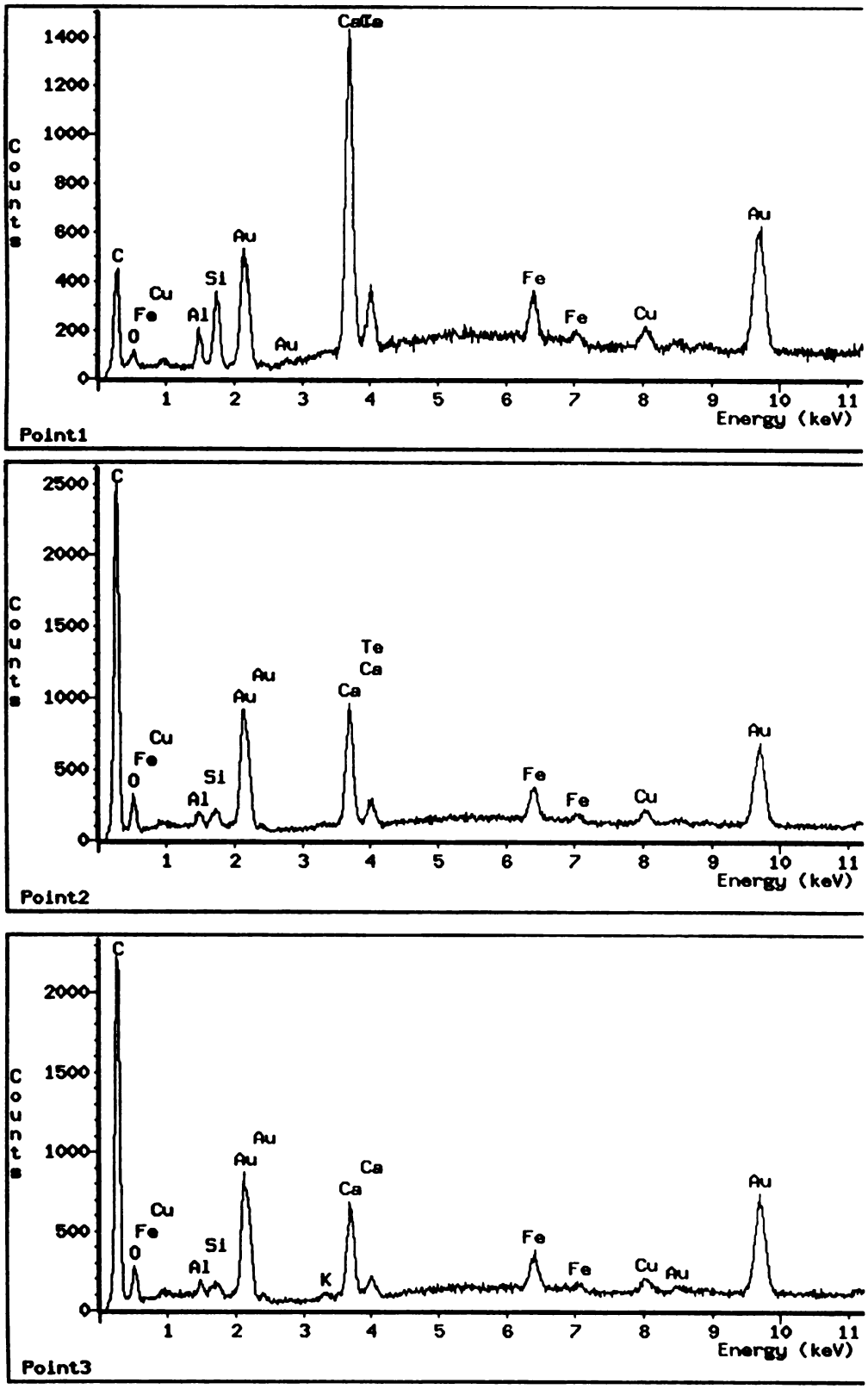

Figure 27. EDS spectra from numbered points in Figure 26. Note high C, Ca, and Fe on EDS spectra. Sample is gold coated (not carbon) and carbon counts usually do not exceed a few hundred.

or diffusion away from the mineral surface (Berner 1978, 1981). The surfaces of minerals dissolving by transport control are smooth, rounded, and featureless (Berner 1978, 1981, Velbel et al. 1996). In contrast, during pure interface-controlled dissolution, ion detachment from the mineral surface is so slow that transport of solutes away from the mineral prevents an increase in ion concentration adjacent to the crystal surface (Berner 1978, 1981, Schott and Petit 1987). Under such circumstances, increased advection or diffusion away from the mineral surface has no effect on the dissolution rate (Berner 1978, 1981). Interface-limited mechanisms result in etch pit formation on mineral surfaces, reflecting the site-selective nature of the interfacial reaction (Berner 1978, 1981, Blum and Lasaga 1987, Velbel et al. 1996).

The ubiquity of etch pits on the surfaces of epidote group minerals collected from Coweeta (Figures 22 and 23) indicates that epidote and allanite weathering occur by interface-controlled dissolution kinetics, like most silicate minerals (Berner 1978, Lasaga 1984, Schott and Petit 1987). This is consistent with the laboratory-determined activation energy for epidote dissolution being 83 kJ mol^{-1} (although this value was determined at pH 1.4; Rose 1991). Etch pit nucleation is favored on surface sites of excess strain energy, in highly undersaturated solutions (Blum and Lasaga 1987). Surface sites of excess energy include twin boundaries and intersections of dislocations with crystal surfaces (Berner 1978, 1981, Brantley et al. 1986, Blum and Lasaga 1987). The presence of line defects intersecting the mineral surface facilitates the migration of molecular water into the crystal (Schott and Petit 1987).

It should be recognized that allanite weathering is rapid, with complete dissolution occurring below the weathering front. The only other mineral displaying any

evidence of weathering during allanite dissolution is biotite, similar to other studies elsewhere (e.g., Delvigne 1998).

Allanite weathering may not have been previously recognized at Coweeta and elsewhere for the following reasons:

(1) Allanite grains are small and occur as accessory phases in unweathered rock. Even if recognized, their small abundances may preclude them from being included with other weatherable minerals that occur in much larger quantities (e.g., plagioclase and biotite).

(2) Allanite may not be distinguishable from epidote in thin section, as is the case in unweathered bedrock at Coweeta. Epidote is generally regarded as being relatively unweatherable, and may be compared to quartz and zircon (e.g., Allen and Hajek 1995, Lång 2000). This is especially true if epidote group minerals are identified in the bedrock, with epidote being noted in the solum. Such observations could easily lead to the conclusion that the epidote group minerals noted in the bedrock are actually epidote, and are relatively unweatherable.

Summary and Conclusions

Allanite and epidote are both present at Coweeta and are indistinguishable petrographically. The only exception is rare epidote-allanite rim-core pairs in the Persimmon Creek Gneiss, in which the allanite may also be sufficiently metamict to be optically isotropic. In general, the Coweeta allanite contains relatively low abundances of REE, and the older allanite cores are more weatherable than the younger allanite rims. Allanite weathering is so rapid that complete dissolution occurs below the weathering front. During allanite weathering Al is mobile and Fe precipitates as goethite. Allanite

weathering is likely accompanied by low permeability and relatively high pH, yielding conditions favorable for carbonate precipitation. With progressive weathering the carbonate is dissolved.

Epidote weathering at Coweeta is much slower than that of allanite, and the epidote persists into the solum with only minor evidence of weathering. Both allanite and epidote weather by interface-limited kinetics, as evidenced by the presence of etch pits on grain surfaces.

CHAPTER 6

RECOGNITION OF A CALCIUM PROBLEM AT THE COWEETA HYDROLOGIC LABORATORY: BULK MAJOR ELEMENT ANALYSES AND THE ISOVOLUMETRIC APPROACH TO WEATHERING

Stream Water Chemistry

The nature of the calcium problem in streams draining silicate terrains has been discussed above. There is little evidence for the calcium problem at Coweeta in older treatments (i.e., Velbel 1992) or in this work (Tables 19 and 20). The only watershed in which the Ca/Na ratio of the stream water substantially exceeds that of the plagioclase stoichiometry is W27 (Table 20). Watershed 27 experienced partial defoliation by fall cankerworm from 1972 to 1979 (Swank and Crossley 1988), which may in part explain the excess Ca. However, W36 was also partially defoliated by fall cankerworm, but only from 1975 to 1979 (Swank and Crossley 1988); the duration of defoliation in W36 may not have been of sufficient duration or extent to result in Ca loss from biomass. Watershed 27 is underlain by the three different lithostratigraphic units of the Coweeta Group. If the Ca/Na ratio of Ridgepole Mountain Formation andesine is used (0.56; Tables 19 and 20) for the watersheds underlain by Coweeta Group bedrock, then any evidence of a calcium problem at Coweeta is eliminated. Therefore, the stream waters of watersheds underlain by Coweeta Group rocks may reflect a combination of elemental contributions from the different lithostratigraphic units present beneath the watershed. In general, the stream water chemistry at Coweeta does not reflect the need to invoke an additional source of Ca. These results include additional microprobe analyses and are consistent with previous findings (i.e., Velbel 1992).

Table 19. Plagioclase compositions for the four lithostratigraphic units found at the Coweeta Hydrologic Laboratory based on the EMPA data of this study (Tables 13, 14, 15, and 16).

Lithostratigraphic Unit	Plagioclase Structural Formula
Otto Formation	$Ca_{0.28}Na_{0.72}Al_{1.28}Si_{2.72}O_8$
Persimmon Creek Gneiss	$Ca_{0.29}Na_{0.71}Al_{1.29}Si_{2.71}O_8$
Coleman River Formation	$Ca_{0.30}Na_{0.70}Al_{1.30}Si_{2.70}O_8$
Ridgepole Mountain Formation	$Ca_{0.36}Na_{0.64}Al_{1.35}Si_{2.65}O_8$

Table 20. Comparison of Ca/Na ratios for stream water from undisturbed control watersheds and plagioclase feldspar stoichiometry (Table 19). Stream flux data from Swank and Waide (1988).

Water-shed	Bed-rock[1]	Stream Flux (mol ha^{-1} yr^{-1})		Ca/Na				
					Plagioclase Feldspar			
		Ca	Na	Stream	Otto Formation	Persimmon Creek Gneiss	Coleman River Formation	Ridgepole Mountain Formation
2	OF	45.4	359.3	0.13	0.39			
14	CG	36.2	183.6	0.20		0.41	0.43	0.56
18	OF	75.6	293.6	0.26	0.39			
27	CG	87.1	170.1	0.51		0.41	0.43	0.56
32	CG	99.8	258.4	0.39		0.41	0.43	0.56
34	OF	122.8	323.6	0.38	0.39			
36	OF	159.7	430.6	0.37	0.39			

[1]OF=Otto Formation, and CG=Coweeta Group

Bulk Major Element Chemistry

Bulk major element analyses of rock, saprolite, and soil at Coweeta have been acquired by Berry (1976), and the data evaluation conducted here is based exclusively on his data (Tables 10 and 11). Berry provides chemical data of cuttings collected during a regolith coring investigation, and includes bulk density measurements (please see Figure 2 for core locations). As there is insufficient data from a single core to gain insight into weathering trends at a single location, all chemical data, along with the respective bulk density measurements, have been combined. In doing so, a landscape-scale assessment of the chemical weathering of heterogeneous bedrock has been completed for the

geographic area defined by the individual core and well locations. This geographic area may be generalized as the northern Coweeta Basin (Figure 2).

Figure 28 displays the empirical reaction progress diagrams for elements analyzed by Berry (1976). The reaction progress diagrams indicate that SiO_2 has experienced the greatest losses from the regolith, and that Al is mobile. Furthermore, Mg and K behave similarly in the profile, as do Na and Ca. Based on petrographic observations, the paired losses of Mg and K reflect biotite dissolution, and the paired losses of Na and Ca reflect plagioclase dissolution. These elemental loss patterns are similar to those reported for granite saprolite in the South Carolina Piedmont/Coastal Plain transition by Gardner et al. (1978) using similar methods.

Recognition of the Calcium Problem

With the concentrations of major elements being volumetric, mass balance methods may be used to investigate element mobility. However, because the mass balance is based on the bedrock and saprolite bulk chemistry, it will reflect the elements that remain in the weathering profile. This contrasts with solutes in ground waters or surface waters, which reflect what is lost from the regolith. Because plagioclase dissolution is the most important weathering reaction in silicate-dominated natural hydrologic systems (Bowser and Jones 1993, 2002; Drever 1997b, Jacobson et al. 2003), the mass balance will be performed for the stage of weathering that begins with the onset to weathering and ends with the loss of plagioclase. From Figure 28(d), this stage starts with a bulk density of 2.92 g cm^{-3}, and ends at approximately bulk density 2.25 g cm^{-3}. For the calculations, the mineralogic compositions are averages for Coweeta based on

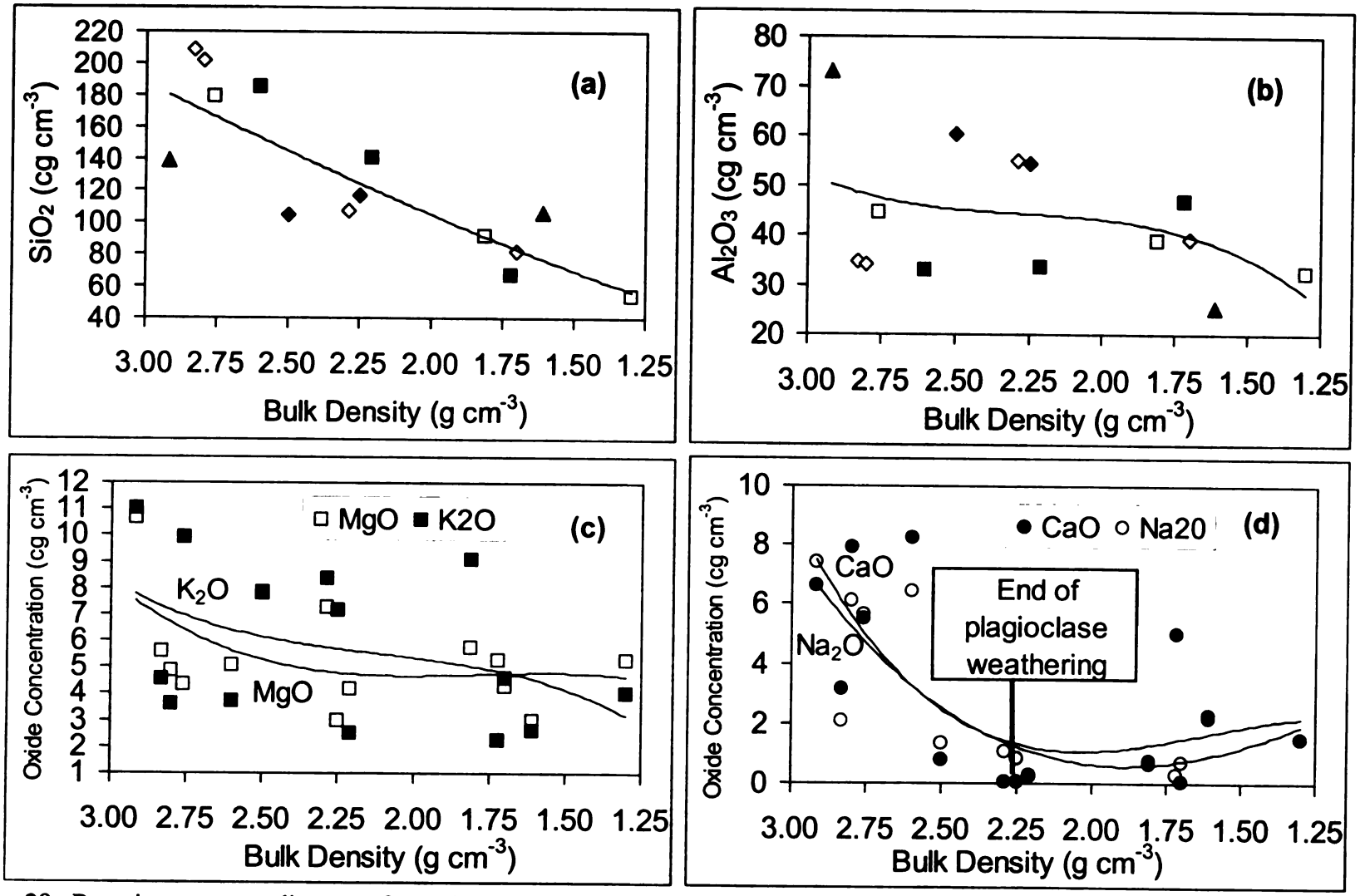

Figure 28. Reaction progress diagrams for major element oxides of bedrock and saprolite at Coweeta. SiO_2 (a), Al_2O_3 (b), K_2O and MgO (c), and CaO and Na_2O (d).

electron microprobe analyses (Tables 13, 14, 15, 16, and 21), and the specific gravities of the minerals are from Klein and Hurlbut (1999) (Table 22).

Table 22 provides an initial attempt on a solid phase mass balance (please see Appendix C for examples of the calculations). In Table 22 the loss of K and Mg attributable to biotite weathering is assumed to be stoichiometric (e.g., Swoboda-Colberg and Drever 1993, Murphy et al. 1998, Jeong and Kim 2003). For this initial balance the modal abundance of garnet lost is assumed to be 0.7%, with garnet ranging from 0 to 8%

Table 21. Average compositions of minerals used in the solid phase mass balance. Compositions calculated from electron microprobe analyses of this study.

Mineral	**Average Coweeta Composition**
Plagioclase	$Ca_{0.30}Na_{0.70}Al_{1.30}Si_{2.70}O_8$
Biotite	$K_{0.89}Na_{0.04}(Mg_{1.44}Fe^{II}_{1.05}Al_{0.29})^{VI}(Al_{1.24}Si_{2.76})^{IV}O_{10}(OH)_2$
Garnet	$Ca_{0.31}Mg_{0.33}Mn^{II}_{0.41}Fe^{II}_{1.94}Al_2Si_3O_{12}$

in the Coweeta bedrock (Table 4). Table 22 indicates that in order for the modeled Na loss to equal the amount lost as determined from the bulk chemistry, plagioclase dissolution would have to account for approximately 25% by volume of the mass lost. This is a realistic value, as reported modal abundances of plagioclase in Coweeta bedrock range from 8 to 36% (Tables 4 and 22). Similarly, based on a balance for K, the amount of biotite lost due to weathering would be approximately 7%, with the range of abundance at Coweeta ranging from 9 to 20%.

From the initial solid phase mass balance in Table 22 Mg and Ca are not balanced. The negative Mg value indicates that too much is being lost, whereas the positive Ca value indicates that not enough Ca is being lost from the weathering profile. Table 23 provides the results of the mass balance calculations where an attempt was made to balance Mg by reducing the amount of modal garnet lost. However, even at no

Table 22. Results of initial solid phase mass balance calculations using the volumetric concentration of saprolite bulk chemistry. In this scenario biotite weathering is occurring stoichiometrically with respect to Mg and K (i.e., Mg/K = 1.44/0.89).

Mineral	Atomic Weight (g mol^{-1})[1]	Specific Gravity (g cm^{-3})[2]	Modal Abundance Range (%)[3]	Modal Abundance Mean (%)	Modal Abundance Lost in Model (%)	Na (mol m^{-3})	K (mol m^{-3})	Mg (mol m^{-3})	Ca (mol m^{-3})
Plagioclase	267.0	2.66	8-36	13.2	25.07	-1748			-749
Biotite	442.2	3.00	9-20	12.3	7.27	-20	-439	-710	
Garnet	481.6	4.32	0-8	1.7	0.70			-21	-19
Totals						-1768	-439	-731	-769
Predicted from Bulk Chemistry						-1768	-439	-681	-1107
Difference						0	0	-50	339

[1]Atomic weight of mineral based on an average Coweeta composition presented in Table 21.
[2]Specific gravity of mineral taken from Klein and Hurlbut (1999).
[3]Range of modal mineral abundances in Coweeta bedrock are presented in Table 4.

Table 23. Results of solid phase mass balance calculations using the volumetric concentration of saprolite bulk chemistry. In this scenario biotite weathering is occurring stoichiometrically with respect to Mg and K (i.e., Mg/K = 1.44/0.89). Note that Mg cannot be made to balance even with no modal loss of garnet.

Mineral	Atomic Weight ($g\ mol^{-1}$)[1]	Specific Gravity ($g\ cm^{-3}$)[2]	Modal Abundance Range (%)[3]	Modal Abundance Mean (%)	Modal Abundance Lost in Model (%)	Na ($mol\ m^{-3}$)	K ($mol\ m^{-3}$)	Mg ($mol\ m^{-3}$)	Ca ($mol\ m^{-3}$)
Plagioclase	267.0	2.66	8-36	13.2	25.07	-1748			-749
Biotite	442.2	3.00	9-20	12.3	7.27	-20	-439	-710	
Garnet	481.6	4.32	0-8	1.7	0.00			0	0
Totals						-1768	-439	-710	-749
Predicted from Bulk Chemistry						-1768	-439	-681	-1107
Difference						0	0	-29	358

[1]Atomic weight of mineral based on an average Coweeta composition presented in Table 21.
[2]Specific gravity of mineral taken from Klein and Hurlbut (1999).
[3]Range of modal mineral abundances in Coweeta bedrock are presented in Table 4.

modal loss of garnet there is still an excess of Mg being lost from the weathering profile. No modal loss of garnet implies that garnet is not weathering at Coweeta, which is inconsistent with microscopic observations. In order to obtain a Mg balance garnet would need to form in the weathering profile. Again, this is a geochemically unreasonable result.

The need for retention of Mg in the weathering profile likely reflects nonstoichiometric release of Mg and K from biotite (e.g., Lin and Clemency 1981, Turpault and Trotignon 1994, Kalinowski and Schweda 1996, Murakami et al. 2003). In Table 24 the ratio of Mg/K release from Coweeta biotite has been lowered (1.339/0.89) relative to the stoichiometric ratio of Mg/K (1.44/0.89; Tables 22 and 23). Also in Table 24 the modal abundance of garnet lost has been returned to 0.7%. By reducing the proportion of Mg released relative to K from biotite during weathering the Mg can now be balanced (Table 24). However, a large abundance (339 mol m^{-3}) of Ca still has not been accounted for (Table 24).

By continuing to reduce the proportion of Mg released relative to K from biotite during weathering the imbalances of both Mg and Ca can be made to equal one another (Table 25). If the Ca imbalance in the solid phase mass balance is simply the result of insufficient loss of garnet, then the modal abundance of garnet lost should now be able to be increased and a balance achieved for both Mg and Ca. With a small decrease in the Mg/K ratio of biotite weathering, and a substantial increase in the modal abundance of garnet lost, a balance can be achieved for all of the base cations in the solid phase mass balance (Table 26). However, the modal abundance of garnet lost required to achieve this balance is almost 13% (Table 26). This garnet loss is geochemically unreasonable

Table 24. Results of solid phase mass balance calculations using the volumetric concentration of saprolite bulk chemistry. In this scenario biotite weathering is occurring nonstoichiometrically with an Mg/K release ratio of 1.339/0.89. Note that Mg has been made to balance, but there is still an unrecognized source of Ca.

Mineral	Atomic Weight ($g\ mol^{-1}$)[1]	Specific Gravity ($g\ cm^{-3}$)[2]	Modal Abundance Range (%)[3]	Modal Abundance Mean (%)	Modal Abundance Lost in Model (%)	Na ($mol\ m^{-3}$)	K ($mol\ m^{-3}$)	Mg ($mol\ m^{-3}$)	Ca ($mol\ m^{-3}$)
Plagioclase	267.0	2.66	8-36	13.2	25.07	-1748			-749
Biotite	442.2	3.00	9-20	12.3	7.27	-20	-439	-660	
Garnet	481.6	4.32	0-8	1.7	0.70			-21	-19
Totals						-1768	-439	-681	-769
Predicted from Bulk Chemistry						-1768	-439	-681	-1107
Difference						0	0	0	339

[1]Atomic weight of mineral based on an average Coweeta composition presented in Table 21.
[2]Specific gravity of mineral taken from Klein and Hurlbut (1999).
[3]Range of modal mineral abundances in Coweeta bedrock are presented in Table 4.

Table 25. Results of solid phase mass balance calculations using the volumetric concentration of saprolite bulk chemistry. In this scenario biotite weathering is occurring nonstoichiometrically with an Mg/K release ratio of 0.651/0.89. Note that the differences in Mg and Ca are equal.

Mineral	Atomic Weight (g mol^{-1})[1]	Specific Gravity (g cm^{-3})[2]	Modal Abundance Range (%)[3]	Modal Abundance Mean (%)	Modal Abundance Lost in Model (%)	Na (mol m^{-3})	K (mol m^{-3})	Mg (mol m^{-3})	Ca (mol m^{-3})
Plagioclase	267.0	2.66	8-36	13.2	25.07	-1748			-749
Biotite	442.2	3.00	9-20	12.3	7.27	-20	-439	-321	
Garnet	481.6	4.32	0-8	1.7	0.70			-21	-19
Totals						-1768	-439	-342	-769
Predicted from Bulk Chemistry						-1768	-439	-681	-1107
Difference						0	0	339	339

[1]Atomic weight of mineral based on an average Coweeta composition presented in Table 21.
[2]Specific gravity of mineral taken from Klein and Hurlbut (1999).
[3]Range of modal mineral abundances in Coweeta bedrock are presented in Table 4.

Table 26. Results of solid phase mass balance calculations using the volumetric concentration of saprolite bulk chemistry. In this scenario biotite weathering is occurring nonstoichiometrically with an Mg/K release ratio of 0.608/0.89. Note that Mg and Ca are now balanced, but with a modal garnet loss of almost 13%.

Mineral	Atomic Weight (g mol^{-1})[1]	Specific Gravity (g cm^{-3})[2]	Modal Abundance Range (%)[3]	Modal Abundance Mean (%)	Modal Abundance Lost in Model (%)	Na (mol m^{-3})	K (mol m^{-3})	Mg (mol m^{-3})	Ca (mol m^{-3})
Plagioclase	267.0	2.66	8-36	13.2	25.07	-1748			-749
Biotite	442.2	3.00	9-20	12.3	7.27	-20	-439	-300	
Garnet	481.6	4.32	0-8	1.7	12.86			-381	-358
Totals						-1768	-439	-681	-1107
Predicted from Bulk Chemistry						-1768	-439	-681	-1107
Difference						0	0	0	0

[1]Atomic weight of mineral based on an average Coweeta composition presented in Table 21.
[2]Specific gravity of mineral taken from Klein and Hurlbut (1999).
[3]Range of modal mineral abundances in Coweeta bedrock are presented in Table 4.

considering that the modal range of garnet in Coweeta bedrock is 0 to 8%, averaging 1.7% (Tables 4 and 26).

By invoking nonstoichiometric dissolution of Mg and K during biotite weathering balances were achieved for all cations except Ca (Table 24). The 339 mol m^{-3} of Ca imbalance indicates that an additional source of Ca is present in the regolith, and that this Ca source is dissolving. Because the mass balance performed is for saprolite bulk densities less than 2.25 g cm^{-3}, the calculations only represent the lower-most (approximately 2 m) portion of the saprolite. The Ca source is also present at the onset of weathering, reflecting a source in the bedrock. Therefore, biomass and/or cation exchange cannot be invoked as Ca sources.

The additional Ca source in the bedrock has either not been previously recognized, or has been noted as being present but not observed weathering. Furthermore, this phase would have to be weathering at comparable rates to the minerals included in the mass balance above in order for its presence to be detected between weathering profile bulk densities of 2.92 and 2.25 g cm^{-3}. The reaction progress diagrams in Figure 28 are a combination of weathering profiles developed on Otto Formation and Coweeta Group lithostratigraphic units. However, the elevated Ca observed at the higher bulk densities is present in both Otto Formation and Coweeta Group samples, indicating that the unidentified Ca source is common to both lithostratigraphic units.

Interestingly, Taylor and Velbel (1991) performed solute-based watershed mass balance calculations on the seven control watersheds at Coweeta, and found that when solving a 3x3 matrix, Ca had to be eliminated from the calculations or unreasonable

results were obtained. Specifically, K, Mg, and Na had to be used in the matrix, because inclusion of Ca yielded a garnet weathering rate that reflects formation during weathering, rather than dissolution.

As discussed above, the previously unrecognized Ca-phase that is present in the bedrock and weathering rapidly is allanite. Apatite, too, is present at Coweeta, but occurs only in trace abundances (too uncommon to be point counted) in the Coweeta Group lithostratigraphic units. Apatite has only been identified in significant abundances in bedrock associated with the Shope Fork Fault. Furthermore, the scarce apatite grains that have been found as a part of this study lack any evidence of weathering. Velbel (personal communication 2002) reports that he observed a saprolite apatite grain using SEM that displayed only slight rounding. Hornblende has also been recognized at Coweeta, but is not present in any of the samples included in the reaction progress diagrams (Berry 1976). Therefore, for watersheds that do not include the Shope Fork Fault (i.e., the watersheds of this study) apatite is not likely to contribute significant Ca to pore and stream waters, and hornblende is not influential on the solid phase mass balance.

The importance of allanite as a Ca source in bedrock is presented in Table 27. Average Coweeta mineral compositions and modal abundances (Table 4) for allanite, garnet, and plagioclase have been used to calculate the relative contributions of each mineral to the Ca content of the bedrock. Note from Table 27, that despite constituting on average <1% of the bedrock by volume, allanite may contain 26% of the bedrock Ca. Furthermore, garnet only contains 8% of the total Ca in the Coweeta bedrock.

A final solid phase mass balance that includes allanite is presented in Table 28. With allanite included, this final mass balance now yields a balance for all cations. In

Table 27. Assessment of the allanite contribution to bedrock Ca at Coweeta Hydrologic Laboratory. Mineral compositions represent an average for Coweeta bedrock.

	Allanite	Garnet	Plagioclase
Specific Gravity ($g\ cm^{-3}$)	3.9[1]	4.32[1]	2.66[1]
Formula	$(Ca_{1.55}Mn_{0.01}Na_{0.07}Ce_{0.014})Fe_{0.49}$-$Mg_{0.05}Al_2O(Al_{0.13}Si_{0.87}O_4)(Si_2O_7)OH$	$Ca_{0.31}Mg_{0.33}Mn_{0.41}Fe_{1.94}Al_2Si_3O_{12}$	$Ca_{0.30}Na_{0.70}Al_{1.30}Si_{2.70}O_8$
Formula Weight	441.9	481.6	267.0
Modal Abundance (%)	0.9	1.7	13.2
Inverse Molar Volume ($mol\ m^{-3}$)	80.1	152.5	1314.9
Ca ($mol\ m^{-3}$)	160.1	47.3	394.5
Ca Fraction in Rock (%)	26	8	66

[1]Data from Klein and Hurlbut (1999).

Table 28. Results of solid phase mass balance calculations using the volumetric concentration of saprolite bulk chemistry. In this scenario biotite weathering is occurring nonstoichiometrically with an Mg/K release ratio of 1.002/0.89, and allanite has been included.

Mineral	Atomic Weight ($g\ mol^{-1}$)[1]	Specific Gravity ($g\ cm^{-3}$)[2]	Modal Abundance Range (%)[3]	Modal Abundance Mean (%)	Modal Abundance Lost in Model (%)	Na ($mol\ m^{-3}$)	K ($mol\ m^{-3}$)	Mg ($mol\ m^{-3}$)	Ca ($mol\ m^{-3}$)
Plagioclase	267.0	2.66	8-36	13.2	24.95	-1740			-745
Biotite	442.2	3.00	9-20	12.3	7.27	-20	-439	-494	
Garnet	481.6	4.32	0-8	1.7	6.10			-181	-170
Allanite	441.9	3.90	0.5-1.4	0.9	1.4	-8		-6	-192
Totals						-1768	-439	-681	-1107
Predicted from Bulk Chemistry						-1768	-439	-681	-1107
Difference						0	0	0	0

[1]Atomic weight of mineral based on an average Coweeta composition presented in Table 21, with average Coweeta allanite composition presented in Table 27.

[2]Specific gravity of mineral taken from Klein and Hurlbut (1999).

[3]Range of modal mineral abundances in Coweeta bedrock are presented in Table 4.

Table 28 the modal abundance lost of both garnet and allanite is relatively high, although still within the range reported in Table 4. Determination of representative modal abundances of Coweeta minerals is complicated by the heterogeneity of the bedrock.

Ciampone (1995) performed major element oxide analyses on saprolite and bedrock composite cuttings sampled during installation of the potable water well at Coweeta (Figure 2, Table 12). Originally, the water well was believed to have been drilled entirely into the Otto Formation to a depth of approximately 61 m (Ciampone 1995). However, based on the proximity of the well to the Shope Fork Fault (Figure 2) and the knowledge that the fault dips approximately 45° to the north (Hatcher 1980, personal communication 2001), the water well likely encounters the fault in the subsurface (Price and Velbel in review). Therefore, the Otto Formation occurs as the hanging wall in the upper portion of well, and the Coweeta Group occurs as the footwall in the deeper portions of the well. The schistose Otto Formation is significantly more micaceous than the gneisses of the Coweeta Group, and thence should be more K-rich. Figure 29 shows plots of K_2O (weight percent) and rubidium (ppm) vs. depth in the water well. Potassium and rubidium concentrations are notably higher above approximately 37 m depth than below, suggesting the transition from Otto Formation (above) to Coweeta Group rocks (below) across the subsurface expression of the Shope Fork Fault. The distinct enrichment of rubidium at approximately 37 m depth may indicate alteration along or adjacent to the shear zone.

The bulk chemistry of the water well samples (Table 12) provides an interesting and important data set, because petrographically allanite is absent in the water well samples. The absence of allanite in water well samples at distances greater than 20 m

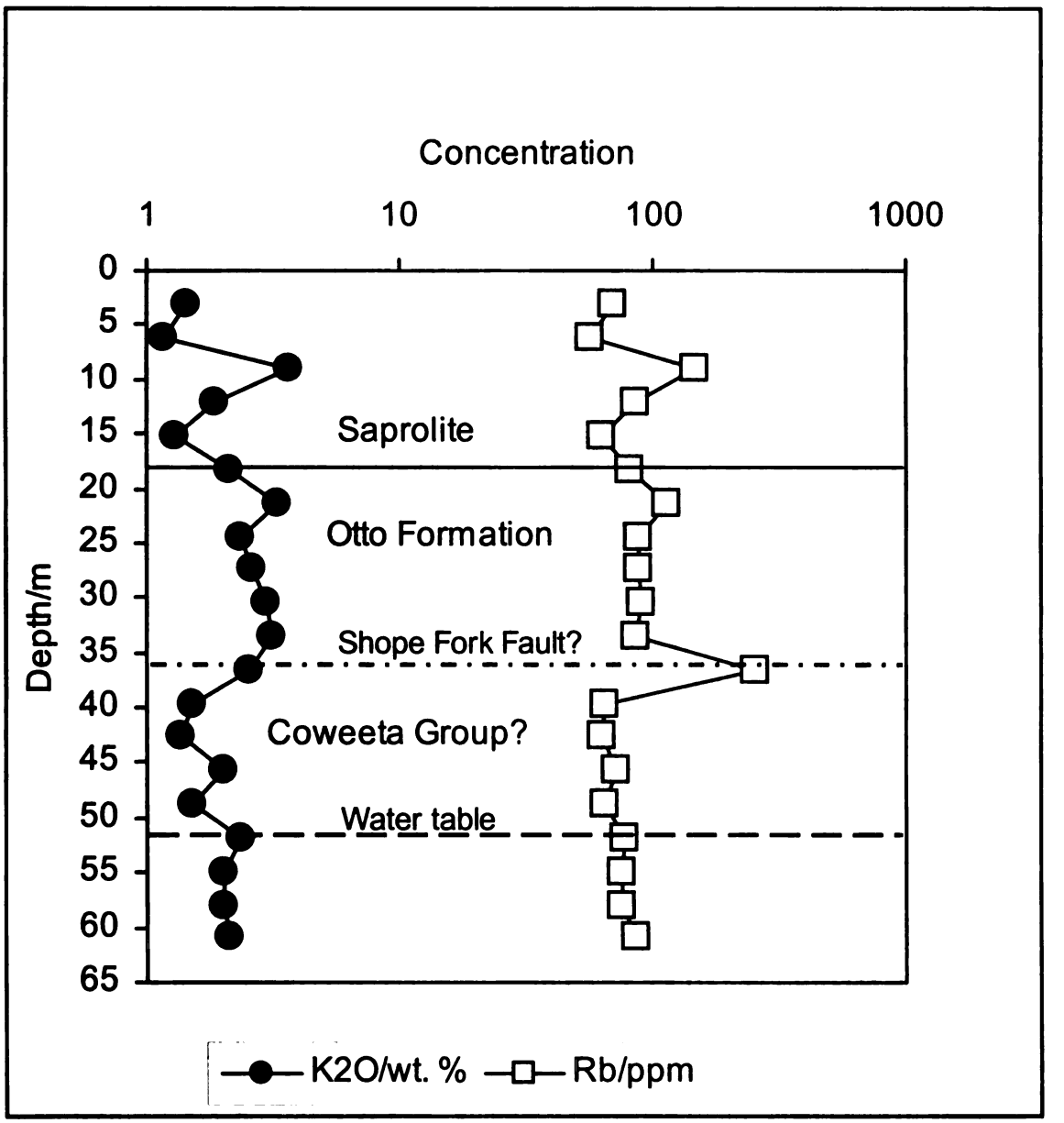

Figure 29. Plot of K_2O and rubidium vs. depth for the water well. Note decrease in K_2O and rubidium below 37 m depth. After Price and Velbel (in review), their Figure 2.

below the fault surface is interpreted to reflect an absence of allanite crystallization in the bedrock, rather than rapid dissolution during fault zone weathering. The water well samples provide a bulk chemistry that may be compared with the more allanite-rich samples collected by Berry (1976) (Figure 30). Bulk chemical analysis for a single Coweeta Persimmon Creek Gneiss bedrock sample is provided by Miller et al. (2000)

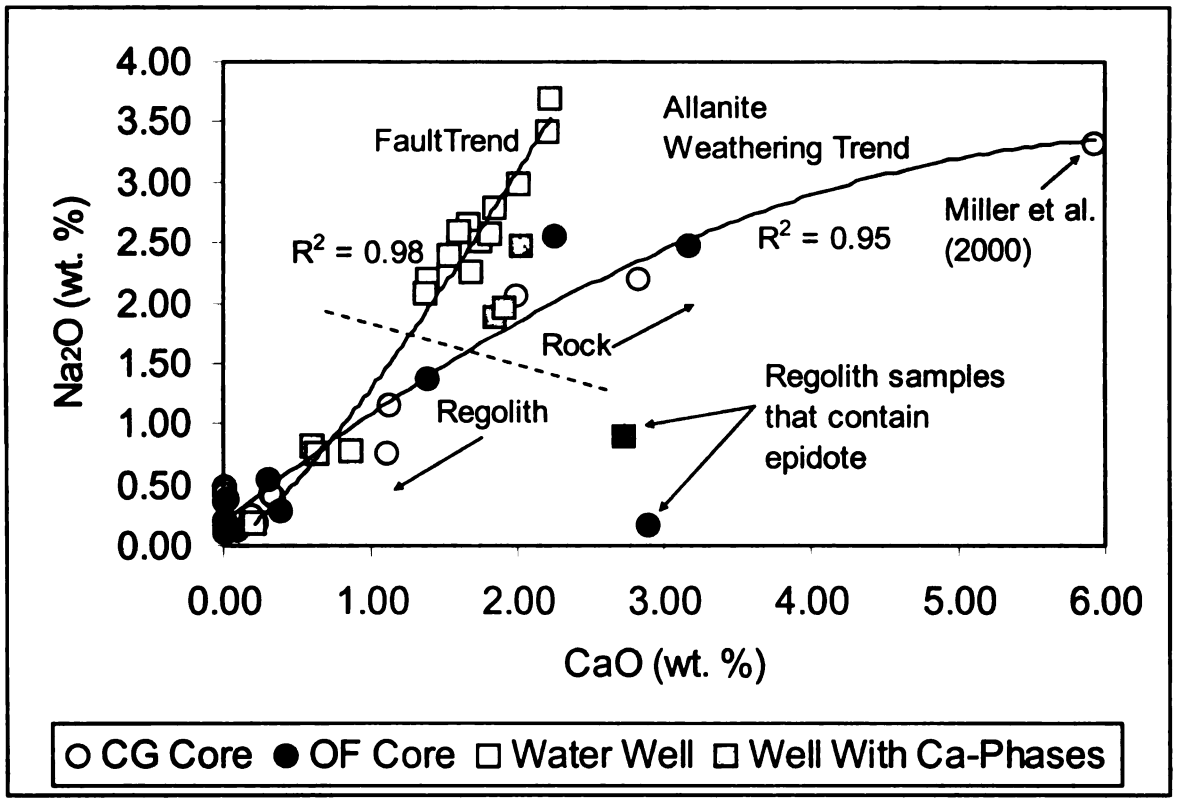

Figure 30. Comparison of the weathering of allanite-bearing bedrock with the weathering of bedrock that lacks epidote group minerals. CG=Coweeta Group and OF=Otto Formation.

(Figure 2). This sample is reported to be particularly high in epidote (Miller et al. 2000) and yields the highest CaO concentration reported for bedrock at Coweeta (Figure 30).

Two trends are visible in Figure 30: a "fault trend" composed of samples from the water well (Ciampone 1995), and an "allanite weathering trend" composed of samples from cores (Berry 1976) and published data on a Persimmon Creek Gneiss bedrock sample (Miller et al. 2000). The influence of garnet on the Ca concentration of the water well samples is negligible compared with that of plagioclase, as garnet occurs in such small quantities relative to plagioclase (Table 4). Therefore, the bulk Na_2O and CaO abundances of the fault trend bedrock samples predominantly reflect plagioclase stoichiometry, with a few exceptions (shaded boxes in Figure 30). These exceptions

contain small abundances of other Ca-bearing phase that include hornblende, calcite, and/or epidote group minerals. Despite this variety of Ca-bearing minerals, apatite was never found. Like many samples collected near the Shope Fork Fault, the mineralogy of these water well samples is anomalous, and may reflect high temperature chemical and mineralogic changes that occurred during mylonitization (Velbel 1985a, Price and Velbel in review). Regardless, water well bedrock samples that contain Ca-bearing minerals in addition to plagioclase and garnet plot towards the allanite weathering trend as a result of the increase in bulk Ca (Figure 30).

Allanite is a highly weatherable epidote group mineral, and is the dominant epidote group mineral at Coweeta. Here, allanite is completely dissolved below the weathering front, and before any other mineral starts to visibly weather, with the possible exception of biotite. Epidote is also present at Coweeta, but is relatively scarce, and, when present, is relatively unweatherable and persists into the solum. Two regolith samples in Figure 30 contain anomalously high Ca concentrations, and do not plot on the allanite weathering trend. From thin section, these two samples contain relatively small, but appreciable quantities of resistant epidote (Figure 30).

Discussion and Conclusions

Allanite weathering is an important Ca source at Coweeta that is readily lost from the bedrock during incipient weathering. However, stream solute chemistry does not reflect a need for an additional source of Ca; i.e., the calcium problem *stricto sensu* is not present at Coweeta. These observations indicate that on the time scales of plagioclase loss from a weathering profile (between regolith bulk densities 2.92 g cm^{-3} and 2.25 g cm^{-3}) Ca is removed from the Coweeta bedrock more so than is indicated by the stream

water for the period of sample. Two hypotheses may be posed to explain this phenomenon: (1) there is a Ca sink in the streams; or (2) the hydrogeochemical conditions that produced the lower saprolite are relict. It is not possible to resolve these apparent inconsistencies with the current data. Gardner (1992) reported a nearly identical observation, but with respect to Al, when comparing saprolites in Brazil and South Carolina with rivers draining these regions. He speculated that Al may precipitate when pH increased in response to degassing of dissolved CO_2 from soil water entering the streams. The molar ratio of bicarbonate to silica that would be expected from weathering reactions for a Georgia Piedmont meta-gabbro weathering profile are reported to be six times higher than the average ground water composition for the area (Schroeder et al. 2000). Schroeder et al. (2000) invoked solute contributions to ground water resulting from silicate weathering of felsic terrains to explain the disparity.

CHAPTER 7

CLAY GENESIS RATES FROM WATERSHED SOLUTE-BASED MASS BALANCE USING MAJOR AND RARE EARTH ELEMENTS: OTTO FORMATION WATERSHEDS 2 AND 34

Watershed Mass Balance and Rare Earth Elements

In order for the number of unknowns (mineral weathering rates) to equal the number of equations (i.e., the number of elements for which stream flux data are available), REE have been included in the mass balance calculations. Rare earth elements are useful in mass balance calculations because they are relatively mobile during weathering, as they are not contained in secondary minerals that remain stable during progressive weathering (e.g., Nesbitt 1979, Cramer and Nesbitt 1983, Banfield and Eggleton 1989, Braun et al. 1990, 1993, 1998 and references therein, Marker and De Oliveira 1990, Braun and Pagel 1994, van der Weijden and van der Weijden 1995, Koppi et al. 1996, Nesbitt and Markovics 1997). The only exception is Ce^{3+}, which oxidizes to Ce^{4+} in the weathering environment and precipitates as cerianite (CeO_2). The behavior of REE during weathering is discussed below.

Prior to performing mass balance calculations using REE, the following topics must be addressed: (1) atmospheric inputs of REE; (2) allanite and other potential mineralogic sources of REE; (3) the abundances of REE associated with vermiculite; (4) the role of REE-hosting secondary phosphate minerals; and (5) the conversion of one-time sampled REE concentrations in stream waters to a flux that approximates a longer term period of record.

Atmospheric Inputs of Rare Earth Elements

At Coweeta, atmospheric major element inputs, both dissolved and particulate, have been measured and subtracted from the stream solute flux data, yielding a stream flux value that reflects only the mineralogic contributions of major elements to surface water (Swank and Waide 1988, their Table 4.11). However, REE concentrations in wet and dry precipitation at Coweeta, or anywhere in the Southern Appalachians, have never been measured. Nevertheless, the atmospheric contribution of REE to Coweeta stream waters is believed to be negligible, for reasons outlined below.

In thick (greater than several meters), unpolluted weathering profiles, the dissolved REE distribution in stream waters will be controlled by bedrock weathering, and atmospheric REE contributions will not be detectable (Goldstein and Jacobsen 1988, Elderfield et al. 1990, Braun et al. 1998, Tricca et al. 1999, Probst et al. 2000, Aubert et al. 2001, 2002). Aubert et al. (2002) used Sr and Nd isotopes, combined with REE, from precipitation, throughfall, soil solutions, spring waters, and stream waters, to investigate the relative influences of mineral weathering and atmospheric inputs on the chemistry of natural waters sampled from catchments in France. They concluded that waters sampled from deeper in the weathering profile, and from streams and springs, have relatively long residence times in the regolith, and are sufficiently influenced by mineral weathering to overwhelm the atmospheric REE and isotopic signature. Similarly, Johannesson and Xiaoping (1997) state that the chemical weathering of rocks is the source of REE to natural terrestrial waters and, consequently, the REE signatures of the rocks can impart their REE signature to associated waters. Because Coweeta contains a thick regolith (on average 6 m, but up to 18m; Berry 1976, Ciampone 1995, Yeakley et al. 1998), the REE

input to natural soil and surface waters from mineral weathering should overwhelm atmospheric inputs. Furthermore, REE contributions to world oceans from rivers are one to two orders of magnitude greater than atmospheric inputs (Zhang and Nozaki 1996), and numerous weathering-related studies of surface water REE ignore precipitation inputs entirely, although this is not always stated explicitly (e.g., Braun et al. 1998, Sholkovitz et al. 1999, Åström 2001, Viers et al. 2000, Aubert et al. 2001).

Natural concentrations of REE in wet and dry precipitation are derived from alteration of the continental crust (Sholkovitz et al. 1993, Grousset et al. 1998, Greaves et al. 1999, Kreutz and Sholkovitz 2000). Rare earth element compositions for unpolluted continental precipitation are shown in Table 29, and are at least one order of magnitude lower in concentration than the Coweeta stream waters. Despite the values in Table 29 being reported as unpolluted, they likely contain pollutants. The REE concentrations reported by Sholkovitz et al. (1993) were collected at Woods Hole, Massachusetts, and Heaton et al. (1990) state that pollutant emissions generated in the Midwest are known to contribute pollutants to the northeast. Furthermore, France is also industrialized, making the REE precipitation concentration collected at the Vosges Catchment (Aubert et al. 2002) suspect of containing at least small quantities of pollutant REE. The REE precipitation concentrations in Table 29, are, therefore, regarded as maximum values for "unpolluted" precipitation. Rare earth element air pollutants may be derived from fossil fuel combustion (Olmez and Gordon 1985, Kitto et al. 1992, Kreutz and Sholkovitz 2000), industrial processes (Aubert et al. 2002), nuclear accidents and weapons testing (Aubert et al. 2002), and/or agricultural fertilizers produced from REE-rich phosphates

Table 29. Tabulation of REE concentrations in unpolluted continental precipitation. Only those REE used in this study have been included.

Study	This Study			Aubert et al. (2002)	Sholkovitz et al. (1993)		
Location	W2	W34	W27	Vosges Catchment, France	Woods Hole, Massachusetts		
Type of Sample	Stream	Stream	Stream	Filtered Rainwater	Filtered Rainwater	Rainwater Particles	Total
La (ppb)	0.08	0.04	0.1	0.0017	0.0012	0.0035	0.0048
Nd (ppb)	0.08	0.04	0.09	0.0008	0.0013	0.0030	0.0043
Gd (ppb)	0.02	0.01	0.02	0.0009	0.0004	0.0005	0.0008
Dy (ppb)	0.02	0.01	0.01	0.0015	0.0002	0.0004	0.0006

(Volokh et al. 1990). None of these potentially atmospheric polluting processes are present in the vicinity of, or upwind from, Coweeta in significant abundance, if at all, to influence atmospheric REE inputs into the watersheds of this study. However, it is recognized that future research involving REE in Coweeta mass balance calculations should include wet and dry precipitation REE analyses.

Allanite Weathering and Other Potential Mineralogic Sources of Rare Earth Elements

Allanite is the only accessory mineral that is weathering and present in significant quantities at Coweeta that contains REE. The abundance and ubiquity of allanite has been observed petrographically. The case for high weatherability of allanite is widespread in the literature (e.g., Goldich 1938, Meintzer 1981, Banfield and Eggleton 1989, Braun et al. 1993, Braun and Pagel 1994, Harlavan and Erel 2002), and allanite has been found to weather more rapidly than other accessory phases, such as apatite and sphene (Banfield and Eggleton 1989, Harlavan and Erel 2002). Apatite is routinely invoked as being the source of REE found in interstitial regolith waters, ground waters, and surface waters (e.g., Banfield and Eggleton 1989, Marker and De Oliveira 1990, Braun and Pagel 1994, van der Weijden and van der Weijden 1995, Braun et al. 1993, 1998, Tricca et al. 1999, Aubert et al. 2001, 2002, Harlavan and Erel 2002). However, at Coweeta, apatite is very rare, particularly in the Otto Formation, and is so scarce that no apatite was encountered during the point counting of bedrock thin sections. Microscopic observations, both optically and by SEM, do not support significant apatite loss during weathering. Velbel (personal communication 2002) reports that using SEM he observed a saprolite apatite grain that displayed only slight rounding. However, the reaction progress diagram for P_2O_5 (Figure 31) does show small losses of a phosphorus-bearing

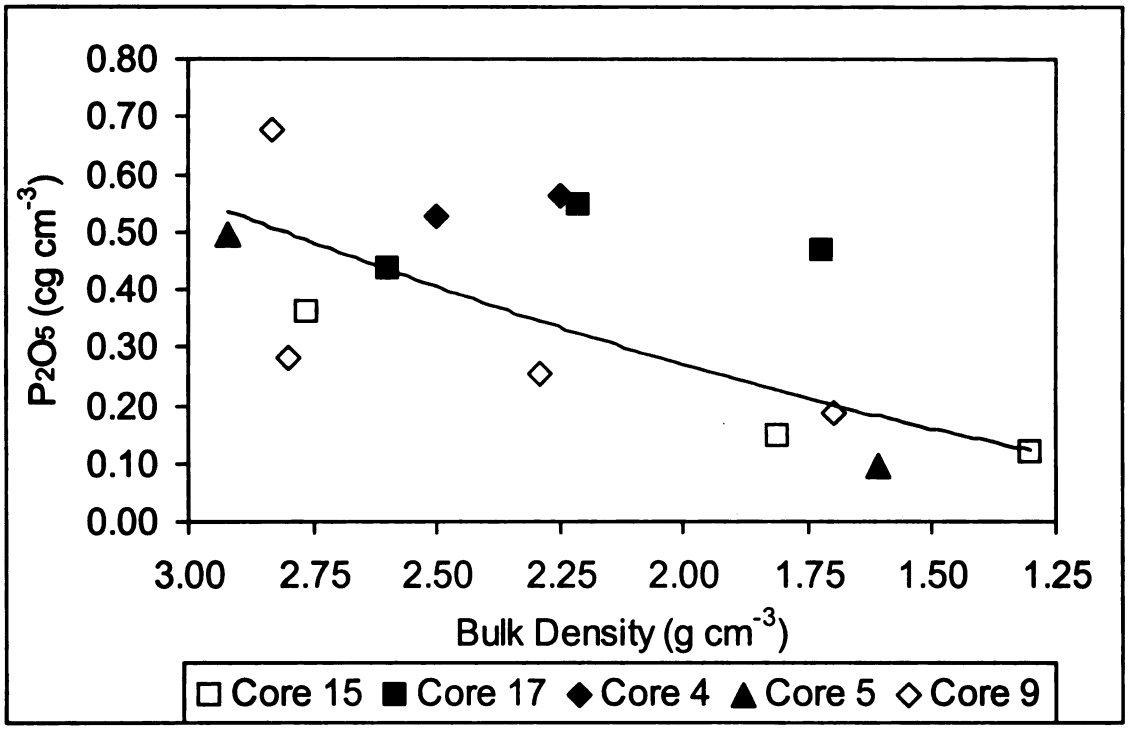

Figure 31. Empirical reaction progress diagram for P_2O_5 showing loss of phosphorus during saprolitization.

phase present in small pre-weathering abundances. The reaction progress diagram may exaggerate the actual losses of phosphorus during weathering because variscite has been identified in the clay-size fraction of incipiently weathered rock (see especially diffractogram for W27-25 in Appendix B). Such a concentration of phosphorus at the onset of weathering would result in the illusion of greater losses of P_2O_5 in the later stages of weathering. Even with this potential phosphorus enrichment during incipient weathering, the change in volumetric concentration of P_2O_5 from rock to top of saprolite is very small (approximately 0.4 cg cm^{-3}; Figure 31). Interestingly, the secondary phosphate present at Coweeta is variscite, not florencite and/or rhabdophane, which are typically found replacing apatite during weathering (e.g., Banfield and Eggleton 1989, Braun et al. 1998, Aubert et al. 2001). Even though very small abundances of apatite are

likely weathering, REE abundances in allanite are reported to be at least two orders of magnitude greater than in apatite (e.g., Gromet and Silver 1983, Grauch 1989, Harlavan and Erel 2002). Therefore, due to small abundances, combined with relatively slow weathering and low REE concentrations, apatite is not believed to be significant in the mass balance calculations for Coweeta. Small increases in apatite and calcite have been found to be associated with the Shope Fork Fault, but do not characterize the bedrock away from the fault.

Rare Earth Element Mobility and Vermiculite

Vermiculite is the only secondary mineral present in the Coweeta regolith that persists into the soil and contains appreciable abundances of REE, especially Ce, whether adsorbed (e.g., Marker and De Oliveira 1990) or providing charge balance in the interlayer (Duddy 1980). The REE concentration in vermiculite has been quantified by ICP-MS and is included in the mass balance calculations (Tables 13 and 14). Exclusion of the REE abundances in vermiculite yields geochemically unreasonable mass balance results and a warning from MATLAB® which reads, "Matrix is close to singular or badly scaled. Results may be inaccurate." The inability to achieve a geochemically reasonable mass balance when REE are not included in the vermiculite stoichiometry may be interpreted to indicate that the REE are not simply adsorbed onto the vermiculite surface, but help balance charge in the mineral structure. Previous studies have demonstrated that kaolinite (Nesbitt 1979, Duddy 1980, Braun et al. 1993), gibbsite, and goethite (Braun et al. 1993) do not host appreciable abundances of structural REE, but probably participate in cation exchange in relatively small, yet significant ways (e.g., Coppin et al. 2002). Regolith, soil solutions, and leachates sampled from upper soil horizons are strongly

depleted in REE, which is attributed to a reduction in pH with decreasing depth (Duddy 1980, Meintzer 1981, Braun et al. 1993, Mongelli 1993, Braun and Pagel 1994, Aubert et al. 2002). The increased solubility of REE with decreasing pH is well documented in the literature (e.g., Nesbitt 1979, Goldstein and Jacobson 1988, Elderfield et al. 1990, Johannesson and Xiaoping 1997, Gaillardet et al. 1997, Sholkovitz et al. 1993, 1999, Tricca et al. 1999 and references therein, Åström 2001, Aubert et al. 2001). However, for a soil extraction performed using pH values between 4.28 and 6.5, Land et al. (1999) found that the amount of extracted, adsorbed, or exchangeable REE increased exponentially with increasing pH. Velbel (1984a, 1985b) reports pH measurements of 6.12 and 5.10 for soil and well water, respectively, at Coweeta Watershed 6; at pH values of less than approximately 6, REE should be present mainly as free ions (Turner et al. 1981, Wood 1990, Smedley 1991). Moreover, the REE concentrations in acid natural waters are reported to be controlled by solid-liquid exchange reactions such as adsorption/desorption and/or ion exchange with secondary minerals, organic carbon, and colloids (Johannesson and Xiaoping 1997 and references therein, Braun et al. 1993, 1998 and references therein, Land et al. 1999, Ingri et al. 2000). The above discussion demonstrates that at the pH levels of Coweeta waters, if all the REE, with the exception of Ce, are not present in solution as free ions, then their concentration will be influenced by cation exchange. As stated above, cation exchange is only a concern for mass balance studies if there is mixing of waters of different chemistries or a temporal change in water chemistry (Drever 1997b, Bowser and Jones 2002), which is not likely at Coweeta.

Gadolinium, unlike any other REE, has been found to be contained exclusively in the dissolved load of Rhine River samples in France (Tricca et al. 1999). These same

researchers also did not find any evidence of changes in REE fractionation when ground water entered the streams of small watersheds. In other words, the REE chemistry of streams draining small watersheds is identical to that of the pore waters of the weathering profile and hence streams contain an unmodified REE weathering signature. Velbel (1984a, 1985b) arrived at the same conclusion at Coweeta with respect to the major element geochemistry (his Table 3-1).

Secondary Phosphate Minerals

Secondary phosphate minerals commonly host REE (e.g., Middelburg et al. 1988, Braun et al. 1993, 1998, Land et al. 1999, Kurtz et al. 2001), but are most influential in natural terrestrial waters with a circumneutral to high pH (Johannesson and Xiaoping 1997). Variscite is widely present in the clay size fraction of incipiently weathered rock at Coweeta (Appendix B), although variscite is not reported to be a REE-bearing phosphate (e.g., Burt 1989). Any phosphates present only precipitate during the earliest stage of weathering, when pH is generally relatively high (e.g., Duddy 1980), and are dissolved during saprolitization with an associated decrease in pH and loss of REE (Nesbitt 1979, Duddy 1980, Meintzer 1981, Banfield and Eggleton 1989, Marker and De Oliveira 1990, Braun et al. 1993, 1998). That is, REE-phosphates will only be associated with the incipient stage of weathering, and there will not be a temporal net change in REE-phosphate abundance. Therefore, the REE stream fluxes do not reflect changes in the abundances of REE-bearing secondary weathering products.

As stated above, the secondary phosphate present at Coweeta is variscite, not florencite and/or rhabdophane which are typically found replacing apatite during weathering, and are known to host REE (e.g., Banfield and Eggleton 1989, Braun et al.

1998, Aubert et al. 2001). This observation may be interpreted to reflect apatite dissolution higher in the Coweeta profile during a later, more acidic, stage of weathering, with P mobilization downward to the weathering front where variscite precipitation occurs. These processes may or may not occur in association with REE. This mechanism of phosphate precipitation differs from previous studies where phosphate precipitation is an apatite replacement phenomenon that occurs during an early stage of weathering (e.g., Banfield and Eggleton 1989, Braun et al. 1998, Aubert et al. 2001).

Conversion of a One-Time Stream Water Analyses to a Long-Term Flux

Like major elements, REE show seasonal and temporal variations in stream waters (Ingri et al. 2000). In order to average out this variability, a minimum seven year period of record of weekly stream water sampling and analysis is needed (Likens and Bormann 1995). The Coweeta major element long-term average solute-flux data used in this study is based on a 20 year period of record (Swank and Waide 1988, Velbel 1993a). However, the Al and REE stream water chemistry used is a one-time sample, collected on May 22, 2002. In order to calculate an approximate long-term average Al and REE solute-flux from the single sample episode, SiO_2 was included with the Al and REE analyses. The ratio of the long-term SiO_2 flux (Swank and Waide 1988) to the one-time May 2002 SiO_2 flux was then used to convert the one-time Al and REE stream solute concentrations to approximate long-term averages (Table 30). Silica was used because it is negligibly influenced by biomass, and, despite relatively small abundances being incorporated into kaolin, it represents the element with the greatest loss from the weathering profile (Figure 32; Bowser and Jones 2002). The conversion of one-time

Table 30. Long-term major element solute flux data, rare earth and major element solute concentrations for the May, 2002 sample episode, and approximate calculated long-term REE solute flux data of W2 and W34 stream waters.

	Watershed 2			Watershed 34		
Element	**May 22, 2002 (ppb)**	**Long-Term Flux (mol ha^{-1} yr^{-1})[1]**	**Ratio (mol ha^{-1} yr^{-1} ppb^{-1})**	**May 22, 2002 (ppb)**	**Long-Term Flux (mol ha^{-1} yr^{-1})[1]**	**Ratio (mol ha^{-1} yr^{-1} ppb^{-1})**
SiO_2	4085	1277	0.31	2643	1321	0.50
Mg	321	94.2	0.29	364	145	0.40
Ca	646	45.4	0.07	709	123	0.17
K	477	74.2	0.16	355	78.8	0.22
Na	NR	359		NR	324	
Al	0	0		0	0	
La	0.08	0.03		0.04	0.02	
Nd	0.08	0.02		0.04	0.02	
Gd	0.02	0.007		0.01	0.006	
Dy	0.02	0.005		0.01	0.005	

[1]Major elements from Swank and Waide (1988), REE calculated from SiO_2 ratios.

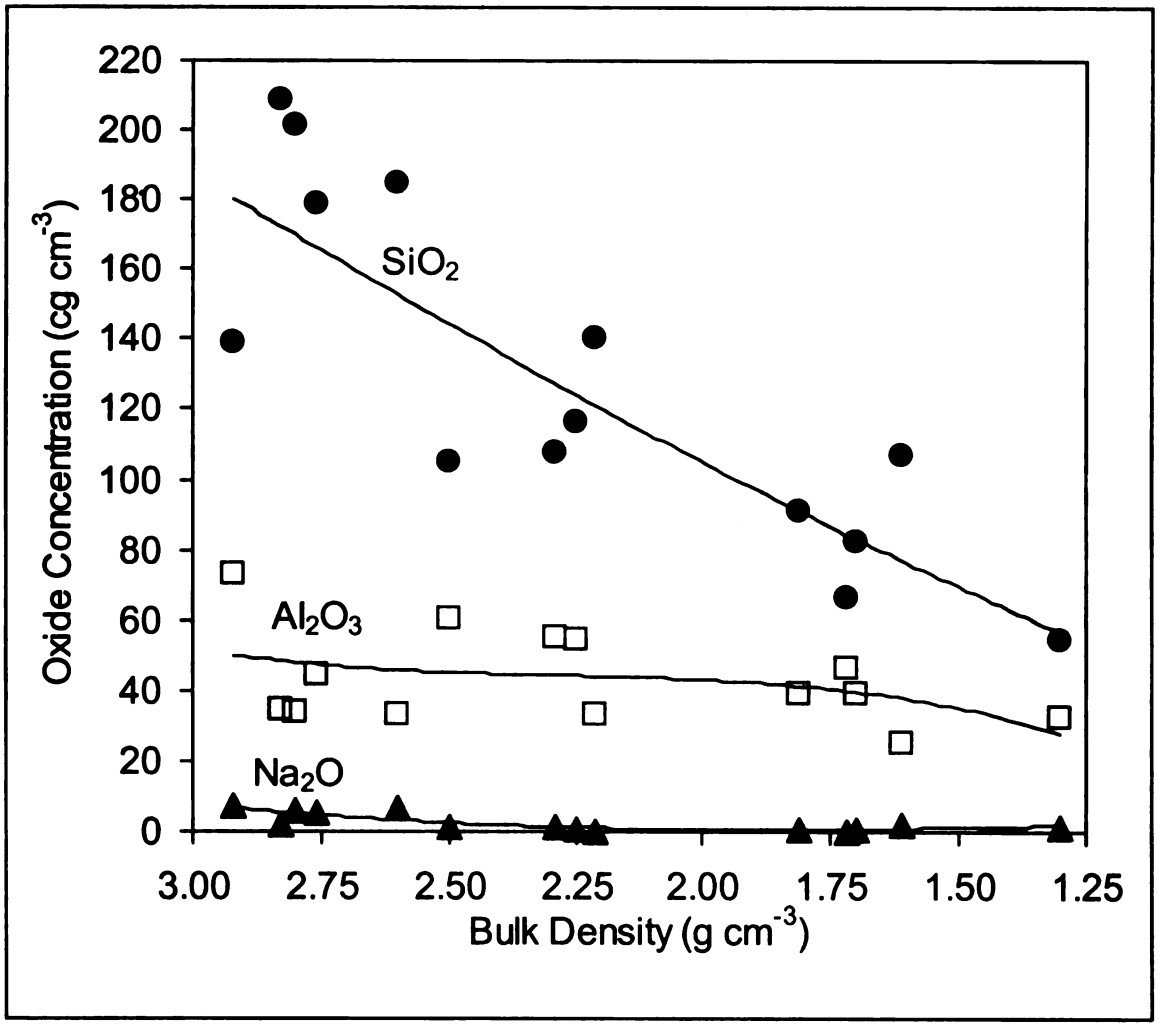

Figure 32. Reaction progress diagrams demonstrating the relatively high mobility of SiO_2 compared to that of Al_2O_3 and Na_2O.

stream solute concentrations to approximate long-term averages assumes that the REE/Al/SiO_2 ratio in a given watershed is invariant with time. Although this assumption cannot be confirmed with the current data set, it is fair to assume consistent behavior among REE, Al, and SiO_2 in the same watershed since none of these cations are significant plant nutrients. The approximate flux values (Al and REE) reported in Table 30 includes subtraction of concentrations found in the field blank.

Watershed Mass Balance for Otto Formation Watersheds 2 and 34

Watersheds 2 and 34 differ only by climate, and are nearly identical with respect to bedrock, aspect, vegetation, weathering history, and being undisturbed control watersheds (Velbel 1993a). Therefore, they provide the opportunity to compare weathering rates for watersheds that vary only by climate. From EMPA and LA-ICP-MS the major element and REE stoichiometries for Otto Formation minerals involved in weathering have been determined (Table 31). For kaolin and gibbsite standard formulae are reported, as these minerals have negligible substitution and do not appreciably host structural REE (e.g., Nesbitt 1979, Duddy 1980, Burt 1989, Braun et al. 1993, Finley and Drever 1997). Fragile clay minerals such as kaolin and gibbsite would also likely not respond well to laser ablation.

The mineral compositions determined by EMPA as part of this study (Table 31) differ from those measured by Velbel (1984a, 1985a, 1995) and Taylor and Velbel (1991). The Otto Formation plagioclase composition determined as part of this study is anorthite 28 (An_{28}; Table 31), whereas the plagioclase composition reported by Velbel (1984a, 1985a, 1995) and Taylor and Velbel (1991) is An_{32}. The most significant compositional difference between the mineral formulae of this study and that of Velbel (1984a, 1985a, 1995) and Taylor and Velbel (1991) is with respect to garnet. The garnet stoichiometry of this study has approximately twice the Ca than that reported by Velbel (1984a, 1985a, 1995) and Taylor and Velbel (1991). Potential sources of difference in mineral stoichiometries may include different instruments, different calibration methods for the instruments, or be a reflection of the mineralogic compositional heterogeneity of the Coweeta bedrock. Regardless, the microprobe analyses performed as part of this

Table 31. Structural formulae for the minerals of the Otto Formation. The biomass term reflects the stoichiometry of ion consumption by the biomass at Coweeta as determined by Day and Monk (1977) and Boring et al. (1981).

Phase	Structural Formula
Allanite	$(Ca_{1.47}Mn_{0.01}Na_{0.14}La_{0.00513}Ce_{0.00982}Nd_{0.00630}Gd_{0.00109}Dy_{0.000660}Yb_{0.000464})Fe_{0.43}Mg_{0.06}Al_2O(Al_{0.06}Si_{0.94}O_4)(Si_2O_7)OH$
Plagioclase (oligoclase)	$Na_{0.72}Ca_{0.28}Al_{1.28}Si_{2.72}O_8$
Garnet	$Ca_{0.41}Dy_{0.0000565}Yb_{0.00039}Mg_{0.36}Mn_{0.50}Fe_{1.76}Al_2Si_3O_{12}$
Biotite	$K_{0.88}Na_{0.041}Ca_{0.001}Ce_{0.000968}(Mg_{1.42}Fe_{1.05}Mn_{0.01}Al_{0.32}Ti_{0.097})(Al_{1.25}Si_{2.75})O_{10}(OH)_2$
Vermiculite	$K_{0.48}Na_{0.032}Ca_{0.026}La_{0.000506}Ce_{0.000224}Nd_{0.000604}Gd_{0.000112}Dy_{0.0000734}Yb_{0.0000284}(Mg_{1.54}$-$Fe^{II}_{0.27}Fe^{III}_{0.55}Mn_{0.005}Al_{0.33}Ti_{0.07})(Al_{1.25}Si_{2.75})O_{10}(OH)_2 \cdot 0.04Al_6(OH)_{15}$
Kaolin	$Al_2Si_2O_5(OH)_4$
Gibbsite	$Al(OH)_3$
Biomass	$Mg_{0.056}Ca_{0.144}Na_{0.008}K_{0.150}$

study will be used in the mass balance calculations. Generally, the mineral formulae (Table 31) reflect an average of multiple analyses (Table 13). However, there was significant variability found for the compositions of biotite and vermiculite. The biotite composition with the highest K stoichiometry was selected for inclusion in the mass balance calculations (analysis C17-3 B3; Table 13). Choosing the biotite composition with the highest K content reduces the likelihood that the analyzed grain has experienced any weathering. Similarly, the vermiculite composition selected was based on the EMPA analyses that yielded both a reasonable charge-balanced formula and the lowest K stoichiometry, presumably representing the most advanced degree of weathering (analysis W2-9 V4; Table 13).

Ten solutes (Table 30) are available for mass balance calculations, although the Otto Formation watersheds only have eight unknowns; i.e., the mineral weathering/ dissolution/formation rates. The solutes used in the mass balance calculations are the six major elements, as well as Dy and La (Table 32). By leaving all element stoichiometries positive in Table 32, the calculated rates of minerals being destroyed will be positive, and rates of minerals forming will be negative (Table 32). Lanthanum was chosen because it has the highest concentrations in stream waters. Dysprosium was included because it occurs in both allanite and garnet. If no REE content for garnet was included in the grand matrix (Table 32), MATLAB® yielded the following message: "Matrix is singular to working precision; all values are infinite." The mass balance calculations were performed with different REE, and geochemically reasonable and very similar results were always obtained. However, mathematically it is always preferable to

Table 32. Grand matrix for W2 and W34 mass balance calculations.[1]

	Allanite	Plagioclase	Garnet	Biotite	Vermiculite	Kaolinite	Gibbsite	Biomass
Si	2.94	2.72	3.00	2.75	2.75	2.00	0.00	0.00
Al	2.06	1.28	2.00	1.57	1.81	2.00	1.00	0.00
Mg	0.06	0.00	0.36	1.42	1.54	0.00	0.00	0.056
Ca	1.47	0.28	0.41	0.001	0.026	0.00	0.00	0.144
Na	0.14	0.72	0.00	0.041	0.032	0.00	0.00	0.008
K	0.00	0.00	0.00	0.88	0.48	0.00	0.00	0.150
Dy	0.000660	0.0000	0.0000565	0.0000	0.0000734	0.0000	0.0000	0.0000
La	0.00513	0.0000	0.0000	0.0000	0.000506	0.0000	0.0000	0.0000

[1]With all element stoichiometries being positive the calculated rates of minerals being destroyed will be positive, and rates of minerals forming will be negative.

incorporate elements that reduce the sparsity (i.e., the number of zeros) of the matrix as much as possible. The results of the mass balance are shown in Table 33.

The significant figures of the rates in Table 33 are important. The REE stream flux data have been limited to one significant figure because the ICP-MS calibration lines were dominated by standards with concentrations higher than that of the solutes. The only mineral that has a rate calculated exclusively from REE solute fluxes is allanite, and appropriately the allanite weathering rate is reported to one significant figure. Garnet too has a rate influenced by Dy and, appropriately the garnet rate will be reported to one significant figure. All of the other minerals, however, have rates calculated from major element fluxes; the biotite and vermiculite rates are calculated from K, plagioclase is calculated from Na, and the neoformed clays are calculated from Si and Al. Therefore, three (or two for rates in tens of mol ha^{-1} yr^{-1}) significant figures are reported for these minerals.

Results and Discussion of Mass Balance Calculations

Table 33 also includes the primary mineral weathering rates for W2 and W34 as calculated by Taylor and Velbel (1991). The differences between the weathering rates of this study and those calculated by Taylor and Velbel (1991) may be the result of any combination of the following: (1) allanite is included in the mass balance of this study; (2) REE are included in this study; (3) the mineral compositions of this study are different than those used in the calculations of Taylor and Velbel (1991); and/or (4) The weathering rates of biotite and vermiculite are decoupled in this study. Factors (1) - (3) have already been discussed above.

Table 33. Results of the mass balance calculations for Watersheds 2 and 34.[1]

	This Study		Taylor and Velbel (1991)[2]		Percent Difference[2]	
Phase	**Watershed 2 (mol ha^{-1} yr^{-1})**	**Watershed 34 (mol ha^{-1} yr^{-1})**	**Watershed 2 (mol ha^{-1} yr^{-1})**	**Watershed 34 (mol ha^{-1} yr^{-1})**	**Watershed 2**	**Watershed 34**
Allanite	40	9				
Plagioclase	478	429	567	500	-16%	-14%
Garnet	70	80	240	304	-71%	-74%
Biotite	469	175	432	294	8.6%	-40%
Vermiculite	-344	-71				
Kaolin	-349	-192				
Gibbsite	-252	-480				

[1]A positive value indicates destruction of a mineral, and a negative value indicates formation.
[2]Previous calculations by Taylor and Velbel (1991) and percent differences are provided for comparison.

Taylor and Velbel (1991) coupled the biotite weathering rate and vermiculite formation rate. The coupling of weathering rates means that the clay genesis rate is calculated from its stoichiometric relationship with the weathering rate of a primary mineral. In the case of the biotite-vermiculite couple, there is the assumption of conservation of the silicate structure during the transformation of biotite to vermiculite, and that once the vermiculite forms the silicate structure will not be destroyed upon further weathering (e.g., Velbel 1984a, 1985a, Taylor and Velbel 1991). As a result, the vermiculite formation rate will simply equal the biotite weathering rate. The vermiculite formation rate being lower than the biotite weathering rate indicates that some fraction of the vermiculite present in the regolith is being destroyed (i.e., converted to solutes) in excess of new production of vermiculite from biotite. Destruction of vermiculite during weathering is consistent with the nature of biotite weathering at Coweeta (Chapter 4). With allanite weathering recognized at Coweeta, and REE included in the calculations, the mass balance calculations may be performed with biotite and vermiculite decoupled.

The largest differences in primary mineral weathering rates are with respect to garnet. Garnet weathering at Coweeta is an important source of solutes to regolith and stream waters (Velbel 1984a, Velbel 1985a), despite composing on average 1.7% of the bedrock by volume (Table 4). The garnet weathering rates of this study are over 70% lower than those calculated by Taylor and Velbel (1991) (Table 33). The weathering rate of any primary mineral calculated by watershed flux-based mass balance methods is influenced by two factors: (1) the actual rate of mineral destruction; and (2) the abundance of the mineral in the bedrock. A low weathering rate may reflect a rapidly weathering mineral that occurs in low abundance (e.g., allanite), or conversely an

abundant mineral that weathers very slowly (e.g., quartz). Garnet at Coweeta weathers to form limonitic protective surface coatings (Figure 33), through which diffusion determines the rate of weathering (Velbel 1984b, 1985a, 1993b). Diffusion-limited weathering is extremely slow relative to what the rate would be in the absence of the protective surface coating. Remnant garnet grains encased in limonitic protective surface coatings are routinely observed in the Coweeta solum (Figure 33). These microscopic

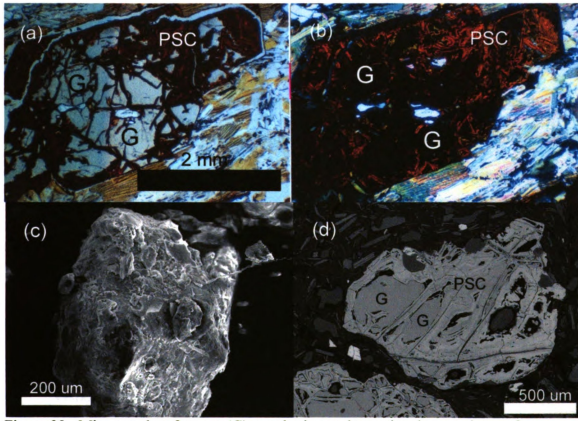

Figure 33. Micrographs of garnet (G) weathering and associated protective surface coatings (PSC). Garnet in thin section in plane-polarized light (a), and crossed-polarized light (b); saprolite sample W27-5 from the Coleman River Formation regolith. SEM image of the exterior of a limonitic (gibbsite, kaolinite, and goethite) protective surface coating (c); saprolite sample W34-6 from the Otto Formation regolith. BSE image of remnant garnet crystals (G) in a limonitic protective surface coating (PSC); B horizon sample W2-5 from the Otto Formation regolith.

observations, combined with the relatively low abundance of garnet in the bedrock, should yield a relatively slow weathering rate when calculated using watershed mass balance methods. In contrast, biotite is very abundant in the Coweeta bedrock, and, other than allanite, is the only other mineral weathering during the earliest stage of weathering (Figure 8). From these observations it may be predicted that biotite should have a relatively high weathering rate at Coweeta when calculated using flux-based mass balance methods. Certainly biotite should have a faster weathering rate than garnet. This is the case for both W2 and W34 for this study. However, Taylor and Velbel (1991) found garnet to weather more rapidly than biotite in W34, which seems questionable based on this discussion. The lower garnet weathering rates calculated in this study likely reflects the inclusion of allanite in the mass balance calculations. Allanite provides an additional Ca source; in the calculations of Taylor and Velbel (1991) garnet weathering had to account for all the stream Ca not provided by the weathering of plagioclase. Plagioclase weathering is constrained by Na, thereby limiting the Ca that can be released by the dissolution of plagioclase. However, the present mass balance ascribes Na fluxes to both plagioclase and allanite sources, so the new plagioclase weathering rates are slightly lower than those of Taylor and Velbel (1991).

Velbel (1993a) used W2 and W34 plagioclase dissolution rates to calculate an apparent activation energy (E_a) of 77 kJ mol^{-1}. The plagioclase weathering rates of this study yield an E_a of 66 kJ mol^{-1}. Both values are well within the range of published activation energies for feldspar dissolution (e.g., Blum and Stillings 1995).

Clay Genesis Rates and Climate

With W2 and W34 only differing by climate, they provide the opportunity to compare clay genesis rates with changes in temperature and precipitation. Table 34 provides a summary of previous studies that were able to correlate clay minerals assemblages with [paleo]climate. Only those clay minerals that dominate the regolith at Coweeta are included in Table 34. From Table 34 it is clear that the only mineral for which there is a consistent relationship between climate and presence are kaolinite in warm and humid climates. Gibbsite appears to form in humid conditions, but there is no consensus on temperature regime.

Table 34. Summary of studies which relate clay minerals in sediments and mudrocks to source area climate. Only those minerals that are significant at Coweeta are included.

	Temperature		Moisture	
Mineral	**Warm**	**Cool**	**Humid**	**Arid**
Gibbsite	A, B	C	A, B, C	
Kaolinite	A, D, E, F,G, J, K, L, N, O, Q, R, S, U, V, W, X, Z		A, E, F, G, H, I, K, L, M, N, O, P, Q, R, S, T, U, V, W, X, Z	
Vermiculite	Y	L, O		I

A=Biscaye (1965)
B=Hill et al. (2000)
C=Norfleet et al. (1993)
D=Yuretich et al. (1999)
E=Gibson et al. (1993)
F=Robert and Kennett (1992)
G=Robert and Chamley (1991)
H=Finkelstein et al. (1998)
I=El-Younsy et al. (1998)
J=Chamley (1989)
K=Kronberg et al. (1986)
L=Pe-Piper and Piper (1985)
M=Hallam et al. (1991)
N=Price et al. (2000)
O=Righi and Meunier (1995)
P=Stoffers and Hecky (1978)
Q=Kalindekafe et al. (1996)
R=Net et al. (2002)
S=Hiscott (1984)
T=Chamley and Müller (1991)
U=Debrabant et al. (1993)
V=Griffin (1962)
W=Robert and Kennett (1994)
X=Tabor et al. (2002)
Y=Protz et al. (1988)
Z=John et al. (2003)

Watershed 2 is warmer and dryer than W34 (Table 1), and has the higher kaolin formation rate (Table 33). Watershed 34 however has the higher gibbsite formation rate (Table 33). These results indicate that kaolin precipitation is favored under a warm and/or dry climate, and gibbsite is favored under a cool and/or wet climate. Additional

calculations have been performed which support these conclusions (Appendix D). Quantifying the relative influences of temperature vs. precipitation cannot be ascertained from these results. Qualitatively, these results indicate that gibbsite abundances may increase in a regolith if small increases in temperature are accompanied by relatively large increases in precipitation. Similarly, kaolin precipitation may be favored in cool climates if precipitation is sufficiently low. Quantifying the relative influences of temperature and precipitation on the neoformation of kaolin and gibbsite at Coweeta would require a third watershed that is identical to W2 and W34, but is climatically either warm and wet or cool and dry.

Discussion and Conclusions

The above results are consistent with previous studies on bauxite genesis. The majority of researchers equate bauxite formation with tropical and seasonal climates (e.g., Bardossy and Aleva 1990, Nahon 1991). However, recent workers have documented bauxitic weathering in cool climates (e.g., Taylor et al. 1990, 1992, Taylor and Eggleton 2001), and Boulangé et al. (1997) believe that bauxite can develop under varying climatic conditions. Taylor and Eggleton (2001) state that only prolonged weathering with ample water over an extended period of time is necessary to produce bauxites. This is consistent with the results of this study which indicate that gibbsite may form under cool conditions, especially if precipitation is relatively high and erosion rates are low.

Using $\delta^{18}O$ values, kaolinite precipitation during cool climates has also been documented in the literature (e.g., Bird and Chivas 1988, Elliott et al. 1995, 1997). These researchers have found kaolinite oxygen isotope ratios which reflect neoformation during

glacial or deglacial times. Bird and Chivas (1988) suggest that efficient leaching of soluble cations is more important in kaolinite formation than temperature.

The watershed mass balance calculations of this study differ from previous studies performed at Coweeta and elsewhere. However, the conclusions based on the mass balance calculations rely on the validity of the following assumptions:

(1) Watershed flux-based mass balance calculations effectively determine mineral weathering/formation rates;

(2) Watersheds 2 and 34 are directly comparable;

(3) The REE stoichiometries of the minerals are real and representative; and

(4) A single stream REE sample episode is representative and can be extrapolated to a long-term average.

Despite these assumptions and limitations the mass balance calculations performed in this study have numerous advantages, including the number of unknowns equaling the number of equations, inclusion of a very important Ca-bearing mineral (allanite), and a garnet weathering rate that is more geochemically reasonable than previous studies. To date, long-term REE fluxes are not available at Coweeta or elsewhere.

What is important from the above calculations, and what can be stated with confidence, is the relationships between the neoformed clay minerals and climate. Kaolin abundances should increase with an increase in temperature and/or a decrease in precipitation, and gibbsite abundances should increase with a decrease in temperature and/or an increase in precipitation.

CHAPTER 8

CLAY GENESIS RATES FROM WATERSHED SOLUTE-BASED MASS BALANCE USING MAJOR AND RARE EARTH ELEMENTS: COWEETA GROUP WATERSHED 27

For purposes of comparison, mass balance calculations using REE have also been performed on W27; a watershed underlain by three lithostratigraphic units (Figure 34), all of which are less reactive than the rocks of the Otto Formation (Velbel 1984a). Watershed 27 is also significantly cooler, with higher precipitation (Table 1) than either W2 or W34.

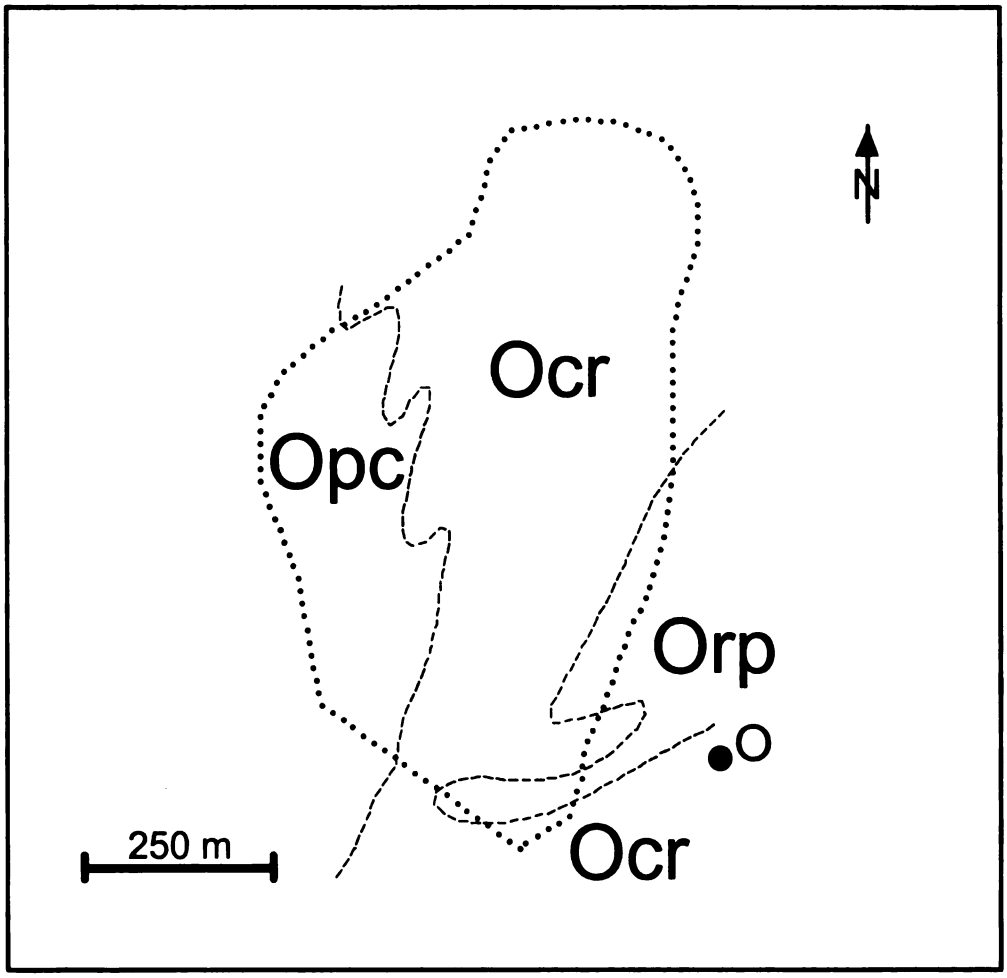

Figure 34. Map of W27 showing lithostratigraphic units and sample locality O.

Watershed Mass Balance for Coweeta Group Watershed 27

The major element and REE stoichiometries for Coweeta Group minerals involved in weathering are provided in Table 35. With the exception of hornblende, the mineral stoichiometries used in the W27 mass balance are those of the Coleman River Formation (Table 35). The mineral compositions of the Coleman River Formation were chosen for the mass balance because the Coleman River Formation is the dominant lithostratigraphic unit in W27, especially at the warmer lower elevations where weathering is most intense in the watershed (Figure 34). All mineral stoichiometries are an average of multiple EMPA and LA-ICP-MS analyses. As in the Otto Formation watersheds, the ratio of the long-term SiO_2 flux (Swank and Waide 1988) to the one-time May 2002 SiO_2 flux has been used to convert the one-time Al and REE stream solute concentrations to approximate long-term averages (Table 36). The grand matrix for W27 is provided in Table 37.

The mass balance has been performed using both hornblende compositions, as well as without hornblende (Table 38). The mass balance includes the six major elements and La, Nd, and Gd. Geochemically reasonable results could not be obtained if Dy was included in the calculations. A detailed investigation into the role of Dy in the calculations revealed that the consumers of Dy (vermiculite and/or solution) are inadequate to deplete the system of the Dy being generated by the weathering of the primary Dy-bearing minerals allanite, garnet, and hornblende. With the present data set, it is not possible to resolve the problem with Dy, although it does not appear to be the result of analytical error, particularly with regard to the mineral compositional data. With

Table 35. Structural formulae for the minerals of lithostratigraphic units from the Coweeta Group[1] used in the mass balance calculations.

Phase	Structural Formula
Allanite	$(Ca_{1.46}Mn_{0.01}Na_{0.06}K_{0.01}La_{0.0134}Ce_{0.0205}Nd_{0.0127}Gd_{0.000287}Dy_{0.00249}Yb_{0.000744})Fe_{0.51}Mg_{0.06}Al_2O(Al_{0.11}Si_{0.89}O_4)(Si_2O_7)OH$
Plagioclase (oligoclase-andesine)	$Na_{0.70}Ca_{0.30}Ce_{0.000251}Al_{1.30}Si_{2.70}O_8$
Garnet	$Ca_{0.30}Dy_{0.000216}Yb_{0.000321}Mg_{0.44}Mn_{0.22}Fe_{2.13}Al_2Si_3O_{12}$
Biotite	$K_{0.91}Na_{0.028}Ce_{0.000360}(Mg_{1.31}Fe_{1.16}Al_{0.33}Ti_{0.093})(Al_{1.25}Si_{2.75})O_{10}(OH)_2$
Hornblende (PCG)	$(Ca_{1.84}Mn_{0.04}Na_{0.36}K_{0.20}La_{0.0000937}Ce_{0.000345}Nd_{0.000383}Gd_{0.000111}Dy_{0.000115})$-$(Mg_{2.60}Fe_{1.77}Al_{0.67}Ti_{0.10})Si_6(Si_{0.50}Al_{1.50})O_{22}(OH)_2$
Hornblende (RMF)	$(Ca_{1.81}Mn_{0.06}Na_{0.42}K_{0.11}Ce_{0.00000433}Gd_{0.0000252}Dy_{0.0000273})(Mg_{2.36}Fe_{1.73}Al_{0.99}Ti_{0.05})Si_6(Si_{0.36}Al_{1.64})O_{22}(OH)_2$
Vermiculite	$K_{0.13}Na_{0.030}Ca_{0.017}Mg_{0.17}(Mg_{0.80}Fe^{II}_{0.55}Fe^{III}_{0.79}Mn_{0.006}Al_{0.33}Ti_{0.12})(Al_{1.25}Si_{2.75})O_{10}(OH)_2 \cdot 0.05Al_6(OH)_{15}$
Kaolin	$Al_2Si_2O_5(OH)_4$
Gibbsite	$Al(OH)_3$
Biomass[2]	$Mg_{0.056}Ca_{0.144}Na_{0.008}K_{0.150}$

[1]All minerals are from the Coleman River Formation, except for the hornblendes which are from the Persimmon Creek Gneiss (PCG) and Ridgepole Mountain Formation (RMF).

[2]The biomass term reflects the stoichiometry of ion consumption by the biomass at Coweeta as determined by Day and Monk (1977) and Boring et al. (1981).

Table 36. Long-term major element solute flux data, rare earth and major element solute concentrations for the May, 2002 sample episode, and approximate calculated long-term REE solute flux data for the W27 stream water.

	May 22, 2002 (ppb)	**Long-Term Flux (mol ha^{-1} yr^{-1})[1]**	**Ratio (mol ha^{-1} yr^{-1} ppb^{-1})**
SiO_2	1206	1083	0.90
Mg	186	111	0.60
Ca	273	87.1	0.32
K	162	62.7	0.39
Na	NR	170	
Al	34	23	
La	0.1	0.09	
Nd	0.09	0.08	
Gd	0.02	0.02	
Dy	0.01	0.01	

[1]Major elements from Swank and Waide (1988), REE calculated from SiO_2 ratios.
NR = Not reported.

Table 37. Grand matrix for the W27 mass balance calculation.

	Allanite (CRF)	Plagioclase (CRF)	Garnet (CRF)	Hornblende (PCG)	Biotite (CRF)	Vermiculite (CRF)	Kaolinite	Gibbsite	Biomass
Si	2.89	2.70	3.00	6.50	2.75	2.75	2.00	0.00	0.00
Al	2.11	1.30	2.00	2.17	1.58	1.88	2.00	1.00	0.00
Mg	0.06	0.00	0.44	2.60	1.31	0.97	0.00	0.00	0.056
Ca	1.46	0.30	0.30	1.84	0.000	0.017	0.00	0.00	0.144
Na	0.06	0.70	0.00	0.36	0.028	0.030	0.00	0.00	0.008
K	0.01	0.00	0.00	0.20	0.91	0.13	0.00	0.00	0.150
La	0.0134	0.00000	0.00000	0.0000937	0.0000	0.000286	0.0000	0.0000	0.0000
Nd	0.0127	0.00000	0.00000	0.000383	0.0000	0.000359	0.0000	0.0000	0.0000
Gd	0.00287	0.00000	0.00000	0.000111	0.0000	0.0000550	0.0000	0.0000	0.0000

Table 38. Results of the mass balance calculations for Watershed 27[1] performed three different ways: (1) hornblende of the Persimmon Creek Gneiss (PCG), (2) hornblende of the Ridgepole Mountain Formation (RMF); and (3) without hornblende.

	This Study				Percent Difference		
Phase	**Hornblende (PCG) (mol ha^{-1} yr^{-1})**	**Hornblende (RMF) (mol ha^{-1} yr^{-1})**	**No Hornblende (mol ha^{-1} yr^{-1})**	**Taylor and Velbel (1991) (mol ha^{-1} yr^{-1})**	**Hornblende (PCG)**	**Hornblende (RMF)**	**No Hornblende**
Allanite	8	8	8				
Plagioclase	241	234	242	230	4.8%	1.7%	5.2%
Garnet	90	21	93	197	-54%	-89%	-53%
Hornblende	3	13					
Biotite	110	105	105	85	29%	24%	24%
Vermiculite	-70	-60	-60				
Kaolin	11	77	2				
Gibbsite	-549	-583	-551				

[1]A positive value indicates destruction of a mineral, and a negative value indicates formation.

multiple EMPA and LA-ICP-MS analyses performed for each mineral, no suite of mineral stoichiometries for Dy could be found that permitted a geochemically reasonable mass balance. However, a small increase in the Dy stream flux from 0.01 to 0.03 mol ha^{-1} yr^{-1} would yield a geochemically reasonable balance. Another potential explanation is that there is an unrecognized Dy sink present in W27. This is not likely because it would have to be a sink that only affects Dy, and is only present in W27. It is worth noting that the problem with Dy is not that an additional source is needed, which supports the assumption that REE inputs from precipitation are negligible at Coweeta.

Although the results of the three sets of mass balance calculation are similar (Table 38), the rates calculated by including the Persimmon Creek Gneiss hornblende composition are favored. The choice of the Persimmon Creek Gneiss hornblende vs. Ridgepole Mountain Formation hornblende is based on the former underlying a substantially larger area of the watershed than the latter, especially at the lower elevations where weathering is most intense (Figure 34).

The reasons for the differences in the primary mineral weathering rates between those calculated as a part of this study and those reported by Taylor and Velbel (1991) are mentioned above, and are: (1) allanite is included in the mass balance of this study; (2) REE are included in this study; (3) the mineral compositions of this study are different than those used in the calculations of Taylor and Velbel (1991); and/or (4) the weathering rates of biotite and vermiculite are decoupled in this study. Also, for reasons already discussed for W2 and W34, the lower garnet dissolution rate of this study (relative to that of Taylor and Velbel 1991) is favored for W27.

The similarity of garnet weathering rates among the three watersheds investigated (Tables 33 and 38) may reflect the influence of protective surface coat formation, in spite of differences in composition, climate, abundance, and the REE used in the calculations. As discussed earlier, when a protective surface coat forms on a garnet grain, the dissolution kinetics become transport-controlled, with diffusion of ions through the protective surface coating being the slow step in the reaction (Velbel 1984b, 1993b). The garnet dissolution rates for W2, W34, and W27 are sufficiently similar (70, 80, and 90 mol ha^{-1} yr^{-1}, respectively) to support the suggestion that diffusion-controlled dissolution kinetics may be sufficiently slow that the influence of climate, composition, and abundance on almandine garnet weathering becomes greatly diminished.

Clay Formation/Dissolution Rates

One interesting aspect of the mass balance calculations in Table 38 is that the W27 kaolin reaction rate indicates destruction (by 11 mol ha^{-1} yr^{-1}), rather than formation, as observed in W2 and W34. Such a low rate may be within the error of calculations. However, what is important is that the W27 rates in Table 38 reflect a very gibbsitic, rather than kaolinitic, regolith, with W27 having the same weathering history as W2 and W34. Furthermore, as the stream flux data in Table 36 indicate, Al is mobile in W27, suggesting destruction of aluminous secondary phases (i.e., kaolin and gibbsite). The progressive weathering of kaolin to dissolved Al would follow the set of reactions:

$$Al_2Si_2O_5(OH)_4 + 5\ H_2O \Leftrightarrow 2\ Al(OH)_3 + 2\ Si(OH)_{4\ (aq)}$$

$$Al(OH)_3 \Leftrightarrow Al(OH)_2^{+}{}_{(aq)} + OH^-$$

This set of reactions demonstrates that the route to dissolved Al in streams is by kaolin dissolution with a gibbsite intermediary. Therefore, the dissolved Al present in the streams of W27 may be viewed as an indicator of kaolin destruction in the regolith.

The gibbsitic nature of the weathering profile in W27 is also supported by XRD data. Figure 35 shows a series of diffractograms of Coleman River Formation regolith samples collected near W27 ("O" in Figure 34 and Appendix A). These diffractograms show an up-profile trend from saprock to the top of the saprolite, with the gibbsitic nature of the profile being evident. The presence of kaolin in the diffractograms may reflect one of three possibilities: (1) kaolin is forming as an intermediary to gibbsite and dissolved Al; (2) the kaolin weathering rate above is incorrect and small amounts of kaolinite are actually forming today; or (3) kaolin is relict from an earlier climate regime that favored kaolin precipitation (e.g., Finley and Drever 1997). Possibilities (1) and (2) may not be resolvable with the current data set. The clay formation/dissolution rates have been calculated using a one-time REE stream analysis that has been adjusted to a long-term average using SiO_2 concentration and flux data. Furthermore, with the exception of the hornblende composition, all the mineral compositions used in the mass balance were from the Coleman River Formation. The mineralogic influence of the other lithostratigraphic units on the stream water chemistry of W27 has not been assessed. From these sources of error, the kinetic behavior of kaolin cannot be addressed with certainty. However, what is known is that W27 has a gibbsitic regolith, which is reflected in both the XRD data and the mass balance calculations, and consistent with the relatively high precipitation regime of the watershed. All of the mass balance

calculations performed for W27 reflect kaolin destruction, which supports the calculated rate.

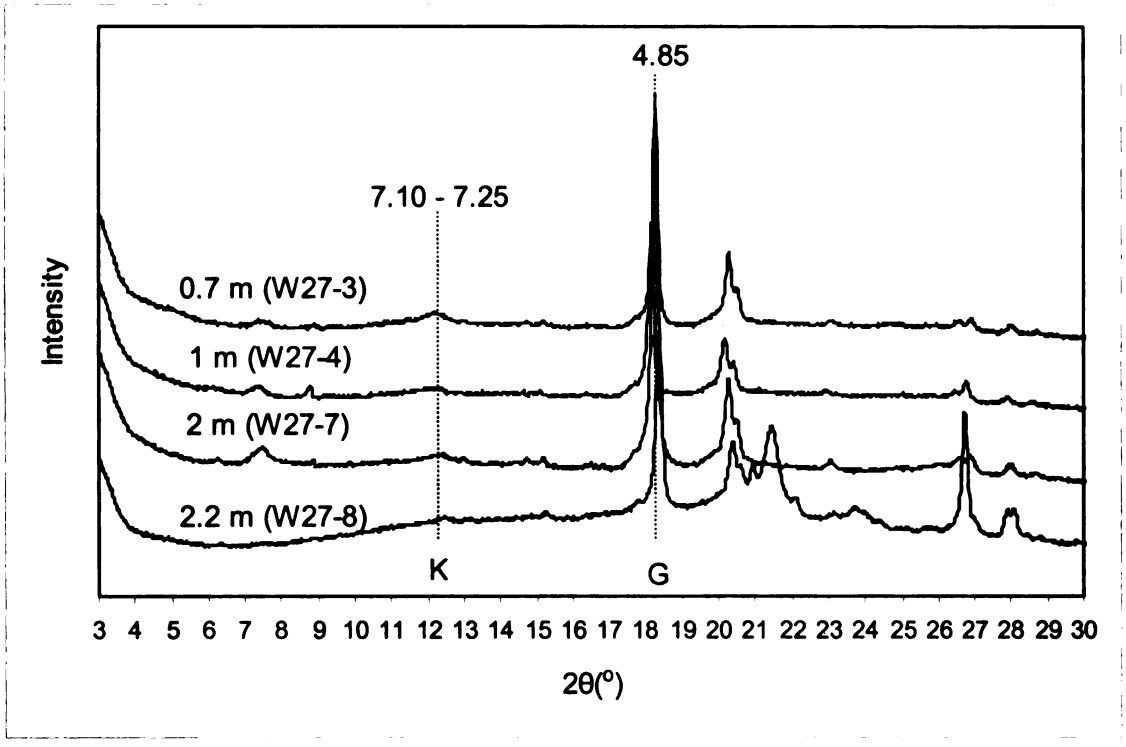

Figure 35. Diffractograms showing the minerals present in the <2 μm size fraction of an up-profile trend in the regolith near W27. Measurements are depth at which sample was collected, with the 2.2 m sample (W27-8) being saprock. Notice abundance of gibbsite (G), and paucity of kaolinite (K). Kaolinite and gibbsite peaks are labeled with their d-spacing in Å. Weathering profile developed on the Coleman River Formation.

Velbel (1984a, 1985a) has argued against the Coweeta saprolite possibly being relict, based on two lines of observation. First, the steep slopes at Coweeta are so conducive to erosion that a relict profile would not likely last long. Second, the clay mineral assemblages are compatible with present day climatic conditions. Velbel's (1984a) argument, however, was to demonstrate that the Coweeta saprolite need not be of Tertiary age; by virtue of its thickness, formation of some of the saprolite in the Pleistocene is almost certainly indicated.

Lithologic Influences on Clay Formation/Dissolution Rates

With W27 being developed on Coweeta Group bedrock, and W2 and W34 being underlain by the Otto Formation, a preliminary assessment of the influence of lithology on clay mineralogy may be made. Figure 36 shows that, despite lithologic differences, kaolin forms faster with increasing temperature and/or decreasing precipitation. Gibbsite formation rates also display nearly monotonic changes with climate, although antithetic to the behavior of kaolinite. Vermiculite formation rates, however, do not display systematic variations with changes in temperature and precipitation, with the W27 vermiculite formation rates being similar to those of W34, despite the significant differences in climate between these two watersheds (Table 1).

The monotonic variations in gibbsite and kaolinite rates with respect to temperature and precipitation are interpreted to reflect a predominantly climatic influence on their formation/dissolution. Lithologic influences on these neoformed clay minerals are believed to be relatively small. The nonsystematic changes in vermiculite formation rates with changes in climate are believed to reflect a significant influence by lithology. With vermiculite being a transformational weathering product of biotite, the vermiculite weathering rate is dependent, at least in part, on the weathering rate of biotite. The weathering rate of biotite may be influenced not only by abundance and climate, but also by composition (e.g., Murakami et al. 2003).

Conclusions

By comparing watersheds that differ by both climate and lithology, it may be concluded that the neoformed clay minerals kaolinite and gibbsite are primarily influenced by climate. In contrast, the transformed clay mineral vermiculite appears to

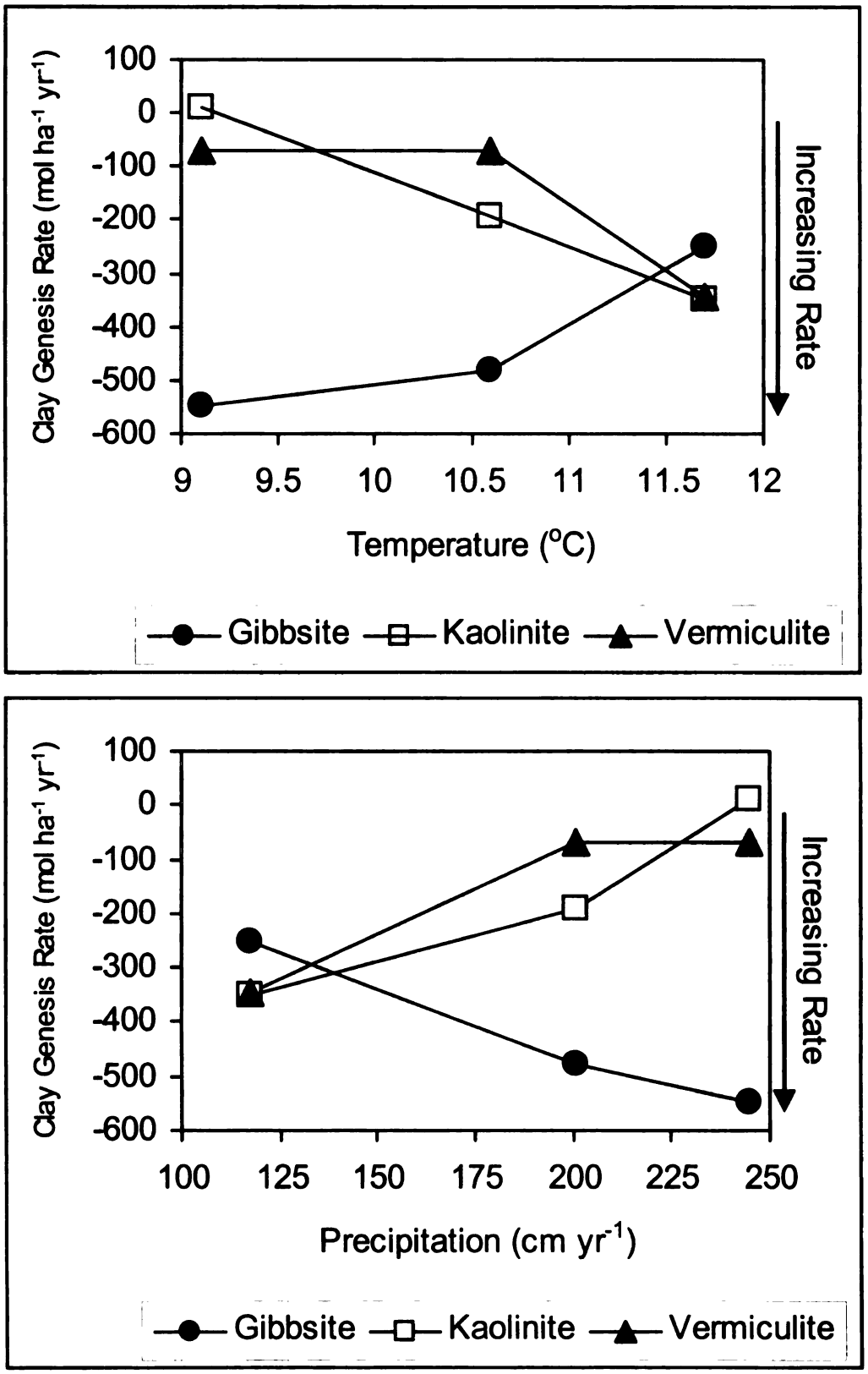

Figure 36. Plots displaying the influence of climatic factors on clay formation/dissolution rates for Coweeta.

be significantly influenced by lithologic factors, as well as climate. These results indicate that kaolinite and gibbsite may be superior climate proxies than vermiculite.

Summary and Conclusions of Mass Balance Calculations using Rare Earth Elements

As discussed in the last chapter, there are numerous sources of potential error within the mass balance calculations performed using REE. The stream water REE chemistry is a one-time sample analysis that has been converted to an approximate long-term flux using stream SiO_2 chemistry. No data have been collected on REE concentrations in precipitation. Furthermore, the REE concentration/flux in the stream waters is only available to one significant figure. Despite all of these potential limitations, the mass balance calculations above have the advantages of including the previously unrecognized, but very important Ca source, allanite, and permitting decoupling of biotite and vermiculite in the matrix. Moreover, the mass balance calculations yield very defensible results that are believed to be the best to date for the watersheds investigated. The calculated mineral weathering rates are the final test on any watershed mass balance calculation. In summary, and perhaps most importantly, the inclusion of REE in mass balance calculations works for the watersheds included in this study, and suggests potential for success of future mass balance calculations that include trace elements.

CHAPTER 9

RESPONSE TIMES OF CLAY MINERAL ASSEMBLAGES TO CLIMATIC CHANGES

The ultimate goal of obtaining the clay mineral kinetic data above is to permit calculation of clay mineral response times. That is, at the current clay formation/ dissolution rates for a given watershed, how much time is required to achieve a 5% (or 50 g kg^{-1}) relative change in regolith clay mineral abundance. The choice of 5% reflects the minimum changes in relative clay abundance that can be detected by changes in XRD peak intensities (e.g., Brown and Brindley 1984, Moore and Reynolds 1997).

Response Times for Watersheds at Coweeta Hydrologic Laboratory

The time required to achieve a change of 50 g kg^{-1} in clay abundance in the Coweeta watersheds investigated is reported in Table 39, and is based on the rates calculated using mass balance methods (Chapters 7 and 8). Table 39 shows that it would take 70,200 years to increase the kaolin abundance in W2 by 5%, at the current kaolin formation rates. The same increase in W34 would take longer (128,000 years). The same relationship exists for vermiculite in W2 and W34, but a gibbsite increase of 50 g kg^{-1} is more rapid in W34 (169,000 years) than W2 (322,000 years). The kaolin destruction rate of W27 (Table 38) has not used to calculate clay response times (Table 39). Although the kaolin destruction rate for W27 is believed to be a robust value, it is not believed to be typical of most Piedmont Terrane weathering profiles. The W27 gibbsite and vermiculite response times are comparable to those of W34. The response times (Table 39) are clearly too long to permit southern Blue Ridge clay mineral assemblages to re-equilibrate with climate during the Holocene (since 12.5 Ka for the

southeastern United States; Delcourt and Delcourt 1985). The use of clay mineral assemblages as proxies for continental paleoclimate interpretations is therefore called into question.

Table 39. Time required for a 5% (50 g kg^{-1}) change in regolith clay abundance (response times) based on calculated rates in Coweeta watersheds.

Watershed	Kaolin (years)	Gibbsite (years)	Vermiculite (years)
2	70,200	322,000	42,400
34	128,000	169,000	317,000
27		148,000	208,000

Clay Formation Rates in the Southern Appalachians

In order to calculate the time needed to form measured regolith clay abundances, additional weathering profile information is needed. Conversion of fluxed-based watershed clay genesis/dissolution rates in mol ha^{-1} yr^{-1} to g kg^{-1} yr^{-1} is easily accomplished, with the rate in g kg^{-1} yr^{-1} then being used to calculate the time needed to produce the measured clay abundance (Appendix C). However, clay abundances in the literature are routinely reported by soil horizon, with each horizon having different physical properties (i.e., bulk density), and constituting different fractions of the overall regolith. Because the clay genesis/dissolution rate from mass balance calculations reflects the mineral-water interactions for the entire profile, an average clay abundance is needed that is weighted to reflect the bulk density and clay mineralogic differences of each horizon. Furthermore, the weighted average regolith should also be representative of the entire landscape, as the weathering profiles of ridges, slopes, and drainages typically vary significantly in both overall thickness and the relative thicknesses of the individual soil horizons.

Yeakley et al. (1998) measured soil horizon thicknesses along a transect perpendicular to the stream of W2. Measurements were taken at 5 or 10 m intervals along the 85 m transect which began at the streambank and ended on the watershed divide (ridge). In total, soil horizon thicknesses were measured at 14 different stations along the transect (Yeakley et al. 1998). These soil horizon thicknesses were then combined with additional measurements that included bulk density, performed by Berry (1976). These data permitted calculation of a representative weathering profile that accounted for variations in soil horizon thickness, soil horizon bulk density, regolith thickness, all of which may be influenced by geomorphic position (Table 40). The calculated representative weathering profile is very comparable to Coweeta regolith data reported by Berry (1976) and Knoepp and Swank (1994).

Table 40. Data for the calculated representative Coweeta regolith.

Horizon	W2 Horizon Thickness (cm; Berry 1976, Yeakley et al. 1998)	Bulk Density ($g\ cm^{-3}$; Berry 1976)	Weighted Profile Bulk Density ($g\ cm^{-3}$)
A	11	1.30	2.11
B	46	1.54	
C	543	2.17	

With clay genesis/formation rates calculated (Tables 33 and 38), and a representative weathering profile developed (Table 40), the time required to form measured clay abundances (herein termed "production times") in Piedmont Terrane (recall that the eastern Blue Ridge and Inner Piedmont together form the Piedmont Terrane; Figure 1) regolith may be determined (Appendix C). In other words, clay genesis/dissolution rates and average regolith physical characteristics, both for Coweeta, will be applied to measured clay abundances in weathering profiles found elsewhere and

reported in the literature (Table 41). The application of Coweeta-derived clay genesis/dissolution rates will be limited to physically comparable regolith, which is going to be a function of bedrock, climate, and geomorphology. Therefore, only clay abundances from Piedmont Terrane regolith have been included. Many of these studies provide clay abundances for the entire regolith, however others only provide clay abundances for the silt- and clay-size fractions. Both types of studies will be included in the calculations herein, with the assumption that quantities of clay in the sand-sized fraction of the weathering profiles are negligible relative to the quantities in the silt- and clay-size fractions. The times needed to generate the abundances of clay reported in Table 41 for southern Appalachian regoliths developed on crystalline rock are contained in Table 42.

The application of Coweeta mineral weathering/formation rates for calculating Piedmont Terrane clay production times assumes that the Coweeta rates are representative of the region. Plagioclase dissolution is the most important weathering reaction in silicate-dominated natural hydrologic systems (Bowser and Jones 1993, 2002; Drever 1997b, Jacobson et al. 2003), especially with respect to Si and Al which constitute the neoformed clays. Plagioclase dissolution rates are also constrained by Na flux, which is minimally influenced by biomass. The Coweeta plagioclase dissolution rates of this study have also changed relatively little from those of Taylor and Velbel (1991) (the small differences noted are due to the use of slightly different plagioclase stoichiometries based on new electron microprobe analyses, and incorporation of a new Na source, allanite, into the mass balance). Therefore, plagioclase dissolution rates may serve as robust proxies for assessing the regional representativeness of Coweeta clay

Table 41. Clay abundances in Piedmont Terrane (Figure 1) regolith as reported in the literature.

Reference			Stolt & Baker (2000)	Norfleet et al. (1993)	Norfleet et al. (1993)	Norfleet et al. (1993)	Coleman et al. (1949)
Physiographic Province			Blue Ridge	Blue Ridge	Blue Ridge	Blue Ridge	Blue Ridge
State			Virginia	NW South Carolina	NW South Carolina	NW South Carolina	North Carolina
Sample Name			Pilot	ED-1	ED-2	ED-3	Rabun Soil
Bedrock			Granites, gneisses, and schists	Mica-rich gneisses or schists	Mica-rich gneisses or schists	Mica-rich gneisses or schists	Basic crystalline rock
A Horizon	Vermiculite (%)	Sand	55	5	3	5	
		Silt					1
		Clay					2
	Kaolin (%)	Sand	20	2	7	3	
		Silt					2
		Clay					15
	Gibbsite (%)	Sand	0	6	1	5	
		Silt					1
		Clay					12
B Horizon	Vermiculite (%)	Sand	36	12	15	15	
		Silt					0
		Clay					5
	Kaolin (%)	Sand	42	1	37	13	
		Silt					1
		Clay					38
	Gibbsite (%)	Sand	1	12	8	14	
		Silt					2
		Clay					31
C Horizon	Vermiculite (%)	Sand	6	3	3	2	
		Silt					0
		Clay					4
	Kaolin (%)	Sand	32	1	11	4	
		Silt					2
		Clay					64
	Gibbsite (%)	Sand	2	11	3	4	
		Silt					1
		Clay					41

Table 41 (cont'd).

Reference			Coleman et al. (1949)	Stolt & Baker (2000)	Coleman et al. (1949)	Calvert et al. (1980a)
Physiographic Province			Blue Ridge	Piedmont	Piedmont	Piedmont
State			North Carolina	Virginia	North Carolina	North Carolina
Sample Name			Fannin Soil	Lovingston	Cecil Soil	--
Bedrock			Mica schist	Granites, gneisses, and schists	Granite and granite gneiss	Granite gneiss
A Horizon	Vermiculite (%)	Sand		44		
		Silt	2		0	
		Clay	2		2	
	Kaolin (%)	Sand		28		14
		Silt	0		0	
		Clay	3		11	
	Gibbsite (%)	Sand		4		
		Silt	2		0	
		Clay	6		3	
B Horizon	Vermiculite (%)	Sand		22		
		Silt	0		0	
		Clay	3		2	
	Kaolin (%)	Sand		54		37
		Silt	0		1	
		Clay	13		34	
	Gibbsite (%)	Sand		2		
		Silt	1		1	
		Clay	16		14	
C Horizon	Vermiculite (%)	Sand		10		
		Silt	0		0	
		Clay	3		0	
	Kaolin (%)	Sand		55		25
		Silt	0		9	
		Clay	8		39	
	Gibbsite (%)	Sand		0		
		Silt	1		3	
		Clay	21		14	

Table 42. Time necessary to form the reported clay abundance in a given Piedmont Terrane (Figure 1) regolith using the clay genesis rates calculated from this study, and assuming a physically comparable weathering profile to that of Coweeta. Clay abundances are reported in Table 41.

Reference		Stolt & Baker (2000)	Norfleet et al. (1993)	Norfleet et al. (1993)	Norfleet et al. (1993)	Coleman et al. (1949)	Coleman et al. (1949)	Stolt & Baker (2000)	Coleman et al. (1949)	Calvert et al. (1980a)	Minimum	Maximum	Mean
Physiographic Province		Blue Ridge	Blue Ridge	Blue Ridge	Blue Ridge	Blue Ridge	Blue Ridge	Piedmont	Piedmont	Piedmont			
State		Virginia	NW South Carolina	NW South Carolina	NW South Carolina	North Carolina	North Carolina	Virginia	North Carolina	North Carolina			
Sample Name		Pilot	ED-1	ED-2	ED-3	Rabun Soil	Fannin Soil	Lovingston	Cecil Soil	---			
Bedrock		Granites, gneisses, and schists	Gneisses and schists	Mica-rich gneisses or schists	Mica-rich gneisses or schists	Basic crystalline rock	Mica schist	Granites, gneisses, and schists	Granite and gneiss	Granite gneiss			
Watershed 2 Rates	Kaolin	500 Ky	10 Ky	200 Ky	70 Ky	900 Ky	100 Ky	800 Ky	700 Ky	400 Ky	10 Ky	900 Ky	400 Ky
	Gibbsite	100 Ky	700 Ky	200 Ky	300 Ky	3 My	1 My	10 Ky	1 My		10 Ky	3 My	800 Ky
	Vermiculite	80 Ky	30 Ky	30 Ky	30 Ky	30 Ky	30 Ky	100 Ky	2 Ky		2 Ky	100 Ky	40 Ky
Watershed 34 Rates	Kaolin	800 Ky	30 Ky	300 Ky	100 Ky	2 My	200 Ky	1 My	1 My	700 Ky	30 Ky	2 My	700 Ky
	Gibbsite	60 Ky	400 Ky	100 Ky	200 Ky	1 My	700 Ky	8 Ky	600 Ky		8 Ky	1 My	400 Ky
	Vermiculite	600 Ky	200 Ky	200 Ky	200 Ky	300 Ky	200 Ky	700 Ky	10 Ky		10 Ky	700 Ky	300 Ky
Watershed 27 Rates	Gibbsite	60 Ky	300 Ky	100 Ky	100 Ky	1 My	600 Ky	7 Ky	500 Ky		7 Ky	1 My	300 Ky
	Vermiculite	400 Ky	200 Ky	200 Ky	100 Ky	200 Ky	100 Ky	500 Ky	8 Ky		8 Ky	500 Ky	200 Ky

genesis rates. Table 43 contains plagioclase dissolution rates calculated as part of this study, as well as from other central and southern Appalachian watersheds as reported in the literature. From Table 43 it is evident that the Coweeta plagioclase dissolution rates fall near the mean calculated of southern and central Appalachian plagioclase dissolution rates. This observation supports the regional representativeness of the Coweeta mass balance calculations, and their use in calculating clay production times for the Piedmont Terrane.

The kaolin destruction rate of W27 (Table 38) has not been used to calculate clay production times for the Piedmont Terrane (Table 42). Again, the kaolin destruction rate for W27 is believed to be a robust value, but its representativeness of the entire Piedmont Terrane is in question.

Discussion

The clay production times reported in Table 42 reflect clay genesis rates calculated for present-day conditions at Coweeta, and are based on a representative Coweeta weathering profile. The production times of clay mineral assemblages range from 2 Ky to 3 My, with mean values ranging from 40 Ky to 800 Ky. Based on the present-day weathering rates of primary minerals, Velbel (1984a, 1985a) reports a Coweeta saprolite residence time of approximately 100 Ky. This residence times fall within the range of mean clay production times for regolith of the Piedmont Terrane.

The influence of periglacial climates on the chemical weathering of Appalachian crystalline bedrock has been discussed by Cleaves (1993). Using an isovolumetric weathering model, he argues that reduced soil CO_2 and decreased ground water moving

Table 43. Comparison of Coweeta plagioclase dissolution rates with southern and central Appalachian plagioclase dissolution rates reported in the literature. Note that the Coweeta rates are near the mean for southern and central Appalachian plagioclase dissolution rates.

Reference	Location	Physiographic Province	Bedrock	Reported Composition	Rate (mol ha^{-1} yr^{-1})
O'Brien et al. (1997)	South Fork Brokenback Run, Virginia	Blue Ridge	Old Rag Granite	An_{22}	666
O'Brien et al. (1997)	Hauver Branch, Maryland	Blue Ridge	Catoctin Formation Metabasalt	An_{53}	514
O'Brien et al. (1997)	Fishing Creek Tributary, Maryland	Blue Ridge	Catoctin Formation Metabasalt	An_{0}	299
Furman et al. (1998)	Shaver Hollow, Virginia	Blue Ridge	Pedlar Granodiorite with Catoctin Basalt Dikes	An_{30}	639
Furman et al. (1998)	White Oak Run, Virginia	Blue Ridge	Chilhowee Metasedimentary Sequence	An_{30}	157
Furman et al. (1998)	Deep Run, Virginia	Blue Ridge	Chilhowee Metasedimentary Sequence	An_{30}	128
White et al. (2002)	Panola Mountain, Georgia	Piedmont	Panola Granite	An_{23}	341
Cleaves et al. (1970)	Pond Branch, Maryland	Piedmont	Lower Schist Member of the Wissahickon Formation	An_{22}	146
O'Brien et al. (1997)	Mill Run, Virginia	Valley and Ridge	Massanutten Sandstone	$An_{0.05}$	158
O'Brien et al. (1997)	Shelter Run, Virginia	Valley and Ridge	Massanutten Sandstone	$An_{0.05}$	243
This Study	W2	Blue Ridge	Otto Formation	An_{28}	478
	W34		Otto Formation	An_{28}	429
	W27		Coweeta Group	An_{30}	241
Mean					341
Minimum					128
Maximum					666

past the weathering front during periglacial times would result in an average rate of saprolitization over the last million years being as little as 24% that of the present. If Cleaves (1993) is correct, then estimates for the mean age of the saprolite at Coweeta is low, and the saprolite may actually have a residence time of approximately 500 Ky. Again, this value falls within the range of Piedmont Terrane clay production times.

The kaolin rate for W27 reflects dissolution and may be the result of either error within the calculations. Alternatively, that the kaolinite identified in diffractograms may be relict from an earlier climatic period and has not yet completely dissolved from the regolith; perhaps the present day conditions in W27 (the time interval on which the mass balance reaction rates are based) are not representative of clay forming conditions over the approximately 500 Ky life of the regolith. If in the past, a warmer and/or drier climate existed in W27, kaolinite may have formed; this kaolinite has certainly been undergoing dissolution since onset of the modern climate, albeit at a very slow rate. From the response and production times of W2 and W34 it is clear that the climatic conditions which favor kaolin precipitation (relatively high temperature and/or relatively low precipitation) would need to persist for approximately 100 Ky for detectable quantities of kaolinite to precipitate. If such a kaolin-favorable climate was followed by the present-day W27 climate, then kaolinite dissolution rates would be so slow that relict kaolinite would remain in the profile for an extended period of time (hundreds of thousands to millions of years).

Since the Middle Pleistocene, episodes of cold climates have been interspersed with interglacial paleoclimates that were warmer than the present (Emiliani 1972, Bowen 1979, Clark 1993, Winograd et al. 1997, Bradley 1999; Figure 37). If the interglacial

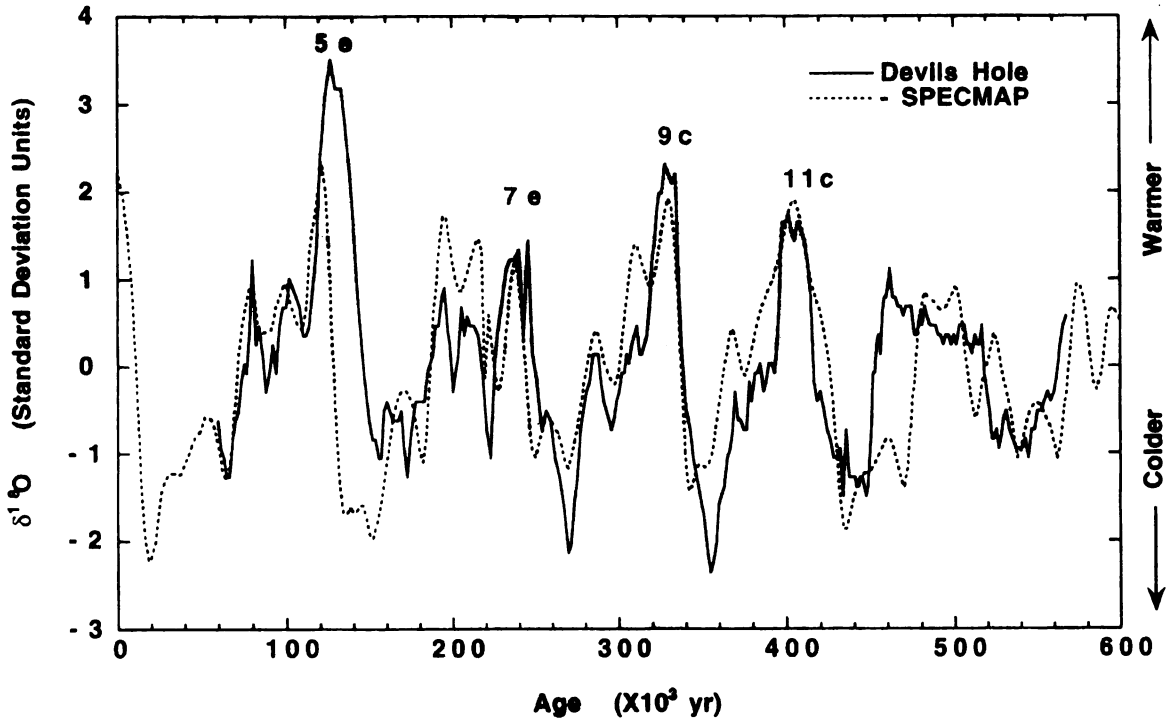

Figure 37. The $\delta^{18}O$ record in a calcite vein from Devil's Hole, Nevada compared to the Spectral Mapping Project (SPECMAP) marine isotope record. The SPECMAP isotope record is a composite chronology for a set of seven superimposed $\delta^{18}O$ records from different ocean basins of the world. Shaded areas represent the last four interglacial periods (isotopic substages 5e, 7e, 9c, and 11c). Modified from Winograd et al. (1997), his Figure 2.

periods were also drier than today, then the climate would have been conducive to kaolin formation. Post-Middle Pliocene interglacials generally lasted approximately 20 Ky to 26 Ky (Winograd et al. 1997; Figure 37). Only if the interglacials were significantly warmer and/or drier than present-day W2 would detectable kaolin potentially precipitate in that relatively short time period. The Coweeta watershed response times indicate that kaolin precipitates at a more rapid rate than it gets dissolved. Relatively small abundances of kaolin may form during interglacials, but not be completely destroyed during a later cooler and/or wetter climate. As a result, all clay abundances including kaolin may reflect a net increase over multiple glacial-interglacial episodes. The last four interglaciations (5e, 7e, 9c, and 11c; Figure 37) sum to 88 Ky. Under such circumstances

it would not be possible to precisely constrain the timing of W27 kaolin formation in the geologic past. However, based on the clay production times (Table 42) it is likely that the present-day mineral abundances in any Coweeta weathering profile reflect the "average" climate that has occurred over the last approximately 500 Ky.

Conclusions

The purpose of this study has been to test Thiry's (2000) argument that the best resolution of the paleoclimatic record in clay-rich sediments and mudrocks 1 or 2 Ma. The conclusions of this study are consistent with those of Thiry (2000).

CHAPTER 10

SUMMARY AND CONCLUSIONS

This study has addressed the influences of climate and lithology on continental clay mineral assemblages. The use of clay minerals as proxies for climate is debated in the literature. Clay mineral formation/dissolution rates have been calculated using watershed mass balance methods at the Coweeta Hydrologic Laboratory located in western North Carolina. The rates have been calculated for three watersheds, two of which only vary by climate (W2 and W34), and a third (W27) which varies from the other two by both climate and lithology. By calculating present-day mineral weathering/formation rates, the rates could be directly correlated with the modern climate. Coweeta is an ideal locality to perform such a study, because it is an intermediate landscape between weathering-limited and transported-limited end-members. The objective of calculating clay formation/dissolution rates at Coweeta has been to determine the resolution of clay minerals in mudrocks as indicators of paleoclimate; Thiry (2000) has argued that the best resolution is 1 to 2 Ma.

The watershed mass balance methods utilized in this study differ from previous mass balance studies completed at Coweeta and elsewhere. The importance of accessory allanite weathering on the Ca (and Na) budget of stream waters has been demonstrated as part of this study, and allanite has been included in all calculations. With allanite weathering recognized, rare earth elements have been included in the mass balance in order to overcome the fundamental problem of the number of unknowns exceeding the number of equations in the matrix algebra. The successful inclusion of REE in the mass balance methods demonstrates that trace elements can be used in such techniques.

The results of this study indicate that kaolin reflects warm and/or dry climates, with gibbsite reflecting cool and/or wet climates. Vermiculite appears to be influenced by both lithology and climate.

The clay formation/dissolution rates calculated for the three watersheds of this study indicate that the neoformed clay minerals kaolin and gibbsite are substantially more sensitive to changes in climate than transformed vermiculite. Lithologic influences on kaolin and gibbsite formation are relatively small, whereas vermiculite formation is strongly linked to biotite weathering. Biotite weathering may be influenced not only by climate, but also by composition (Murakami et al. 2003). Therefore, the use of vermiculite as a paleoclimatic indicator is called into question.

Based on the present-day clay formation rates determined by mass balance methods for Coweeta, detectable changes in relative clay mineral abundance (i.e., 50 g kg^{-1} using XRD) occur on time scales of tens of thousands to hundreds of thousands of years. Such time scales exceed the time scales of glacial-interglacial oscillations (approximately 100 Ky). As a result, clay mineral assemblages in the sedimentary record at best reflect long-term (tens of thousands to hundreds of thousands of years) average climate changes. Certainly, the clay mineral assemblages present in the Coweeta regolith today have not equilibrated with the modern Holocene interglacial climate. Furthermore, the results of this research suggest that Thiry (2000) is correct: the best paleoclimatic resolution of clay minerals in the rock record is 1 to 2 My.

Future Research

Calcium Loss Differences Between Solid and Solute Phase Chemistry

At Coweeta, the solid phase bulk chemistry reflects a greater loss of Ca from the lower saprolite than does the modern stream water chemistry. The likely Ca sink at Coweeta that reduces the present-day stream water Ca/Na ratio is vermiculite. Vermiculite at Coweeta contains one to three orders of magnitude more Ca than parent biotite, with relatively little difference in Na (Tables 13 and 14). Furthermore, there is preliminary evidence that the vermiculite formation rate increases with increasing temperature (Figure 36, Appendix D). The modern interglacial climate may potentially provide an optimal climate for vermiculite genesis, thereby providing a Ca sink that may not be significant during glacials. It may also further be hypothesized that the greater the biotite abundance in the bedrock, the less likely a calcium problem will be manifested in stream waters. The role of vermiculite as a Ca sink during interglacial periods can only be resolved with future research.

Kaolin and Climate

Based on the oxygen isotope ratios of clay, Elliott et al. (1995, 1997) determined that pedogenic kaolinite found in saprolite of the Virginia Piedmont Province formed under a cooler climatic regime than exists today. They suggested that the kaolinite possibly formed during or shortly after Pleistocene glaciation. Bird and Chivas (1988) had similar findings for kaolinite sampled from Permian clayrocks of eastern Australia. They also concluded that kaolinite neoformation occurred during a glacial or deglacial period. The results of this study indicate that kaolin formation is favored in a warmer and/or drier climate. From the current data set it is not possible to resolve the relative

importance of temperature vs. precipitation on kaolin formation. However, when combining the results of Elliott et al. (1995, 1997) and Bird and Chivas (1988) with those of this study, it may be suggested that kaolin precipitation may actually be favored in a cooler climate if precipitation is sufficiently low. If so, then perhaps the glacial periods, rather than the interglacials, provide adequately dry conditions that may be conducive to kaolin formation despite the cooler temperatures. Approximately 75% of the last 500 Ky were cooler glacial periods (Winograd et al. 1997; Figure 37). If Elliott et al. (1995, 1997) are correct and southern Appalachian kaolin formed during a glaciation, than 375 Ky of the last 500 Ky may have provided climatic conditions that favored kaolin precipitation. During the present interglacial, this relict kaolin is slowly undergoing dissolution in W27. Kaolin precipitation in cool and dry climates is contrary to previous research which has always reported kaolinite to reflect warm and humid climates (Tables 2 and 34).

From the production times of W2 and W34 it is evident that it may take as much as 2 My to generate a kaolin-rich regolith (Table 42). However, if the present-day kaolin formation rates are slow relative to cooler/drier glacial times, then the 2 My needed to produce a kaolin-rich weathering profile may be substantially reduced. Modern clay mineral assemblages likely reflect an average long-term climate that is significantly longer than the glacial-interglacial oscillations (average approximately 100 Ky; Winograd et al. 1997) identified for the last 500 Ky (Figure 37).

It is important to recognize that the above discussion is based on clay genesis rates calculated for modern interglacial watersheds (Figure 37) and may only be applicable to weathering during interglaciations. Furthermore, resolving the relative

influence of temperature vs. precipitation on clay neoformation would require identical watersheds including one that is relatively warm and wet and the other relatively cool and dry. The results of this study are limited by the fact that temperature increases for Coweeta watersheds are accompanied by precipitation decreases. The possibility of kaolin precipitating during cooler and dryer interglacial climatic conditions can only be resolved with future research.

APPENDICES

APPENDIX A

MAP OF SAMPLE LOCATIONS

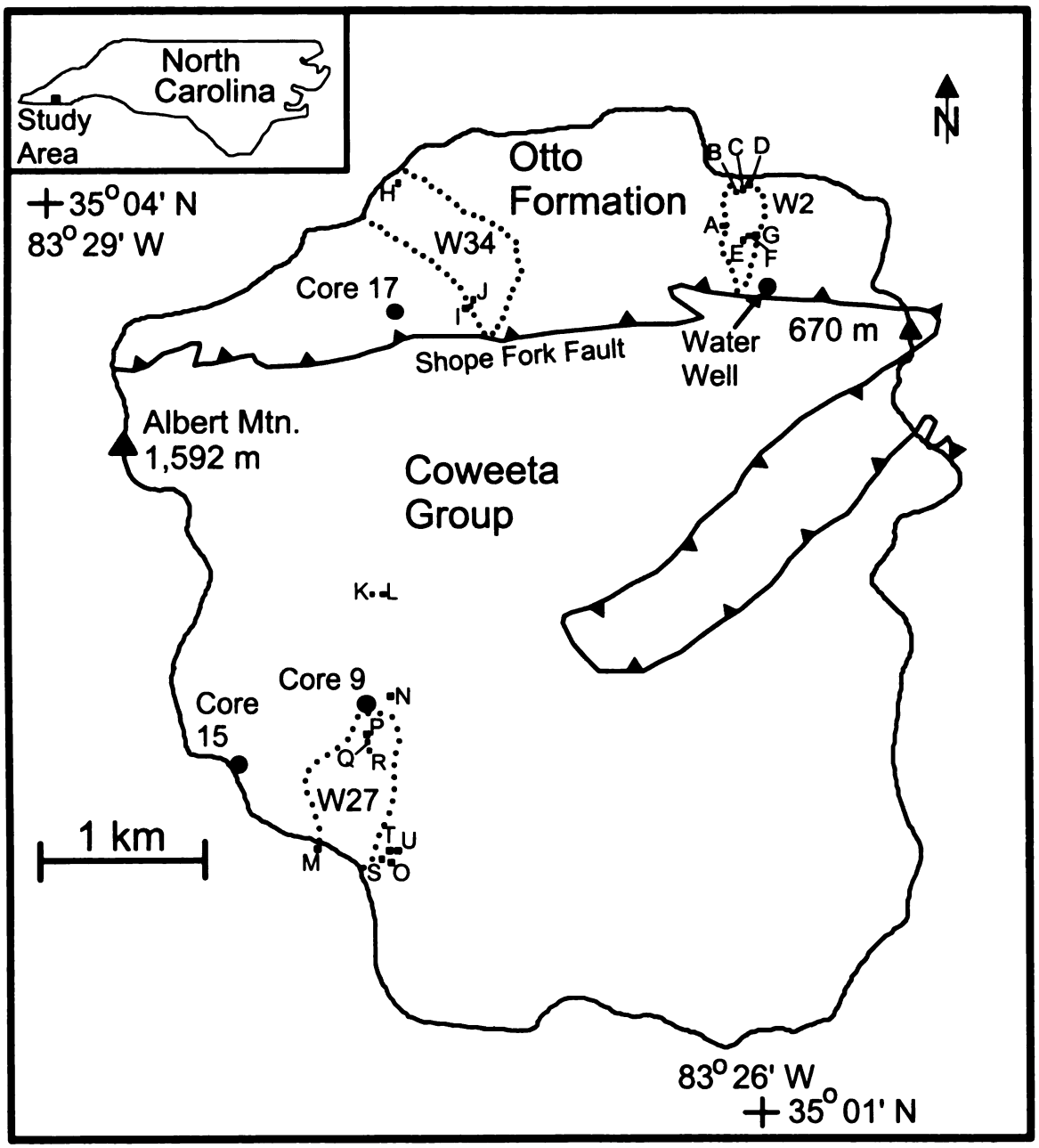

Key for Sample Locations

A: W2-1, W2-2, W2-3, W2-4
B: W2-16, W2-17
C: W2-14, W2-15
D: W2-11, W2-12, W2-13
E: W2-9, W2-10
F: W2-7, W2-8
G: W2-5, W2-6
H: W34-4, W34-5, W34-6, W34-7
I: W34-1, W34-2
J: W34-12, W34-13
K: W27-14, W27-15, W27-16, W27-17
L: W27-18, W27-19, W27-2O, W27-21
M: W27-1, W27-2
N: W27-9, W27-10, W27-11, W27-12, W27-13
O: W27-3, W27-4, W27-5, W27-6, W27-7, W27-8
P: LSS27-1, LSS27-3
Q: LMS27-1, LMS27-2
R: LRS27-1, LRS27-3
S: W27-22
T: W27-23, W27-24
U: W27-27, W27-28, W27-29

APPENDIX B

SAMPLE X-RAY DIFFRACTION PATTERNS

Key to Diffractogram Notation

Pattern Labels

Mg → Indicates sample was Mg-saturated.
K → Indicates sample was K-saturated.
Air Dried → Indicates sample did not receive any pretreatment.
B → Scan of hand-picked biotite grains; no pretreatment.

Peak Labels

H → Hydrobiotite
S → Smectite
K/H → Interlayered kaolinite and hydroxy-interlayered material
V → Vermiculite
M → Mica
K → Kaolinite
Va → Variscite
G → Gibbsite
Ha → Halloysite
Go → Goethite
? → Unknown peak

Numbers above peaks are d-spacings in angstroms (Å).

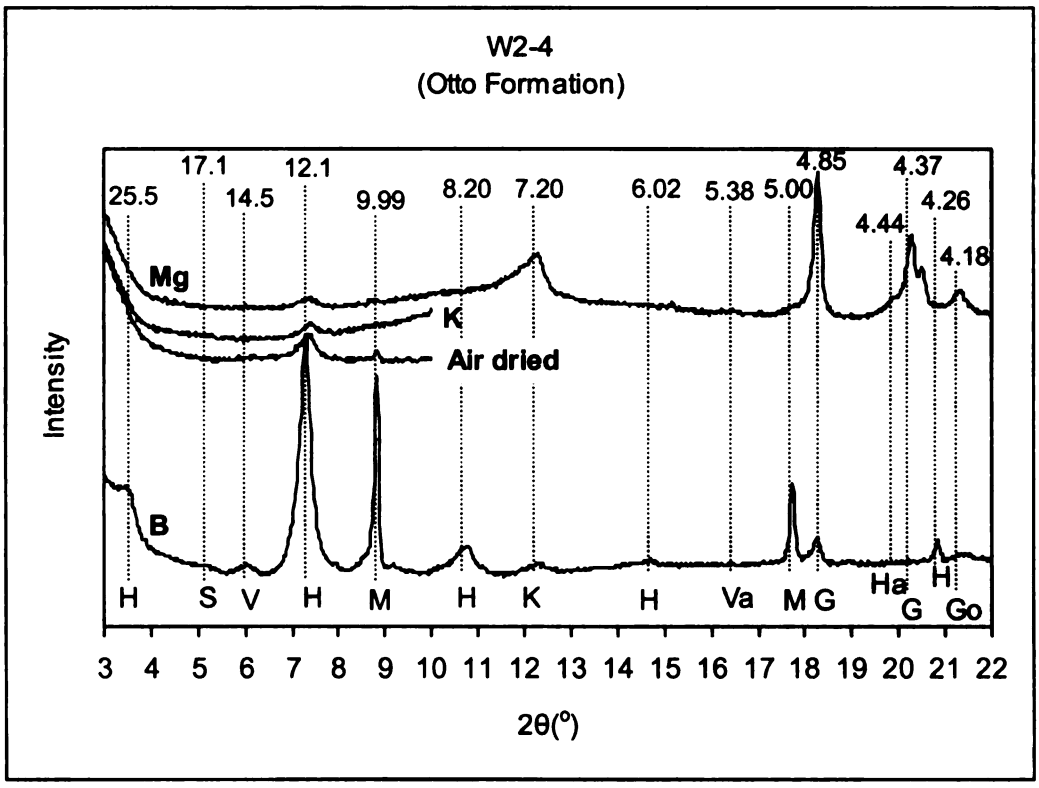
W2-4
(Otto Formation)
Intensity
Mg
K
Air dried
B
25.5
17.1
14.5
12.1
9.99
8.20
7.20
6.02
5.38
5.00
4.85
4.44
4.37
4.26
4.18
H
S
V
H
M
H
K
H
Va
M G
Ha
G
H
Go
3 4 5 6 7 8 9 10 11 12 13 14 15 16 17 18 19 20 21 22
2θ(°)

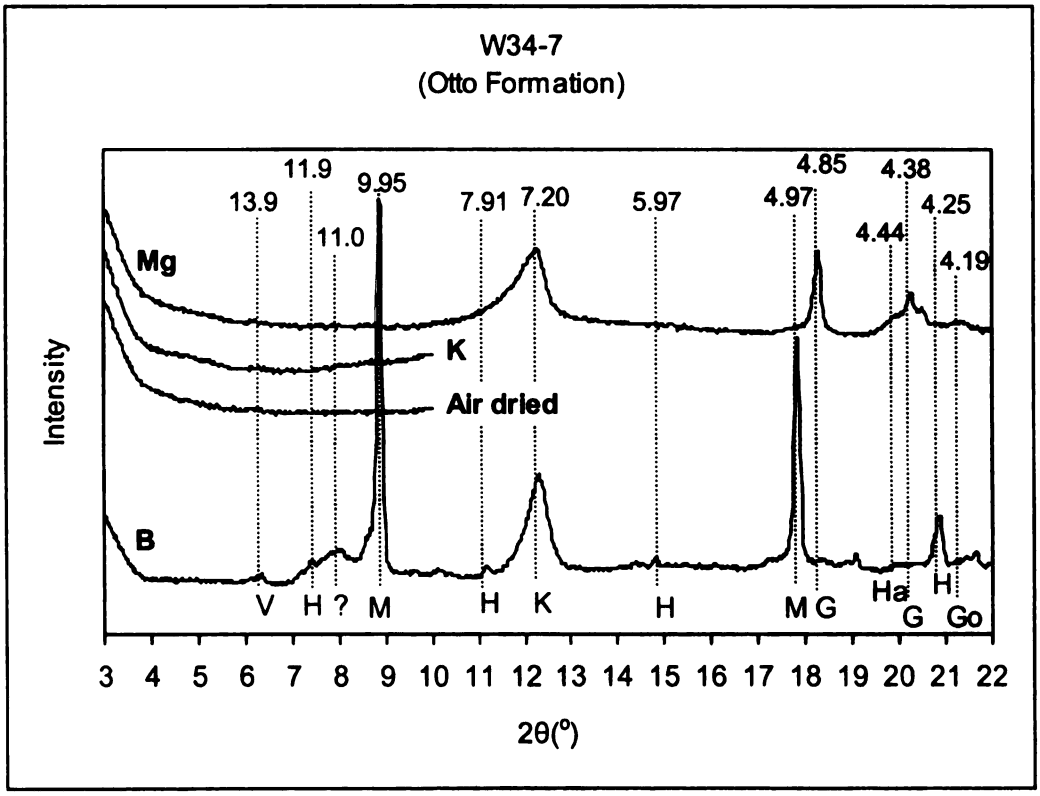
W34-7
(Otto Formation)
Intensity
Mg
K
Air dried
B
13.9
11.9
11.0
9.95
7.91
7.20
5.97
4.97
4.85
4.44
4.38
4.25
4.19
V
H
?
M
H
K
H
M G
Ha
G
H
Go
3 4 5 6 7 8 9 10 11 12 13 14 15 16 17 18 19 20 21 22
2θ(°)

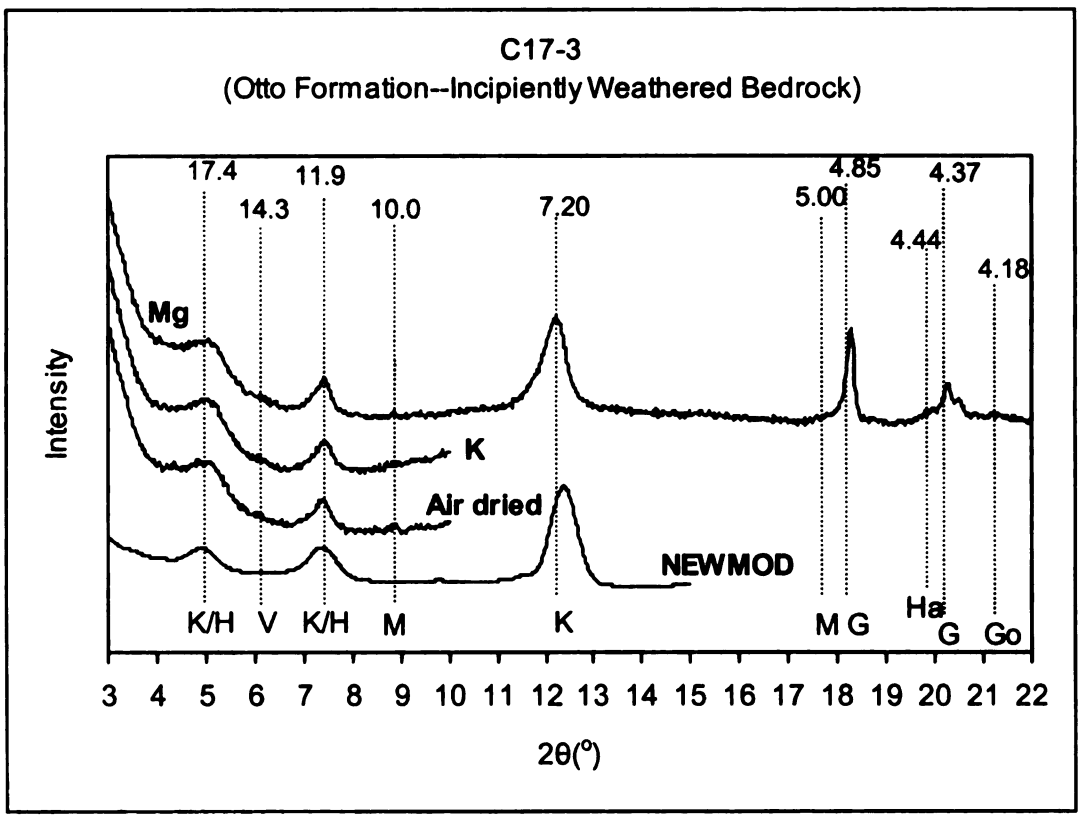
C17-3
(Otto Formation--Incipiently Weathered Bedrock)
17.4
11.9
14.3
10.0
7.20
4.85
5.00
4.37
4.44
4.18
Mg
K
Air dried
NEWMOD
K/H
V
K/H
M
K
M G
Ha
G
Go
Intensity
3 4 5 6 7 8 9 10 11 12 13 14 15 16 17 18 19 20 21 22
2θ(°)

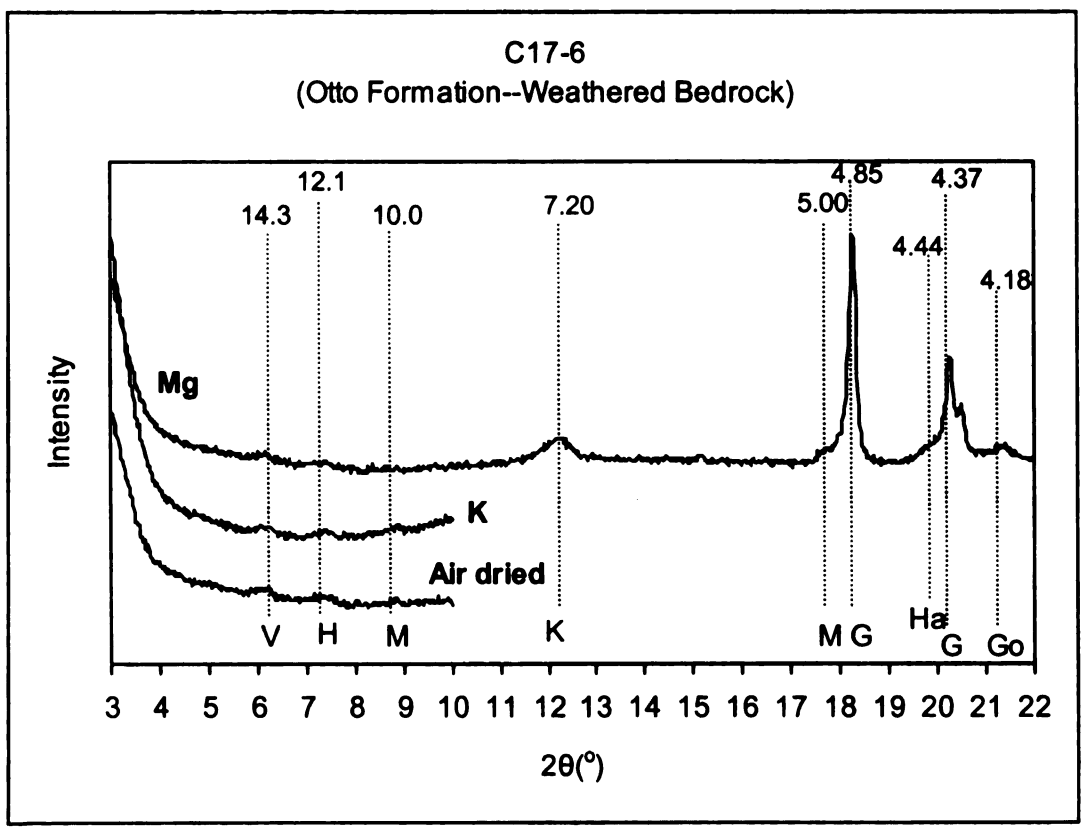
C17-6
(Otto Formation--Weathered Bedrock)
12.1
14.3
10.0
7.20
4.85
5.00
4.37
4.44
4.18
Mg
K
Air dried
V
H
M
K
M G
Ha
G
Go
Intensity
3 4 5 6 7 8 9 10 11 12 13 14 15 16 17 18 19 20 21 22
2θ(°)

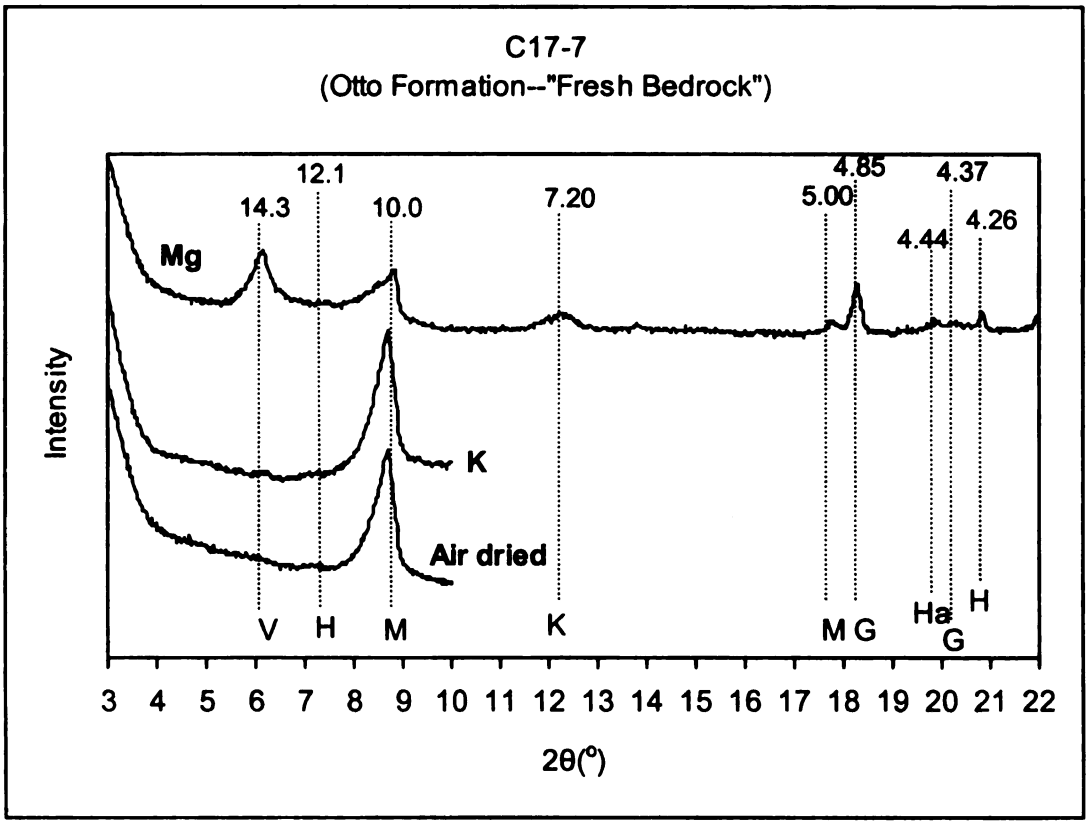
C17-7
(Otto Formation--"Fresh Bedrock")
Intensity
Mg
K
Air dried
14.3
12.1
10.0
7.20
5.00
4.85
4.44
4.37
4.26
V
H
M
K
M G
Ha
G
H
3 4 5 6 7 8 9 10 11 12 13 14 15 16 17 18 19 20 21 22
2θ(°)

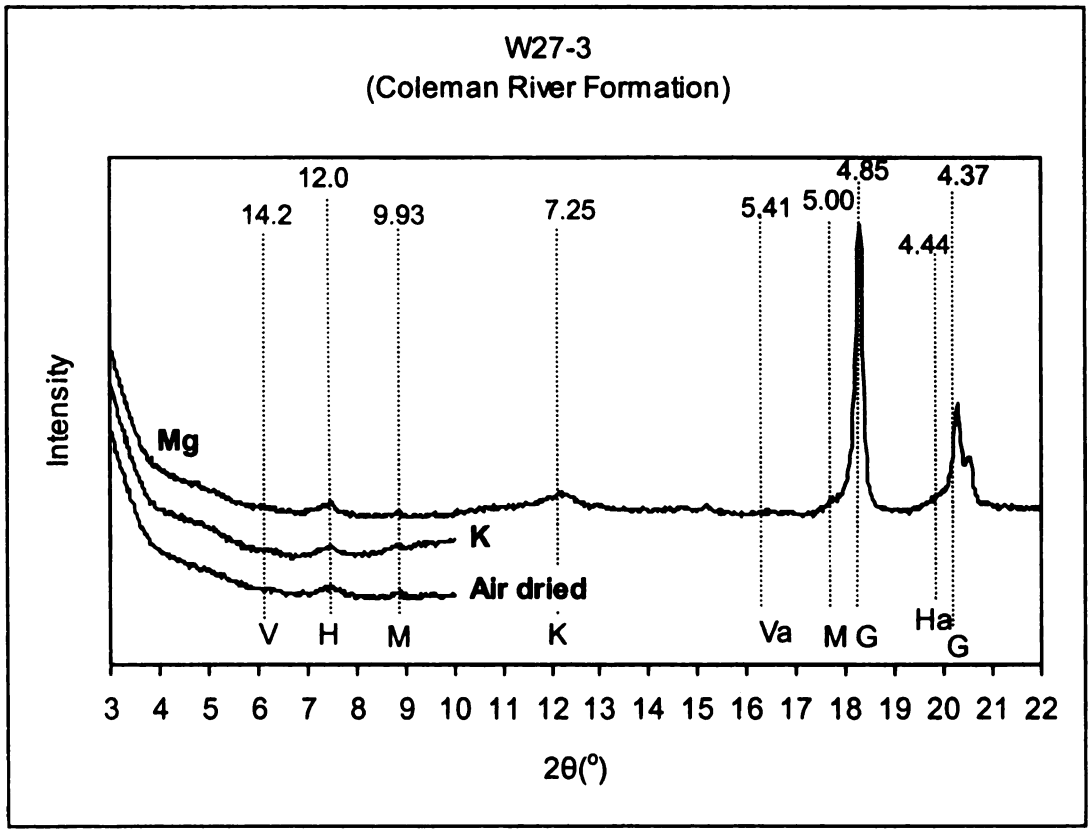
W27-3
(Coleman River Formation)
Intensity
Mg
K
Air dried
14.2
12.0
9.93
7.25
5.41
5.00
4.85
4.44
4.37
V
H
M
K
Va
M G
Ha
G
3 4 5 6 7 8 9 10 11 12 13 14 15 16 17 18 19 20 21 22
2θ(°)

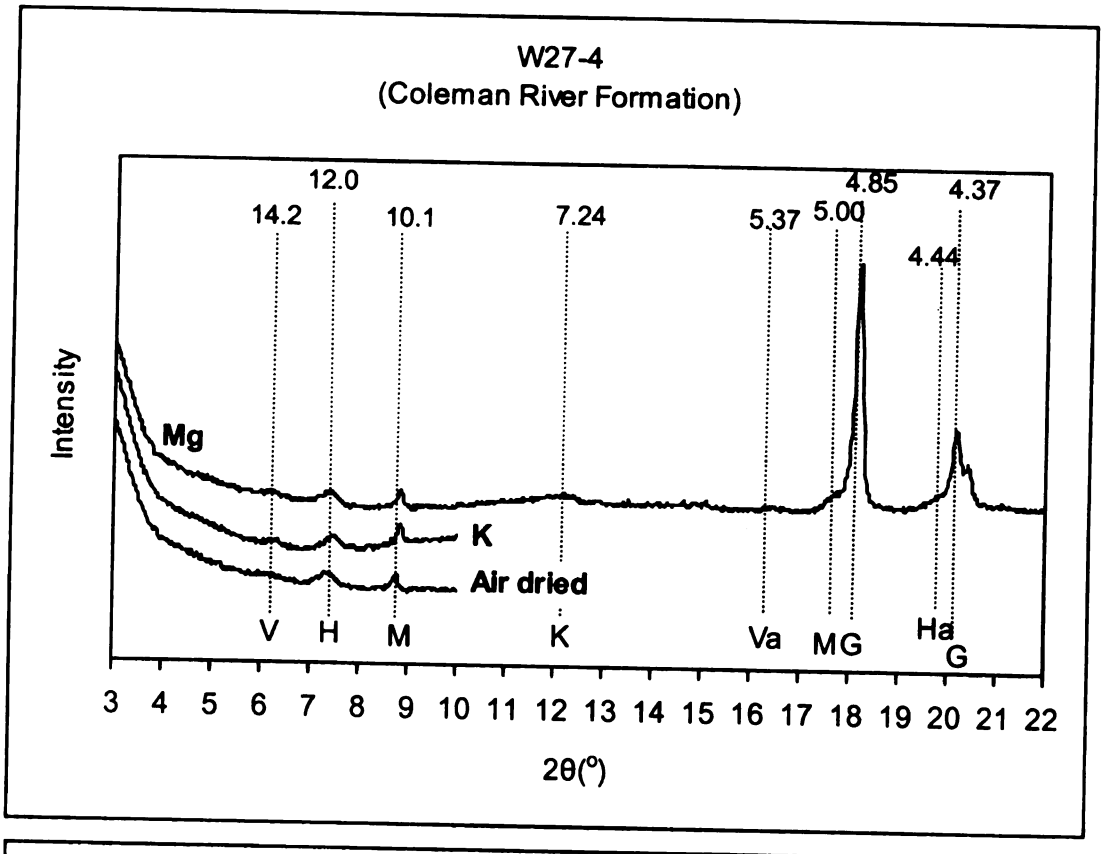
W27-4
(Coleman River Formation)
Intensity
12.0
14.2
10.1
7.24
5.37
5.00
4.85
4.37
4.44
Mg
K
Air dried
V
H
M
K
Va
MG
Ha
G
3 4 5 6 7 8 9 10 11 12 13 14 15 16 17 18 19 20 21 22
2θ(°)

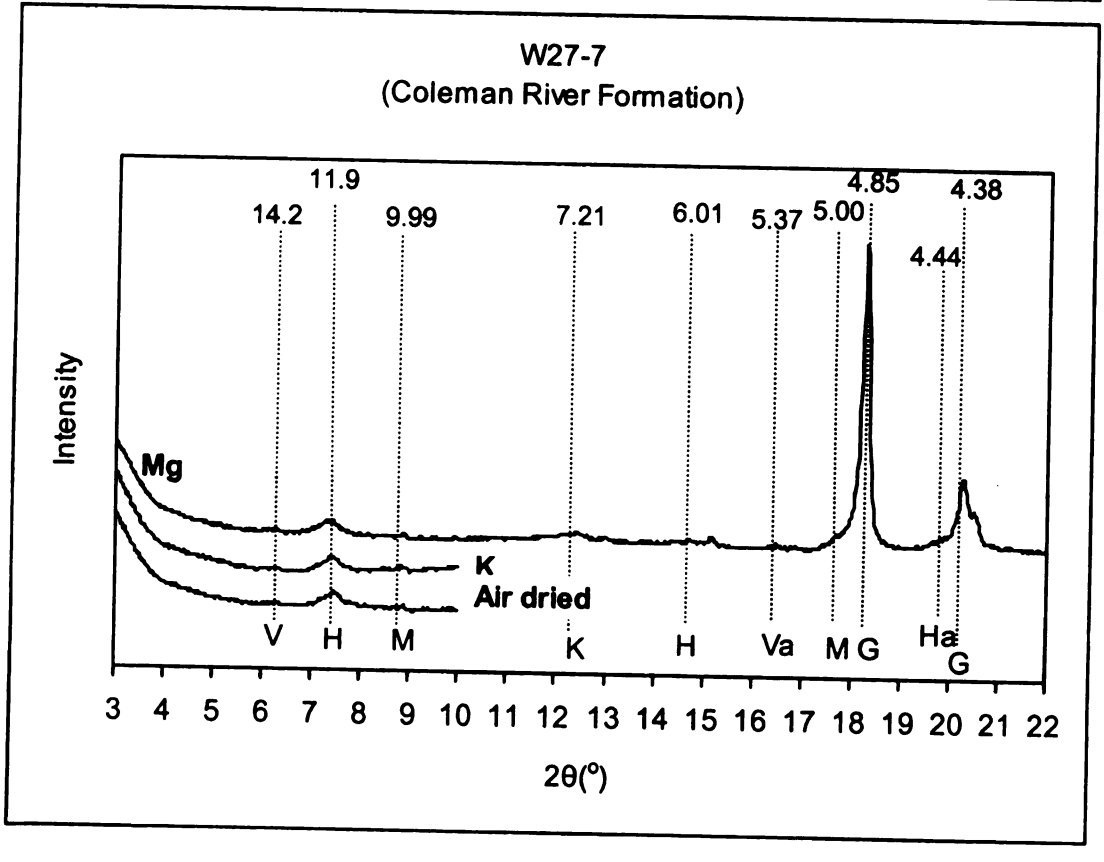
W27-7
(Coleman River Formation)
Intensity
11.9
14.2
9.99
7.21
6.01
5.37
5.00
4.85
4.38
4.44
Mg
K
Air dried
V
H
M
K
H
Va
MG
Ha
G
3 4 5 6 7 8 9 10 11 12 13 14 15 16 17 18 19 20 21 22
2θ(°)

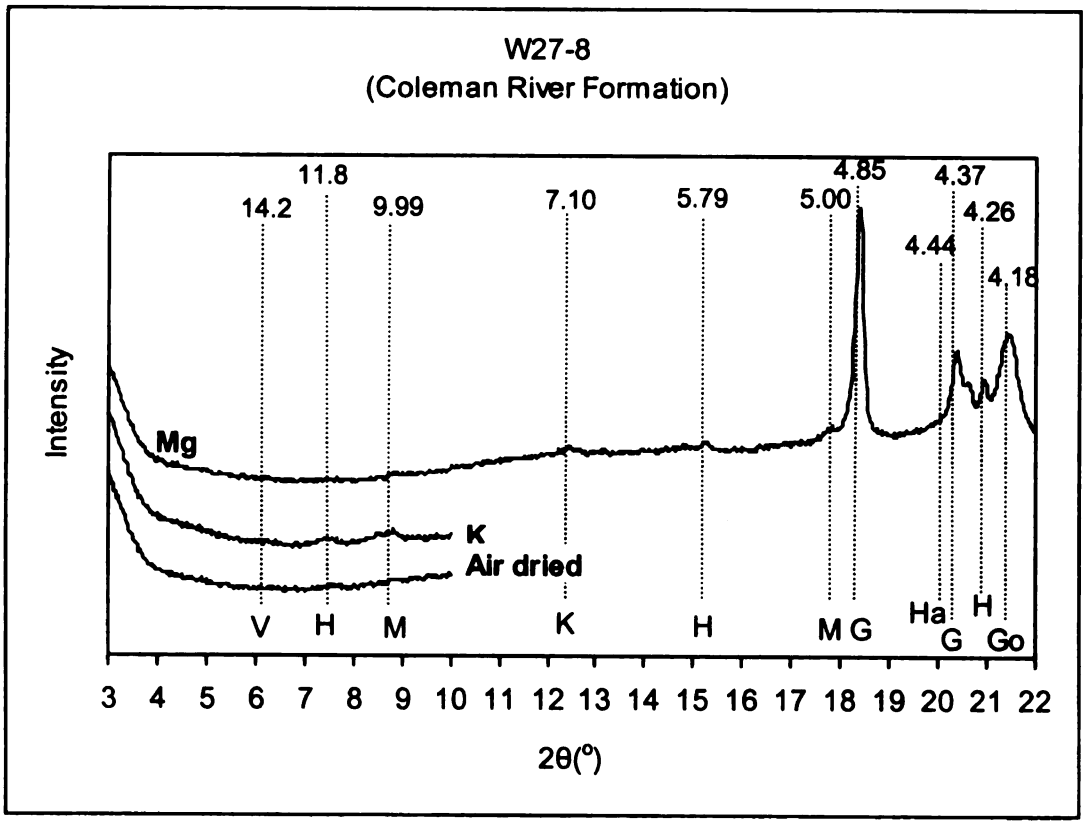
W27-8
(Coleman River Formation)
Intensity
14.2
11.8
9.99
7.10
5.79
5.00
4.85
4.37
4.26
4.44
4.18
Mg
K
Air dried
V
H
M
K
H
M G
Ha
G
H
Go
3 4 5 6 7 8 9 10 11 12 13 14 15 16 17 18 19 20 21 22
2θ(°)

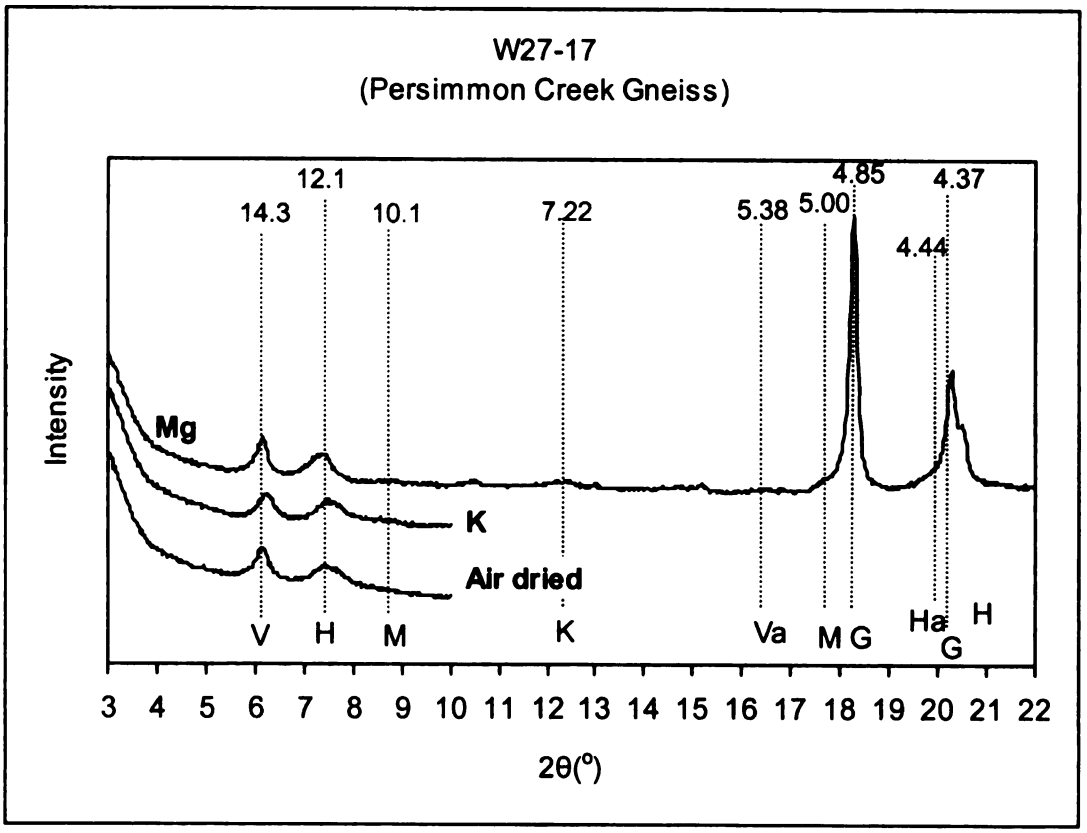
W27-17
(Persimmon Creek Gneiss)
Intensity
14.3
12.1
10.1
7.22
5.38
5.00
4.85
4.37
4.44
Mg
K
Air dried
V
H
M
K
Va
M G
Ha
G
H
3 4 5 6 7 8 9 10 11 12 13 14 15 16 17 18 19 20 21 22
2θ(°)

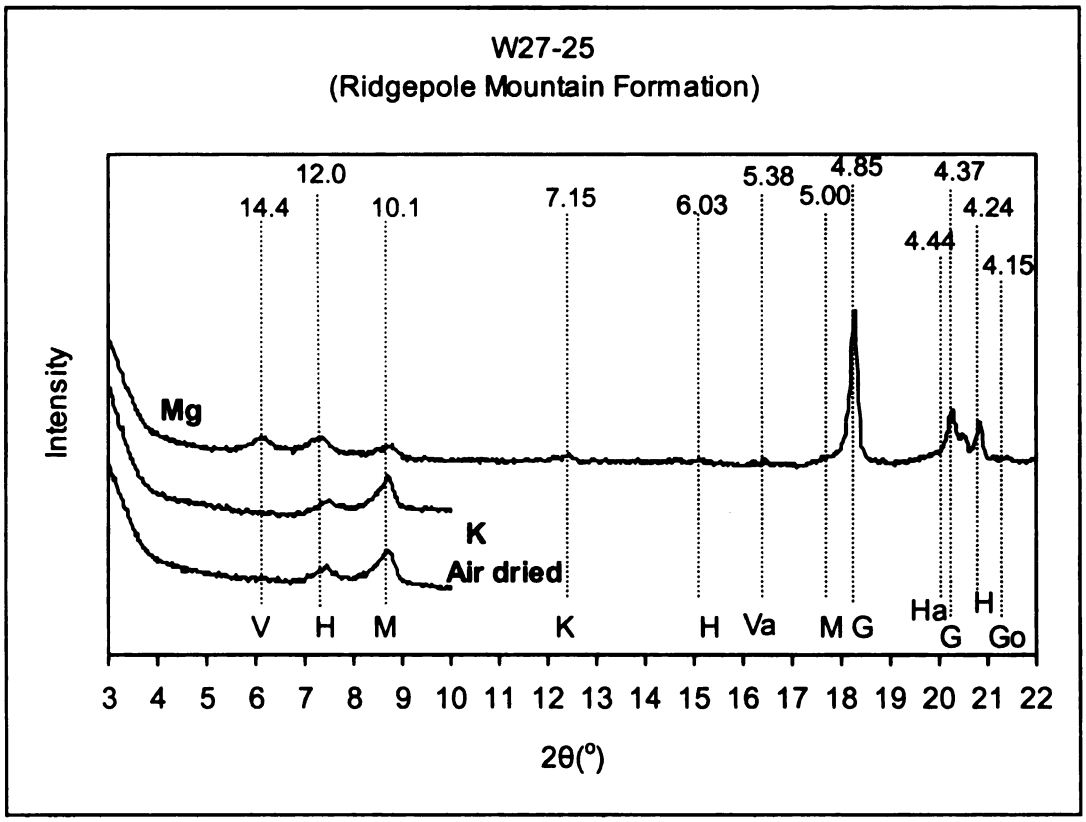
W27-25
(Ridgepole Mountain Formation)
Intensity
Mg
K
Air dried
14.4
12.0
10.1
7.15
6.03
5.38
5.00
4.85
4.44
4.37
4.24
4.15
V
H
M
K
H
Va
M
G
Ha
G
H
Go
3 4 5 6 7 8 9 10 11 12 13 14 15 16 17 18 19 20 21 22
2θ(°)

APPENDIX C

EXAMPLES OF ELEMENTARY CALCULATIONS

Elementary calculations have been completed using an Excel spreadsheet. Examples of each type of calculation are provided below.

Calculation of elements lost from the saprolite in the solid phase mass balance:

Example using Na lost due to plagioclase weathering:

$$2.66 \frac{g}{cm^3} * \frac{1 \text{ mole}}{267 \text{ g}} * \frac{25.07\%}{100} * \frac{100^3 \text{ cm}^3}{\text{m}^3} * \frac{0.7 \text{ moles Na}}{1 \text{ mole plag}} = 1{,}748 \text{ moles Na m}^{-3}$$

- Specific gravity of plagioclase
- Molecular weight of plagioclase
- Percentage of plagioclase dissolved
- Moles of Na per mole of plagioclase

Conversion of clay formation/dissolution rates in mol ha^{-1} yr^{-1} to rates in g kg^{-1} yr^{-1}:

Example using W2 kaolinite formation rate:

$$349 \frac{\text{moles}}{\text{ha} \cdot \text{yr}} * \frac{258 \text{ g}}{\text{mole}} * \frac{1 \text{ hectare}}{10{,}000 \text{ m}^2} * \frac{1}{6 \text{ m}} * \frac{1 \text{ m}^3}{10^6 \text{ cm}^3} * \frac{1 \text{ cm}^3}{2.11 \text{ g}} * \frac{1{,}000 \text{ g}}{\text{kg}}$$

$$= 7.12 * 10^{-4} \text{ g kg}^{-1} \text{ yr}^{-1}$$

- Formula weight of clay
- Profile thickness
- Average profile bulk density

Conversion of clay formation/dissolution rates in g kg^{-1} yr^{-1} to a response/production time in years:

Example using W2 kaolinite formation rate to calculate a response time:

$$50 \text{ g kg}^{-1} * \frac{\text{years}}{7.12 * 10^{-4} \text{ g kg}^{-1}} = 70{,}200 \text{ years}$$

APPENDIX D

CLAY GENESIS RATES AND CLIMATE

Climate consists of both temperature and precipitation. White and Blum (1995a,b) and White et al. (1999a,c) have determined that only the weathering fluxes of SiO_2 for worldwide watersheds underlain by granitoid rock types exhibit statistically significant systematic changes with fluctuations in both precipitation and temperature. They also provided a function that quantitatively describes the weathering flux of SiO_2 as a coupled product of precipitation and temperature. This equation may be used to adjust the SiO_2 flux of either W2 or W34 for the temperature or precipitation of the other, with the adjusted/corrected SiO_2 flux then being used in the mass balance calculations. In doing so, either temperature or precipitation may be held constant in order to evaluate the influence of the other climatic parameter on clay formation rates at Coweeta. The equation developed by White and Blum (1995a,b) and White et al. (1999a,c), is as follows:

$$Q_{i,w} = (a_i * P) \exp\left[-\frac{E_a}{R} \left[\frac{1}{T} - \frac{1}{T_o} \right] \right] \quad (1)$$

Where,

$Q_{i,w}$	Average flux of species i (mol ha^{-1} yr^{-1})
P	Average annual precipitation (mm yr^{-1})
a_i	Fitted precipitation dependence
T_o	Temperature of reference watershed (K)
T	Temperature of specific watershed (K)
E_a	Arrhenius activation energy
R	Gas constant

The pre-exponential term on the right-hand side of Eqn. 1 assumes a linear correlation between precipitation and SiO_2 flux, where a_i is the slope (White and Blum 1995a,b,

White et al. 1999a,c). T_o is a reference temperature and was chosen to be the mean of W2 and W34.

Naturally weathering plagioclase at Coweeta (Velbel 1983, 1986b, 1990a; Figure 38) and elsewhere (e.g., Wilson, 1975, Keller 1976, 1978, Berner and Holdren 1977, 1979, Hochella and Banfield 1995) is known to dissolve by interface-controlled kinetics, which indicates that the flushing rate of meteoric water through a weathering profile does not influence the weathering rate. Allanite weathering (this study) follows the same interface-controlled dissolution kinetics as plagioclase. Garnet weathering at Coweeta too will not be influenced by changes in regolith hydrology, as its weathering is controlled by either diffusion of ions through a protective surface coating (Velbel 1984b, 1993b), or interface-controlled dissolution.

Clay Genesis Rates at Constant Precipitation

The results of the mass balance calculations in which the SiO_2 flux of W34 was calculated from the precipitation of W2 (1,153 mol ha^{-1} yr^{-1}) is presented in Table 44. By making such adjustments, the clay genesis rates of W2 and W34 (Table 44) only reflect the difference in temperature of the two watersheds. Interestingly, the apparent activation energy based on SiO_2 flux calculated as part of this study using only W2 and W34 is 62.1 kJ mol^{-1}, whereas the apparent activation energy for the 68 worldwide watersheds of White and Blum (1995a,b) and White et al. (1999a,c) is 59.4 kJ mol^{-1}. The strong similarity between these two apparent activation energies indicates that, despite being only two watersheds, W2 and W34 are relatively representative of the global average in terms of SiO_2 flux.

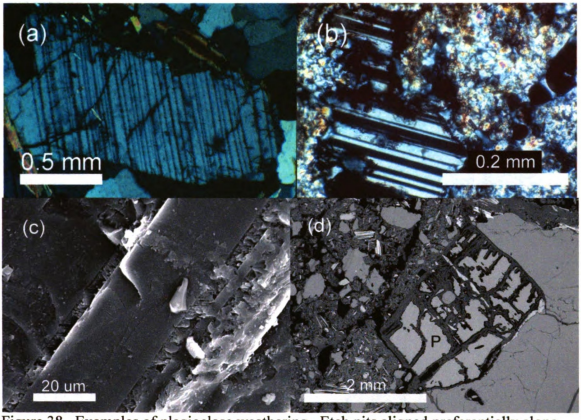

Figure 38. Examples of plagioclase weathering. Etch pits aligned preferentially along one set of twin lamellae in an incipiently weathered rock of the Persimmon Creek Gneiss (a); sample C15-9 in crossed-polarized light. Plagioclase and its weathering products of predominantly gibbsite with lesser kaolin in Persimmon Creek Gneiss saprolite (b); sample W27-14 in crossed-polarized light. SEM image of preferentially etching along one set of twin lamellae in an incipiently weathered rock of the Persimmon Creek Gneiss (c); sample C15-9. BSE image of plagioclase and its weathering products of predominantly gibbsite, goethite, and lesser kaolin in a B horizon of Otto Formation regolith (d); sample W2-17 in crossed-polarized light.

The results of the calculations show that in the warmer watershed (W2) the rates of vermiculite and kaolin formation are higher than those of the cooler watershed (W34). Gibbsite, however, has a faster formation rate in W34. These results indicate that with increasing temperature and constant precipitation, kaolin should form at the expense of gibbsite. The formation of kaolin at the expense of gibbsite in a warmer climate with constant precipitation reflects increased SiO_2 being released to the interstitial waters of

the regolith as a result of the higher weathering rates of plagioclase and biotite (Table 44).

Table 44. Comparison weathering rates for watersheds that vary only by temperature. Precipitation corrected using Eqn. 1 (White and Blum 1995a,b, and White et al. 1999a,c).

Phase	Watershed 2 (mol ha^{-1} yr^{-1})	Watershed 34 Corrected for W2 Precipitation (mol ha^{-1} yr^{-1})
Allanite	40	9
Plagioclase	478	429
Garnet	70	80
Biotite	469	175
Vermiculite	-344	-71
Kaolin	-349	-276
Gibbsite	-252	-312

Watershed 2 has both a higher biotite weathering rate and vermiculite weathering relative to W34. The quantity of Si and Al in the weathering profile pore waters resulting from biotite destruction is actually dependent on the resistance of the vermiculite intermediary to solubilization. That is, the difference between the biotite weathering rate and vermiculite formation rate is a measure of the solute contribution from biotite weathering. The difference in the biotite weathering rate and vermiculite formation rate is greater in W2 than W34 (Table 44), supporting the statement that biotite weathering contributes more solutes available for clay neoformation in a warmer climate than a cooler climate, if precipitation is constant. Therefore, from the results in Table 44, it may also be concluded that warmer temperatures and constant precipitation not only increase the rate of biotite weathering and vermiculite formation, but also increases the fraction of vermiculite ultimately being destroyed. However, with the vermiculite formation rate being higher in W2 relative to W34, vermiculite appears to be an indicator of a warmer climate if precipitation is constant.

In summary, based on the mass balance calculations above, and if precipitation remains constant, vermiculite and kaolin should be indicators of a warmer climate. Gibbsite, in contrast, is an indicator of a decrease in temperature at constant precipitation.

Clay Genesis Rates at Constant Temperature

As stated previously, White and Blum (1995a,b) and White et al. (1999a,c) have determined that only the watershed flux of SiO_2 exhibits statistically significant systematic changes with fluctuations in precipitation. When the W34 SiO_2 flux was adjusted for precipitation, the only rates that change are for kaolin and gibbsite. This may be interpreted to suggest that precipitation only influences the concentration of SiO_2 in weathering profile interstitial waters (e.g., Lowe 1986, Parfitt 1993), and hence the neoformed clay minerals. Plagioclase and allanite dissolve by interface-controlled kinetics (e.g., Wilson, 1975, Keller 1976, 1978, Berner and Holdren 1977, 1979, Velbel 1983, 1986b, 1990a, Hochella and Banfield 1995; Figure 38), and garnet weathering is controlled by either diffusion of ions through a protective surface coating (Velbel 1984b, 1993b) or interface-controlled dissolution. For these reasons it is suggested that the only difference between Watersheds 2 and 34 when temperature is held constant is the SiO_2 flux. Therefore, when comparing weathering rates from W2 and W34, only the SiO_2 flux used to calculate the rates will be different. Equation 1 has been used to adjust the SiO_2 flux of W34 for the temperature of W2. The W34 SiO_2 flux rate increases to 1,448 mol ha^{-1} yr^{-1} when the temperature of W2 is used.

A comparison of weathering rates by which only precipitation has been adjusted, with temperature held constant, is provided in Table 45. Not surprisingly, the watershed

Table 45. Comparison weathering rates for watersheds that vary only by precipitation. Temperature corrected using Eqn. 1 (White and Blum 1995a,b, and White et al. 1999a,c).

Phase	Watershed 2 (mol ha^{-1} yr^{-1})	Watershed 34 Corrected for W2 Temperature (mol ha^{-1} yr^{-1})
Allanite	40	40
Plagioclase	478	478
Garnet	70	70
Biotite	469	469
Vermiculite	-344	-344
Kaolin	-349	-263
Gibbsite	-252	-423

with the highest precipitation (W34), when temperature is held constant, has the highest gibbsite formation rate and the lowest kaolin formation rate. Because the vermiculite transformation rate is apparently only influenced by temperature, it shows no change with change in precipitation.

Conclusions

Isolating temperature and precipitation in the calculations above supports the conclusion that kaolin precipitation is favored under a warm and/or dry climate, and gibbsite is favored under a cool and/or wet climate. Not over-interpreting these results is important because they are only robust if the following assumptions are valid:

(1) The relationships between temperature and solute flux, and precipitation and solute flux as determined by White and Blum (1995a,b) and White et al. (1999a,c) are true.

(2) Only SiO_2 needs adjusting for temperature and precipitation between W2 and W34.

REFERENCES

Afifi, A.A., and Bricker, O.P., 1983, Weathering reactions, water chemistry and denudation rates in drainage basins of different bedrock types: I—sandstone and shale: in Dissolved Loads of Rivers and Surface Water Quantity/Quality Relationships, Proceedings of the Hamburg Symposium, IAHS Publication no. 141, p. 193-203.

Ahn, J.H., and Peacor, D.R., 1987, Kaolinitization of biotite: TEM data and implications for an alteration mechanism: American Mineralogist, v. 72, p. 353-356.

Allen, B.L., and Hajek, B.F., 1995, Mineral occurrence in soil environments: in Dixon, J.B., and Weed, S.B. (eds.), Minerals in Soil Environments, Soil Science Society of America, Madison, Wisconsin, p. 199-278.

Apello, C.A.J., and Postma, D., 1996, Geochemistry, Ground water, and Pollution: A.A. Balkema, Rotterdam, Netherlands, 536 p.

Åström, M., 2001, Hydrological and soil geochemical controls of the abundance and fractionation patterns of rare earth elements in a periodically acidic Boreal stream: Geochemistry; Exploration, Environmental, Analysis, v. 1, p. 101-108.

Aubert, D., Stille, P., and Probst, A., 2001, REE fractionation during granite weathering and removal by waters and suspended loads: Sr and Nd isotopic evidence: Geochimica et Cosmochimca Acta, v. 65, p. 387-406.

Aubert, D., Stille, P., Probst, A., Gauthier-Lafaye, F., Pourcelot, L., and Del nero, M., 2002, Characterization and migration of atmospheric REE in soils and surface waters: Geochimica et Cosmochimica Acta, v. 66, p. 3339-3350.

Banfield, J.F., and Eggleton, R.A., 1988, Transmission electron microscope study of biotite weathering: Clays and Clay Minerals, v. 36, p. 47-60.

Banfield, J.F., and Eggleton, R.A., 1989, Apatite replacement and rare earth mobilization, fractionation, and fixation during weathering: Clays and Clay Minerals, v. 37, p. 113-127.

Bardossy, G., and Aleva, G.J.J., 1990, Lateritic Bauxites: Elsevier Science Publishers, Amsterdam, The Netherlands, 624 p.

Barman, A.K., Varadachari, C., and Ghosh, K., 1992, Weathering of silicate minerals by organic acids. I. Nature of cation solubilisation: Geoderma, v. 53, p. 45-63.

Barshad, I., 1955, Soil Development: in Bear, F.E. (ed.), Chemistry of the Soil, Reinhold Publishing Corporation, New York, p. 1-52.

Barshad, I., 1957, Factors affecting clay formation: Proceedings of the 6th National Conference on Clays and Clay Minerals, p. 110-132.

Barshad, I., 1966, The effect of a variation in precipitation on the nature of clay mineral formation in soils from acid and basic igneous rocks: Proceedings of the International Clay Conference, Jerusalem, v. 1, p. 167-173.

Becker, G.F., 1895, Reconnaissance of the gold fields of the southern Appalachians: U.S. Geological Survey 16th Annual Report, 1894-1895, Part 3, U.S. Government Printing Office, Washington, D.C., p. 251-331.

Benoit, G., 1994, Clean technique measurement of Pb, Ag, and Cd in freshwater: A redefinition of metal pollution: Environmental Science and Technology, v. 28, p. 1987-1991.

Benoit, G., Hunter, K.S., and Rozan, T.F., 1997, Sources of trace metal contamination artifacts during collection, handling, and analysis of freshwaters: Analytical Chemistry, v. 69, p. 1006-1011.

Berner, R.A., 1978, Rate control of mineral dissolution under earth surface conditions: American Journal of Science, v. 278, p. 1235-1252.

Berner, R.A., and Holdren, G.R., Jr., 1977, Mechanism of feldspar weathering: some observational evidence: Geology, v. 5, p. 369-372.

Berner, R.A., and Holdren, G.R., Jr., 1979, Mechanism of feldspar weathering—II. Observations of feldspars from soils: Geochimica et Cosmochimica Acta, v. 43, p. 1173-1186.

Berner, R.A., 1981, Kinetics of weathering and diagenesis: in Lasaga, A.C., and Kirkpatrick, R.J. (eds.), Kinetics of Geochemical Processes: Reviews in Mineralogy Volume 8, Mineralogical Society of America, Washington, D.C., p. 111-134.

Berner, E.K., and Berner, R.A., 1987, The global water cycle: Geochemistry and environment: Englewood Cliffs, Prentice-Hall, Inc., Englewood Cliffs, New Jersey, 397 p.

Berry, J.L., 1976, Study of chemical weathering in the Coweeta Hydrologic Laboratory, Macon County, North Carolina: Unpublished Report, 62 p.

Berry, J.L., 1977, Chemical weathering and geomorphological processes at Coweeta, North Carolina: Geological Society of America Abstracts with Programs, v. 9, p. 120.

Bird, M.I., and Chivas, A.R., 1988, Stable-isotope evidence for low-temperature kaolinitic weathering and post-formational hydrogen-isotope exchange in Permian kaolinites: Chemical Geology, v. 72, p. 249-265.

Biscaye, P.E., 1965, Mineralogy and sedimentation of recent deep-sea clay in the Atlantic Ocean and adjacent seas and oceans: Geological Society of America Bulletin, v. 76, p. 803-832.

Bish, D.L., 1994, Quantitative x-ray diffraction analysis of soils: in Amonette, J.E., and Zelazny, L.W. (eds.), Quantitative Methods in Soil Mineralogy, Soil Science Society of America Miscellaneous Publications, Madison, Wisconsin, p. 267-295.

Blum, A.E., 1994, Feldspar in weathering: in Parson, I. (ed.), Feldspars and Their Reactions, Kluwar Academic Publishers, Netherlands, p. 595-630.

Blum, A.E., and Stillings, L.L., 1995, Feldspar dissolution kinetics: in White, A.F., and Brantley, S.L. (eds.), Chemical Weathering Rates of Silicate Minerals, Mineralogical Society of America Reviews in Mineralogy Volume 31, Washington, D.C., p. 291-342.

Blum, A.E., and Lasaga, A.C., 1987, Monte Carlo simulations of surface reaction rate laws: in Stumm, W. (ed.), Aquatic Surface Chemistry, John Wiley & Sons, New York, p. 255-292.

Boring, L.R., Monk, C.D., and Swank, W.T., 1981, Early regeneration of a clear-cut southern Appalachian forest: Ecology, V. 62, p. 1244-1253.

Boulongé, B., Ambrosi, J.-P., and Nahon, D., 1997, Laterites and bauxites: in Paquet, H., and Clauer, N., (eds.), Soils and Sediments, Mineralogy and Geochemistry, Springer-Verlag, New York, p. 49-65.

Bowen, D.Q., 1979, Glaciations past and future: Geographical Magazine, v. 52, p. 62-67.

Bowser, C.J., and Jones, B.F., 1993, Mass balances of natural water: Silicate dissolution, clays, and the calcium problem: Biogeomon Symposium on Ecosystem Behavior: Evaluation of Integrated Monitoring in Small Catchments, Prague, Czech Republic, p. 30-31.

Bowser, C.J., and Jones, B.F., 2002, Mineralogic controls on the composition of natural waters dominated by silicate hydrolysis: American Journal of Science, v. 32, p. 582-662.

Bradley, R.S., 1999, Paleoclimatology: Reconstructing Climates of the Quaternary, 2nd Ed., Volume 68 of the International Geophysics Series: Academic Press, New York, 613 p.

Brantley, S.L., Crane, S.R., Crerar, D.A., Hellmann, R., and Stallard, R., 1986, Dissolution at dislocation etch pits in quartz: Geochimica et Cosmochimica Acta, v. 50, p. 2349-2361.

Braun, J-J., Pagel, M., Muller, J.P., Bilong, P., Michard, A., and Guillet, B., 1990, Cerium anomalies in lateritic profiles: Geochimica et Cosmochimica Acta, v. 51, p. 597-605.

Braun, J-J., Pagel, M., Herbillon, A., and Rosin, C., 1993, Mobilization and redistribution of REE and thorium in a syenitic lateritic profile: a mass balance study: Geochimica et Cosmochimica Acta, v. 57, p. 4419-4434.

Braun, J.-J., and Pagel, M., 1994, Geochemical and mineralogic behavior of REE, Th, and U in the Akongo lateritic profile (SW Cameroon): Catena, v. 21, p. 173-177.

Braun, J.-J., Viers, J., Dupré, B., Ndam, J., and Muller, J.-P., 1998, Solid/liquid REE fractionation in the lateritic system of Goyoum, East Cameroon: the implications for the present dynamics of the soil covers of the humid tropical regions: Geochimica et Cosmochimica Acta, v. 62, p. 273-299.

Bricker, O., Katz, B., Afifi, A., Puckett, L., Olson, C., and Kennedy, M., 1983, Geochemistry of small Appalachian watersheds developed on silicate bedrock: Science Géologie Mémoires, v. 73, p. 41-52.

Bricker, O.P., 1986, Geochemical investigations of selected Eastern United States watersheds affected by acid deposition: Journal of the Geological Society, London, v. 143, p. 621-626.

Brindley, G.W., 1984, Quantitative x-ray mineral analysis of clays: in Brindley, G.W., and Brown, G. (eds.), Crystal Structures of Clay Minerals and Their X-ray Identification, Mineralogical Society of London, London, p. 411-438.

Bromley, A.V., 1964, Allanite in the Tan-Y-Grisiau microgranite, Merionethshire, North Wales: American Mineralogist: v. 49, p. 1747-1754.

Brown, G., and Brindley, G.W, 1984, X-ray diffraction procedures for clay mineral identification: in Brindley, G.W., and Brown, G. (eds.), Crystal Structures of Clay Minerals and Their X-ray Identification, Mineralogical Society of London, London, p. 305-360.

Bryan, D.S., 1994, Factors controlling the occurrence and distribution of hematite and goethite in soils and saprolites derived from schists and gneisses in western North Carolina [unpublished M.S. thesis]: Michigan State University, East Lansing, Michigan, 125 p.

Burt, D.M., 1989, Compositional and phase relations among rare earth element minerals: in Lipin, B.R. and McKay, G.A. (eds.), Geochemistry and Mineralogy of Rare Earth Elements, Review in Mineralogy Volume 21, The Mineralogical Society of America, Washington, D.C., p. 259-308.

Calvert, C.S., Buol, S.W., and Weed, S.B., 1980a, Mineralogical characteristics and transformations of a vertical rock-saprolite-soil sequence in the North Carolina Piedmont: I. Profile morphology, chemical composition, and mineralogy: Soil ScienceSociety of America Journal, v. 44, p. 1096-1103.

Calvert, C.S., Buol, S.W., and Weed, S.B., 1980b, Mineralogical characteristics and transformations of a vertical rock-saprolite-soil sequence in the North Carolina Piedmont: II. Feldspar alteration products—their transformations through the profile: Soil Science Society of America Journal, v. 44, p. 1096-1103.

Carver, R.E., 1986, Rates of intrastratal solution of heavy minerals in southeast Atlantic Coastal Plain and their potential of dating sedimentary events: American Association of Petroleum Geologists Bulletin, v. 70, p. 572.

Chamley, H., 1989, Clay Sedimentology: Springer-Verlag, New York, 623 p.

Chamley, H., 1997, Clay mineral sedimentation in the ocean: in Paquet, H., and Clauer, N., (eds.), Soils and Sediments, Mineralogy and Geochemistry, Springer-Verlag, New York, p. 269-302.

Chamley, H., and Debrabant, P., 1984, Paleoenvironmental history of the north Atlantic region from mineralogical and geochemical data: Sedimentary Geology, v. 40, p. 151-167.

Chamley, H., and Müller, D.W., 1991, Clay mineralogy in southeast Spain during the late Miocene: climatic, paleoceanographic and tectonic events in the Eastern Betic seaway: Geologie en Mijnbouw, v. 70, p. 1-19,

Ciampone, M.A., McVey, D.E., Gerke, T.L., Briggs, W.D., Zhang, Y., Maynard, J.B., and Huff, W.D., 1992, Non-systematic weathering profile in the Blue Ridge Mountains, N.C.: Role of geochemical variables: Geological Society of America Abstracts with Programs, v. 24, p. A214.

Ciampone, M.A., 1995, Non-systematic weathering profile on metamorphic rock in the southern Blue Ridge Mountains, North Carolina: Petrography, bulk chemistry, and mineral chemistry of biotite [unpublished M.S. thesis]: University of Cincinnati, Cincinnati, Ohio, 86 p.

Clark, G.M., and Ciolkosz, E.J., 1988, Periglacial geomorphology of the Appalachian Highlands and Interior Highlands south of the glacial border: a review: Geomorphology, v. 1, p. 191-220.

Clark, G.M., 1993, Quaternary Geology and Geomorphology of Part of the Inner Piedmont of the Southern Appalachians in the Columbus Promontory Upland Area, Southwestern North Carolina and Northwestern South Carolina: Carolina Geological Society Guidebook, p. 67-84.

Clayton, J.L., 1979, Nutrient supply to soil by rock weathering: in Impact of Intensive Harvesting on Forest Nutrient Cycling, State University of New York, College of Environmental Science and Forestry, Syracuse, New York, p. 75-96.

Clayton, J.L., 1986, An estimate of plagioclase weathering rate in the Idaho batholith based upon geochemical transport rates: in Colman, S.M., and Dethier, D.P. (eds.), Rates of Chemical Weathering of Rocks and Minerals, Academic Press, Inc., New York, New York, p. 453- 467.

Clayton, J.L., 1988, Some observations of the stoichiometry of feldspar hydrolysis in granitic soils: Journal of Environmental Quality, v. 17, p. 153-157.

Clayton, J.L., Megahan, W.F., and Hampton, D., 1979, Soil and bedrock properties: Weathering and alteration products and processes in the Idaho batholith: United States Forest Service Research Paper INT-237, 35 p.

Clayton, T., Pearce, R.B., and Peterson, L.C., 1999, Indirect climatic control on the clay mineral composition of Quaternary sediments from the Cariaco basin, northern Venezuela (ODP Site 1002): Marine Geology, v. 161, p. 191-206.

Cleaves, E.T., Godfrey, A.E., and Bricker, O.P., 1970, Geochemical balance of a small watershed and its geomorphic implications: Geological Society of America Bulletin, v. 81, p. 3015-3032.

Cleaves, E.T., Fisher, D.W., and Bricker, O.P., 1974, Chemical weathering of serpentinite in the eastern Piedmont of Maryland: Geological Society of America Bulletin, v. 85, p. 437-444.

Cleaves, E.T., 1993, Climatic impact on isovolumetric weathering of a coarse-grained schist in the northern Piedmont Province of the Central Atlantic states: Geomorphology, v. 8, p. 191-198.

Cocker, M.D., 1998, Defining the heavy mineral potential in the upper coastal plain of Georgia with the use of NURE stream sediment geochemical data and a geographical information system: Proceedings, 33rd Forum on the Geology of Industrial Minerals, Proceedings, Canadian Institute on Mining and Metallurgy Special Volume 50, Montreal, p. 131-144.

Coleman, N.T., Jackson, M.L., and Mehlich, A., 1949, Mineral composition of the clay fraction: II. of several Coastal Plain, Piedmont, and mountain soils of North Carolina: Proceedings, Soil Science of America, v. 14, p. 81-85.

Coppin, F., Berger, G., Bauer, A., Castet, S., and Loubet, M., 2002, Sorption of lanthanides on smectite and kaolinite: Chemical Geology, v. 182, p. 57-68.

Cramer, J.J., and Nesbitt, H.W., 1983, Mass-balance relations and trace-element mobility during continental weathering of various igneous rocks: Science Géologique Mémoires, v. 73, p. 63-73.

Curtis, C.D., 1990, Aspects of climatic influence on the clay mineralogy and geochemistry of soils, palaeosols, and clastic sedimentary rocks: Journal of the Geological Society, London, v. 147, p. 351-357.

Daniels, N., and Kochel, R.C., 1998, Role of debris flows in landscape evolution, Blue Ridge Mountains, Madison County, Virginia: Abstracts with Programs, Geological Society of America, v. 30, p. 9.

Day, F.P., and Monk, C.D., 1977, Seasonal nutrient dynamics in the vegetation on a southern Appalachian watershed: American Journal of Botany, v. 64, p. 1126-1139.

Debrabant, P., Fagel, N., Chamley, H., Bout, V., and Caulet, J.-P., 1993, Neogene to Quaternary clay mineral fluxes in the Central Indian basin: Palaeography, Palaeoclimatology, Palaeoecology, v. 103, p. 117-131

DeConinck, J.F. and Bernoulli, D., 1991, Clay mineral assemblages of Mesozoic pelagic and flysch sediments of the Lombardian Basin (Southern Alps): implications for palaeotectonics, palaeoclimate and diagenesis: Geologische Rundschau, v. 80, p. 1-17.

Deer, W.A., Howie, R.A., and Zussman, J., 1986, Rock-Forming Minerals, Volume 1B, Disilicates and Ring Silicates, John Wiley & Sons, Inc., New York, 629 p.

Delcourt, H.R., and Delcourt, P.A., 1985, Quaternary palynology and vegetational history of the Southeastern United States: in Bryant, V.M., and Holloway, R.G. (eds.), Pollen Records of Late-Quaternary North American Sediments, American Association of Stratigraphic Palynologists Foundation, Dallas, Texas, p. 1-37.

Delvigne, J.E., 1998, Atlas of Micromorphology of Mineral Alteration and Weathering: The Canadian Mineralogist Special Publication 3, Mineralogical Association of Canada, Ottawa, Ontario, 494 p.

Dennis, A.J., and Wright, J.E., 1997, Middle and late Paleozoic monazite U-Pb ages, Inner Piedmont, South Carolina: Abstracts with Programs, Geological Society of America, v. 29, p. 12.

Derry, L.A., and France-Lanord, C., 1997, Himalayan weathering and erosion fluxes: climate and tectonic controls: in Ruddiman, W.F. (ed.), Tectonic Uplift and Climate Change, Plenum Press, New York, p. 289-312.

Dill, H.G., 1995, Heavy mineral response to the progradation of an alluvial fan: implications concerning unroofing of source area, chemical weathering and palaeo-relief (Upper Cretaceous Parkstein fan complex, SE Germany): Sedimentary Geology, v. 95, p. 39-56.

Dollase, W.A., 1971, Refinement of the crystal structure of epidote, allanite and hancockite: American Mineralogist, v. 56, p. 447-464.

Dong, H., Peacor, D.R., and Murphy, S.F., 1998, TEM study of progressive alteration of igneous biotite to kaolinite throughout a weathered soil profile: Geochimica et Cosmochimica Acta, v. 62, p. 1881-1887.

Douglass, J.E., and Hoover, M.D., 1988, History of Coweeta: in Swank, W.T., and Crossley, Jr., D.A. (eds.), Forest Hydrology and Ecology at Coweeta, Springer-Verlag, New York, p. 17-31.

Drever, J.I., 1973, The preparation of oriented clay mineral specimens for X-ray diffraction analysis by a filter-membrane peel technique: American Mineralogist, v. 58, p. 553-554.

Drever, J.I., and Hurcomb, D.R., 1986, Neutralization of atmospheric acidity by chemical weathering in an alpine drainage basin in the North Cascade Mountains: Geology, v. 14, p. 221-224.

Drever, J.I., and Zobrist, J., 1992, Chemical weathering of silicate rocks as a function of elevation in the southern Swiss Alps: Geochimica et Cosmochimica Acta, v. 56, p. 3209-3216.

Drever, J.I., 1997a, The Geochemistry of Natural Waters: Surface and Ground water Environments, 3rd Edition: New Jersey, Prentice Hall, 436 p.

Drever, J.I., 1997b, Catchment mass balance: in Saether, O.M., and de Caritat (eds.), Geochemical Processes, Weathering and Ground water Recharge in Catchments, A.A. Balkema, Rotterdam, Netherlands, p. 241-261.

Duddy, I.R., 1980, Redistribution and fractionation of rare earth and other elements in a weathering profile: Chemical Geology, v. 30, p. 363-381.

Eaton, L.S., and McGeehin, J.P., 1997, Frequency of debris flows and their role in long term landscape evolution in the central Blue Ridge, Virginia: Abstracts with Programs, Geological Society of America, v. 29, p. 410.

Ehlmann, A.J., 1968, Clay mineralogy of weathered products and of river sediments, Puerto Rico: Journal of Sedimentary Petrology, v. 38, p. 885-894.

Ehrmann, W.U., Melles, M., Kuhn, G., and Grobe, H., 1992, Significance of clay mineral assemblages in the Antarctic Ocean: Marine Geology, v. 107, p. 249-273.

Ehrmann, W., 1998, Implications of late Eocene to early Miocene clay mineral assemblages in McMurdo Sound (Ross Sea, Antarctica) on paleoclimate and ice dynamics: Palaeography, Palaeoclimatology, Palaeoecology, v. 139, p. 213-231.

Elderfield, H., Upstill-Goddard, R., and Sholkovitz, E.R., 1990, The rare earth elements in rivers, estuaries, and coastal seas and their significance to the composition of ocean waters: Geochimica et Cosmochimica Acta, v. 54, p. 971-991.

Elliott, W.C., Savin, S.M., Dong, H., and Peacor, D.R., 1995, Clay mineralogy and stable isotope geochemistry of a Piedmont Province Saprolite, Woodbridge, Virginia: Abstracts with Programs, Geological Society of America, v. 27, p. 51.

Elliott, W.C., Savin, S.M., Dong, H., and Peacor, D.R., 1997, A paleoclimate interpretation derived from pedogenic clay minerals from the Piedmont Province, Virginia: Chemical Geology, v. 142, p. 201-211.

El-Younsey, A.R.M., Soliman, M.A., Ahmed, E.A., and Abdel-Mottaleb, E.D.A., 1998, Sedimentology and mineralogy of the Neogene and more recent sediments in Wadi El-Assiuti area, Assiut, Egypt: Bulletin of the Faculty of Science, Assiut University, v. 27, p. 253-282.

Emiliani, C., 1972, Quaternary Hypsithermals: Quaternary Research, v. 2, p. 270-273.

Ercit, T.S., 2002, The mess that is "allanite": The Canadian Mineralogist, v. 40, p. 1411-1419.

Eslinger, E., and Pevear, D., 1988, Clay Minerals for Petroleum Geologists and Engineers: Society of Economic Geologists and Paleontologists Short Course Notes No. 22.

Ewing, R.C., 1976, Metamict mineral alteration: an implication for radioactive waste disposal: Science, v. 192, p. 1336-1337.

Ewing, R.C., and Haakar, R.F., 1981, Amorphous structure of metamict minerals observed by TEM: Nature, v. 293, p. 449-450.

Ezzaïm, A., Turpault, M.-P., and Ranger, J., 1999, Quantification of weathering processes in an acid brown soil developed from tuff (Beaujolais, France) Part I., Formation of weathered rind: Geoderma, v. 87, p. 137-154.

Finkelstein, D.B., Leckie, R.M., and Yuretich, R.F., 1998, Kaolinite as a proxy for continental weathering in the Late Cretaceous Greenhorn cyclothem of the Western Interior Seaway: Geological Society of America Abstracts with Programs, v. 30, p. 220.

Finley, J.B., and Drever, J.I., 1997, Chemical mass balance and rates of mineral weathering in a high-elevation catchment, West Glacier Lake, Wyoming: Hydrological Processes, v. 11, p. 745-764.

Friis, H., 1974, Weathered heavy-mineral associations from the young-Tertiary deposits of Jutland, Denmark: Sedimentary Geology, v. 12, p. 199-213.

Frondel, J.W., 1964, Variation of some rare earths in allanite: American Mineralogist, v. 49, p. 1159-1177.

Frye, J.C., William, H.B., and Glass, H.D., 1960, Gumbotil, Accretion-Gley, and the Weathering Profile: Illinois State Geological Survey Circular 295, 39 p.

Fryer, B.J., Jackson, S.E., and Longerich, H.P., 1995, The design, operation and role of the laser-ablation microprobe coupled with inductively coupled plasma-mass spectrometer (LAM-ICP-MS) in the earth sciences: Canadian Mineralogist, v. 33, p. 303-312.

Furman, T., Thompson, P., and Hatchl, B., 1998, Primary mineral weathering in the central Appalachians: A mass balance approach: Geochimica et Cosmochimica Acta, v. 62, p. 2889-2904.

Gaillardet, J., Dupré, B., Allègre, and Négrel, P., 1997, Chemical and physical denudation in the Amazon River Basin: Chemical Geology, v. 142, p. 141-173.

Gardner, L.R., 1980, Mobilization of Al and Ti during rock weathering—isovolumetric geochemical evidence: Chemical Geology, v. 30, p. 151-165.

Gardner, L.R., 1992, Long-term isovolumetric leaching of aluminum rocks during weathering: Implications for the genesis of saprolite: Catena, v. 19, p. 521-537.

Gardner, L.R., Kheoruenromne, I., and Chen, H.S., 1978, Isovolumetric geochemical investigation of a buried granite saprolite near Columbia, SC, U.S.A.: Geochimica et Cosmochimica Acta, v. 42, p. 417-424.

Gardner, L.R., Kheoruenromne, I., and Chen, H.S., 1981, Geochemistry and mineralogy of an unusual diabase saprolite near Columbia, South Carolina: Clays and Clay Minerals, v. 29, p. 184-190.

Gardner, T.W., and Sevon, W.D., 1989, Appalachian Geomorphology: Elsevier Science Publishers, Amsterdam, The Netherlands, 318 p.

Garrels, R.M., 1967, Genesis of some ground waters from igneous rocks: in Abelson, P.H. (ed.), Researches in Geochemistry, v. 2, John Wiley & Sons Ltd., New York, p. 405-420.

Garrels, R.M., and Mackenzie, F.T., 1967, Origin of the chemical compositions of some springs and lakes: in Stumm, W. (ed.), Equilibrium Concepts in Natural Water Systems, American Chemical Society Advances in Chemistry Series No. 67, p. 222-242.

Gerrard, A.J., 1994, Weathering of granitic rocks: environment and clay mineral formation: in Robinson, D.A., and Williams, R.B.G. (eds.), Rock weathering and Landform Evolution, Chichester, p. 3-20.

Gibbs, R.J., 1977, Clay mineral segregation in the marine environment: Journal of Sedimentary Petrology, v. 47, p. 237-243.

Gibson, T.G., Bybell, L.M., and Owens, J.P., 1993, Latest Paleocene lithologic and biotic events in the neritic deposits of southwestern New Jersey: Paleoceanography, v. 8, p. 495-514.

Gilkes, R.J., and Suddhiprakarn, A., 1979a, Biotite alteration in deeply weathered granite. I. Morphological, mineralogical, and chemical properties: Clays and Clay Minerals, v. 27, p. 349-360.

Gilkes, R.J., and Suddhiprakarn, A., 1979b, Biotite alteration in deeply weathered granite. II. The oriented growth of secondary minerals: Clays and Clay Minerals, v. 27, p. 361-367.

Goldich, S.S., 1938, A study in rock-weathering: Journal of Geology, v. 46, p. 17-58.

Goldstein, S.J., and Jacobsen, S.B., 1988, Rare earth elements in river water: Earth and Planetary Science Letters, v. 89, p. 35-47.

Graham, R.C., Weed, S.B., Bowen, L.H., and Buol, S.W., 1989a, Weathering of iron-bearing minerals in soils and saprolite of the North Carolina Blue Ridge Front: I. Sand-size primary minerals: Clays and Clay Minerals, v. 37, p. 19-28.

Graham, R.C., Weed, S.B., Bowen, L.H., Amarasiriwardena, D.D., and Buol, S.W., 1989b, Weathering of iron-bearing minerals in soils and saprolite of the North Carolina Blue Ridge Front: II. Clay mineralogy: Clays and Clay Minerals, v. 37, p. 29-40.

Graham, R.C., and Buol, S.W., 1990, Soil-geomorphic relations on the Blue Ridge Front II. Soil characteristics and pedogenesis: Soil Science Society of America Journal, v. 54, p. 1367-1377.

Grant, W.H., 1963, Weathering of Stone Mountain granite: Clays and Clay Minerals, v. 11, p. 65-73.

Grant, W.H., 1964, Chemical weathering of biotite-plagioclase gneiss: Clays and Clay Minerals, v. 12, p. 455-463.

Grant, W.H., 1988, Debris Avalanches and the Origin of First-Order Streams: in Swank, W.T., and Crossley, Jr., D.A. (eds.), Forest Hydrology and Ecology at Coweeta, Springer-Verlag, New York, New York, p. 103-110.

Grantham, J.H., and Velbel, M.A., 1988, The influence of climate and topography on rock-fragment abundance in modern fluvial sands of the southern Blue Ridge Mountains, North Carolina: Journal of Sedimentary Petrology, v. 58, p. 219-227.

Grauch, R.I., 1989, Rare Earth elements in metamorphic rocks: in Lipin, B.R. and McKay, G.A. (eds.), Geochemistry and Mineralogy of Rare Earth Elements, Review in Mineralogy Volume 21, The Mineralogical Society of America, Washington, D.C., p. 147-168.

Greaves, M.J., Elderfield, H., and Sholokovitz, E.R., 1999, Aeolian sources of rare earth elements to the Western Pacific Ocean: Marine Chemistry, v. 68, p. 31-38.

Griffin, G.M., 1962, Regional clay-mineral facies—products of weathering intensity and current distribution in the northeastern Gulf of Mexico: Geological Society of American Bulletin, v. 73, p. 737-768.

Griffin, J.J., Windom, H., and Goldberg, E.D., 1968, The distribution of clay minerals in the world ocean: Deep-Sea Research, v. 15, p. 433-459.

Gromet, L.P., and Silver, L.T., 1983, Rare earth element distributions among minerals in a granodiorite and their petrogenetic implications: Geochimica et Cosmochimica Acta, v. 47, p. 925-939.

Grousset, F.E., Parra, M., Bory, A., Martinez, P., Bertrand, P., Shimmield, G., and Ellam, M., 1998, Saharan wind regimes traced by the Sr-Nd isotopic composition of subtropical Atlantic sediments: last glacial maximum vs. today: Quaternary Science Reviews, v. 17, p. 395-409.

Gupta, R.K., and Talwar, C.L., 1997, Mineralogy of soils developed on Karewas in Baramula and Kupwara areas of Kashmir: Clay Research, v. 16, p. 31-34.

Hack, J.T., 1980, Rock control and tectonism: Their importance in shaping the Appalachian Highlands: U.S. Geological Survey Professional Paper 1126-B, 17 p.

Hallam, A., Grose, J.A., and Ruffell, A.H., 1991, Palaeoclimatic significance of changes in clay mineralogy across the Jurassic-Cretaceous boundary in England and France: Palaeography, Palaeoclimatology, Palaeoecology, v. 81, p. 173-187.

Harlavan, Y., and Erel, Y., 2002, The release of Pb and REE from granitoids by the dissolution of accessory phases: Geochimica et Cosmochimica Acta, v. 66, p. 837-848.

Hartmann, B.H., Bodnár, K.J., Ramseyer, K., and Matter, A., 1999, Effect of Permo-Carboniferous climate on illite-smectite, Haushi Group, Sultanate of Oman: Clays and Clay Minerals, v. 47, p. 131-143.

Hata, S., 1939, The alteration of allanite: Scientific Papers of the Institute of Physical and Chemical Research, v. 36, p. 301-311.

Hatcher, R.D., 1980, Geologic map of Coweeta Hydrologic Laboratory, Prentiss Quadrangle, North Carolina: State of North Carolina, Department of Natural Resources and Community Development, in Cooperation with the Tennessee Valley Authority, scale 1:14,400.

Hatcher, R.D., 1988, Bedrock geology and regional geologic setting of Coweeta Hydrologic Laboratory in the Eastern Blue Ridge: in Swank, W.T., and Crossley, Jr., D.A. (eds.), Forest Hydrology and Ecology at Coweeta, Springer-Verlag, New York, p. 81-92.

Heaton, R.W., Rahn, K.A., and Lowenthal, D.H., 1990, Determination of trace elements, including regional tracers, in Rhode Island precipitation: Atmospheric Environment, v. 24A, p. 147-153.

Helvey, J.D., and Patric, J.H., 1988, Research on interception losses and soil moisture relationships: in Swank, W.T., and Crossley, Jr., D.A. (eds.), Forest Hydrology and Ecology at Coweeta, Springer-Verlag, New York, p. 129-137.

Hermann, J., 2002, Allanite: thorium and light rare earth element carrier in subducted crust: Chemical Geology, v. 192, p. 289-306.

Hewlett, J.D., 1961, Soil moisture as a source of base flow from steep mountain watersheds: Southeastern Forest Experiment Station Paper no. 132, U.S. Department of Agriculture–Forest Service, Asheville, North Carolina, 11 p.

Hewlett, J.D., and Hibbert, A.R., 1963, Moisture and energy conditions within a sloping soil mass during drainage: Journal of Geophysical Research, v. 68, p. 1081-1087.

Hiscott, R.N., 1984, Clay mineralogy and clay-mineral provenance of Cretaceous and Paleogene strata, Labrador and Baffin shelves: Bulletin of Canadian Petroleum Geology, v. 32, p. 272-280.

Hill, I.G., Worden, R.H., and Meighan, I.G., 2000, Geochemical evolution of a palaeolaterite: the Interbasaltic Formation, Northern Ireland: Chemical Geology, v. 166, p. 65-82.

Hochella, M.F., and Banfield, J.F., 1995, Chemical weathering of silicates in nature: a microscopic perspective with theoretical considerations: in White, A.F., and Brantley, S.L. (eds.), Chemical Weathering Rates of Silicate Minerals, Mineralogical Society of America Reviews in Mineralogy Volume 31, Washington, D.C., p. 353-406.

Horowitz, A.J., Demas, C.R., Fitzgerald, K.K., Miller, T.L., and Rickert, D.A., 1994, U.S. Geological Survey protocol for the collection and processing of surface-water samples for the subsequent determination of inorganic constituents in filtered water: USGS Open-File Report 94-0539, 57 p.

Horowitz, A.J., Lum, K.R., Garbarino, J.R., Hall, G.E.M., Lemieux, C., and Demas, C.R., 1996, The effect of membrane-filtration on dissolved trace element concentrations: Water, Air, and Soil Pollution, v. 90, p. 281-296.

Howard, S.A., and Preston, 1989, Profile fitting of powder diffraction patterns: in Bish, D.L., and Post, J.E. (eds.), Modern Powder Diffraction, Mineralogical Society of America Reviews in Mineralogy Volume 20, Washington, D.C., p. 217-276.

Hughes, R.E., Moore, D.M., and Reynolds, R.C., 1993, The nature, detection, occurrence, and origin of kaolinite/smectite: in Murray, H., Bundy, W., and Harvey, C. (eds.), Kaolin Genesis and Utilization, Clay Minerals Society Special Publication No. 1, Boulder, Colorado, p. 291-324.

Hughes, R.E., Moore, D.M., and Glass, H.D., 1994, Qualitative and quantitative analysis of clay minerals in soils: in Amonette, J.E., and Zelazny, L.W. (eds.), Quantitative Methods in Soil Mineralogy, Soil Science Society of America Miscellaneous Publications, Madison, Wisconsin, p. 330-359.

Hurley, J.P., Shafer, M.M., Cowell, S.E., Overdier, J.T., Hughes, P.E., and Armstrong, D.E., 1996, Trace metal assessment of Lake Michigan tributaries using low-level techniques: Environmental Science and Technology, v. 30, p. 2093-2098.

Ingri, J., Widerlund, A., Land, M., Gustafsson, Ö., Andersson, P., and Öhlander, B., 2000, Temporal variations in the fractionation of the rare earth elements in a boreal river; the role of colloidal particles: Chemical Geology, v. 166, p. 23-45.

Jackson, M.L., 1963, Interlayering of expandable layer silicates in soils by chemical weathering: Clays and Clay Minerals, v. 11, p. 29-46.

Jackson, S.E., Longerich, H.P., Dunning, G.R., and Fryer, B.J., 1992, The application of laser ablation microprobe-inductively coupled plasma-mass spectrometry (LAM-ICP-MS) to in situ trace element determination in minerals: Canadian Mineralogist, v. 30, p. 1049-1064.

Jacobson, A.D., Blum, J.D., Chamberlain, C.P., Craw, D., and Koons, P.O., 2003, Climatic and tectonic controls on chemical weathering in the New Zealand Southern Alps: Geochimica et Cosmochimica Acta, v. 67, p. 29-46.

Janeczek, J., and Eby, R.K., 1993, Annealing of radiation damage in allanite and gadolinite: Physics and Chemistry of Minerals, v. 19, p. 343-356.

Jeffries, T.E., Perkins, W.T., and Pearce, N.J.G., 1995, Measurements of trace elements in basalts and their phenocrysts by laser probe microanalysis inductively coupled plasma mass spectrometry (LPMA-ICP-MS): Chemical Geology, v. 121, p. 131-144.

Jenner, G.A., Foley, S.F., Jackson, S.E., Green, T.H., Fryer, B.J., and Longerich, H.P., 1993, Determination of partition coefficients for trace elements in high pressure-temperature experimental run products by laser ablation microprobe-inductively coupled plasma-mass spectrometry (LAM-ICP-MS): Geochimica et Cosmochimica Acta, v. 57, p. 5099-5103.

Jeong, G.Y., and Kim, H.B., 2003, Mineralogy, chemistry, and formation of oxidized biotite in the weathering profile of granitic rocks: American Mineralogist, v. 88, p. 352-364.

Johannesson, K.H., and Xiaoping, Z., 1997, Geochemistry of the rare earth elements in natural terrestrial waters: a review of what is currently known: Chinese Journal of Geochemistry, v. 16, p. 20-42.

John, C.M., Mutti, M., and Adatte, T., 2003, Mixed carbonate-siliciclastic record on the North African margin (Malta)—coupling of weathering processes and mid Miocene climate: Geological Society of America Bulletin, v. 115, p. 217-229.

Johnsson, M.J., 1992, Chemical weathering controls on sand composition: Encyclopedia of Earth Systems Science, v. 1, p. 455-466.

Jolicoeur, S., Ildefonse, P., and Bouchard, M., 2000, Kaolinite and gibbsite weathering of biotite within saprolites and soils of central Virginia: Soil Science Society of America Journal, v. 64, p. 1118-1129.

Kahle, M., Kleber, M., and Jahn, R., 2002, Review of XRD-based quantitative analyses of clay minerals in soils: the suitability of mineral intensity factors: Geoderma, v. 109, p. 191-205.

Kalindekafe, L.S.N., Dolozi, M.B., and Yuretich, R., 1996, Distributions and origin of clay minerals in the sediments of Lake Malawi: in Johnson, T.C., and Odada, E.O. (eds.), The Limnology, Climatology and Paleoclimatology of the East African Lakes, Gordon and Breach Publishers, Canada, p. 443-460.

Kalinsowski, B.E., and Schweda, P., 1996, Kinetics of muscovite, phlogopite, and biotite dissolution and alteration at pH 1-4, room temperature: Geochimica et Cosmochimica Acta, v. 60, p. 367-385.

Kalinowski, B.E., Faith-Ell, C., and Schweda, P., 1998, Dissolution kinetics and alteration of epidote in acidic solutions at 25°C: Chemical Geology, v. 151, p. 181-197.

Katz, B.G., Bricker, O.P., and Kennedy, M.M., 1985, Geochemical mass-balance relationships for selected ions in precipitation and stream water, Catoctin Mountains, Maryland: American Journal of Science, v. 285, p. 931-962.

Katz, B.G., 1989, Influence of mineral weathering reactions on the chemical composition of soil water, springs, and ground water, Catoctin Mountains, Maryland: Hydrological Processes, v. 3, p. 185-202.

Keller, W.D., 1976, Scan electron micrographs of kaolins collected from diverse environments of origin: I.: Clays and Clay Minerals, v. 24, p. 107-113.

Keller, W.D., 1978, Kaolinization of feldspar as displayed in scanning electron micrographs: Geology, v. 6, p. 184-188.

Kenoyer, G.J., and Bowser, C.J., 1992, Ground water chemical evolution in a sandy silicate aquifer in northern Wisconsin: 2. Reaction modeling: Water Resources Research, v. 28, p. 591-600.

Khan, A.M., and Kim, S.J., 1998, Control of physico-chemical conditions on the mineralogical characteristics of weathering profile of anorthositic rocks of Suryun area, Korea: Acta Mineralogica Pakistanica, v. 9, p. 1-6.

Kitto, M.E., Anderson, D.L., Gordon, G.E., and Olmez, I., 1992, Rare earth element distributions in catalyst and airbourne particles: Environmental Science and Technology, v. 26, p. 1368-1375.

Klein, C., and Hurlbut, C.S., 1999, Manual of Mineralogy: John Wiley & Sons, Inc., New York, 681 p.

Knoepp, J.D., and Swank, W.T., 1994, Long-term soil chemistry changes in aggrading forest ecosystems: Soil Science Society of America Journal, v. 58, p. 325-331.

Kochel, R.C., and Johnson, R.A., 1984, Geomorphology and sedimentology of humid-temperate alluvial fans, central Virginia: in Koster, E.H., and Steel, R.J. (eds.), Sedimentology of Gravels and Conglomerates: Memoirs of the Canadian Society of Petroleum Geology, Calgary, Canada, p. 109-122.

Koppi, A.J., Edis, R., Field, D.J., Geering, H.R., Klessa, D.A., and Cockayne, D.J.H., 1996, Rare earth element trends and cerium-uranium-manganese associations in weathered rock from Koongarra, Northern Territory, Australia: Geochimica et Cosmochimica Acta, v. 60, p. 1695-1707.

Kreutz, K.J., and Sholkovitz, E.R., 2000, Major element, rare earth element, and sulfur isotopic composition of a high-elevation firn core: Sources and transport of mineral dust in central Asia: Geochemistry, Geophysics, Geosystems, v. 1, Paper number 2000GC000082.

Kronberg, B.I., Nesbitt, H.W., and Lam, W.W., 1986, Upper Pleistocene Amazon deep-sea fan muds reflect intense chemical weathering of their mountainous source lands: Chemical Geology, v. 54, p. 283-294.

Kurtz, A.C., Derry, L.A., Chadwick, O.A., 2001, Accretion of Asian dust to Hawaiian soils: Isotopic, elemental, and mineral mass balances: Geochimica et Cosmochimica Acta, v. 65, p. 1971-1983.

Land, M., Öhlander, B., Ingri, J., and Thunberg, J., 1999, Solid speciation and fractionation of rare earth elements in a spodosol profile from northern Sweden as revealed by sequential extraction: Chemical Geology, v. 160, p. 121-138.

Lång, L.-O., 2000, Heavy mineral weathering under acidic soil conditions: Applied Geochemistry, v. 15, p. 415-423.

Lasaga, A.C., 1984, Chemical kinetics of water-rock interactions: Journal of Geophysical Research, v. 89, p. 4009-4025.

Liebens, J., and Schaetzl, R.J., 1997, Relative-age relationships of debris flow deposits in the Southern Blue Ridge, North Carolina: Geomorphology, v. 21, p. 53-67.

Likens, G.E., and Bormann, 1995, Biogeochemistry of a Forested Ecosystem: Springer-Verlag New York, Inc., New York, 159 p.

Loferski, P.J., 1981, Clay mineralogy of weathering profiles from the Carolina Piedmont: Southeastern Geology, v. 22, p. 193-202.

Lin, F.-C., and Clemency, C.V., 1981, Dissolution kinetics of phlogopite. I. Closed-system: Clays and Clay Minerals, v. 29, p. 101-106.

Logan, W.S., and Dyer, L.J., 1996, Influence of mineral weathering reactions, road salt and cation exchange on ground water chemistry, Catoctin Mountain, Central Maryland: Geological Society of America Abstracts with Programs, v. 28, p. 31-32.

Longerich, H.P., Jackson, S.E., and Gunther, D., 1996, Laser ablation inductively coupled plasma mass spectrometric transient signal data acquisition and analyte concentration calculation: Journal of Analytical Atomic Spectrometry, v. 11, p. 899-904.

Losche, C.K., McCraken, R.J., and Davey, C.B., 1970, Soils on steeply sloping landscapes in the southern Appalachian Mountains: Soil Science Society of America Proceedings, v. 34, p. 473-478.

Lowe, D.J., 1986, Controls on the rates of weathering and clay mineral genesis in airfall tephras: a review and New Zealand case study: in Colman, S.M., and Dethier, D.P. (eds.), Rates of Chemical Weathering of Rocks and Minerals, Academic Press, Inc., New York, New York, p. 265-330.

Macías Vazquez, F., 1981, Formation of gibbsite in soils and saprolites of temperate-humid zones: Clay Minerals, v. 16, p. 43-52.

Marker, A., and De Oliveira, J.J., 1990, The formation of rare earth element scavenger minerals in the weathering products derived from alkaline rocks of SE-Bahia, Brazil: Chemical Geology, v. 84, p. 373-374.

Mast, M.A., Drever, J.I., and Baron, J., 1990, Chemical weathering in the Loch Vale watershed, Rocky Mountain National Park, Colorado: Water Resources Research, v. 26, p. 2971-2978.

Mast, M.A., 1992, Geochemical characteristics: in Baron, J.S. (ed.), Biogeochemistry of an Alpine Ecosystem, Springer-Verlag, New York, p. 93-107.

Medeira, M.A.V., and Sanches Furtado, A.F.A., 1987, The instability of gibbsite and occurrence of other aluminous products in soils of perhumid climate regions of Portugal: Garcia de Orta, Sér. Geol., v. 10, p. 35-41.

Meintzer, R.E., 1981, Thorium and rare earth element migration incipient to the weathering of an allanite pegmatite, Amherst County, Virginia [unpublished M.S. thesis]: University of Virginia, 107 pp.

Menking, K.M., 1997, Climatic signals in clay mineralogy and grain-size variations in Owens Lake core OL-92, southeast California: Geological Society of America Special Paper 317, p. 25-36.

Merschat, A.J., and Kalbas, J.L., 2002, Geology of the southwestern Brushy Mountains, North Carolina Inner Piedmont: a summary and synthesis of recent studies: in Hatcher, R.D., Jr., and Bream, B.R. (eds.), Inner Piedmont Geology in the South Mountains-Blue Ridge Foothills and the Southwestern Brushy Mountains, Central-Western North Carolina, North Carolina Geological Survey, Carolina Geological Society Annual Field Trip Guidebook, p. 101-126.

Michalek, D.D., 1969, Fanlike features and related periglacial phenomena of the Southern Blue Ridge [unpublished Ph.D. dissertation]: University of North Carolina, Chapel Hill, North Carolina, 206 pp.

Middelburg, J.J., van der Weijden, C.H., and Woittiez, J.R.W., 1988, Chemical processes affecting the mobility of major, minor and trace elements during weathering of granitic rocks: Chemical Geology, v. 68, p. 253-273.

Migoń, P., and Lidmar-Bergström, K., 2002, Deep weathering through time in central and northwestern Europe: problems of dating and interpretations of geological record: Catena, v. 49, p. 25-40.

Migoń, P., and Thomas, M.F., 2002, Grus weathering mantles—problems and interpretation: Catena, v. 49, p. 5-24.

Miller, C.F., Hatcher, R.D., Jr., Ayers, J.C., Coath, C.D., and Harrison, T.M., 2000, Age and zircon inheritance of eastern Blue Ridge plutons, southwestern North Carolina and northeastern Georgia, with implications for magma history and evolution of the southern Appalachian orogen: American Journal of Science, v. 300, p. 142-172.

Millot, G. and Bonifas, M., 1955, Transformations isovolumetriques dans les phénomènes da lateritisation et de bauxitisation: Bulletin Service Carte Geologique Alsace Lorraine, v. 8, p. 3-20 (in French).

Millot, G., 1964, Géologie des Argiles: Masson, Paris, 499 p.

Millot, G., 1970, Geology of Clays: Springer-Verlag, New York, New York.

Mills, H.H., 1981, Some observations on slope deposits in the vicinity of Grandfather Mountain, North Carolina, USA: Southeastern Geology, v. 22, p. 209-222.

Mills, H.H., 1982, Long-term episodic deposition on mountain foot slopes in the Blue Ridge province of North Carolina: Evidence from relative-age dating: Southeastern Geology, v. 23, p. 123-128.

Mills, H.H., 1983, Pediment evolution at Roan Mountain, North Carolina, USA: Geographic Annalar, v. 65A, p. 111-126.

Mills, H.H., Brackenridge, G.R., Jacobson, R.B., Newell, W.L., Pavich, M., and Pomery, J.S., 1987, Appalachian mountains and plateaus: in Graf, W.L. (ed.), Geomorphic Systems of North America, Geological Society of America Centennial Special Volume 2, Boulder, Colorado, p. 5-50.

Mitchell, R.S., 1966, Virginia metamict minerals: allanite: Southeastern Geology, v. 7, p. 183-195.

Mongelli, G., 1993, REE and other trace elements in a granitic weathering profile from "Sette", southern Italy: Chemical Geology, v. 103, p. 17-25.

Moore, D.M., and Reynolds, Jr., R.C., 1997, X-ray Diffraction and the Identification and Analysis of Clay Minerals: Oxford University Press, New York, 378 p.

Mossa, J., 1998, The promise for geomorphic discovery in the south: Journal of Geography, v. 97, p. 151-161.

Murakami, T., Utsunomiya, S., Yokoyama, T., and Kasama, T., 2003, Biotite dissolution processes and mechanisms in the laboratory and in nature: Early stage weathering environment and vermiculitization: American Mineralogist, v. 88, p. 377-386.

Murphy, S.F., Brantley, S.L., Blum, A.E., White, A.F., and Dong, H., 1998, Chemical weathering in a tropical watershed, Luquillo Mountains, Puerto Rico: II. Rate and mechanism of biotite weathering: Geochimica et Cosmochimica Acta, v. 62, p. 227-243.

Nagy, K.L., 1995, Dissolution and precipitation kinetics of sheet silicates: in White, A.F., and Brantley, S.L. (eds.), Chemical Weathering Rates of Silicate Minerals, Reviews in Mineralogy Volume 31, Mineralogical Society of America, Washington, D.C., p. 173-234.

Nahon, D.B., 1991, Introduction to the Petrology of Soils and Chemical Weathering: John Wiley & Sons, Inc., New York, 313 p.

Neal, C.R., Davidson, J.P., and McKeegan, K.D., 1995, Geochemical analysis of small samples: micro-analytical techniques for the nineties and beyond: Reviews in Geophysics, Supplement, p. 25-32.

Neary, D.G., and Swift, L.W., 1984, Rainfall thresholds for triggering a debris avalanching event in the southern Appalachians: Geological Society of America Abstracts with Programs, v. 16, p. 609.

Nesbitt, H.W., 1979, Mobility and fractionation of rare earth elements during weathering of granodiorite: Nature, v.279, p. 206-210.

Nesbitt, H.W., and Markovics, G., 1997, Weathering of granodiorite crust, long-term storage of elements in weathering profiles, and petrogenesis of siliclastic sediments: Geochimica et Cosmochimca Acta, v. 61, p. 1653-1670.

Net, L.I., Alonso, M.S., and Limarino, C.O., 2002, Source rock and environmental control on clay mineral associations, Lower Section of Paganzo Group (Carboniferous), Northwest Argentina: Sedimentary Geology, v. 152, p. 183-199.

Newman, A.C.D., 1987, Chemistry of Clays and Clay Minerals: John Wiley & Sons, New York, 480 p.

Nickel, E., 1973, Experimental dissolution of light and heavy minerals in comparison with weathering and intrastratal solution: Contributions to Sedimentology, v. 1, p. 1-68.

Norfleet, M.L., and Smith, B.R., 1989, Weathering and mineralogical classification of selected soils in the Blue Ridge Mountains of South Carolina: Soil Science Society of America Journal, v. 53, p. 1771-1178.

Norfleet, M.L., Karathanasis, A.D., and Smith, B.R., 1989, Gibbsite-kaolinite equilibria in gneiss-derived southern Appalachian soils: Agronomy Abstracts, v. 81, p. 322.

Norfleet, M.L., Karathanasis, A.D., and Smith, B.R., 1993, Soil solution composition relative to mineral distribution in Blue Ridge Mountains soils: Soil Science Society of America Journal, v. 57, p. 1375-1380.

Norman, M.D., Pearson, N.J., Sharma, A., and Griffin, W.L., 1996, Quantitative analysis of trace elements in geological materials by laser ablation ICPMS: Instrumental operating conditions and calibration values of NIST glasses: Geostandards Newsletter, v. 20, p. 247-261.

Nriagu, J., Lawson, G., Wong, H.K.T., and Azcue, J.M., 1993, A Protocol for Minimizing Contamination in the Analysis of Trace Metals in Great Lakes Waters: Journal of Great Lakes Research, v. 19, p. 175-182.

Nriagu, J., Lawson, G., Wong, H.K.T., and Cheam, V., 1996, Dissolved trace metals in Lake Superior, Erie and Ontario: Environmental Science and Technology, v. 30, p. 178-187.

O'Brien, A.K., Rice, K.C., Bricker, O.P., Kennedy, M.M., and Anderson, R.T., 1997, Use of geochemical mass balance modeling to evaluate the role of weathering in determining stream chemistry in five Mid-Atlantic watersheds on different lithologies: Hydrological Processes, v. 11, p. 719-744.

O'Hara, K.D., Kirschner, D.L., and Moecher, D.P., 1995, Petrologic constraints on the source of fluid during mylonitization in the Blue Ridge Province, North Carolina and Virginia, U.S.A.: Journal of Geodynamics, v. 19, p. 217-287.

Olmez, I., and Gordon, G.E., 1985, Rare earths: atmospheric signature for oil-fired power plants and refineries: Science, v. 229, p. 966-968.

Pačes, T., 1983, Rate constants of dissolution derived from the measurements of mass balance in hydrological catchments: Geochimica et Cosmochimica Acta, v. 47, p. 1855-1863.

Pačes, T., 1986, Rates of weathering and erosion derived from mass balance in small drainage basins: in Colman, S.M., and Dethier, D.P. (eds.), Rates of Chemical Weathering of Rocks and Minerals, Academic Press, Inc., New York, p. 531- 550.

Palmquist, J.C., 1990, Metamict allanite in Archean gneiss, Bighorn Mountains, Wyoming: Geological Society Abstracts with Programs, v. 22, p. 41.

Parfitt, R.L., Russell, M., and Orbell, G.E. 1983, Weathering sequence of soils from volcanic ash involving allophane and halloysite, New Zealand: Geoderma, v. 29, p. 41-57.

Pavich, M.J., 1989, Regolith residence time and the concept of the surface age of the Piedmont "peneplain": Geomorphology, v. 2, p. 181-196.

Pavich, M.J., Leo, G.W., Obermeier, S.F., and Estabrook, J.R., 1989, Investigations of the characteristics, origin, and residence time of the upland residual mantle of the Piedmont of Fairfax County, Virginia: U.S. Geological Survey Professional Paper 1352, United States Government Printing Office, Washington, D.C., 58 p.

Pédro, G., 1968, Distribution des principaux types de'altération chimique à la surface du globe, présentation d'une esquisse géographique: Rev. Géogr. Phys. Géol. Dyn., v. 10, p. 457-470.

Peng, M., and Ruan, D., 1986, A spectroscopic study on the allanite from a granite body in northeastern Guangdong: Journal of Central-South Institute of Mining and Metallurgy, Issue 1, p. 1-9.

Pe-Piper, G., and Piper, D.J.W., 1985, Late-Cenozoic clays and climatic change in the post-orogenic Lakonia Graben, southern Greece: Neues Jahrbuch Miner. Abh., v. 151, p. 301-313.

Perkins, W.T., Pearce, N.J.G., and Jeffries, T.E., 1993, Laser ablation inductively coupled plasma mass spectrometry: a new technique for the determination of trace element and ultra-trace elements in silicates: Geochimica et Cosmochimica Acta, v. 57, p. 475-482.

Plummer, L.N., and Back, W., 1980, The mass balance approach: Application to interpreting the chemical evolution of hydrologic systems: American Journal of Science, v. 280, p. 130-142.

Poitrasson, F., Paquette, J.-L., Montel, J.-M., Pin, C., and Duthou, J.-L., 1998, Importance of late-magmatic and hydrothermal fluids on the Sm-Nd isotope mineral systematics of hypersolvus granites: Chemical Geology, v. 146, p. 187-203.

Poppe, L.J., Commeau, J.A., and Luepke, G., 1995, Silt fraction heavy-mineral distributions in a lateritic environment: the rivers and insular shelf of north-central Puerto Rico: Sedimentary Geology, v. 95, p. 251-268.

Potter, P.E., Heling, D., Shimp, N.F., and Van Wie, W., 1975, Clay mineralogy of modern alluvial muds of the Mississippi River Basin: Bull. Centre Rech. Pau – SNPA, v. 9, p. 353-389.

Power, E.T., Smith, B.J., 1994, A comparative study of deep weathering and weathering products: case studies from Ireland, Corsica and southeast Brazil: in Robinson, D.A., and Williams, R.B.G. (eds.), Rock weathering and Landform Evolution, Chichester, p. 21-40.

Price, G.D., Ruffell, A.H., Jones, C.E., Kalin, R.M., and Mutterlose, J., 2000, Isotopic evidence for temperature variation during the early Cretaceous (late Ryazanian—mid-Hauterivian): Journal of the Geological Society, London, v. 157, p. 335-343.

Price, J.R., and Velbel, M.A., in review, Applications of chemical weathering indices to weathering profiles developed on heterogeneous felsic metamorphic parent rocks: Chemical Geology.

Probst, A., El Gh'Mari, A., Aubert, D., Fritz, B., and McNutt, R., 2000, Strontium as a tracer of weathering processes in a silicate catchment polluted by acid atmospheric inputs, Strengbach, France: Chemical Geology, v. 140, p. 203-219.

Protz, R., Ross, G.J., Martini, I.P., and Terasmae, J., 1984, Rate of podzolic soil formation near Hudson Bay, Ontario: Canadian Journal of Soil Science, v. 64, p. 31-49.

Protz, R., Ross, G.J., Shipilato, M.J., Terasmae, J., 1988, Podzolic soil development in the southern James Bay lowlands, Ontario, Canadian Journal of Soil Science, v. 68, p. 287-305.

Prowell, D.C., and Owens, J.P., 1987, Late Cenozoic deformation in the eastern U.S.: speculation from studies of Cretaceous and Early Cenozoic tectonism: Geological Society of America Abstracts with Programs, v. 19, p. 127.

Prowell, D.C., 1989, Crustal compression, uplift, and extension in the eastern United States during the Cretaceous and Cenozoic as implied by fault geometries: Geological Society of America Abstracts with Programs, v. 21, p. 54.

Prowell, D.C., and Obermeier, S.F., 1991, Evidence of Cenozoic Tectonism: in Horton, J.W., Jr., and Zullo, V.A., (eds.), The Geology of the Carolinas, Carolina Geological Society Fiftieth Anniversary Volume, p. 309-318.

Prowell, D.C., and Christopher, R.A., 1993, Evidence for Cenozoic uplift of the Appalachian Mountains in the southeastern United States: Geological Society of America Abstracts with Programs, v. 24, p. 62-63.

Prowell, D.C., and Christopher, R.A., 2000, The last Appalachian orogeny: evidence for Cenozoic tectonism and uplift of mountains in the eastern Unites States: Geological Society of America Abstracts with Programs, v. 32, p. 67.

Ramspott, L.D., 1965, Earliest effects of weathering in Elberton Granite: Bulletin of the Georgia Academy of Science, v. 23, p. 34-35.

Rateev, M.A., Gorbunavo, Z.N., Lisitzin, A.P., and Nosov, G.I., 1969, The distribution of clay minerals in the oceans: Sedimentology, v. 13, p. 21-43.

Rebertus, R.A., Weed, S.B., and Buol, S.W., 1986, Transformations of biotite to kaolinite during saprolite-soil weathering: Soil Science Society of America Journal, v. 50, p. 810-819.

Reynolds, R.C., Jr., and Reynolds, R.C., III, 1996, NEWMOD-For-Windows™. The Calculation of One-Dimensional Diffraction Patterns of Mixed-Layer Clay Minerals: R.C. Reynolds, Jr., 8 Brook Road, Hanover, NH.

Righi, D., and Meunier, A., 1995, Origin of clays by rock weathering and soil formation: in Velde, B. (ed.), Clays and the Environment, Springer, New York, p. 43-161.

Robert, C., and Chamley, H., 1991, Development of early Eocene warm climates, as inferred from clay mineral variations in oceanic sediments: Palaeogeography, Palaeoclimatology, Palaeoecology, v. 89, p. 315-331.

Robert, C., and Kennett, J.P., 1992, Paleocene and Eocene kaolinite distribution in the South Atlantic and Southern Ocean: Antarctic climatic and paleoceanographic implications: Marine Geology, v. 103, p. 99-110.

Robert, C., and Kennett, J.P., 1994, Antarctic subtropical humid episode at the Paleocene-Eocene boundary: clay-mineral evidence: Geology, v. 22, p. 211-214.

Robie, R.A., Hemingway, B.S., and Fisher, J.R., 1978, Thermodynamic properties of minerals and related substances at 298.15 K and 1 bar (10^5 Pascals) pressure and at higher temperatures: U.S. Geological Survey Bulletin 1452 , 456 p.

Romero, N.L., 1989, Mineral weathering in the Loch Vale watershed, Rocky Mountain National Park, Front Range, Colorado [unpublished M.S. thesis]: Michigan State University, East Lansing. Michigan, 92 p.

Rose, N.M., 1991, Dissolution rates of phrenite, epidote and albite: Geochimica et Cosmochimica Acta, v. 55, p. 3273-3286.

Schalscha, E.B., Appelt, H., and Schaltz, A., 1967, Chelation as a weathering mechanism—I. Effect of complexing agents on the solubilization of iron from minerals and granodiorite: Geochimica et Cosmochimica Acta, v. 31, p. 587-596.

Schoeller, H., 1942, La diorite d'Anglars (LOT): Proces-verbaux de la Societe Linneene de Ordeaux, Séance du 18, p. 1-6 (in French).

Schott, J., and Petit, J.-C., 1987, New evidence for the mechanisms of dissolution of silicate minerals: in Stumm, W. (ed.), Aquatic Surface Chemistry, John Wiley & Sons, New York, p. 255-292.

Schroeder, P.A., Melear, N.D., West, L.T., and Hamilton, D.A., 2000, Meta-gabbro weathering in the Georgia Piedmont, USA: implications for global silicate weathering rates: Chemical Geology, v. 163, p. 235-245.

Schroeder, P.A., Melear, N.D., Bierman, P., Kashgarian, M., and Caffee, M.W., 2001, Apparent gibbsite growth ages for regolith in the Georgia Piedmont: Geochimica et Cosmochimica Acta, v. 65, p. 381-386.

Schwertmann, U., and Taylor, R.M., 1995, Iron oxides: in Dixon, J.B., and Weed, S.B. (eds.), Minerals in Soil Environments, Soil Science Society of America, Inc., Madison, Wisconsin, p. 379-438.

Scott, R.C., Jr., 1972, The geomorphic significance of debris avalanching in the Appalachian Blue Ridge Mountains [unpublished Ph.D. dissertation]: University of Georgia, Athens, Georgia, 185 p.

Sholkovitz, E.R., Curch, T.M., and Arimoto, R., 1993, Rare earth element composition of precipitation, precipitation particles, and aerosols: Journal of Geophysical Research, v. 98, p. 20587-20599.

Sholkovitz, E.R., Elderfield, H., Szymczak, R., and Casey, K., 1999, Island weathering: river sources of rare earth elements to the Western Pacific Ocean: Marine Chemistry, v. 68, p. 39-57.

Singer, A., 1980, The paleoclimatic interpretation of clay minerals in soils and weathering profiles: Earth Science Review, v. 15, p. 303-326.

Singer, A., 1984, The paleoclimatic interpretation of clay minerals in sediments—a review: Earth-Science Review. v. 21, p. 251-293.

Smedley, P.L., 1991, The geochemistry of rare earth elements in ground water from the Carnmenellis area, southwest England: Geochimica et Cosmochimica Acta, v. 55, p. 2767-2779.

Stallard, R.F., and Edmond, J.M., 1983, Geochemistry of the Amazon 2. The influence of the geology and weathering environment on the dissolved load: Journal of Geophysical Research, v. 88, p. 9671-9688.

Stauffer, R.E., 1990, On granite weathering and the sensitivity of alpine lakes to acid deposition: Limnology and Oceanography, v. 50, p. 1109-1130.

Stoffers, P., and Hecky, R.E., 1978, Late Pleistocene-Holocene evolution of the Kivu-Tanganyika Basin: in Matter, A., and Tucker, M.E. (eds.), Modern and Ancient Lake Sediments, International Association of Sedimentologists Special Publication Number 2, Blackwell Scientific Publications, London, p. 43-55.

Stolt, M.H., Baker, J.C., and Simpson, T.W., 1991, Micromorphology of the soil-saprolite transition zone in the Hapludults of Virginia: Soil Science Society of America Journal, v. 55, p. 1067-1075.

Stolt, M.H., and Baker, J.C., 2000, Quantitative comparison of soil and saprolite genesis: examples from the Virginia Blue Ridge and Piedmont: Southeastern Geology, v. 39, p. 129-150.

Strens, R.G.J., 1966, Properties of the Al-Fe-Mn epidotes: Mineralogical Magazine, v. 25, p. 928-944.

Sun, S.-S., and McDonough, W.F., 1989, Chemical and isotopic systematics of oceanic basalts: implications for mantle composition and processes: in Saunders, A.D., and Norry, M.J. (eds.), Magmatism in the Ocean Basins, Geological Society Special Publication No. 42, p. 313-345.

Suwa, K., Matsuzawa, I., Iida, C., and Yamasaki, K., 1958, Mineralogical and geochemical studies on the weathering of a quartz porphyry: The Journal of Earth Sciences, Negoya University, v. 6, p. 75-100.

Sverdrup, H.U., 1990, The Kinetics of Base Cation Release due to Chemical Weathering: Lund University Press, Lund, Sweden, 246 p.

Sverdrup, H., and Warfvinge, P., 1993, Calculating field weathering rates using a mechanistic geochemical model PROFILE: Applied Geochemistry, v. 8, p. 273-283.

Sverdrup, H., and Warfvinge, P., 1995, Estimating weathering rates using laboratory kinetics: in White, A.F., and Brantley, S.L. (eds.), Chemical Weathering Rates of Silicate Minerals, Mineralogical Society of America Reviews in Mineralogy v. 31, Washington, D.C., p. 485-542.

Swank, W.T., and Douglass, J.E., 1977, Nutrient budgets for undisturbed and manipulated hardwood forest ecosystems in the mountains of North Carolina: in Correll, D.L. (ed.), Watershed Research in Eastern North America, Smithsonian Institution, Washington, D.C., p. 343-364.

Swank, W.T., and Crossley, Jr., D.A., 1988, Introduction and Site Description: in Swank, W.T., and Crossley, Jr., D.A. (eds.), Forest Hydrology and Ecology at Coweeta, Springer-Verlag, New York, p. 3-16.

Swank, W.T., and Waide, J.B., 1988, Characterization of baseline precipitation and stream chemistry and nutrient budgets for control watersheds: in Swank, W.T., and Crossley, Jr., D.A. (eds.), Forest Hydrology and Ecology at Coweeta, Springer-Verlag, New York, New York, p. 57-79.

Swift, Jr., L.W., Cunningham, G.B., and Douglass, J.E., 1988, Climatology and Hydrology: in Swank, W.T., and Crossley, Jr., D.A. (eds.), Forest Hydrology and Ecology at Coweeta, Springer-Verlag, New York, p. 35-56.

Swoboda-Colberg, N.G., and Drever, J.I., 1993, Mineral dissolution rates in plot-scale field and laboratory experiments: Chemical Geology, v. 105, p. 51-69.

Tabor, N.J., Montanez, I.P., and Southard, R.J., 2002, Paleoenvironmental reconstruction from chemical and isotopic compositions of Permo-Pennsylvanian pedogenic minerals: Geochimica et Cosmochimica Acta, v. 66, p. 3093-3107.

Taylor, A.B., 1988, Mineral transformations and geochemical mass balance of a disturbed forested watershed [unpublished M.S. thesis]: Michigan State University, East Lansing, Michigan, 132 p.

Taylor, A.B., and Velbel, M.A., 1991, Geochemical mass balances and weathering rates in forested watersheds of the southern Blue Ridge II. Effects of botanical uptake terms: Geoderma, v.51, p. 29-50.

Taylor, G., Truswell, E.M., Eggleton, R.A., and Musgrave, R., 1990, Cool climate bauxite: Geochemistry of the Earth's Surface and of Mineral Formation 2nd International Symposium, Aix en Provence, France, Chemical Geology, v. 84, p. 183-184.

Taylor, G., Eggleton, R.A., Holzhauer, C.C., Maconachie, L.A., Gordon, M., Brown, M.C., and McQueen, K.G., 1992, Cool climate lateritic and bauxitic weathering: Journal of Geology, v. 100, p. 669-677.

Taylor, A.S., Blum, J.D., Lasaga, A.C., and MacInnis, I.N., 2000, Kinetics of dissolution and Sr release during biotite and phlogopite weathering: Geochimica et Cosmochimica Acta, v. 64, p. 1191-1208.

Taylor, G., and Eggleton, R.A., 2001, Regolith Geology and Geomorphology: John Wiley & Sons, Ltd., New York, 375 p.

Tardy, Y., Bocquier, G., Paquet, H., Millot, G., 1973, Formation of clay from granite and its distribution in relation to climate and topography: Geoderma, v. 10, p. 271-284.

Thiry, M., 2000, Palaeoclimatic interpretation of clay minerals in marine deposits: an outlook from the continental origin: Earth-Science Reviews, v. 49, p. 201-221.

Thompson, H.J., 1969, The James River flood of August 1969 in Virginia: Weatherwise, v. 22, p. 180-183.

Tricca, A., Stille, P., Steinmann, M., Kiefel, B., Samuel, J., and Eikenberg, J., 1999, Rare earth elements and Sr and Nd isotopic compositions of dissolved and suspended loads from small river systems in the Vosges mountains (France), the river Rhine and ground water: Chemical Geology, v. 160, p. 139-158.

Turk, J.T., and Spahr, N.E., 1991, Rocky Mountains: Controls on lake chemistry: in Charles, D.F. (ed.), Acid Deposition and Aquatic Ecosystems: Regional Case Studies, Springer-Verlag, New York, p. 471-501.

Turner, D.R., Whitfield, M., and Dickson, A.G., 1981, The equilibrium speciation of dissolved components in fresh water and seawater at 25 C and 1 atm pressure: Geochimica et Cosmochimica Acta, v. 45, p. 855-881.

Turpault, M.P., and Trotignon, L., 1994, The dissolution of biotite single crystals in dilute HNO_3 at 24°C: Evidence of an anisotropic corrosion process of micas in acidic solutions: Geochimica et Cosmochimica Acta, v. 58, p. 2761-2775.

Uddin, A., and Lundberg, N., 1998, Unroofing history of the eastern Himalaya and the Indo-Burman ranges: heavy-mineral study of Cenozoic sediments from the Bengal Basin, Bangladesh: Journal of Sedimentary Research, v. 68, p. 465-472.

Vance, E.R., and Routcliffe, P., 1976, Heat treatment of some metamict allanites: Mineralogical Magazine, v. 40, p. 521-523.

van der Weijden, C.H., and van der Weijden, R.D., 1995, Mobility of major, minor and some redox-sensitive trace elements and rare-earth elements during weathering of four granitoids in central Portugal: Chemical Geology, v. 125, p. 149-167.

Varadachari, C., Barman, A.K., and Ghosh, K., 1992, Weathering of silicate minerals by organic acids II. Nature of residual products: Geoderma, v. 61, p. 251-268.

Velbel, M.A., 1983, A dissolution-reprecipitation mechanism for the pseudomorphous replacement of plagioclase feldspar by clay minerals during weathering: Science Géologie Mémoires, v. 71, p. 139-147.

Velbel, M.A., 1984a, Mineral transformations during rock weathering, and geochemical mass-balances in forested watersheds of the southern Appalachians [unpublished Ph.D. dissertation]: Yale University, New Haven, Connecticut, 175 p.

Velbel, M.A., 1984b, Natural weathering mechanisms of almandine garnet: Geology, v. 12, p. 631-634.

Velbel, M.A., 1985a, Geochemical mass balances and weathering rates in forested watersheds of the southern Blue Ridge: American Journal of Science, v. 285, p. 904-930.

Velbel, M.A., 1985b, Hydrogeochemical constraints on mass balances in forested watersheds of the southern Appalachians: in Drever, J.I. (ed.), The Chemistry of Weathering: Reidel Publishing Co., Dordrecht, Holland, p. 231-247.

Velbel, M.A., 1986a, The mathematical basis for determining rates of geochemical and geomorphic processes in small forested watersheds by mass balance: examples and implications: in Colman, S.M., and Dethier, D.P. (eds.), Rates of Chemical Weathering of Rocks and Minerals, Academic Press, Inc., New York, p. 439- 451.

Velbel, M.A., 1986b, Influence of surface area, surface characteristics, and solution composition on feldspar weathering rates: in Davis, J.A., and Hayes, K.F. (eds.), Geochemical Processes at Mineral Surfaces, American Chemical Society Symposium Series, v. 323, American Chemical Society, Washington, D.C., p. 615-634.

Velbel, M.A., 1987, Mechanisms and products of hornblende weathering at the Coweeta Hydrologic Laboratory, North Carolina: Abstracts, Clay Minerals Society 24th Annual Meeting, p. 135.

Velbel, M.A., 1988, Weathering and soil-forming processes: in Swank, W.T., and Crossley, Jr., D.A. (eds.), Forest Hydrology and Ecology at Coweeta, Springer-Verlag, New York, New York, p. 93-102.

Velbel, M.A., 1989a, Effect of chemical affinity on feldspar hydrolysis rates in two natural weathering systems: Chemical Geology, v. 78, p. 245-253.

Velbel, M.A., 1989b, Weathering of hornblende to ferruginous products by a dissolution-reprecipitation mechanism: petrography and stoichiometry: Clays and Clay Minerals, v. 37, p. 515-524.

Velbel, M.A., 1990a, Influence of temperature and mineral surface characteristics on feldspar weathering rates in natural and artificial systems: a first approximation: Water Resources Research, v. 26, p. 3049-3053.

Velbel, M.A., 1990b, Mechanisms of saprolitization, isovolumetric weathering, and pseudomorphous replacement during rock weathering—a review: Geochemistry of the Earth's Surface and of Mineral Formation 2nd International Symposium, Aix en Provence, France, Chemical Geology, v. 84, p. 17-18.

Velbel, M.A., 1992, Geochemical mass balances and weathering rates in forested watersheds of the southern Blue Ridge. III. Cations budgets and the weathering rate of amphibole: American Journal of Science, v. 292, p. 58-78.

Velbel, M.A., 1993a, Temperature dependence of silicate weathering in nature: How strong a negative feedback on long-term accumulation of atmospheric CO_2 and global greenhouse warming?: Geology, v. 21, p. 1059-1062.

Velbel, M.A., 1993b, Formation of protective surface layers during silicate-mineral weathering under well-leached, oxidizing conditions: American Mineralogist, v. 78, p. 405-414.

Velbel, M.A., 1993c, Constancy of silicate-mineral weathering-rate ratios between natural and experimental weathering: implications for hydrologic control of differences in absolute rates: Chemical Geology, v. 105, p. 89-99.

Velbel, M.A., 1993d, Weathering and pedogenesis at the watershed scale: some recent lessons from studies of acid-deposition effects: Chemical Geology, v. 107, p. 337-339.

Velbel, M.A., 1995, Interaction of ecosystem processes and weathering processes: in Solute Modelling in Catchment Systems, Trudgill, S.T. (ed.), John Wiley & Sons Ltd., New York, New York, p. 193-209.

Velbel, M.A., Basso, C.L., and Zieg, M.J., 1996, The natural weathering of staurolite: Crystal-surface textures, relative stability, and the rate-determining step: American Journal of Science, v. 296, p. 453-472.

Viers, J., Dupré, B., Braun, J.-J., Deberdt, S., Angeletti, B., Ngoupayou, J.N., and Michard, A., 2000, Major and trace element abundances, and strontium isotopes in the Nyong basin rivers (Cameroon): constraints on chemical weathering processes and elements transport mechanisms in humid tropical environments: Chemical Geology, v. 169, p. 211-241.

Volokh, A.A., Gorbunov, A.V., Gundorina, S.F., and Revich, B.A., 1990, Phosphorus fertilizer production as a source of rare-earth element pollution of the environment: Science of the Total Environment, v. 95, p. 141-148.

Wagner, T., Pletsch, T., Kuhnt, W., 1997, Cretaceous to late Oligocene development of sedimentary and organic facies at ODP Leg 159; paleoenvironmental implications for the eastern Equatorial Atlantic: American Association of Petroleum Geologists Bulletin, v. 81, p. 1567.

Warfvinge, P., and Sverdrup, H., 1992, Calculating critical loads of acid deposition with PROFILE—A steady-state soil chemistry model: Water, Air, Soil Pollution, v. 63, p. 119-143.

Watson, T.L., 1917, Weathering of allanite: Bulletin of the Geological Society of America, v. 28, p. 463-500.

Weaver, C.E., 1989, Clays, Muds, and Shales: Developments in Sedimentology 44, Elsevier Science Publishers B.V., New York, 819 p.

White, A.F., and Blum, A.E., 1995a, Effects of climate on chemical weathering in watersheds: Geochimica et Cosmochimica Acta, v. 59, p. 1729-1747.

White, A.F., and Blum, A.E., 1995b, Climatic effects in chemical weathering in watersheds: Applications of mass balance approaches: in Trudgill, S.T. (ed.), Solute Modeling in Catchment Systems, John Wiley & Sons Ltd., New York, p. 101-131.

White, A.F., Blum, A.E., Bullen, T.D., Vivit, D.V., Schulz, M., and Fitzpatrick, J., 1999a, The effect of temperature on experimental and natural chemical weathering rates of granitoid rocks: Geochimica et Cosmochimica Acta, v. 63, p. 3277-3291.

White, A.F., Bullen, T.D., Vivit, D.V., Schulz, M.S., and Clow, D.W., 1999b, The role of disseminated calcite in the chemical weathering of granitoid rocks: Geochimica et Cosmochimica Acta, v. 63, p. 1939-1953.

White, A.F., Bullen, T.D., Vivit, D.V., Schulz, M.S., and Blum, A.E., 1999c, The effect of climate on chemical weathering of silicate rocks: in Ármannsson, H. (ed.), Geochemistry of the Earth's Surface, Balkema, Netherlands, p. 79-82.

White, A.F., Bullen, T.D., Schulz, M.S., Blum, A.E., Huntington, T.G., and Peters, N.E., 2001, Differential rates of feldspar weathering in granitic regoliths: Geochimica et Cosmochimica Acta, v. 65, p. 847-869.

White, A.F., Blum, A.E., Schulz, M.S., Huntington, T.G., Peters, N.E., and Stonestrom, D.A. 2002, Chemical weathering of the Panola Granite: Solute and regolith elemental fluxes and the weathering rate of biotite: in Hellmann, R., and Wood, S.A., (eds.), Water-Rock Interactions, Ore Deposits, and Environmental Geochemistry: A Tribute to David A. Crerar, The Geochemical Society, Special Publication No. 7, p. 37-59.

Whitton, J.S., and Churchman, G.J., 1987, Standard Methods for Mineral Analysis of Soil Survey Samples for Characterization and Classification in New Zealand Soil Bureau: New Zealand Soil Bureau Scientific Report, v. 79, New Zealand Soil Bureau, Lower Hutt, New Zealand, 27 pp.

Williams, H., and Hatcher, R.D., Jr., 1982, Suspect terranes and accretionary history of the Appalachian orogen: Geology, v. 10, p. 530-536.

Williams, H., and Hatcher, R.D., Jr., 1983, Suspect terranes: a new look at the Appalachian orogen: in Hatcher, R.D., Jr., Williams, H., and Zietz, I. (eds.), Contributions to the tectonics and geophysics of mountain chains, Geological Society of America Memoir 158, p. 33-54.

Willman, H.B., Glass, H.D., and Frye, J.C., 1963, Mineralogy of Glacial Tills and Their Weathering Profiles in Illinois, Part I. Glacial Tills: Illinois State Geological Survey Circular 347, 55p.

Wilson, A.F., 1966, Metamict allanite from pegmatites cutting basic charnockitic granulites in the Fraser Range, Western Australia: Journal of the Royal Society of Western Australia, v. 49, p. 85-87.

Wilson, M.J., 1975, Chemical weathering of some primary rock-forming minerals: Soil Science, v. 119, p. 349-355.

Wilson, M.J., 1987, X-ray powder diffraction and methods: in Wilson, M.J. (ed.), A Handbook of Determinative Methods in Clay Mineralogy, Chapman and Hall, New York, New York, p. 26-98,

Windom, H.L., 1976, Lithogeneous material in marine sediments: in Riley, J.P., and Chester, R. (eds.), Chemical Oceanography, Volume 5, Academic Press, New York, p. 103-135.

Winograd, I.J., Landwehr, J.M., Ludwig, K.R., Coplen, T.B., and Riggs, A.C., 1997, Duration and structure of the past four interglaciations: Quaternary Research, v. 48, p. 141-154.

Wood, S.A., 1990, The aqueous geochemistry of the rare earth elements and yttrium: Chemical Geology, v. 82, p. 159-186.

Yeakley, J.A., Swank, W.T., Swift, L.W., Hornberger, G.M., and Shugart, H.H., 1998, Soil moisture gradients and controls on a southern Appalachian hillslope from drought through recharge: Hydrology and Earth System Sciences, v. 2, p. 41-49.

Yuretich, R., Melles, M., Sarata, B., and Grobe, H., 1999, Clay minerals in the sediments of Lake Baikal: a useful climate proxy: Journal of Sedimentary Research, v. 69, p. 588-596.

Zhang, J., and Nozaki, Y., 1996, The REE concentrations of the rainwaters over Tokyo, Japan: Implications for dissolution of REE from aerosol and atmospheric input to the oceans: Abstracts, 30th International Geological Congress, v. 3, p. 49.